

REPORT NO.
UCB/EERC-82/08
AUGUST 1982

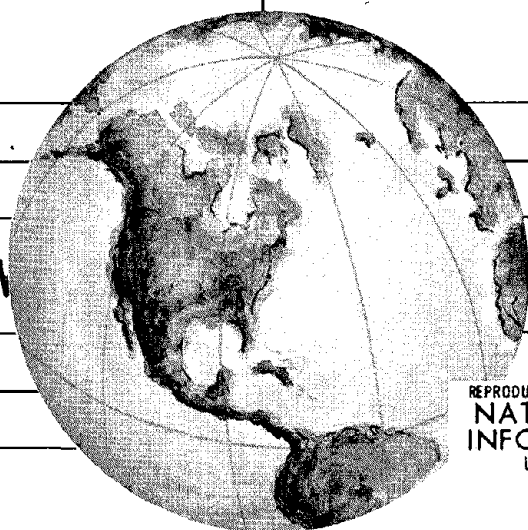
EARTHQUAKE ENGINEERING RESEARCH CENTER

AN EVALUATION OF THE DESIGN AND ANALYTICAL SEISMIC RESPONSE OF A SEVEN-STORY REINFORCED CONCRETE FRAME-WALL STRUCTURE

by

FINLEY A. CHARNEY
VITELMO V. BERTERO

Report to National Science Foundation



REPRODUCED BY
NATIONAL TECHNICAL
INFORMATION SERVICE
U.S. DEPARTMENT OF COMMERCE
SPRINGFIELD, VA. 22161

COLLEGE OF ENGINEERING

UNIVERSITY OF CALIFORNIA • Berkeley, California

For sale by the National Technical Information Service, U.S. Department of Commerce, Springfield, Virginia 22161.

See back of report for up to date listing of EERC reports.

DISCLAIMER

Any opinions, findings, and conclusions or recommendations expressed in this publication are those of the authors and do not necessarily reflect the views of the National Science Foundation or the Earthquake Engineering Research Center, University of California, Berkeley

REPORT DOCUMENTATION PAGE		1. REPORT NO. NSF/CEE-82064	2.	3. Recipient's Accession No.
4. Title and Subtitle An Evaluation of the Design and Analytical Seismic Response of a Seven-Story Reinforced Concrete Frame-Wall Structure				5. Report Date August 1982
7. Author(s) Finley A. Charney and V. V. Bertero				6.
9. Performing Organization Name and Address Earthquake Engineering Research Center University of California, Berkeley 47th Street and Hoffman Blvd. Richmond, Calif. 94804				8. Performing Organization Rept. No. UCB/EERC-82/08
12. Sponsoring Organization Name and Address National Science Foundation 1800 G. Street, N.W. Washington, D.C. 20550				10. Project/Task/Work Unit No.
				11. Contract(C) or Grant(G) No. (C) (G) PFR-8009478
				13. Type of Report & Period Covered
				14.
15. Supplementary Notes				
16. Abstract (Limit: 200 words) <p>This report describes the analytical studies regarding the response of a reinforced concrete test building that have been conducted at the University of California, Berkeley, as part of a US-Japan cooperative research program on the behavior of structures subjected to earthquake induced loading. This work, which begins with a review of the prototype design according to the 1979 Uniform Building Code specifications for seismic resistant buildings, shows that while the test building, a 1/5 scale model of a 7-story reinforced concrete frame-wall structure, does not satisfy all code specifications, it can be considered to be a good design from the point of view of the strong column-weak beam philosophy.</p> <p>The elastic properties of the structure are investigated through the use of flexibility matrices; the inelastic response of the structure to monotonically increasing lateral loads is studied; and a nonlinear dynamic analysis using the computer program DRAIN-2D, which indicates that the response of the test building to different recorded ground motions is governed by the behavior of the centrally located shearwall, is presented.</p> <p>In order to obtain an understanding of the response of the structure to the ground motions, detailed analysis of the response for the duration of pulses inducing maximum response is considered. Errors that occur in the response due to modeling procedures are discussed and methods are suggested for improved analysis.</p>				
17. Document Analysis a. Descriptors				
b. Identifiers/Open-Ended Terms				
c. COSATI Field/Group				
18. Availability Statement Release Unlimited		19. Security Class (This Report)		21. No. of Pages 196
		20. Security Class (This Page)		22. Price

**An Evaluation of the Design
and Analytical Seismic Response
Of a Seven-Story Reinforced Concrete
Frame-Wall Structure**

By

Finley A. Charney
Graduate Student

and
Vitelmo V. Bertero
Professor of Civil Engineering

Report Number 82-08
Earthquake Engineering Research Center
College of Engineering
University of California
Berkeley, California

July 1982

ABSTRACT

As part of the comprehensive US-Japan cooperative research program on the behavior of structures subjected to earthquake induced loading, a 1/5 scale model of a 7-story reinforced concrete frame-wall structure is to be tested on the University of California's shaking table located at Richmond Field Station. This model is one of many different types and sizes of models that will be tested at research institutions in both the United States and Japan. In addition to the experimental work, analytical studies are being carried out on the models to be tested. Through the correlation and the study of the results obtained from these analytical and experimental investigations, it is hoped that the behavior of models will be better understood, and thus provide valuable information to those planning future experimental research programs. Also, the results from these tests will supply data on the adequacy of the design and construction techniques currently used for seismic resistant structures.

This report describes the analytical studies that have been conducted at Berkeley regarding the response of the reinforced concrete test building. This work, which begins with a review of the prototype design according to the 1979 Uniform Building Code specifications for seismic resistant buildings, shows that while the test building does not satisfy all code specifications, it can be considered to be a good design from the point of view of the strong column-weak beam philosophy. After the UBC checks, the results of three types of analysis are presented. First, the elastic properties of the structure are investigated through the use of flexibility matrices. Next, the inelastic response of the structure to monotonically increasing lateral loads is studied. The final type of analysis is a nonlinear dynamic analysis using the computer program DRAIN-2D, which indicates that the response of the test building to different recorded ground motions is governed by the behavior of the centrally located shearwall. Once the wall yields in flexure at its base, the beams begin to yield, followed by the columns at the base of the structure. In every case, the structure is able to dissipate the energy demanded by the earthquake induced loading. Also, in order to obtain an understanding of the response of the structure to the ground motions, detailed analysis of the response for the duration of pulses inducing maximum response is considered.

To provide improved analysis, within the limitations inherent in the modelling of structures using DRAIN-2D, the errors that occur in the response due to modeling procedures are discussed and methods are suggested for improved analysis. Finally, main conclusions are drawn and recommendations for future research are formulated.

ACKNOWLEDGEMENTS

The research reported herein is part of the US-Japan Cooperative Research Program Utilizing Large Scale Testing Facilities, formulated by a US-Japan Planning Group in 1979. Funding for this project was provided by the National Science Foundation under Grant No. PFR-8009478, as part of the total support to the US-Japan Cooperative Research Program. Any opinions, findings, conclusions, and recommendations expressed in this publication are those of the authors and do not necessarily reflect the view of the National Science Foundation.

F.A.Charney conducted this research, under the supervision of V.V. Bertero, Principal Investigator, in partial fulfillment of the requirements for the degree of Doctor of Philosophy in Civil Engineering.

Many people have contributed to these studies, and the authors especially wish to thank A.E. Aktan, R.W. Clough, G.H. Powell, and S. Mahin for their comments and guidance. Also, the excellent illustrations, executed by Gail Feazell, Gloria Pelatowski, Deborah Moss, and Richard Steele are greatly appreciated. Editing assistance was provided by Susan Gardner. This report was typed by F.A. Charney on a TRS-80 Microcomputer, using the program "EDDIE", developed at Berkeley by E.L. Wilson.

TABLE OF CONTENTS

SECTION	TITLE	PAGE
	Abstract	iii
	Acknowledgements	v
	Table of Contents	vii
	List of Tables	xi
	List of Figures	xiii
	Chapter 1: Introduction	1
1.1	Objectives	2
1.2	Scope and Layout of Report	3
	Chapter 2: Review of Prototype Design	5
2.1	Materials	6
2.1.1	Concrete	6
2.1.2	Steel Reinforcement	6
2.2	Cross Sectional Analysis	7
2.2.1	Beams	7
2.2.2	Columns	9
2.2.3	Shearwall	11
2.3	Joints and Anchorage	13
2.4	Prototype Loading	14
2.4.1	Gravity Loading	14
2.4.2	Structural Mass and Lateral Loading	15
2.5	UBC Lateral Load Analysis	17
2.5.1	Lateral Load Analysis	17
2.5.2	Ultimate Strength of Prototype	19
2.5.3	Strength of Wall Acting Alone	19
2.6	Discussion of UBC Analysis	20
	Chapter 3: Elastic Properties of Prototype	23
3.1	Prototype Flexibility	23
3.2	Mode Shapes and Periods of Vibration	26
	Chapter 4: Strength Under Monotonically increasing Lateral Load	27
4.1	Static Load to Collapse Analysis	27
4.2	Element Yield Surfaces	28
4.3	Results of Collapse Analysis	28
4.3.1	Force-Displacement Response	29
4.3.2	Plastic Hinge Formation	30
4.4	Effect of Wall Hinging	31
4.5	Analysis of the P-Delta Effect	32

	Chapter 5: Response of Prototype to Earthquake Loading	33
5.1	Nonlinear Analysis Using DRAIN-2D	33
4.1.1	Step by Step Analysis Procedures	35
5.1.2	Element Properties and Behavior	35
5.2	Properties of the Analytical Model	36
5.2.1	Damping	36
5.3	Selection of Time step	36
5.4	Introduction to Results	37
5.4.1	Organization of Results	38
5.5	Prototype Response to Miyagi Oki	39
5.5.1	Discussion of Overall Response	39
5.5.2	Detailed Analysis of Three Pulses	40
5.5.2.1	Pulse One (MO1)	40
5.5.2.2	Pulse Two (MO2)	41
5.5.2.3	Pulse Three (MO3)	42
5.5.2.4	Discussion of MO Response	43
5.6	Prototype Response to Pacoima Dam	46
5.6.1	Discussion of Overall Response	46
5.6.2	Detailed Analysis of a Single Pulse	47
5.7	Comparison of the MO and DPD Response	49
5.8	Ductility : Supply vs Demand	50
5.9	Conclusions on MO and DPD Response	53
	Chapter 6: Accuracy of Computed Response	55
6.1	Global Modelling Errors	55
6.1.1	Flexural Frame to Frame Coupling	55
6.1.2	Affect of Large Displacements	57
6.1.3	Rigidity of Foundation	57
6.2	Local Modelling Errors	57
6.2.1	Column Elements	58
6.2.2	Beam Elements	59
6.2.2.1	Initial Beam Stiffness	60
6.2.2.2	Strain Hardening Stiffness	61
6.2.2.3	Positive Moment Strength	61
6.2.2.4	Negative Moment Strength	62
6.2.2.5	The Takeda Model	62
6.2.3	Shearwall Elements	63
6.2.4	Conclusions on Local Modelling	65
6.3	Structural Loads, Mass, and Damping	65
6.3.1	Loads	65
6.3.2	Mass	66
6.3.3	Damping	66
6.4	Numerical Errors	67
	Chapter 7: Summary and Research Needs	69
7.1	Conclusions	70
7.2	Future Analytical Research Needs	72
7.3	Future Experimental Research Needs	73

List of References	75
Tables	77-91
Figures	93-157
Appendix A: Plans of 1/5 Scale Model	159

LIST OF TABLES

TABLE	TITLE OF TABLE	PAGE
2.1	Table 23-I From the Uniform Building Code	79
2.2	U.S.A. vs Metric Bar Sizes	79
2.3	Summary of Beam Strengths	80
3.1	Elastic Stiffness of Frame Elements	81
3.2	Structural Flexibility Matrices	82
3.3	Experimental Flexibility Matrix (Japan)	83
4.1	Flexibility of Yielded Structure	84
5.1	Summary of Response During Pulse 1 of M0	85
5.2	Summary of Response During Pulse 2 of M0	86
5.3	Summary of Response During Pulse 3 of M0	87
5.4	Summary of Response During Single DPD Pulse	88
5.5	Comparison of M0 and DPD Response	89
5.6	Available Section Curvature Ductility	90
5.7	Ductility Demands for the DPD Analysis	91

List of Figures

	FIGURE	PAGE NUMBER
Fig. 1.1	Plan of Prototype Structure	95
Fig. 1.2	Section of Prototype Structure	95
Fig. 2.1	Concrete Stress-Strain Curve	96
Fig. 2.2	Reinforcement Stress-Strain Curve	96
Fig. 2.3	Typical Beam Cross Section	97
Fig. 2.4	Typical Beam Elevation	97
Fig. 2.5	Moment-Curvature Relationship for Typical Beam	98
Fig. 2.6	Improved Detail for Typical Beam	98
Fig. 2.7	Typical Column Cross Section	99
Fig. 2.8	Moment-Curvature Relationships for Typical Column	99
Fig. 2.9	Axial Load-Moment Interaction Diagram for Typical Column	100
Fig. 2.10	Axial Load-Moment Controlled by Shear Strength Envelope for Typical Column	100
Fig. 2.11	Ductility Diagram for Typical Column	101
Fig. 2.12	Typical Column Tie Details	101
Fig. 2.13	Tie Requirements According to UBC	102
Fig. 2.14	Spacing of Ties to Prevent Buckling of Column Bars	103
Fig. 2.15	Improved Detail for Typical Column	104
Fig. 2.16	Typical Cross-Section of Shearwall	104
Fig. 2.17	Shearwall Moment-Curvature Diagram	104
Fig. 2.18	The Mechanism of Sliding Shear Failure	105
Fig. 2.19	Improved Shearwall Detail	105
Fig. 2.20	Improved Joint Detail	105
Fig. 2.21	Prototype Gravity Loading	106
Fig. 2.22	Reactive Mass and Lateral Load Distributions	106
Fig. 2.23	UBC Lateral Loads and Resulting Displacements	106
Fig. 2.24	Beam Moments from UBC Analysis	107
Fig. 2.25	Column Forces from UBC Analysis	107
Fig. 2.26	Beam Moments vs Beam Strengths from UBC Analysis	108
Fig. 2.27	Column Forces vs Column Strengths from UBC Analysis	109
Fig. 2.28	Assumed Plastic Hinge Pattern for Strength Analysis	109
Fig. 3.1	Model of Prototype used for Linear and Nonlinear Analysis	110
Fig. 3.2	Elastic Displacement Profiles for Component Frames	110
Fig. 3.3	Elastic Frame Interactive Forces	110

	FIGURE	PAGE NUMBER
Fig. 3.4	Displacement Superposition for Interaction	111
Fig. 3.5	Mode Shapes and Periods of Vibration	111
Fig. 4.1	ULARC3 Yield Surface for Beam-Columns	112
Fig. 4.2	ULARC3 Yield Surface for Beams	112
Fig. 4.3	Actual Yield Surface Used for Beam-Columns	113
Fig. 4.4	Actual Yield Surface Used for Beams	113
Fig. 4.5	Actual Yield Surface Used for Shearwall	114
Fig. 4.6	Element Strain Hardening Parameters	114
Fig. 4.7a	Force vs Displacement at Roof from ULARC3 Analysis	115
Fig. 4.7b	Force vs Displacement at Level One from ULARC3 Analysis	115
Fig. 4.8	Interactive Forces for Triangular Lateral Load from ULARC3 Analysis	116
Fig. 4.9	Interactive Forces for Uniform Lateral Load from ULARC3 Analysis	116
Fig. 4.10	Plastic Hinge Pattern for Triangular Lateral Loading	117
Fig. 4.11	Plastic Hinge Patterns for Uniform Lateral Loading	117
Fig. 4.12	Maximum Plastic Hinge Rotations as a Result of Triangular Lateral Loading	118
Fig. 4.13	Force vs Displacement Including P-Delta	118
Fig. 5.1	Incremental Equations of Motion	119
Fig. 5.2	Single Component Beam Model with Degrading Stiffness	120
Fig. 5.3	Modified Takeda Bi-Linear Moment-Rotation Diagram	120
Fig. 5.4	Yield Surface for Single Component Model	120
Fig. 5.5	Ground Acceleration Record for Miyagi-Oki Analysis	121
Fig. 5.6	Ground Acceleration Record for Derived Pacoima Dam Analysis	121
Fig. 5.7	Time-History of Top Story Displacement Resulting from Miyagi-Oki Ground Motion	122
Fig. 5.8	Time-History of First Story Displacement Resulting from Miyagi-Oki Ground Motion	122
Fig. 5.9	Time-History of Structure Base Shear Resulting from Miyagi-Oki Ground Motion	123
Fig. 5.10	Time-History of Frame A' Base Shear Resulting from Miyagi-Oki Ground Motion	123
Fig. 5.11	Time-History of Frame B Base Shear Resulting from Miyagi-Oki Ground Motion	124
Fig. 5.12	Time-History of Shearwall Base Shear Resulting from Miyagi-Oki Ground Motion	124
Fig. 5.13	Time-History of Shearwall Base Moment Resulting from Miyagi-Oki Ground Motion	125

FIGURE	TITLE	PAGE NUMBER
Fig. 5.14	Envelope of Maximum Lateral Displacements Resulting from Miyagi-Oki Ground Motion	125
Fig. 5.15	Envelope of Maximum Element Moments Resulting from Miyagi-Oki Ground Motion	126
Fig. 5.16	Envelope of Maximum Element Shears Resulting from Miyagi-Oki Ground Motion	126
Fig. 5.17	Envelope of Maximum Element Axial Forces Resulting from Miyagi-Oki Ground Motion	127
Fig. 5.18	Envelope of Maximum Beam Plastic Hinge Rotations Resulting from Miyagi-Oki Ground Motion	127
Fig. 5.19	Plastic Hinges Resulting from first part of Pulse One of Miyagi-Oki Ground Motion	128
Fig. 5.20	Plastic Hinges Resulting from Second Part of Pulse One of Miyagi-Oki Ground Motion	128
Fig. 5.21	Plastic Hinges Resulting from Pulse Two of Miyagi-Oki Ground Motion	129
Fig. 5.22	Plastic Hinges Resulting from Pulse Three of Miyagi-Oki Ground Motion	129
Fig. 5.23	Distribution of Base Shears Resulting from Pulse One of Miyagi-Oki Ground Motion	130
Fig. 5.24	Distribution of Base Shears Resulting from Pulse Two of Miyagi-Oki Ground Motion	130
Fig. 5.25	Distribution of Base Shears Resulting from Pulse Three of Miyagi-Oki Ground Motion	130
Fig. 5.26	Base Shear vs First Story Displacement Resulting from Pulse One of Miyagi-Oki Ground Motion	131
Fig. 5.27	Base Shear vs First Story Displacement Resulting from Pulse Two of Miyagi-Oki Ground Motion	131
Fig. 5.28	Base Shear vs First Story Displacement Resulting from Pulse Three of Miyagi-Oki Ground Motion	132
Fig. 5.29	Base Shear vs Roof Displacement Resulting from Pulse One of Miyagi-Oki Ground Motion	132
Fig. 5.30	Base Shear vs Roof Displacement Resulting from Pulse Two of Miyagi-Oki Ground Motion	133
Fig. 5.31	Base Shear vs Roof Displacement Resulting from Pulse Three of Miyagi-Oki Ground Motion	133
Fig. 5.32	Frame Interaction Forces Resulting from Pulse One of Miyagi-Oki Ground Motion	134
Fig. 5.33	Frame Interaction Forces Resulting from Pulse Two of Miyagi-Oki Ground Motion	135
Fig. 5.34	Frame Interaction Forces Resulting from Pulse Three of Miyagi-Oki Ground Motion	136
Fig. 5.35	Lateral Force Profile Time-History Resulting from Pulse One of Miyagi-Oki Ground Motion	137
Fig. 5.36	Lateral Force Profile Time-History Resulting from Pulse Two of Miyagi-Oki Ground Motion	137
Fig. 5.37	Lateral Force Profile Time-History Resulting From Pulse Three of Miyagi-Oki Ground Motion	137
Fig. 5.38	Time-History of Roof Displacement Resulting from Derived Pacoima Dam Ground Motion	138

	FIGURE TITLE	PAGE NUMBER
Fig. 5.39	Time History of First Story Displacement Resulting from Derived Pacoima Dam Ground Motion	138
Fig. 5.40	Time-History of Structure Base Shear Resulting from Derived Pacoima Dam Ground Motion	139
Fig. 5.41	Time-History of Frame A' Base Shear Resulting from Derived Pacoima Dam Ground Motion	139
Fig. 5.42	Time-History of Frame B Base Shear Resulting from Derived Pacoima Dam Ground Motion	140
Fig. 5.43	Time-History of Shearwall Base Shear Resulting from Derived Pacoima Dam Ground Motion	140
Fig. 5.44	Time-History of Shearwall Base Moment Resulting from Derived Pacoima Dam Ground Motion	141
Fig. 5.45	Envelope of Maximum Lateral Displacements Resulting from Derived Pacoima Dam Ground Motion	141
Fig. 5.46	Envelope of Maximum Element Moments Resulting from Derived Pacoima Dam Ground Motion	142
Fig. 5.47	Envelope of Maximum Element Shears Resulting from Derived Pacoima Dam Ground Motion	142
Fig. 5.48	Envelope of Maximum Element Axial Forces Resulting from Derived Pacoima Dam Ground Motion	143
Fig. 5.49	Plastic Hinge Patterns Resulting from First Part of Pulse One of Derived Pacoima Dam Ground Motion	143
Fig. 5.50	Plastic Hinge Patterns Resulting from Second Part of Pulse One of Derived Pacoima Dam Ground Motion	144
Fig. 5.51	Maximum Plastic Hinge Rotations Resulting From Derived Pacoima Dam Ground Motion	144
Fig. 5.52	Distribution of Base Shears Resulting from Pulse One of Derived Pacoima Dam Ground Motion	145
Fig. 5.53	Base Shear vs First Story Displacement Resulting from Pulse One of Derived Pacoima Dam Ground Motion	146
Fig. 5.54	Base Shear vs Roof Displacement Resulting from Pulse One of Derived Pacoima Dam Ground Motion	146
Fig. 5.55	Frame Interactive Forces Resulting from First Part of Pulse One of Derived Pacoima Dam Ground Motion	147
Fig. 5.56	Frame Interactive Forces Resulting from Second Part of Pulse One of Derived Pacoima Dam Ground Motion	148
Fig. 5.57	Lateral Force Profile Time History Resulting from Pulse One of Derived Pacoima Dam Ground Motion	149
Fig. 5.58	Relationship Between Plastic Hinge Rotation and Curvature Ductility	150
Fig. 6.1	Frame to Frame Flexural Coupling	151
Fig. 6.2	Model Including Coupling	152
Fig. 6.3	Model of Base of Table	152
Fig. 6.4	Method for Obtaining Improved Column Stiffness	153
Fig. 6.5	Method for Obtaining Improved Beam Stiffness	153
Fig. 6.6	Hysteresis for Typical Beam as Computed	154
Fig. 6.7	Hysteresis for Japanese 1/2 Scale Model	154

	FIGURE TITLE	PAGE NUMBER
Fig. 6.8	Lateral Load Distributions Affecting Wall Hinging	155
Fig. 6.9	Simple Shear Yielding Model	155
Fig. 6.10	Effect of Equilibrium Corrections on Response	156
Fig. 6.11	Multi-Component Model to Reduce Equilibrium Errors	157

CHAPTER 1

INTRODUCTION

1.0 Introduction

Due to the infrequent occurrence of major earthquakes, and the sparse instrumentation in place in currently existing buildings, earthquake engineers often require more information on the behavior of structures than can be supplied by field observations alone. Therefore, it is sometimes necessary to design research programs, which utilize physical and/or mathematical models, in order to obtain quantitative data on the response of structures which have been designed to absorb earthquake induced loadings. In general, these research programs involve both experimental and analytical techniques. Analytical procedures are used to predict or verify some aspect of the experimental response of the experimental model. Or, less often, experimental programs may be developed in which the reliability of a certain new analytical procedure is investigated. Several methods are currently in use for performing both experimental and analytical analyses of model structures. For example, physical models may represent the entire structure, or only a single component or subassembly, and these models may be either full-scale, or smaller. The loads may be applied statically, quasi-statically, pseudo-dynamically, or dynamically through the use of shaking tables or other such dynamic load inducing devices. For mathematical models, there are various types of finite elements to consider, and several ways to represent the force-deformation characteristics of the material.

In order to determine the relationship between some of the different experimental and analytical techniques used in earthquake engineering research, and for the further purpose of improving seismic resistant design procedures, an extensive research program has been developed in which earthquake engineers from both the United States and Japan are participating. In this research program, JAPAN-USA, several different physical models of the same prototype structure will be tested experimentally and analyzed using digital computers.[1] The results of these tests will be shared among all participants of the cooperative venture so that the nature of the different research techniques may be better understood and, therefore,

provide insight into how future experimental and analytical work might be more efficiently carried out.

A present phase of the project deals with the experimental investigation of the design and behavior of a seven-story reinforced concrete frame-wall system, which has been denominated the R/C Test Building. An Illustration of this structure, (henceforth, Prototype), is given in Figs. 1.1 and 1.2. This structure represents to some extent a common design for mid-rise apartment or office buildings, although a seven-story frame-wall system may be somewhat unusual since buildings with a similar configuration of walls and frames would likely be more than seven stories in height.

Several models of this R/C Test Building will be designed, constructed, and tested by research institutions in both the United States and Japan. In Japan, a full-scale model has been constructed, and has already undergone pseudo-dynamic tests.[2] In addition, the Japanese have built and tested several 1/2-scale models of components or subassemblages.[3] In the United States, at the Portland Cement Association, component tests are being carried out on the shear wall. At the University of Texas at Austin, tests are being performed on models of the beam-column joints. A small scale (1/10-scale) model is being developed for the shaking table at the University of Illinois. At the University of California at Berkeley, a 1/5-scale model will be tested on the earthquake simulator at Richmond Field Station.

In order to be able to plan the experimental work, and to study the correlation between experimental results and those obtained using present analytical techniques, extensive analytical investigations are being carried out on the prototype model to be tested at Berkeley. This report deals with some of these analytical investigations, having the following objectives.

1.1 Objectives

The main objectives of the work described in this report are as follows:

- 1) To review, and improve if necessary, the design of the reinforced concrete test building in which the seismic resistant structural system

consists of an interacting wall and moment resisting space frames.

2) To determine the reliability of predicting the seismic response of the test building through the use of available linear and nonlinear structural analysis computer programs, and to give recommendations for improved analysis, but within the constraints of using the currently available programs.

3) To produce the required analytical information to formulate a rational experimental program of studies on the 1/5-scale model, to determine the type and sequence of ground motions, and to design the required instrumentation.

4) To evaluate the implications of the results obtained regarding the seismic resistant design and construction of the R/C frame-wall structural system.

1.2 Scope and Layout of Report

In Chapter 2, an overall description of the Prototype is given, with a detailed analysis of the stiffness, strength, and ductility of the individual elements. The cross section analysis is discussed in terms of both the theoretical computations and the simplified techniques of the ACI [4] and UBC [5] building codes. The placement of the reinforcement is also discussed in terms of concrete confinement, longitudinal bar buckling, and anchorage. If necessary, improved details are presented. Finally, the ability of the Prototype to resist UBC lateral earthquake loading is investigated.

In Chapter 3, the results of a series of elastic analyses are described and the global flexibility of the structure is discussed in terms of its flexibility matrix. The theoretical periods of vibration and the associated mode shapes are also presented and compared to those (periods) obtained through the use of the simplified UBC equations.

The results of a series of static load to collapse analyses are presented in Chapter 4. Here, a particular distribution of lateral load is monotonically increased until a state of impending collapse is reached. The distribution of plastic hinges is explained, and will be used as reference for some of the material of Chapter 5. As in Chapter 3, a series of structural flexibility matrices will be presented, which if compared to the elastic matrices, will give an indication of the global damage due

to the formation of plastic hinges. Finally, the effects of gravity loading on the overall response (the P-Delta effect) is presented.

In Chapter 5, a detailed presentation of the results of two nonlinear dynamic analyses is given. The prototype was subjected to two very different earthquake ground motions, and the response is explained through the study of force and displacement time-history curves, as well as very detailed looks at the response to pulses contained within each earthquake.

The material presented in Chapters 3, 4, and 5 is discussed in Chapter 6, and any anomalies in the response are explained. Errors introduced due to assumptions made during the analysis will be used as a basis for recommendations for improved methods of analysis which incorporate existing computer programs but more intelligently utilize their options.

Finally, in Chapter 7, the results of the preceeding five chapters are summarized and general conclusions given. Also, specific recommendations are presented with respect to the proper sequence of ground motions that should be considered for the loading of the 1/5-scale model. The chapter ends with suggestions for future research.

CHAPTER 2

REVIEW OF PROTOTYPE DESIGN

2.0 Introduction

The prototype building is a seven-story, two by three bay reinforced concrete frame-wall structure. The primary structural system consists of two parallel moment resisting space frames on the exterior of the building (henceforth, Frames A and C), and one interior frame-wall (Frame B). The plan and elevation of the prototype structure are presented in Figs. 1.1 and 1.2, and a set of detailed drawings for the 1/5-scale model to be tested at Berkeley is given in Appendix A.

This structure would classify as a UBC type 3 structure (a dual bracing system consisting of a shear wall interacting with a ductile moment resisting space frame) only if it can be shown that the elements are detailed to behave in a ductile manner, that is, satisfy section 2626 of the same code. Also, UBC gives strict guidelines as to how the different components of the interacting frame-wall system should be designed to resist the lateral load, as shown in Table 2.1, which is part of Table 23-I of the Uniform Building Code.

Before any analysis could be carried out, several basic assumptions had to be made with regard to loading, mass, and stiffness of the prototype. These assumptions are as follows and are applicable for all the analysis, unless otherwise noted, which was carried out and described in this report:

- 1) The lateral loading, which results from earthquake induced inertial forces, occurs simultaneously with vertical gravity loads which consist of the weight of the structure itself, superimposed dead load such as partitions and mechanical equipment, and live load.
- 2) The reactive mass consists of the weight of the structure, plus all superimposed dead load. Live load is not included.
- 3) The earthquake ground motion has only a horizontal component, and that is parallel to the primary structural system consisting of Frames A, B, and C.
- 4) All references to the "code" are references to the 1979 edition of the Uniform Building Code.

5) For the UBC code checks, the structural analysis was based on uncracked section properties for all elements.

6) For non-UBC lateral load analysis, (Chapters 3, 4, and 5), the initial stiffness and damping properties correspond to those which might be measured after the structure had been subjected to a minor to moderate earthquake. Thus it is assumed that the majority of the beams and columns, as well as the shearwall, is significantly cracked.

2.1 Materials

At the time this analytical investigation started, there was very little data available on the characteristics of the materials that would be used in the prototype. What was available, was the concrete ultimate compressive stress, and some mill reports for some of the Japanese reinforcement. For the analysis, attempts were made to originate realistic stress-strain curves from this sparse data.

2.1.1 Concrete

The concrete to be used in the prototype was specified to have a 28-day cylinder strength of 3850 psi, and be made of normal weight aggregates and Type 1 Portland cement. In order to determine the moment-rotation characteristics of the beam and columns it was necessary to derive constitutive relations for both the confined and unconfined concrete. For both of these, the well known Park-Kent relationship for confined concrete was utilized [6]. In Fig. 2.1, the derived concrete stress-strain curves are illustrated.

For the beams, the concrete was not assumed to be confined, because the detailing of the steel in the compression zones at the face of the columns is not adequate to provide the necessary confining forces (according to UBC). For the columns, the confining steel, in general, is not adequate either, but special details which have been supplied for the bottom of the first-story columns do provide some confinement in those areas. The topic of confinement is discussed in more depth later when the beam, column, and shearwall details are analyzed.

2.1.2 Steel Reinforcement

From the Japanese mill reports on samples of D13 and D22 bars, the average yield

stress was 59.25 ksi, and the average breaking stress was 85.0 ksi. Note that this average yield stress is 18.5 percent greater than the specified value of 50 ksi. For the cross section analyses discussed in the next few paragraphs, all steel was assumed to have a yield stress of 60 ksi, and a breaking stress of 85 ksi. Strain hardening was assumed to commence at a strain of 0.03 in/in, and the initial strain hardening modulus was 441 ksi; however, it should be noted that these values are high and low, respectively, for American grade 60 steel. A cubic polynomial defines the stress-strain relationship in the strain hardening range. This derived constitutive relationship is shown in Fig. 2.2.

The bar types illustrated in the figures and in the following discussion are metric sizes, where for example a D19 bar is 19 mm in diameter. These metric bars have close counterparts in the United States, as illustrated in Table 2.2.

2.2 Cross Section Analysis

The strength, stiffness, and ductility of the beams, columns, and shearwall were derived through the use of the computer program RCCOLA [7]. This program uses a layer approach, in which the concrete within a layer may be either confined, unconfined, or both. The stress-strain relationships for the concrete and steel are directly specified. The program iterates on the equilibrium of internal forces throughout the cross section, and sets the convergence limit as one kip.

2.2.1 Beams

The typical beam cross section is given in Fig.2.3, and the beam profile is shown in Fig.2.4. These details represent all the beams of Frames A, B, and C. The layout of the principal beam reinforcement, as shown in Fig.2.4, satisfies all of the requirements of the code, including the requirement that the positive moment capacity at the face of the support be at least 50 percent of the negative moment capacity. For the determination of the negative moment strength, stiffness, and ductility of the sections of the beam near the face of the columns, the flange width which is assumed to be effective plays a very important role. For this analysis, a total width of 60 inches was used, which will result in an intermediate strength, much less than that which would be obtained if a center-to-center slab width (218 inches) was used. This full width could only be considered effective if the whole

beam-slab system is very ductile, thus all the slab steel could yield and contribute to the maximum strength.[8] For the determination of the positive moment strength, stiffness, and ductility, the same 60 inch slab was considered effective. In Chapter 6, discussion is presented on what affect these assumptions might have on the overall response of the structure to lateral loads.

The results of the RCCOLA analysis for the beams are given in Table 2.3 and in Fig.2.5. In the table, the flexural strengths of a typical beam are given and compared to the values obtained using the ACI analysis. (Note that the ACI capacity reduction factors have been ignored unless otherwise indicated.) The fact that the positive moment strengths from RCCOLA are larger than those following ACI can be attributed to the effects of strain hardening in the longitudinal reinforcement. The shear strength of the section, following ACI, is also given in the table. In Fig.2.5, a slightly simplified moment-average curvature relationship for each cross section type within the typical beam is presented. The moment curvature relationships are simplified by using the transformed cracked section moment of inertia to define the initial stiffness. This simplification is based on the assumption made at the start of the dynamic analysis, that the structure had already been subjected to a moderate earthquake prior to the time the major earthquake struck. As expected, the positive moment sections exhibit much more ductility than the negative moment sections, and the initial stiffness is somewhat greater. The positive moment sections have a larger strain hardening stiffness because of the greater steel strains developed in this section before the concrete in the compression zone crushes.

Since the shear strength of this beam, according to ACI, is 70.7 kips, the indications are that any failures which occur would be of a ductile flexural mode, assuming that the longitudinal bars do not buckle as a result of poor lateral restraint provided by the stirrup-ties.

An improved beam detail is shown in Fig. 2.6. In this detail, two changes have been made. First, all three of the bottom longitudinal reinforcing bars are extended into the supports. The extra bar lengths have been added to avoid cutoffs in tension zones, and to enhance the ductility of the negative moment sections at the face of the columns. Second, at the critical regions adjacent to the supports, special

supplementary cross ties have been added, so that the concrete will have better confinement properties, and the center longitudinal bar will have better lateral restraint against buckling.

2.3.2 Columns

The typical column section is illustrated in Fig.2.7. This section, except for the ties, represents all the columns of the building. The tie details for the columns vary throughout the structure, as will be explained later. The moment-average curvature relationships for the column at different levels of axial load are shown in Fig.2.8. The figure illustrates the typical increase of stiffness but decrease in ductility which is associated with columns subjected to increasing levels of compressive axial loads. The axial load-moment interaction diagram for the column is given in Fig.2.9. The figure shows two curves, one for a maximum concrete strain of 0.003 in/in, and another at a strain of 0.004 in/in. The fact that the latter curve exhibits lower strengths in the high axial load range is due to the assumption of concrete spalling at a strain of 0.0035 in/in.

In modern seismic design philosophy, one main objective is to provide a structure which will not collapse as a result of the infrequent major earthquake. If the structure is designed to resist strong ground motion it is very important to be sure that sudden brittle failures of the elements, especially the columns, are avoided. This can be achieved by supplying large ductility and particularly large energy dissipation to the structure. In the columns, two types of non-ductile failure; shear, and the combination of flexure with high axial load, are discussed with respect to the prototype.

In order to avoid shear failures, adequate tie details must be provided. These ties may be required to carry 100 percent of the shear force when the axial compressive stress in the column is less than $0.12f_c'$. The shear force to be resisted is as follows:

$$V_u = (1/L_c) \times 1.25 (M_a + M_b)$$

where L_c is the clear span of the column, and M_a and M_b are the ultimate strengths

of ends a and b of the column under some axial load N_u . The moments are multiplied by 1.25 to take into account strain hardening and the fact that the actual yield strength is likely somewhat greater than the nominal yield strength of the longitudinal reinforcement of the column. If the shear strength of the column can be estimated as the sum of the concrete shear strength and the strength of the ties in resisting diagonal tensile forces, an axial-moment controlled by shear strength envelope can be plotted on the axial load moment interaction curve for the column, as shown in Fig. 2.10. Since the shear envelope falls outside the interaction curve for all values of M and N, it can be assumed that a shear failure will not occur in this column.

In Fig. 2.11, the ductility of the column is plotted together with the moment-axial load interaction curve. This illustrates clearly that the ductility of this column is rather low (curvature ductility less than 4) for axial load levels greater than 150 kips in compression. The maximum axial load expected in any column for the prototype is about 300 kips (as obtained from static and dynamic inelastic analysis), which corresponds to a ductility of about 2. It is obvious then that large column inelastic deformations cannot be tolerated.

For the prototype, there are three different column tie details, as shown in Fig. 2.12. For all of the columns from the second story on up, the ties consist simply of a D10 square hoop, one located every four inches along the height of the structure. As can be seen from the figure, the hoops extend through the joint at the same 4 inch spacing. At the bottom third of the first-story column, and for the entire height of the shearwall boundary elements, the square ties are supplemented with cross ties, as shown in the figure.

In no case do these tie details satisfy UBC in terms of the requirements for confinement. In Fig. 2.13, the formulas given by UBC to determine the total area A_{sh} of rectangular hoop reinforcement are given. The results obtained through the use of the controlling equation are summarized in table shown in Fig. 2.14. As can be seen from the table, a hoop spacing of roughly 2-1/2 inches is required with the D10 hoops, or a spacing of 4 inches if the hoops are changed from D10 to D13 bars. Other options for hoop details and spacing are also given in the table.

Another function that the hoops perform is to prevent the longitudinal bars in the

column from buckling once the concrete has spalled away. Although the tie details given in the original design do satisfy the minimum spacing requirements for hoops (aside from confinement and shear strength considerations), it can be shown from rational analysis that the D22 longitudinal bars in the columns may well buckle if the cover is lost. In Fig. 2.14, computations are presented which show that a hoop spacing of about two inches would be required to prevent the buckling of the main column reinforcement if the ties are not properly touching the longitudinal reinforcement ($k=1$).

An improved column detail, which would satisfy the UBC requirements, is shown in Fig. 2.15. The significant change from the prototype detail is the reduction in spacing of the ties in the third of the column region adjacent to the joint from 4 inches, to 2-1/2 inches. Also, the cross tie detail shown is more effective in confining the concrete than is the present detail.

2.2.3 Shearwall

The shearwall, located in the center of the structure, is without doubt the dominant element in the building. The wall is of the bar-bell type where the boundary elements are of the same design as the typical column of Fig. 2.6 and Fig. 2.12c. The panel of the wall is 7.87 inches thick, and has D10 bars at 7.87 inches running both vertically and horizontally at each face of the panel. A cross sectional view of the wall is given in Fig. 2.16. Note that the panel reinforcement, which is 0.355 percent of the panel cross sectional area, easily satisfies the code minimum (0.250 percent).

Since the wall is centrally located, the axial loads it will develop will be due primarily to the effects of gravity loading. These levels of load which are accurately estimated with approximate analysis, were used as the datums for establishing the moment curvature relationships for sections of the wall. The results of the RCCOLA analysis of the wall, given in Fig. 2.17, show that the cracked stiffness of the typical section at the base of the building is 50 percent greater than at the top. The yield moment at the base of the wall ($N=740k$) is correspondingly 50 percent greater than at the top ($N=105k$). It is interesting to note that the stiffness of the cross section of the wall is 500 to 1000 times that of

the cross sections of the beams or columns, and has a flexural strength 75 times that of the beams that frame into it.

It is difficult to accurately determine the shear strength of a reinforced concrete shearwall. Components of shear in a cracked section will be carried by the horizontal and vertical panel reinforcement, by aggregate interlock, by dowell action of the vertical reinforcement, particularly those of the edge members, and by shear resistance of the uncracked concrete or diagonal compressive forces in the panel concrete. If the horizontal steel, together with a concrete strength of $3.3\sqrt{f'_c}$ in shear is considered, the strength of the wall is roughly 574 kips, of which 278 kips is from the concrete, and the remaining 296 kips is from the horizontal panel steel. In tests of a 1/2-scale model of the wall, the Japanese researchers reported a strength of about 350 kips.[2] In these tests, a three story segment of the wall was loaded with a single lateral load at the top, together with an axial load of roughly 550 kips.

It is interesting to note that there are different philosophies concerning the way the shear strength of the wall should be determined. For example, it has been recommended by Paulay that over the length of the plastic hinge, the contribution of all mechanisms to shear strength should be ignored, except that of the web reinforcement.[9] This seems to be a logical design procedure, since after a few cycles of inelastic deformation, there will be little concrete intact to carry the shear. However, Bertero has indicated that if the boundary elements are well confined with closely spaced ties, there may be a significant contribution to the overall shear strength of the wall since the vertical steel in the boundary elements will act as very effective dowell reinforcement.[10]

The failure mechanism of the wall not only depends on the geometry of the cross section, but also on the way the wall is loaded. If the wall is subjected to a large moment which produces yielding with low shear, the mechanism will be completely different than if loaded with low moment but large shear. The way the wall undergoes inelastic deformations will determine the path of force redistribution, and entirely dominate the subsequent response of the building. Also, the loading history will have a pronounced affect on the behavior of a shearwall since as a result of reversed cyclic loading and the residual plastic strains in the walls

flexural reinforcement, large continuous cracks may form, and the effectiveness of the horizontal web reinforcement will be reduced.[10] This may result in a sliding failure across the plastic hinge zones, as shown in Fig.2.18.

Finally, with regards to improvements for the shearwall details, see Fig. 2.19. Here, the only major change has been to alter the details of the boundary elements similarly to what was done for the columns.

2.3 Joints and Anchorage

The VBC has two requirements for the joints in ductile moment resisting space frames. First, in terms of the anchorage of bars of flexural members terminating in a column, the bars must extend into the opposite face of the column, and terminate in a standard 90 degree hook. This detail is satisfied for the majority of the exterior joints, the exception being some joints for the first floor level, where the hook is anchored only midway into the column. This detail apparently represents the Japanese practice, and would have been applicable for all of the exterior joints, except an agreement was made to change the detail and use the American practice. Since the first story of the Japanese model had been cast prior to the agreement, a few of these details remain. It is interesting to note that this inconsistent detailing has been carried through to the Berkeley 1/5-scale model, in order to obtain a maximum degree of similarity between the models.

First, in terms of anchorage for the D19 beam bars, the basic required development length is 18 inches for bottom bars, and 25.2 inches for top bars. The hooks can develop a stress of 27.92 ksi, and thus may be considered to contribute 11.71 inches to the total. The leading length of these bars is 12.94 inches, resulting in a total effective development length of $12.94 + 11.71 = 24.65$ inches, which is slightly less than required, but probably sufficient.

The second VBC requirement for joints has to do with the way the column ties are placed through the joint [VBC Section 2626(g)1]. Since the prototype tie details are not adequate initially, it is clear that the joint detail is also not adequate according to VBC. It should be noted, however, that since the present (exterior) joint maximum shear stress is only $4.35\sqrt{f'_c}$, the detailing is probably adequate. The fact that little confinement exists within the joint is disturbing however, so a new

joint detail for the exterior beam-column connections is proposed, as shown in Fig.2.20. This joint design follows the recommendation of the ACI-ASCE Committee 352 on joints in monolithic reinforced concrete structures.[11] Similar details should be designed for the interior joints, which are confined on all four faces by beams, and the corner joints at the top of the building.

2.4 Prototype Loading

For the analysis of the prototype, only the gravity loading and the earthquake loading are of importance. Wind loading will not be a factor. For the earthquake loading, only the equivalent lateral forces as given by UBC will be discussed in this chapter. The response of the prototype to actual ground motions is discussed in Chapter 5.

2.4.1 Gravity loading

The magnitude and distribution of gravity loading is very important in the non-linear analysis of frame-wall structures. Some of the reasons for this are as follows:

- 1) The pattern of plastic hinge formation depends on the initial state of the structure as subjected to gravity load alone. Those elements with the largest ratio of gravity moment to yield moment will hinge first when subjected to the seismic forces. The subsequent response of the structure will depend on the new stiffness, which is based on when and where the hinges form.
- 2) The accurate correlation between section moment-curvature and element hinge moment-rotation depends on the length of the plastic hinge, which in turn depends on the distribution of moments along the length of the member, and this can be affected significantly by the gravity load moments.
- 3) The initial stiffness of the columns and wall depends on the average level of axial load present in the element during the response. Since the load in the elements will oscillate about the gravity load level, this is a good datum for establishing the initial elastic stiffness.
- 4) Similar to the above consideration, the geometric stiffness of the axially loaded members depends on the initial level of gravity load in that element.

The only way to accurately establish the initial gravity load distribution is by doing a complex three-dimensional analysis of the floor system. In fact, this

analysis should be iterative, since the elements stiffness depends on the moments along the length of the section, and the moments along the length depend on the stiffnesses of the elements. At the end of the analysis the correct gravity load distribution is obtained, together with a good estimate of the element stiffness coefficients.

For the prototype , the analysis as decribed above was not carried out. Instead, an approximation of the distribution of gravity loading was obtained by visually estimating tributary areas. The resulting loads are given in Fig.2.21, which shows the tributary areas, and the loading on a typical beam element of Frame A or Frame B. Note that the live loads have been reduced as allowed by UBC. Also, distributed loads which were triangular or trapezoidal in shape, were simplified into uniformly distributed loads. This assumption has little effect on the fixed end moments in this case. The loads of Fig.2.21 were used to establish the fixed end forces which were required for the non-linear analysis presented in Chapters 4 and 5, and the UBC analysis discussed later on in this chapter.

2.4.2 Prototype Mass and Lateral Load

The reactive masses of Fig. 2.22a include all the dead load of the bare structure, as well as an additional 15 pounds per square foot reactive mass for partitions, ceiling, and mechanical equipment, or anything else that might be tied down. The 15 psf partition, which is less than the 20 psf as required by UBC, is used as a compromise value between Japanese and U.S. practice.[1] These translational masses were used as input for the evaluation of mode shapes and frequencies, in the nonlinear dynamic analysis, and for the evaluation of the equivalent lateral earthquake loading of UBC.

The Uniform Building Code assumes that the above mass will be effective primarily in the first mode of vibration of the structure. Using the UBC procedure for determining the effective lateral loads from the mass distribution results in the loading pattern given in Fig.2.22b. In this figure, the loads are given in terms of the as yet undetermined total base shear, V_{total} .

In order to determine the base shear, UBC gives the following formula:

$$V_{\text{total}} = Z I K S C W$$

The factors in the formula are defined below for the prototype.

Z = 1.0 for a building in "zone 4",

I = 1.0 for a non-essential facility,

K = 0.8 or 1.0 as described later,

S = 1.0 for good soil conditions,

C = $1.0 / 15\sqrt{T}$ where T is the first mode period of vibration, and

W = the weight of the total reactive mass of the building = 2501 kips.

As mentioned at the beginning of this chapter, Table 23-I of the Uniform Building Code gives certain requirements that a structure must satisfy in order to classify as a "ductile" moment resisting space frame. Since some of the details given in the original prototype design are inadequate, it must be assigned a **K** factor of 1.0. If the improved details are used, the **K** factor of 0.8 for ductile frames is applicable.

In order to determine the factor **C**, the fundamental period of vibration, T, must be known. UBC gives two equations for the determination of T. The first of these assumes the period is a function of only the building height and width, and has nothing to do with materials or framing system. This formula is:

$$T = 0.05h_n / \sqrt{D}$$

Where h_n and D are the building's height, and width in the direction of ground motion, respectively. Using this formula, the period of vibration is T=0.475 seconds.

The other method of the code is more accurate, as it assumes a first mode shape proportional to the lateral displacements induced by the UBC lateral loading. This mode shape is then used in a Rayleigh quotient in order to obtain the period of vibration. Using this method, a period of vibration of 0.45 seconds was obtained, which by coincidence, agrees well with the value determined from the simpler formula. With T and **K** known, the total base shear that the structure should be able to resist can be computed. Using **K**=1.0 (since strictly speaking, the frames of this building cannot be classified as "ductile"), and taking T as 0.475 seconds

(since the 0.45 seconds obtained from the Rayleigh analysis is a lower bound) the value of C is 0.0967, and the total base shear to be resisted is 242 kips.

2.5 UBC Lateral Load Analysis

In the following discussion, the prototype will be looked at in three ways. First, the results of an elastic lateral load analysis is presented, and the ability of the prototype to resist the forces developed is discussed. Second, a very simple ultimate strength analysis of the building is given, which estimates the relative strengths of the exterior and interior frames. Finally, the strength of the shearwall is discussed, in association with the requirement that it be able to resist the entire base shear as if it were acting alone.

2.5.1 Lateral Load Analysis

The prototype was subjected to a combination of UBC lateral load and gravity load where the dead load was increased by the factor 1.05, the live load was increased by the factor 1.275, and the lateral load was increased by the factor 1.4. This loading is consistent with the assumption that the frames are not "ductile", ie $K=1$. The applied lateral loading, together with the resulting lateral displacements are shown in Fig.2.23. For the analysis, it was assumed that all sections remained uncracked, that there was no out of plane interaction between frames, that the floor slabs acted as a diaphragm rigid in their own planes, and that the bases of the columns and shearwall were totally fixed. Also, the joints were assumed to be completely rigid. This model, except for the neglect of out-of-plane coupling, represents an upper bound on the stiffness of the bare frame and is the model that was used to determine the period of vibration via the Rayleigh analysis. With these assumptions, and the assumption that $K=1$, the base shear of 242 kips unfactored, or 338 kips factored, is also an upper bound. Of course, the lateral displacements shown in Fig.2.23 then represent a lower bound for displacements.

The forces developed in the frame members as a result of the lateral loading of Fig.2.23 are shown in Figs 2.24 and 2.25. In Fig 2.24, the beam moments (at the face of the supports) are written over the locations at which they occur. Positive values represent moments that produce tension in the bottom of the sections, and negative values produce tension in the top. Note that for Frames A and C, values are also

given for the maximum midspan moments.

Two things are immediately noticed in the figure. First, the negative moments adjacent to the shearwall in Frame B are the maximum that occur. Second, only in Frames A or C do large positive midspan moments occur (associated with locations of zero shear). The reason for this obviously has to do with the boundary conditions for these beams, those in Frame B having one support which is essentially rigid.

In Fig. 2.25, the moments, shears, and axial loads are given for all of the column elements. Here, there are two significant points to be made. First, none of the columns develop axial tension loading, and second, Frame B carries 95 percent of the total base shear.

The forces developed in the elements are compared to their capacities in Figs 2.26 and 2.27. Here, the comparison is made with the ACI strengths without the capacity reduction factors. In Fig 2.26, the ratios of actual moment to ACI strength are given for the moments at the face of the support for all the beams, and at midspan of the exterior bays of Frames A and C. Any value which exceeds 1.00 is over-stressed in relation to the ideal ACI strengths. Any factor which exceeds 0.9 is over-stressed with respect to the reduced strengths. Note that all values which exceed 0.9 have been circled on the figure. For Frame B, almost all of the negative moment sections are overstressed. Then it can be concluded that if the redistribution allowed by UBC and ACI is neglected, this structure is not correctly designed. If the maximum allowable redistribution of 20 percent is considered, however, the maximum factor in Fig. 2.26 reduces to 0.86, and the design of the prototype is acceptable. The actual amount of redistribution allowed for the beams in the prototype is 18.4 percent. Using this value, the maximum factor of Fig. 2.26 is 0.88, and the design, therefore, can be considered acceptable.

Recall from earlier discussion, that only a 60 inch effective flange width was assumed in the determination of the negative moment capacities of these over-stressed sections. Since the true strength of the sections will likely be greater than assumed, the fact that the beams are over stressed is not important. What is significant, is that these are the beams that will have the largest ductility demands, since they will be the first to form plastic hinges. Also, these are the

beams sections that have the lowest ductility available. It is for this reason, that these negative moment sections must be carefully detailed in order that these ductility demands can be achieved. Finally, for the beams, it should be noted that there is no danger of a brittle shear failure developing, since the maximum shear force developed (33.8 kips) is only 48 percent of the available strength (70.7 kips).

The actual column forces are compared to their strengths in Fig.2.27. Here, the axial-load moment pair for each column is shown by a dot in the column interaction diagram. It is clear that there is no danger of column failure (for well-detailed columns).

Finally, it should be noted that the shearwall easily resists its developed forces. The ratio of wall shear force to shear strength is 0.540, and the ratio of wall moment to flexural strength is 0.593. Later on in this chapter, the wall is investigated in terms of the requirement that it be able to resist the entire UBC base shear, as if it were acting alone.

2.5.2 Ultimate Strength of Prototype

One of the requirements that the UBC has for frames to classify as parts of a dual bracing system, is that they be able to resist 25 percent of the required lateral loads. See Table 2.1. In order to check out this requirement, a limit analysis was carried out. For this analysis, it was assumed that the plastic hinges follow an ideal elastic-perfectly plastic moment rotation relationship. The analysis was based on the plastic hinge pattern of Fig. 2.28 and the RCCOLA member strengths from Table 2.5. Note that this is the same hinge pattern as developed in the static load to collapse analysis of Chapter 4, and the dynamic analysis of Chapter 5. According to the above assumptions, the strength of each of the exterior frames is 136 kips, and the strength of the interior frame is 335 kips. The ratio of the total exterior frame strength, to the required lateral load is $272/338$ or 0.805. The requirements of the code, in this case, are easily satisfied. If the frames and walls have sufficient ductilities to develop the assumed plastic hinge pattern the maximum lateral resistance would be $272+335=607$ kips.

2.5.3 Strength of Wall Acting Alone

The last requirement that must be met by a structure so that it may classify as a dual bracing system ($K=0.8$) is that its shearwall must be able to resist the entire lateral load, as if it were acting alone. For the prototype, this requirement is not satisfied, as will now be shown.

In terms of shear strength, there is no problem with the prototype. The total base shear that must be resisted is 242 kips, times a load factor of 2.0 for shear, times the K factor of 0.8 or 387.2 kips. Recall that the strength of this wall in shear is 574 kips without the capacity reduction factor, or 488 kips with a reduction factor of 0.85.

For flexure, however, the strength requirements are not satisfied. The total base moment that must be resisted is 162400 inch-kips (resulting from the 242 kip total lateral load with a load factor = 1.4 and $K=0.8$), but the capacity (neglecting strain-hardening) is only 150000 inch-kips without the reduction factor of 0.90, or 135000 inch-kips with the factor. From this point of view then, the design does not satisfy the requirements of UBC. Another point that should be mentioned, is the fact that the 150000 in-k capacity of the wall was based in part on the contribution of panel reinforcement to flexural strength. UBC, however, states explicitly that only the reinforcement that is in the boundary elements should be considered in determining the flexural strength. If this is done, the flexural strength of the wall is only 57000 in-k, which is only 35 percent of the factored base moment equal to 162400 in-k as shown above.

At this point it is appropriate to mention that the UBC requirement that the panel reinforcement in the wall be ignored in computing flexural strength is a potentially dangerous requirement. If this panel reinforcement is ignored in these computations, the predicted flexural strength of the wall will be substantially less than the actual strength, as demonstrated above. Therefore, the shear forces that the wall will attract will be significantly greater than assumed, thus resulting in the possibility of a brittle shear failure occurring in the wall.

2.6 Discussion of UBC Analysis

The only major difficulty with the design of the prototype involves the tie details in the critical regions of the beams and the columns. If the improved tie details,

which were shown earlier, were used in lieu of the existing details, IC could be taken as 0.8, and the overstress in the beams would be marginal. However, according to UBC, the flexural capacity of the shearwall would be low. This should not be of concern for the following reasons:

- 1) The total lateral force was based on a lower bound period of vibration, thus itself is an upper bound.
- 2) The fact that the maximum nominal unit shear in all beams, columns, and wall is very low guarantees a good flexural yielding mechanism in these members.
- 3) The (well-detailed wall) should exhibit excellent ductility, and the frames can pick-up considerable force after the wall yields in flexure.

Aside from the detailing of the individual elements, another question that should be addressed is whether or not the conceptual design of the prototype itself is good. In order to answer this, two facts will be mentioned. First, in the elastic range, the exterior frames each carry only 2.5 percent of the total lateral load. Second, in the inelastic range, each exterior frame is capable of carrying a total 136 kips of lateral load. This would seem to be good design because, under moderate ground motions, most of the forces would be taken elastically by the shearwall. For more severe earthquakes, the exterior frames would dissipate a good amount of energy because the wall has sufficient ductility to allow the frames to develop their flexural mechanisms.

This can be looked at in another way, however. If the center frame-wall were replaced by a frame similar to the exterior frames, the strength of the structure would be 408 kips, much in excess of the required code lateral forces (which would be smaller in this case, since the structure is more flexible, weighs somewhat less, and would be classified as a ductile moment resisting space frame with $IC=0.67$). If it could be demonstrated that under moderate earthquakes this modified ductile space frame structure would respond somewhat elastically, remain serviceable, and stiffness and drift requirements were met, it might offer considerable advantages over the frame-wall structure, particularly from architectural and economic points of view.

Finally, this question should be asked : Why does the UBC allow a R_C factor of 0.67 for framed structures, but only allow a R_C of 0.8 for frame-wall structures? Apparently, UBC assumes that the shearwall type structure will not be able to develop the ductility that a framed structure would. Recent tests, however, have shown this not to be the case.[12,13]

which were shown earlier, were used in lieu of the existing details, RC could be taken as 0.8, and the overstress in the beams would be marginal. However, according to UBC, the flexural capacity of the shearwall would be low. This should not be of concern for the following reasons:

- 1) The total lateral force was based on a lower bound period of vibration, thus itself is an upper bound.
- 2) The fact that the maximum nominal unit shear in all beams, columns, and wall is very low guarantees a good flexural yielding mechanism in these members.
- 3) The (well-detailed wall) should exhibit excellent ductility, and the frames can pick-up considerable force after the wall yields in flexure.

Aside from the detailing of the individual elements, another question that should be addressed is whether or not the conceptual design of the prototype itself is good. In order to answer this, two facts will be mentioned. First, in the elastic range, the exterior frames each carry only 2.5 percent of the total lateral load. Second, in the inelastic range, each exterior frame is capable of carrying a total 136 kips of lateral load. This would seem to be good design because, under moderate ground motions, most of the forces would be taken elastically by the shearwall. For more severe earthquakes, the exterior frames would dissipate a good amount of energy because the wall has sufficient ductility to allow the frames to develop their flexural mechanisms.

This can be looked at in another way, however. If the center frame-wall were replaced by a frame similar to the exterior frames, the strength of the structure would be 408 kips, much in excess of the required code lateral forces (which would be smaller in this case, since the structure is more flexible, weighs somewhat less, and would be classified as a ductile moment resisting space frame with $RC=0.67$). If it could be demonstrated that under moderate earthquakes this modified ductile space frame structure would respond somewhat elastically, remain serviceable, and stiffness and drift requirements were met, it might offer considerable advantages over the frame-wall structure, particularly from architectural and economic points of view.

Finally, this question should be asked : Why does the UBC allow a **K**C factor of 0.67 for framed structures, but only allow a **K**C of 0.8 for frame-wall structures? Apparently, UBC assumes that the shearwall type structure will not be able to develop the ductility that a framed structure would. Recent tests, however, have shown this not to be the case.[12,13]

CHAPTER 3

ELASTIC PROPERTIES OF PROTOTYPE

3.0 Introduction

The prototype structure is somewhat typical of frame-wall systems in general, except for the fact that a real structure with a similar configuration of frames and walls would likely be taller than seven stories in height. The effect of frame-wall interaction has been well documented for tall buildings [14] yet little information is available for buildings as short as the prototype. For this reason, a series of analyses have been carried out in which the mechanisms of elastic frame-wall interaction for the prototype were investigated.

It is apparent from the size of the shearwall with respect to the size of the beams and columns in the frames that the shearwall will dominate the response of the structure to a given set of loads. In order to illustrate this, and for the further purpose of understanding the contribution of the exterior frames to the structural stiffness (flexibility) a series of structural flexibility matrices have been calculated. Flexibility matrices are used here instead of stiffness matrices because the coefficients in the flexibility matrix give a direct indication of the displacement response due to an arbitrary loading. In Chapter 4 a flexibility matrix will be presented for the structure with a plastic hinge at the base of the shearwall and this matrix will be compared to the matrix for the uncracked structure first presented in this chapter.

3.1 Description of Prototype Flexibility

The flexibility matrices for the prototype were obtained through use of the SAP-80 structural analysis program. All of the properties of Frames A and C (they are identical) were added to form a new frame, henceforth termed A', which is twice as stiff (and strong) as Frame A or C. In the analysis, rigid end zones were considered, but the effect of flexural coupling via the beams and slabs between Frame A' and Frame B were not. The effects of flexural coupling will be discussed in Chapter 6. An illustration of the assumed model is presented in Fig.3.1 showing

the general structural topology and the rigid end zones. The dashed lines between Frame A' and Frame B indicate that the lateral displacements of the two structures are slaved, thus approximating the effect of a diaphragm totally rigid in its own plane. Also, it is important to note that the structural properties and modeling used in this analysis were also used to model the elastic response component of the non-linear static and dynamic analyses as described in Chapters 4 and 5.

The elastic member properties used in the analysis are listed in Table 3.1. These properties correspond to cracked transformed section moments of inertia (see Section 2.0 of Chapter 2). Shear deformations were ignored.

In the analysis of the flexibility matrices, only the story lateral degrees of freedom are considered, thus each matrix is 7 by 7 in size. The matrices were evaluated by solving for the displacements at each story due to a 1000 kip lateral load, acting one story at a time. In the matrices of Table 3.2, for example, the first column represents the displacement profile of the structure due to a 1000 kip lateral force at level 7. The integer indices at the top of each matrix simply indicate the story level at which the unit force was applied. The integer indices along the right hand side indicate the story level at which the resulting displacement was measured.

The first matrix, for Frame A', shows clearly that the frame displaces primarily in a shear mode. Note that the displacement profile for a 1000 kip force at level 1 produces an almost constant displacement of about 3.9 inches above level 2, and that a 1000 kip force at level 2 produces an almost constant displacement above level 3. A similar pattern follows for the force at any level. If all the columns of the flexibility matrix are added together, the result is a displacement profile for Frame A' with a 1000 kip force at each level. This profile, which has been normalized to a maximum displacement of one inch, is shown in Fig.3.2-A. The result is typical of plane frames.

For Frame B, which includes the wall, a completely different type of flexibility matrix exists. In this case, a 1000 kip force at level 1 produces a linear increasing displacement profile above level 1. A similar pattern follows for a force at any one level. The displacement profile for Frame B with a uniform lateral load is given by the curve B in Fig.3.2. The ever so slight reverse curvature near the top of the

diagram is due to the influence of the beams and columns of Frame B. In Fig.3.2, the curve C is the displaced shape of the total structure due to the uniform lateral load. Note that it is almost identical in shape to the displaced shape for Frame B alone. This clearly indicates the dominance of the wall on the stiffness of the entire structure. A further indication of the dominating nature of the wall can be obtained by noting that although the global flexibility of the structure is much less than that of the wall, the form of the flexibility matrix is almost identical.

The elastic interactive forces between Frame A' and Frame B are shown in Fig.3.3, where the total structure was subjected to a uniform lateral load of magnitude 431.9 kips. This level of load is slightly less than the amount that would cause the first plastic hinge to form in one of the beams of Frame B. At this level of loading, the shearwall of Frame B is carrying 418 kips, which is 96 percent of the total amount.

There appear to be three major components involved in the elastic force distributions of Fig.3.3. First, the reverse load of 21.6 kips at the top of Frame B, second, the large force at level 6, and third, the large force at level one of Frame B. Equally as important are the counterparts of these forces acting on Frame A'. It is obvious from looking at Figs 3.2 and 3.3 that these interactive forces come from Frame B forcing Frame A to displace in a "cantilever mode." This is further illustrated by the superposition of forces shown in Fig.3.4. Here, Frame A' was first loaded with a single lateral load of 83.3 kips at level 7, and the resulting displacements calculated giving a maximum displacement of 2.4 inches. Next, a load of -21.9 kips was applied at level 6, and these increments of displacement added to those previously calculated, to obtain a maximum displacement of 1.8 inches. Note that at this point the displacements at levels 4 through 7 are very near the final values, but the displacements at level 1 through 3 are still rather bad. The application of the -40.2 kip force at level 1 corrects this, and the final displacement profile is very nearly approximated, with the maximum being 1.6 inches, compared to the exact value of 1.7 inches.

It is interesting to compare the flexibility matrix obtained analytically with that obtained by the Japanese during the testing of the full-scale model.[2] This experimental flexibility matrix, as shown in Table 3.3, is quite different from the

analytical matrix , mainly in terms of the size of the individual entries. This gives an indication that the use of transformed cracked section properties in the analysis represents a lower bound on the initial stiffness of the structure, and that the omission of frame to frame flexural-torsional coupling may be an important source of error.

3.2 Mode shapes and Frequencies

The elastic mode shapes and frequencies for the prototype were evaluated by the SAP-80 program. The elastic properties as described in Section 3.1 were used, together with the lumped story masses of Fig. 2.22. Only the first three frequencies were calculated. The results of this analysis are shown in Fig.3.5, which gives both the periods of vibration and the associated mode shapes.

The ratio of the first period to the second period of vibration is approximately equal to 4.5. The fact that this ratio differs somewhat from the usual ratio for framed buildings, $T_1 / T_2 = 3.0$, can be used as further evidence of the dominance of the shear wall on the response of the structure. This is explained as follows: Consider a structure with uniform mass and stiffness throughout its height. In one instance, assume the beams are all very rigid as compared to the columns. In this case, we have a shear building, where the ratio of T_1 to T_2 is 3.00. Next consider a building with very rigid columns as compared to the beams. In this case, we have a cantilever structure with the ratio of T_1 to T_2 equal to 6.3. Any real structure with uniform mass and stiffness should remain within these bounds. For the prototype structure, the wall is quite rigid as compared to the beams and columns, so a ratio of 4.5 should not be too surprising.

Recall from Chapter 2, Section 2.4.2, that the first mode period of vibration as calculated from the Rayleigh quotient was about 0.45 seconds, which is significantly less than that shown in Fig. 3.5 for the cracked structure. The reason for this, of course, is that in Chapter 2 the elastic properties of the structure were derived from the assumption that the sections remained uncracked. When the uncracked sections are considered in computing the periods, the values indicated also in Fig. 3.5 are obtained. The period for the first mode is very close (0.47 secs vs 0.45 secs) to that obtained in section 2.4.2.

CHAPTER 4

STRENGTH UNDER MONOTONICALLY INCREASING LATERAL LOAD

4.0 Introduction

In this chapter, the behavior of the structure as subjected to a monotonically increasing lateral load is discussed. The response is traced from first yielding all the way through to collapse. This static load to collapse analysis is important for several reasons. First, this analysis will be very useful as background information when the response of the structure to dynamic earthquake induced loading is presented. The inelastic response to earthquake loading is much more complicated than the inelastic response to a static load, since the effects of inertial forces and damping need not be considered in the static analysis. Also, the static analysis gives an indication of the way the individual frames share the lateral load and the way the total structure reacts to different load patterns, and thus to the general strength and stiffness of the individual frame components as yielding progresses throughout the response. Finally, the static analysis can serve as a check on the dynamic analysis. Any strange phenomena that occur in the (very uncertain) dynamic analysis that do not occur in the static analysis may lead to the source of any problems encountered with the dynamic analysis.

4.1 Static Load to Collapse Analysis

In order to carry out this analysis, the computer program ULARC was used, which was recently modified to include the effects of axial load-moment interaction yield surfaces for the columns, beam and column rigid end zones, slaved degrees of freedom, geometric stiffness for the columns, and uniform gravity load distribution for the beams.[15] A new modification enabling the use of (kinematic) strain-hardening, was made to the program, together with improved input-output options. This latest version of the program has been termed ULARC3, and a complete users manual has been prepared.[16]

ULARC3 works on an event-to-event basis, where an increment of load is added until a single plastic hinge is formed. After the formation of this hinge, the

structural stiffness matrix is re-formed, and a new load increment is applied so that another hinge will form. The analysis is continued until the maximum global displacement exceeds some input limiting value, or the number of iterations as specified by the user has been exceeded. The program assumes all elements have unlimited strength and ductility.

4.2 Element Yield Surfaces

ULARC3 provides a single yield surface type, which is for a general beam-column element. The input parameters for this element are illustrated in Fig.4.1. If a beam element is desired, the program will ignore the axial strength parameters and assume the simple yield surface of Fig.4.2.

The yield surfaces input for this static load to collapse analysis are shown in Figs. 4.3 thru 4.5 for the columns, beams, and wall respectively. Note that seven different strength parameters are given for the wall, each corresponding to the level of axial load present in the wall at the start of the analysis.

The elastic properties of the structure were exactly as given in Chapter 3 for the analysis of the flexibility matrices (see Table 3.1). However, since the elements may yield, strain hardening stiffnesses are also assigned. In Fig.4.6, the assumed bi-linear force-deformation relationships for the elements are illustrated, together with a table giving the assumed strain hardening stiffness as a percentage of the initial stiffness. In general, these strain hardening stiffnesses were taken as the slope of the strain hardening portion of the moment-curvature relationships of the sections as given in Chapter 2. For the beams, however, the strain hardening stiffness was taken as a weighted average for the positive and negative moment sections. The positive moment stiffness was given a greater weight in this computation since the positive moment inelastic deformations occur over a greater length of the beam than do the negative moment deformations.

4.3 Results of Collapse Analysis

In this section, the results of two different analyses are reported. The first is a static load to collapse with a monotonically increasing upper triangular "first mode" lateral loading. The second is similar to the first, except that a uniformly

distributed lateral load was used. In both cases, gravity loading was applied as the first load increment. In both of these analyses, the effect of geometric stiffness on the columns and wall were ignored. Later on in this chapter, another analysis is presented in which geometric stiffness is considered, and is compared to a similar analysis without geometric stiffness.

4.3.1 Force-Displacement Response

The response of the structure to the triangular and uniform lateral loads is illustrated by the force-displacement curves of Fig.4.7. The response is nearly linear up until the time the shearwall hinges, with the slight nonlinearity being due to the formation of plastic hinges in some of the beams of Frame B prior to the formation of the wall hinge. After the wall hinges (in a flexural manner), the structural stiffness decreases rather dramatically (by about 60 percent), and further losses of stiffness are due to flexural hinging of the remainder of the Frame A' and B beam elements.

The maximum shear force developed in the wall was 471 kips for the case of uniform loading. This is somewhat less than the capacity of the wall, which is about 574 kips according to the UEC. This indicates that a flexural yielding of the wall has to take place. For this reason it is important to determine whether the structure can supply the overall displacement ductility (ultimate displacement / yield displacement at first story) of about 12, as indicated in Fig 4.7b. It will be shown in Chapter 5 that this ductility can be supplied and is controlled by the ductility of the wall and the beam negative moment plastic hinges.

The fact that the structural overturning moment due to the triangular load is 50 percent larger than that of the uniform load (for the same total base shear) explains why the wall yields at a lower total lateral force for the triangular load. Also, the displacement increments for equal force increments are larger for the triangular loads, which explains why the initial stiffness for the triangular loading is less than it is for the uniform load. Finally, it can be deduced that the lower the resultant of the lateral forces, the higher the yield strength of the structure, and the higher the initial tangential stiffness in the V_B vs δ_y diagram.

The fact that the shear wall yields at a displacement of approximately 2.2 inches

for both load cases is an indication of the importance of frame-wall interaction, and the dominance of the wall on the behavior of the total structure. In order to illustrate this, the story shear forces for Frames A', B and the total structure are plotted along the height of the structure before and after the wall hinge forms. These forces are given in Figs. 4.8 and 4.9 for the triangular and uniform load cases respectively. The first thing that is noticed from the figures is that the frame interactive force distributions do not change significantly after the wall hinges. The large interactive force at the top, and the rather large reverse interactive force at the bottom of Frame A' remains almost constant. Note also, that the distribution of interactive forces is very similar for the triangular load and the rectangular loading, indicating that the interactive forces between Frames A' and B develop almost independent of the loading pattern. As expected, Frame A' picks up a larger percentage of the total force after the wall hinges, and this percentage increases as more and more plastic hinges form in the beams of Frame B.

Since the wall hinges when the global displacement at the top story is about 2.2 inches, and since the distribution of interactive forces is almost the same for both load cases, except that for uniform loading the frames resist a little larger portion of the total shear, it can be concluded that Frame B, most particularly the shearwall of Frame B, completely dominates the elastic and inelastic response of this structure. It is apparent that the modeling of the wall, not only in terms of its stiffness and strength, but also in terms of the type of failure mechanism that develops, is of fundamental importance in predicting the response of the entire structure to static or dynamic loads.

4.3.2 Plastic Hinge Formation

The sequence of plastic hinge formations is given in Figs 4.10 and 4.11 for the two load cases. The hinge patterns are almost identical. The most significant difference is that the wall hinge forms slightly sooner (with respect to when the other hinges form) for the rectangular load than it does for the triangular load. This is consistent with the fact that the total lateral load at the time the hinge forms is somewhat greater than for the triangular load.

The distribution of plastic hinges will be explained with reference to Fig. 4.10. The hinges form in groups, with the groups usually representing either the hinges at the left end, or the right end of nearly all the beams of a particular bay. The first group of hinges to form is located at the right ends of the beams of Frame B. These ends of the beams are in an initial state of negative moment (tension in the top fibers of the beams), and the lateral loading increases negative moment. The hinges that form first are adjacent to the shear wall. Since the wall is so rigid as compared to the beams, the negative moment here under gravity loading will be larger than anywhere else in the structure. This, in combination with the fact that the rotation of the beam-wall joints are larger than the rotations of the beam-column joints, explains why these hinges form first. Then the hinges form in the right ends of the beams in the right hand bay of Frame B for similar reasons, except that here, large carry-over moments from the left ends of the beams are responsible for the negative moment increments at the right end of the beam. The next major group of hinges to form include the left ends of the beams of Frame A'. The center bay beams hinge first under positive moment since the span is smaller and the effect of gravity loading is less. Also, recall that the positive yield moment for these beams is roughly equal to one-half the negative moment capacity. The remaining hinges form somewhat randomly through Frame A', and then Frame B. Note that the hinges that form last are those at the base of the columns of the structure (with the exception of the lower right hand column of Frame A', which hinges 65th). This is a desirable result, indicating that a sidesway failure mode will occur only after all of the beams have hinged. In Fig 4.12, the maximum plastic hinge rotations resulting from the triangular loading are illustrated.

4.4 Effect of Wall Hinging on Structure

Once the shearwall hinges, the stiffness or flexibility of the structure undergoes a dramatic change. This fact is illustrated through the use of structural flexibility matrices, computed before and after the wall yields. These matrices, which are given in Table 4.1, are not only different from the point of view of their norm, but also by the form of the individual rows and columns.

By adding all the elements in the top row of either matrix, the displacement at the roof of the building due to a uniform lateral load is obtained. The stiffness of the

building after the hinge forms is 40 percent of that before. This is completely consistent with the results shown in the right hand side of Fig.4.9, which shows K_T going from 236 kips/in to 91 kips/inch.

4.5 Analysis of the P-Delta effect

In order to study the P-Delta effect, a ULARC3 analysis was made in which the geometric stiffness of the columns and shearwall was included. The loading was gravity plus a uniform lateral load. The response of the structure including P-Delta is compared to that without P-Delta in Fig.4.13. As can be observed, the only effect was a slight reduction in overall stiffness. The maximum displacements for each analysis are nearly the same, but the ultimate load for no P-Delta is about 5 percent more. The conclusion here is that the errors introduced by leaving out P-Delta are insignificant with respect to the overall response of the structure.

CHAPTER 5

RESPONSE OF PROTOTYPE TO EARTHQUAKE LOADING

5.0 Introduction

In this chapter, the response of the prototype to two different ground motions is presented and discussed. The goals of this analysis are as follows:

- 1) Obtain a basic understanding of the inelastic behavior of the prototype as it responds to major ground excitations.
- 2) Determine the sequence and magnitude of ground motions to be used in the 1/5-scale model shaking table tests, and gather data on the magnitude of forces, displacements, rotations, and accelerations that will occur, such that instrumentation for the 1/5-scale model may be properly designed.

5.1 Nonlinear Analysis Using DRAIN-2D

Before discussing in detail the response of the Prototype to two different ground motions, it is important to describe the basic tool used in performing this analysis. The computer program used for this work has been the nonlinear dynamic analysis program DRAIN-2D, developed at Berkeley by Kaaran and Powell [17]. This program is designed to perform a time-history response analysis of an arbitrary planar structure to an earthquake ground motion.

The structure is idealized as an assemblage of beams, columns, and rigid joints, all positioned in the same plane. The effects of finite dimensional joints and simple nodal constraints may be considered. The basic source of the nonlinearity is in the behavior of the elements, which are assumed to follow a bi-linear force deformation relationship. Throughout the analysis, equilibrium is based on the initial configuration of the nodes, thus large displacement effects are ignored. It is possible, however, to include a linearized geometric stiffness in order to approximate any P -delta effects due to large lateral displacements. The basic analysis procedures, together with a description of the local element modeling will now be given.

5.1.1 Step-by-Step Analysis Procedure

DRAIN carries out a step-by-step analysis of the structure through the use of the Newmark constant average acceleration integration scheme. In this method, the acceleration during a particular time step is assumed to remain constant, therefore, the velocity varies linearly and the displacements vary quadratically. The formulation of the incremental equations of motion is given in Figure 5.1. Note that the dynamic problem is transformed into a series of static problems. In these equations, the mass matrix, \mathbf{M} , is strictly diagonal (zero entries possible), and the damping matrix, \mathbf{C} , is assumed proportional to the mass and the tangential stiffness matrix, \mathbf{K}_t . It is possible to base the damping on the initial stiffness matrix as well, but this was not done in the present analysis. The constant average acceleration scheme is known to be unconditionally stable for linear problems, yet it has been shown that the procedure may become unstable for nonlinear problems.[18]

If all of the elements in the structure remain elastic during a particular timestep, the incremental displacements, velocities, and accelerations computed by the step-by-step procedure will be very accurate, thus equilibrium will be very nearly satisfied at the end of the timestep. If, on the other hand, one or more elements do yield during the timestep, the incremental displacements calculated at the end of the timestep will be underestimated since the structural stiffness is greater at the start of the timestep than it is at the end. Since the incremental velocities and accelerations, which are derived from the incorrect displacements, will also be incorrect, the equilibrium at the end of the timestep will not be satisfied. If these errors are not corrected, the computed response will soon diverge from the true response. The DRAIN program uses a "modified forces" procedure to approximately correct the equilibrium errors.[19] The incorrect displacement increment is assumed to be the true displacement, and the equilibrium is "satisfied" by adding a corrective force to the load vector during the subsequent timestep. This corrective load is present only for the duration of the timestep in which it is applied.

5.1.2 Element Properties and Behavior

Of the several elements available from DRAIN, only two different element types were utilized. For all of the columns in the structure, the two component beam-column element was used. This element, which yields on the basis of a moment-axial load interaction yield surface, is in all ways similar to that used by the program ULARC3, as described in detail in Chapter 4 of this report. Refer again to Fig.4.1 for an illustration of the two-component model and it's associated yield surface.

For all of the (horizontal) beam elements and for the shearwall, a degrading stiffness single component model was used. In this model, all of the inelastic action is assumed to occur in concentrated rotational springs, one located at each end of the element. The center portion of the beam has the stiffness property of the beam as if it were considered to be linear elastic. In this model, the moment-rotation relation of the concentrated inelastic rotational spring follows a set of degrading stiffness rules similar to those first established by Takeda at Illinois [20]. In this case, however, the spring stiffness is assumed to be only bi-linear, whereas in the original Takeda model, the stiffness was tri-linear. In this bi-linear degrading stiffness model, the yielding is a function of the moment in the hinge only, and is completeley independent of the level of axial load present in the element. Figures 5.2 through 5.4 illustrate the one-component model, the Takeda hysteretic model, and the yield surface respectively.

It is apparent from the moment-curvature relationships of the shearwall (see Fig. 2.17) that the level of axial load in the wall has a significant effect on the stiffness and flexural yield strength of the element. In order to use the degrading stiffness beam element for the wall, it had to be assumed that the axial load in the wall remained relatively constant throughout the response. This assumption is very accurate for the prototype, since the wall is centrally located in the structure and since the axial stiffness of the columns does not change (due to DRAIN modeling procedures). Note, however, that in the real structure, neutral axis migration might occur in the wall, thus removing the symmetry of the structure and causing the axial load levels in the wall to vary throughout the response.

5.2 Properties of the Analytical Model

For the nonlinear dynamic analysis, the stiffness and strength properties of the elements, the gravity loading, and the structural topology, were exactly the same as used in the static load to collapse analysis of Chapter 4. The reactive mass is the same as given for the UBC analysis of Chapter 2. These properties will not be repeated here. Note that the effects of geometric stiffness in the columns, and shear deformations in all of the elements were ignored in this analysis. Also, as in the ULARC3 analysis, the effect of out of plane frame to frame flexural-torsional coupling, via the slab-beam floor system connecting Frames A and C to Frame B, was not included.

5.2.1 Damping

As mentioned earlier, the equivalent viscous damping was assumed to be proportional to the mass and tangential stiffness:

$$C(t) = a * M + b * K_t(t)$$

where in this analysis,

$$a = 1.49 \quad \text{and} \quad b = 0.00094$$

With these values of a and b , an average of 6 percent damping was provided in the first three modes. (Only as long as the structure remains elastic, since changes in K_t will cause changes in C)

5.3 Selection of Time-Step

The time-step used in the DRAIN analysis of the Prototype to both ground excitations was 0.01 seconds. To check the accuracy of this timestep, a short 2 second analysis was made of the structure subjected to seconds 2 through 4 of the Miyagi-Okai earthquake (to be described later). For this analysis, a timestep of 0.02 was used, and compared to the results from a similar analysis with the 0.01 second timestep. These two analyses showed very little difference in terms of displacements, but the forces differed in some cases by as much as 5 percent. Another short analysis with a time-step of 0.005 seconds should be carried out, but

the results of such an analysis would likely produce similar displacements but slightly different forces. In any event, the fact that the forces do not "match up" as well as displacements should be expected since the forces are derived from the displacements, and any errors contained in the displacements will be amplified in the resulting forces.

5.4 Introduction to the Results

In this analysis, the basic assumption was that the prototype structure had already been subjected to some minor serviceability earthquake prior to the time the major earthquake struck. For this reason, all of the element properties described in previous discussion correspond to the cracked transformed section properties. The gravity loading includes structural dead weight, superimposed dead load such as partitions and mechanical equipment, and reduced live load. For the mass, the structural dead weight plus the superimposed dead load was included, but live load was not.

It is very important to note here that in no way should the response of the analytical model be construed to be the same as the response of the actual prototype structure to the actual earthquake ground motion. The response of the model is only as good as the assumptions made when creating the model, and is very sensitive to other parameters such as the length of the timestep, the equilibrium correction procedure, and the roundoff and truncation occurring in the computer during the solution of the incremental equilibrium equations. Hopefully, however, this analytical response will give a clear indication of the type behavior that can be expected from the real structure.

In the analysis, two very different earthquake ground motions are considered. The first record used was the first 12 seconds of the Japanese Miyagi-Oki [MO] earthquake, which was normalized to a maximum acceleration of 0.36 g. A time-history of this ground motion is given in Fig. 5.5. This ground motion, supplied by the Japanese, seems to have been filtered somehow since there is a conspicuous absence of the jagged peaks that are typical of earthquake records.

The second ground motion used was the first 4 seconds of the "Derived" Pacoima Dam earthquake record [DPD]. This record was normalized to a maximum

acceleration of 0.40 g, as shown in Fig. 5.6. The DPD earthquake has some very long pulses associated with it, in particular one that starts at time 3.04 seconds and reaches its peak acceleration of 0.4 g at 3.28 seconds. For comparison, the incremental velocities of the DPD record are approximately 1.5 times those of the maximum occurring in the MO record. It can, therefore, be expected that although the maximum acceleration for DPD is only 11 percent greater than that of MO, the displacements produced by DPD may be relatively much greater. This is confirmed later.

5.4.1 Organization of the Results

For each earthquake, two different types of analysis of the results have been carried out. First, the overall response of the prototype to the particular ground motion is studied. This analysis includes time-history plots of the entire response, diagrams showing envelope values of element forces and deformations and nodal displacements. This analysis attempts to quantify the response over the entire time period considered.

The second type of analysis involved a detailed investigation of the response of the structure to a particular pulse within the entire response. For the DPD analysis, this pulse lasts from time 2.4 to 4.0 seconds. For MO, three pulses are studied, 2.4 to 3.6 seconds, 7.0 to 8.2 seconds, and finally 10.4 to 11.6 seconds. In each of the three pulses for MO, and in the single pulse of DPD, significant inelastic response occurs. In doing this analysis, five types of plots were produced for every fourth time step within the pulse. These are as follows:

- 1) A table summarizing the significant aspects of the response to the pulse.
- 2) A profile of the lateral displacements showing the lateral displacement at each story and the contribution of the shearwall plastic hinge rotation to the overall displacements.
- 3) Plots of the story shear forces and the story overturning moments for the total structure and the individual contributions of Frame A', Frame B, and the shearwall to the total.
- 4) Plots showing the "inertial forces" acting at each story of each frame component. These inertial forces are actually the concentrated lateral loads acting at each story that would produce the shears and moments

shown in the plots of (3) above, if these forces were applied statically.

5) Diagrams giving a time history of the way the plastic hinges progress through the structure during the pulse. Different symbols in the plot represent plastic hinges that are either new, loading, or unloading.

These plots, however, are not included within the body of this report. They have been bound separately and can be obtained from the author.[21] After all of the data has been presented and discussed for each earthquake, the responses will be compared and the important differences analyzed with respect to the overall goals given at the start of this chapter.

5.5 Prototype Response to Miyagi-Oki

5.5.1 Discussion of Overall Response

The overall response of the prototype to the Miyagi-Oki ground motion is given by the time history plots of Figures 5.7 through 5.13, and the maximum response envelope diagrams of Figures 5.14 through 5.17. The maximum lateral displacements (at level 7) are 6.36 inches at time equals 7.45 seconds, and -7.03 inches at time equals 10.87 inches. From Fig. 5.14, it can be seen that the maximum positive or negative displacements at each level occur practically at the same time, thus the diagram showing the displacement envelopes also represents the actual displacement profile of the structure at the given time. Note that the displaced shape of the structure is essentially linear above the second story, in fact the inter-story drift indices above the second story remain almost constant. It can be concluded, therefore, that when displacements are at their maximum, the "rigid body" rotation of the shearwall, which has hinged at it's base, is controlling the displaced shape of the structure.

The maximum shear force developed in the structure is 770 kips and occurred at time equals 3.14 seconds. At this time, 23 percent of the shear is taken by Frame A', and the remaining 77 percent is taken by Frame B, which includes the shearwall. The shearwall itself absorbs 547 kips at this time, which is 71 percent of the total, and 93 percent of the shear in Frame B. Recall again, that the strength of the wall in shear, according to UBC, is about 574 kips. This indicates that the wall may actually yield either in flexure or in shear. Also, the maximum base shear of 547 kips in the wall results in a unit nominal shear stress of about 401 psi or $6.46\sqrt{f'_c}$

which can be considered enough to start some deterioration in its hysteretic behavior.

The maximum shears and moments developed in the beam elements are simply the result of the beams hinging at each end since the strain hardening stiffness assigned to these elements was rather low. However, the beams in Frame B have slightly higher shear forces than those in Frame A', because the rotations developed in Frame B are larger than those in Frame A'. The maximum shear recorded in any beam was 27.22 kips, resulting in a unit nominal shear stress of about 115 psi, or only $1.86\sqrt{f_c'}$, which is sufficiently low to guarantee good hysteretic behavior. Figure 5.18 illustrates the maximum rotations developed in each plastic hinge.

The column axial force envelopes show that at no time do the columns have tension loading (note that the minimum compressive loads for the first story columns are given in Fig. 5.17) Recall that when determining the beam strengths, only a 60 inch flange width was assumed, thus the strengths could be considered as lower bounds. It would take a flange width of approximately 120 inches in the beams to cause the exterior columns of the frames to be loaded in tension, assuming of course, that these new stiffer and stronger beams yield at both ends.

The axial force levels in the shearwall remained almost constant throughout the response, thus validating the assumption made when assigning the wall elements to be of the degrading stiffness type. (See Chapter 2, Section 2.2.3)

5.5.2 Analysis of Response to 3 Pulses

In each of the three pulses studied, the response is split into two parts. The first part includes the response of the structure to a negative incremental velocity, thus causing "positive" displacements and forces to occur along the height of the structure. The second part of the pulse is just the opposite, that is the structure is responding to a positive incremental velocity, and produces "negative" displacements and forces. The signs of the forces are of course relative, and in this discussion, positive is taken as from left to right.

5.5.2.1 Pulse One (MO1)

The first pulse studied lasts from time equals 2.4 to 3.6 seconds (see Fig.5.7) and includes the first yielding of the structure. A summary of the important response parameters is given in Table 5.1. In the first part of the pulse, the structure is responding to an incremental velocity of approx. -19.9 in/sec, and a maximum ground acceleration of 0.209 g. During this first part of the pulse, the structure yields for the first time, and the inelastic behavior is limited to two beams of Frame B, and the base of the shearwall, as shown in Fig.5.19. This is very minor yielding as compared to what happens in the second part of the pulse, where there is very extensive yielding throughout the entire structure. See Fig. 5.20. In Figs 5.19 and 5.20 the number assigned to the black dot representing the plastic hinge indicates when that hinge formed relative to the others. For example, in both cases the wall hinge forms first, thus this is indicated by the number 1 next to the hinge. (Note that for the dynamic analysis, several hinges form during the same time step, so it is not possible to exactly follow the hinge progression as done for the static analysis. Therefore, the hinge progressions of Fig. 5.19 and 5.20 are not true progressions, but still give the general tendency of progression and show the extent of damage at the end of a pulse.) Recall that an entire time-history of the yielding is given in the separate volume of plots and tables.[21] This progression of plastic hinges is discussed later, in conjunction with similar figures for the other two pulses. Note that in the second part of the pulse, the response is due to an incremental velocity of 30.6 in/sec, and a maximum acceleration of 0.251 g.

The maximum base shear developed in the structure during the entire response is 767 kips, and occurs at time equals 3.12 seconds, during the second part of the pulse. The shear of 547 kips in the base of the shearwall is also a maximum for the entire response.

5.5.2.2 Pulse Two (MO2)

In the second pulse studied, which lasts from time equals 7.0 to 8.2 seconds, the incremental velocity for the first part of the pulse is -34.8 in/sec, and the associated acceleration is -.24 g. In the second part of the pulse, the incremental velocity is only 25.9 in/sec, but the associated acceleration is 0.36 g, which is the maximum value for the ground motion used. In Table 5.2, the response values are summarized.

For this second pulse, yielding was associated only with the positive displacements, which were the maximum recorded in the response. This yielding, as shown in Fig. 5.21, is even more extensive than that of the first pulse, with hinges forming at each end of almost every beam in the structure. Note that the only portion of the structure remaining elastic are the roof beams and columns of Frame A'.

At this point it is interesting to note that the pulse which is associated with the peak acceleration of 0.36 g is not effective in producing any yielding in the structure. The yielding which takes place during pulse 2 can be attributed mainly to the first part of the pulse, which has a peak acceleration of only 0.24 g, but an incremental velocity 34 percent greater than that associated with the 0.36 g portion.

The roof displacement of 6.35 inches, which occurs at time equals 7.44 seconds, is the largest positive displacement occurring during the entire response. Associated with this large displacement are relatively large overturning moments for each component of the structure, the total being 378,000 inch kips. The base shears developed in the structure at time 7.28 seconds are only 84 percent of the maximum value observed in the first pulse.

5.5.2.3 Pulse Three (MO3)

The third pulse studied lasts from time equals 10.4 to 11.6 seconds, and is different from the other two pulses, because the negative response occurs prior to the positive response. In pulse three, the first part of the pulse has an incremental velocity of 35.4 in/sec and an acceleration of 0.334 g, while the second part of the pulse has an incremental velocity of only 25.4 in/sec, and an acceleration of 0.285 g. Table 5.3 lists a summary of the response of the prototype to this pulse.

The third pulse is similar to the second pulse in that there is only one yield excursion, this time associated with the first part of the pulse, corresponding to the positive accelerations. The extent of yielding is given in Fig. 5.22. In this case, the behavior is very similar to that occurring during pulse two.

The maximum negative displacement of 7.03 inches, which occurs at time equals 10.87 seconds, is in magnitude the largest displacement recorded in the analysis. Associated with these displacements, are the largest overturning moments of 382,000 in-k, which also occurs at time equals 10.87 seconds. The maximum base shear recorded during pulse three is 644 kips, and is 84 percent of the maximum which occurs during pulse one.

5.5.2.4 Discussion of MO Response

For each of the three pulses, it is the shearwall that hinges first, followed by the beams of Frame B, and then the beams of Frame A'. This hinging pattern is very similar to that derived from the ULARC3 analysis of Chapter 4, except for the fact that in the ULARC3 analysis, the wall did not hinge first. This hinging progression is mainly a function of the rigid body rotation of the shearwall, as explained in section 4.2.2 of Chapter 4. It is not entirely clear why the wall hinges at different relative times for the dynamic analysis than it does for the static analysis. The trend from the static analysis was that the lower the location of the resultant of the applied lateral forces, the sooner the formation of the wall hinge. For the three pulses studied here, the resultant of the "inertial forces" was always between that of a (UBC) triangular load and a uniform load, thus indicating that the wall hinge should have formed seventh or eighth (as compared to the ULARC3 analysis). Such comparisons are difficult to justify, however, due to the extreme complexity of the dynamic interaction between wall and frames.

This dynamic interaction just described is very interesting, so it is now discussed in detail. In Figures 5.23 through 5.25, a distribution of the base shears developed in Frame A', Frame B, the shearwall, and the total structure, is plotted as a function of time, for the three pulses respectively. At the bottom of the figures, the ground accelerations and the lateral displacement at the first story are also plotted against time, except here the curves are normalized so that they have a maximum value of 1.0 during the pulse. From these figures, two things are immediately noticed. First, the shears in Frame B and the wall are always dominant, and second, the shear in Frame A' is almost proportional to the lateral displacements at the first story. The fact that the shears in Frame B are so large has been well documented, so this will not be pursued further, but it should be

noted that while the structure remains elastic Frame B takes about 95 percent of the shear. Only when the wall yields does Frame A' begin to absorb more shear, up to a maximum of about 23 percent. The proportionality of the forces and first story displacements in Frame A' is quite remarkable, considering the fact that almost all of the beams in Frame A' have hinged in each case.

In order to get a clearer picture of the proportionality phenomenon, the time variable has been eliminated by plotting the base shear in the various frame components versus the first story lateral displacements, as shown in Figs. 5.26 to 5.28. In each case the shear in Frame A' is essentially linear, and causes a rotation of the force-displacement diagram for the total structure. An entirely different picture of the frame-wall interaction is obtained if the base shears are plotted versus the roof displacements, as in Figs 5.29 thru 5.31. Here the force-displacement relationship for Frame A' is no longer linear, and while the loop for the total structure proceeds in a clockwise manner, the loop for Frame A' is counterclockwise.

The reverse loops for Frame A' as displayed in Figs 5.29 to 5.31 are difficult to explain since they may be due to several effects, all coupled through the inelastic frame-wall interaction. One explanation for the reverse loops is that the relative stiffness of Frame A' increases with each cycle of inelastic deformation. This increase is due to the fact that DRAIN assigns a new lower stiffness to the elements after each yield excursion. Since the stiffness of Frame B, which is dominated by the stiffness of the wall, is much greater than that of Frame A', its stiffness will decay at a greater rate than that of Frame A', thus making that frame relatively stiffer after each cycle.

Even though the curves for Frame A' in Figs. 5.26 to 5.28 appear linear, in fact, there is some minor nonlinearity present, which becomes noticeable only by calculating the slope of the curves. In each case, the average slope is about 260 kips per inch, or 270 kips/inch at the origin, and about 255 kips per inch at maximum displacement. Recall from the plastic hinge patterns, that the lower story columns do not yield. For this reason, this near linearity seems reasonable for the curves of base shear versus first story displacement for Frame A'.

One further comment on the curves of Figures 5.26 to 5.31 is that the loops in the figures should not be taken to be a measure of the energy dissipated or absorbed by component frames of the structure. This is true because the base shear moving through either the first story or the roof displacement is not representative of the total work being done by the structure. The only true measure of this is the summation of the energy dissipated by all of the plastic hinges in all of the beams and the shearwall.

In the separate volume of plots, the story inertial forces are plotted along the height of the structure every fourth time step. In these plots, the length of the vector which indicates the force direction is proportional to the magnitude of the force. These force distributions give a good indication of the complex nature of the dynamic frame wall interaction. For convenience, nine of these plots are reproduced as Figures 5.32 to 5.34. These plots indicate the distribution of elastic forces just prior to the wall yield, just after the wall yield, and at maximum displacement for each pulse. (For the first pulse, the second part of the response is used.) In all of these plots, the general tendency is for the interaction to be dominated by the large reverse force present at the top of Frame B. This is exactly the same as noticed in the static load to collapse analysis of Chapter 4. See Figures 4.8 and 4.9 for comparison. In the case of the dynamic loading, however, the magnitudes of the force differ from pulse to pulse, but the general arrangement of the forces is the same. Also, note there is no sudden redistribution of force from Frame B to Frame A' once the shearwall yields, but rather a gradual transition. At this stage of the response, the force redistribution seems to be more of a function of overall displacement than of the relative stiffnesses of the individual frames. It is also interesting to note that although the total shears are nearly the same after yielding and at maximum displacement, the wall and Frame B carries a smaller portion of the total base shear as compared to the pre-yielding or just yielded state.

As a final indication of the lateral force distributions, the inertial force profiles for the total structure are shown again in Figures 5.35 to 5.37. In these diagrams, the maximum forces are all drawn as positive, so they may more easily be compared. In each figure, the time at which different events occur are clearly indicated. Two items are worth mentioning:

1) The later the pulse, the less spread out over time the events occur. To be more specific, it takes 0.28 seconds for the wall to yield and unload in the first pulse, 0.20 seconds in the second pulse, and only 0.12 seconds in the third pulse. This is probably due to the progressive softening of the structure which occurs as a result of increasing cycles of yielding and unloading.

2) These force profiles are almost never upper triangular. At maximum displacement however, the profiles are top heavy, or sort of upper parabolic. At maximum shear, they are uniform for the first two pulses, and upper parabolic for the last pulse.

Facts (1) and (2) above are very important from the point of view of testing the 1/5-scale model on the shaking table, and the comparison of the results of this test with the pseudo-dynamic tests that are being performed by the researchers in Japan.

With respect to Fact (1), and referring to the last pulse of MO, all of the yielding occurs within a time frame of 0.12 seconds. For the tests on the 1/5-scale model, the time scale is compressed by the factor $1/\sqrt{5}$. This results in the response frame of 0.12 seconds being reduced to only 0.054 seconds. If the data acquisition unit scans at a rate of only one cycle per 0.01 seconds, only 5 or 6 readings will be available for study, and the significant aspects of the response may or may not be captured.

With respect to Fact (2), in the pseudo-dynamic tests being carried out in Japan, the loading pattern was upper triangular in shape, and varied only in magnitude and direction. If the results from the shaking table tests on the 1/5-scale model to be carried out at Berkeley indicate a non-triangular loading, as suggested by the response of the analytical model to MO, it may be difficult to correlate the behavior of the full scale and 1/5-scale scale models.

5.6.0 Prototype Response to Pacoima Dam

5.6.1 Discussion of Overall Response

Only the first 4 seconds of the Derived Pacoima Dam (DPD) earthquake were used in this analysis. The response is illustrated by the time-history curves of Figures

5.38 thru 5.44, and the envelope diagrams of Figures 5.45 thru 5.48.

The maximum lateral displacements at level 7 are 11.14 inches at time equals 3.71 seconds, and -8.04 inches at 3.05 seconds. From the displacement envelopes given in Fig. 5.45, it can be seen that the maximum story displacements practically occur at the same relative time, thus the displacement envelopes also represent the displacement profiles at the times given. Except for the slight slope discontinuity present at level 1, the displacements are essentially linear, and are dominated by the rigid body rotation of the wall.

The maximum shear force developed at the base of the structure is -869 kips, and occurs at time equals 2.84 seconds. At this time, 24 percent of the shear is taken by Frame A', and the remaining 76 percent is taken by Frame B, which also includes the wall. The shearwall itself absorbs -614 kips, which is 70 percent of the total, or 93 percent of that in Frame B. Note that these are not the maximum shears developed in Frame B, or the wall. These occur at time equals 3.36 seconds, and are 657 kips for Frame B, 648 kips for the wall, and only 693 kips for the total structure. If the code computed shear strength for the wall, 574 kips, could be a reliable value, then the shear force of 648 kips in the wall indicates that there may be some danger of a shear failure. If a shear failure did occur, the subsequent response would of course be vastly different from the analysis presented, where a flexural failure in the shearwall is assumed. More is said about this in Chapter 6.

As in the Miyagi-Oki analysis, the maximum forces in the columns and beams are essentially the yield forces plus some small amount of moment from the strain hardening component of the elements. Since the maximum plastic hinge rotations for DPD are greater than those for MO, the DPD beam moments and shears are correspondingly greater.

5.6.2 Detailed Analysis of a Single Pulse

This single pulse lasts from 2.6 to 4.0 seconds (see Fig. 5.38) and contains all of the inelastic response of the prototype. A summary of the important response parameters is given in Table 5.4. Note that the first part of the response is due to a maximum acceleration of 0.34 g, and a corresponding incremental velocity of 54.2 in/sec, while the second part of the response is due to the maximum ground

acceleration of -0.4 g, and an incremental velocity of -51.5 in/sec.

Each part of the response contains extensive inelastic behavior, with plastic hinges forming in all of the beams except the mid-bay roof beam of Frame A', and with hinges forming in the base of the shearwall and all of the first story columns.

In the volume of plots, a complete time history of the progression of plastic hinges is given. In each direction, the shearwall hinges first, followed by the beams of Frame B and those of Frame A'. This is entirely the same as the Miyagi-Oki response, (except for the column base hinges) but is different from the static load to collapse since in that case the shearwall did not hinge first. For convenience, these hinge patterns are compiled into two figures, Fig 5.49 and 5.50, which summarize the plastic hinge progressions. In Fig. 5.51, the maximum values of plastic hinge rotation are given.

In Fig. 5.52, a time-history of the base shear forces in the different frame components is given. At the bottom of the figure, the normalized first story displacements and the ground accelerations are also shown. The general behavior that was observed during the Miyagi-Oki response is also apparent here, that is, Frame B takes the majority of the shear throughout the response, more than 90 percent during the elastic range, and then the Frame A' starts to resist a large portion only after the yielding of the wall starts. Furthermore the forces in Frame A' seem to be somewhat proportional to the displacements at level one.

Recall that in the Miyagi-Oki analysis, a plot of base shear versus first story displacement displayed an almost linear behavior for Frame A'. This is not the case in the DPD response, however, as shown in the plot of base shear versus first story lateral displacement as shown in Fig. 5.53 Here, there is distinct looping in the lower left quadrant, and very distinct clockwise looping in the positive quadrant. This effect is entirely due to the hinging of the base of the first story columns of the structure. If the base shears are plotted against the roof displacement, the loop for Frame B is clockwise, as is the positive portion of the loop for Frame A'. (This is true for the positive displacements but not the negative displacements since there was only minor column yielding for negative displacements.) This is illustrated in Fig. 5.54. Again, the difference in this DPD

response from the MO response is due to the effect of the base column hinges.

The inertial force profiles shown in the volume of plots give an indication of the frame-wall interactions occurring from time to time. These force patterns are similar to those observed for MO and the static load to collapse analysis. The force distributions before and after the wall hinges, or before and after the columns hinge, and at maximum displacement are shown for both the positive and negative parts of the pulse in Figs. 5.55 and 5.56. For the first yielding of the wall, there does appear to be some minor redistribution occurring after the hinge, but for the second wall hinging the increase in base shear force in Frame A' is large (from 37 kips to 101 kips). The maximum base shear force developed in Frame A' of 277 kips occurs only after all of the columns at the base of the structure have hinged. Note that in each case of column hinging, the columns which are being put into tension by the earthquake loading (acting alone) hinge first. This is significant from the point of view that a lower bound strength was taken for the girders. A higher strength for these elements would have caused the columns to hinge relatively sooner, thus altering the subsequent behavior of the structure. This also implies that it might be possible for the columns to hinge during the Miyagi-Oki earthquake if the beam strengths had been greater.

As a final indication of the lateral force distributions for the DPD response, Fig. 5.57 shows the inertial force profiles for the total structure over the entire time interval of the pulse. Significant events are clearly indicated on the figure. The same general conclusions that were reached for the MO analysis apply here, that is, that the later the pulse, the less spread out over time the events occur, and that in general, the force profiles are not upper triangular. On the contrary, the force profiles at wall yielding are very nearly uniformly distributed.

5.7 Comparison of the MO and DPD Response

In order to be able to develop a structural mechanism it is necessary that

- 1) The wall yields
- 2) The beams yield

3) The columns yield at their base.

Only the first two events occurred during the Miyagi-Oki response, while all three occurred during the Derived Pacoima Dam response. The fact that the overall response of the prototype to DPD was greater than MO is due almost entirely to the incremental velocities of that earthquake being greater, by a factor of almost 1.5 to 1. The fact that the maximum acceleration occurring in the DPD ground motion was greater than that in MO (0.4 g to 0.36 g) is comparatively insignificant, since the 0.36 g acceleration was associated with a relatively small incremental velocity, and did not in itself produce any yielding. In Table 5.5, the maximum response values for each earthquake are indicated. The significant differences occur mainly in the displacements, the plastic hinge rotations, and in the number of load reversals that produce wall yielding. The force values do not differ much since the strain hardening stiffness assigned to the elements was rather low.

In general, the response of the structure to the earthquakes is very similar before the first story columns yield. The behavior up to that time is completely controlled by the rigid body rotations of the shearwall after it yields. The forces picked up by Frame A' are essentially proportional to the first story displacements, until the columns hinge. After the columns hinge, the force in Frame A' reaches its maximum value (except for some minor subsequent increases due to strain hardening).

Before making final conclusions about the response of the prototype, it is necessary to discuss the ductility demands of the response, and relate this to the ductility supplied. This is done in the next section.

5.8 Ductility : Supply vs Demand

To be able to judge if the designed structure would be capable to resist the earthquake ground motions considered it is necessary to analyze if the energy dissipation capacity of the structure is larger than that demanded from the response to these ground motions. Although it is possible to compute such available and demand energy, at present there are two simpler methods that are used to make such judgments. One of the most commonly used is to compare the available with the demanded curvature ductility at the critical section. The other is

to compare directly the maximum plastic hinge rotation demanded with the estimated available rotation capacity at each of the critical regions.

The second method is better because what is measured experimentally is rotation and not curvature. The ideal would be to have tables where the available plastic hinge rotations for different members (beams, columns, and walls) are given as a function of their dimensions and detailing as well as their loading conditions. Unfortunately such tables, or even the data on which to base these tables, is not available. Furthermore, even for a given designed element, i.e. of given dimensions and reinforcement detailing, the available plastic hinge rotations, or energy dissipation capacity, depends on the shear that is developed at the inelastic regions during flexural yielding as well as the amount of axial force and number of yielding deformation reversals to which the critical regions of members are subjected.

Using the first method, the information given in Table 5.7 was computed. This shows that the energy dissipation supplied to each of the members is larger than demanded, not only because the maximum and cumulative plastic hinge rotations are small, but also because the amount of shear and the number of reversals are relatively small. Values considerably higher than those required have been measured in tests conducted at Berkeley.[12,13]

The details of the method used to compute the values shown in Table 5.7 are now explained. Since the hinge rotations occurring during the DPD response were greater than those in the MO response, only the DPD ductility demands need be discussed. In Chapter 2 the moment-curvature diagrams for the individual elements were given. For these curves, it is necessary to define a curvature ductility for the sections. This ductility, μ_c is defined as follows:

$$\mu_c = \text{curvature at maximum concrete strain} / \text{curvature at yield}$$

where yield curvature is the curvature at first yield, and the maximum concrete strain is taken as 0.0045 for the beams, columns, and boundary elements of the shearwall. These available ductility values are summarized in Table 5.6. Note that several ductility values are shown for the columns. It is important to note that these are the assumed ductilities, assumed from the point of view that they are

based on the assumption that the main longitudinal reinforcement does not buckle, and that shear failure will not occur prior to flexural failure.

Since DRAIN-2D gives only plastic hinge rotations as a measure of the inelastic behavior of the elements, it is necessary to relate these values to the curvature ductilities for the elements in order to assess the ductility demands for the individual critical regions. The derivation of equations relating the curvature ductility demands to the maximum plastic hinge rotation as printed by the computer program are given in Fig. 5.58. Essentially, this ductility factor comes from assuming a plastic hinge length, which is based on the moment gradient in the element. This plastic hinge length, together with the maximum hinge rotation and the yield curvature of the element, defines the curvature ductility demand:

$$\mu_{cd} = (\Theta_u / (L_p * \phi_y)) + 1$$

where μ_{cd} is the curvature ductility demand

Θ_u is the output hinge rotation

L_p is the equivalent plastic hinge length

and ϕ_y is the yielding curvature.

The envelope values of plastic hinge rotation demands, Θ_u , for the DPD response were given in Fig.5.51. The required ductilities, as computed from the above equation, are shown in Table 5.7, together with the other relevant quantities. For the beam elements, there are four required ductilities shown, which correspond to the maximum positive and negative hinge rotations in Frame A' and Frame B. In Frame B, the critical beam is the beam at level 5, with a positive hinge rotation of 0.012 radians, and a negative hinge rotation of 0.016 radians. These large plastic hinge rotations are primarily a result of the hinge rotation at the base of the shearwall of 0.01 radians.

From Table 5.7, it can be seen that for the negative moment region of the critical beam of Frame B, the required ductility may not be supplied, since these values are roughly the same. Assuming that the hinge rotation of 0.016 radians is fixed, the only way to alter the properties of the beam in order to meet the ductility demand

would be to use better confinement or reduce the percentage of tension steel. Recall from earlier discussion, however, that the 60 inch flange width assumed is already a lower bound, and that a wider flange might be more realistic. If a greater flange width was used, the effective tensile steel area would be greater, and the ductility would be reduced. It must also be kept in mind that the ductility supplied was based on a limiting concrete strain of 0.0045 in/in. If for the beams, the steel in the critical region was better detailed, ie more ties, the confined concrete would have a greater ultimate strain, resulting in a greater supplied ductility. Note that for the positive moment region of the same beam, the ductility supplied is far in excess of that which is required.

The critical beam for Frame A' is the sixth level center bay beam, where the maximum positive and negative plastic hinge rotations are 0.0112 and 0.0077 radians, respectively. Slightly larger negative moment hinges occur in some of the negative moment regions of the exterior bays, but since these beams have a longer clear span, their moment gradients are not as steep as for the center bay and, therefore, the plastic hinge lengths are longer for the exterior bay beams, resulting in smaller ductility demands. In no case, however, are the required ductilities greater than that which can be supplied by the beams.

For the shearwall, the required curvature ductility of 6.26 is much smaller than the supplied ductility of 18.9. Also, the columns which yield, yield demanding low ductility. The supplied ductility is in excess of that required because the axial forces are not severe and the shear stresses are small.

Although the response to the Miyagi-Oki record requires more yielding reversals than Derived Pacoima Dam, it is clear that there is no problem in supplying the required ductilities for the MO ground motion, normalized to a peak acceleration of 0.36 g.

5.9 Conclusions on MO and DPD Responses

Some conclusions are made with respect to which of the two earthquakes might provide more useful information on the shaking table tests. In this discussion, it must be assumed that the analytically predicted responses just described give a

fair indication of the general behavior of the structure to the two different ground motions. In the next chapter, reasons are given why this analysis might not be so reliable, and methods are suggested which are thought capable of providing a better (more dependable) response, still using the basic DRAIN package.

As mentioned earlier, the responses of the prototype to the two earthquakes are quite similar before the columns hinge at their bases. Also, the degree of damage depends on the initial conditions at the start of a particular acceleration pulse, and on the incremental velocity contained within that pulse. In the MO response, the structure was forced to undergo several yield excursions, while in the DPD response, the structure yielded only once in each direction. The displacements for the DPD response were much greater than those in the MO response, although the forces were similar. While in the MO response there was no problem supplying the required ductility, the ductility requirements of some of the negative moment regions in the beams adjacent to the shearwall for the DPD response were slightly greater than supplied.

From these considerations alone, it seems that the Miyagi-Oki earthquake would probably produce the more interesting response, mainly because the structure was forced to undergo several cycles of inelastic deformation, and the progression of damage could be more closely followed.

What is needed for the shaking table tests on the 1/5-scale model is an earthquake which produces several cycles of yielding, yields over a "longer" time period, and produces some column hinging, but preferably near the end of the response. Except for the fact that the response intervals for MO were short from a data acquisition point of view, a MO type earthquake with a greater maximum ground acceleration than .36 g may prove to be a good solution. Or, the 0.36 g earthquake could be followed by a 0.40 or 0.45 g ground motion, depending on the amount of damage desired. In any event, the 0.36 g Miyagi-Oki ground motion provides a response that will permit the study of the effect of degradation upon dissipation of energy with several yielding reversals. Furthermore it provides a bit of safety from total destruction of the model occurring during the first pulse.

CHAPTER 6

ACCURACY OF COMPUTED RESPONSE

6.0 Introduction

The analytical response of the Prototype structure to the static loadings of Chapter 4, and the dynamic loadings of Chapter 5, is only as good as the assumptions made while performing the analysis. For this reason, it is of fundamental importance that the possible sources of error in the analysis be studied carefully. For the discussion in this chapter, the sources of error are grouped as follows:

- 1) Errors in the global modeling of the entire structure.
- 2) Errors associated with the local modeling of the individual elements.
- 3) Errors in estimation of structural loads, mass, and damping.
- 4) Errors associated with the numerical methods used to determine the response.

The purpose of this chapter is to discuss these errors, and determine their affect on the response of the prototype. Also, through this discussion, methods for obtaining an improved response are outlined.

6.1 Global Modeling Errors

6.1.1 Flexural Frame to Frame Coupling

In Chapter 3, the manner in which the structure was modeled was discussed, and illustrated in Fig. 3.1. The two exterior frames were added together to form a new frame, Frame A', and this frame was linked to the interior frame, Frame B, through the use of horizontal constraints. Recall that the flexural coupling of the exterior frame to the interior frame, via the transverse slab-beam system, was ignored.

The omission of flexural coupling can be an important source of error in this building. In Fig. 6.1, the two frames are shown in a deformed configuration. Note that here, although the joints at the tops of the interior columns of Frame A' displace very little in the vertical direction, the corresponding points in Frame B

do displace due to the rotation of the shearwall. In the real structure, the beams connecting these points (the beams between Frames A' and B) will be forced to deform accordingly, thus transferring forces between the two frames. Since in the analytical model this transfer was ignored, the analytical model is more flexible than the real structure, all other things being equal.

It is also important to realize that this inter-frame coupling may have a pronounced effect on the way the interior columns of Frame A yield. Calculations on the response of the prototype to the DPD ground motion have shown that the axial loads in these interior columns may change by 50 to 75 percent if coupling is considered. Also, the moment entering the beam-column joint from the transverse beams is not negligible in this case. These moments can be significant enough to cause the interior columns of Frame A' to yield in a biaxial bending mode. Only a uniaxial bending yield surface was assumed in the analysis. It is clear then, that due to the omission of flexural coupling, the moments and axial loads in the interior columns of Frame A' were not very accurately estimated. This could have a significant effect on the response of the prototype to a Miyagi-Oki type ground motion, since the base columns of Frame A' might yield in the real structure, while they did not in the computed response. Recall the change in behavior of Frame A' once the columns yielded in the DPD analysis.

In future analysis, there is no doubt that the frame to frame flexural coupling needs to be included. In Fig. 6.2 a very simple flexural coupling model is described. The basic idea behind this model is that for a rotation Θ at joint I of the shearwall, joint J will displace an amount Δ , thus causing a reaction at K via the flexural stiffness of the transverse beam. Assuming that Frame A' has no flexural stiffness out of plane, so no moments are transferred to that frame from Frame B, this reaction, R_1 , can be computed as shown in Fig. 6.2. If it is assumed that the joints J and K have the same coordinates, ie Frames A' and B lie in the same position of the same plane, an equivalent reaction, R_2 will be transmitted to K via the fictitious beam I-K, with stiffness EI_E . Setting R_1 equal to R_2 , and noting that there are two frames A which make up Frame A', the necessary equivalent stiffness for the fictitious beam is:

$$EI_E = (EI_T/2) * (L_W/L_T)^2$$

6.1.2 Effect of Large Displacements

Since the incremental equilibrium equations for the structure were based on the initial topology, second order or large displacement effects were ignored. Recall from Chapter 4, however, that the inclusion of linearized geometric stiffness on the static load to collapse analysis had a small, but significant effect on the load-displacement response. Therefore, for future analysis using DRAIN, second order effects should be included.

6.1.3 Rigidity of Foundation

One of the basic assumptions made at the start of this analysis was that the foundation of the structure is totally rigid. For the 1/5 scale-model, however, the fact that the shaking table may not provide a totally rigid base must be taken into account. In particular, there is the possibility of global rotations and vertical displacements of the table itself. These extra degrees of freedom could be included through the use of linear constraints, however, this would be difficult using the current version of DRAIN. Instead, a massive support structure will have to be modelled, as shown in Fig.6.3. The numerical values of the spring constants have to be worked out, and this can be done only through studying the response of past models that were tested on the table.

6.2 Local Modeling

Of all assumptions made in setting up the analytical model, those associated with assigning strength and stiffness to the individual elements are certainly the most error prone. In general, the analyst has to produce a bilinear moment rotation relationship that represents the entire behavior of a particular critical region of an element. This bi-linear model has only four parameters: positive moment yield strength, negative moment yield strength, elastic stiffness EI , and strain hardening stiffness. Note that both positive and negative moment sections are assigned the same stiffness parameters, and that flexural stiffness is completely independent of the level of axial load in the element. In the next few sections, the local modeling used for the prototype structure is reviewed. Errors associated with

the modeling are discussed and methods for improved analysis are given.

6.2.1 Column Elements

Although the majority of the columns did not yield as a result of the two earthquakes considered, they were loaded well above their cracking load. The result is a flexural stiffness for these elements somewhere between gross and cracked-transformed. Since in the analysis the entire length of the columns was assumed to be represented by the same cracked-transformed stiffness, the overall stiffness of the prototype with respect to the columns alone was underestimated.

Although the method used to estimate the column flexural stiffness for the previous analysis contributes little to the total modeling errors, a better method should be derived for future work. The main problem associated with deriving this sort of model is the effect of the axial load-moment interaction on the flexural stiffness of the column. For high levels of compressive axial load, the flexural stiffness will be much greater than sections that are subjected to lower levels of axial load. Moreover, for sections that are in tension, the flexural stiffness is drastically reduced. Unfortunately, using the current version of DRAIN, there is no way to take these variations in stiffness due to axial load into account. Therefore, it becomes necessary to make assumptions with respect to the average level of axial load that will occur in a column during the response, and assign the flexural stiffness accordingly. If it can be shown that the columns will never carry tensile axial loads, the gravity loads acting alone should be used as the basis for the determination of the column flexural stiffness. Using this axial load, in association with a moment gradient over the length of the column with the end moments being somewhere between the cracking moment and the yield moment (for that axial load), the appropriate element stiffness coefficients can be assigned, as shown in Fig. 6.4.

If it is possible for some of the columns to be loaded axially in tension due to the lateral inertial forces occurring during an earthquake, it would be necessary to provide a new element for DRAIN that changes in stiffness due to changes in axial load in the column elements. Since the columns do not yield, in general, this new element would not need to include the effects of degrading stiffness as associated with the beam elements.

The potential bi-axial moment yielding in the first story interior columns of Frame A', as described in the last section, would be impossible to model with current elements available in the element library of DRAIN. As an estimate the yield surface might be slightly altered to account for the bi-axial eccentricities, but the uncertainties would remain to be rather large.

Recall also that the columns yield only in a flexural mode and axial yielding is not possible. In the present analysis this is of no concern since at no time did the axial load levels in the columns approach their yielding load. In future analysis, however, where the effects of frame to frame flexural coupling will be included and stronger beams may be utilized, it is very possible that the columns may yield in an axial manner. The neglect of column axial yielding in this case would indeed be a serious source of error.

6.2.2 Beam Elements

As mentioned earlier, the beam elements in DRAIN-2D are modeled through the use of a bi-linear moment rotation relationship, in which only four parameters are used. These parameters must somehow represent both positive and negative moment yielding, and initial and strain hardening stiffness. For rectangular beams, with equal top and bottom steel, and constant moment along the length, this model is fairly accurate. For a T-beam subjected to gravity loading in addition to earthquake loading, the bi-linear model cannot exactly represent the true behavior of the element. Even if the bi-linear model was good, the task of determining the values of the four parameters for reinforced concrete structures is full of uncertainties, some of which are:

- 1) For a T-beam, as most reinforced concrete sections are, the initial stiffness and the strain hardening stiffness will be quite different at positive and negative moment regions. DRAIN allows only one initial, and one strain hardening stiffness for the entire beam.
- 2) For a reinforced concrete beam which is part of a frame which is being subjected to lateral loadings, one end of the beam may have tension on the top, while the other end will have tension on the bottom. In this case, the 2 by 2 element stiffness matrix is not doubly symmetric, but rather biased to one side (ie the k_{11} term is greater than the k_{22} term). When the signs of the moments change, the bias should switch to the other direction. This

effect is completely ignored by DRAIN.

3) DRAIN assumes that the gravity loading does not produce yielding, and the fixed end moments are input on the basis of that assumption. However, as the element stiffnesses change along their length, the fixed end moments will also change.

There are many more uncertainties that could be added to this list. It is clear that any method used to assign the numerical values to the four parameters is only approximate. What must be done, is to determine which aspects of the behavior of the elements are the most important to capture. In the next few sections of this chapter, the methods used to set the parameters for the analysis are described, and wherever possible, improved methods are recommended.

6.2.2.1 Initial Beam Stiffness

The initial stiffness of the sections was taken as the average of the positive and negative moment cracked transformed section stiffness. This is clearly a lower bound, since regions of the beam remain relatively crack free, while other sections are fully cracked and yielding. Since the beam stiffness is only 1/1000 times that of the shearwall, the errors in the response due to a "too low" beam stiffness are probably small. However, when the beams are looked at as part of Frame A', the effect on the overall lateral stiffness of the structure is significant, as demonstrated by the flexibility matrices presented in Table 3.2, which shows Frame A' being only slightly more flexible than the wall alone. Of course, this flexibility matrix for Frame A' is also a function of the column flexural and axial stiffnesses. In order to judge the true sensitivity of the structure to the initial stiffness of the beams, more extensive calculations should be made, where changes in structural stiffness due to changes in beam stiffness only are measured.

In any event, it is necessary that a better representation of the beam initial stiffness be derived. Although it can be expected that the beams will normally be loaded with a combination of gravity and lateral loading, resulting in positive moment at one end of the beam, and negative moment at the other end, this moment pattern will be continuously changing, with the moments under gravity load alone being the "average" measured during the response. Using this gravity load moment diagram, together with the moment-curvature relationship for the positive and negative moment sections, a more accurate beam stiffness can be determined than

derived from the transformed cracked section alone. See Fig. 6.5 for an illustration of the proposed method.

6.2.2.2 Strain Hardening Stiffness

Once all of the beams have hinged at both ends in Frame A', for example, the stiffness of the entire frame is represented mainly by the strain hardening stiffness of the individual beams and the flexural and axial stiffness of the columns. On an element basis, it is the increase in moment beyond the yield moment that determines the plastic hinge length, thus strain hardening is important in establishing the actual strength as well as the ductility demands of a particular critical region. For these reasons, and others, it can be seen that strain hardening stiffness is an important modeling parameter.

For the analysis of the prototype, an average positive-negative moment strain hardening stiffness was used to model the inelastic behavior of the beams. Thus, in the negative moment regions this stiffness was overestimated, and was underestimated in the positive moment regions. If the relationships between curvature ductility and plastic hinge length (see Chapter 5, Section 8) can be assumed to be at least qualitatively accurate, it can be shown that the practice of using the average strain hardening stiffness will result in unconservative estimates of required ductility for the negative moment regions. The reason for this is that when the negative moment strain hardening stiffness is overestimated, too-large moments will occur in those regions. Since the higher negative moments will produce longer plastic hinges, the computed curvature ductility requirements will be too low. In the case of the beams for Frame B, this can be significant since it was the negative moment regions of these beams that came the closest to being unable to supply the required curvature ductility. This, combined with the fact that the supplied ductility for these sections might have been overestimated due to an (assumed) too narrow flange width, indicates that there may be some problems in actually achieving the amount of deformation required in these regions during the DPD earthquake.

6.2.2.3 Positive Moment Strength

The positive moment yield strength is relatively easy to estimate if most of the

properties of the materials, and the location and distribution of the longitudinal reinforcement are accurately established. For this reason, the positive moment yield strength used in the prototype analysis is probably a good estimate. However, strengths beyond yield may not be correctly modeled since a too low strain hardening stiffness was assigned in order to accommodate the bi-linear model. In future analysis, it might be a good idea to alter the positive moment yield strength so that at some limiting plastic hinge rotation the ultimate moment is correctly modeled. The ultimate moment is more important to get right than is the yield moment, since it is this ultimate moment, together with the ultimate negative moment that determines the maximum shear in the element, thus the axial forces in the columns and the overall frame overturning moment. Note that if the above idea is used, the computed ductility demands for the section will be altered. This should be of no concern, however, since the positive moment ductility demands are easily attained.

6.2.2.4 Negative Moment Strength

For T-beams, in which the flange is part of a monolithically cast slab, the negative moment strength is difficult to predict, due to the uncertainty in assigning an effective slab width. In the prototype analysis, a 60 inch flange width was assumed, which is probably alright for the yielding moment but is probably a lower bound for the maximum moment when large ductilities are required. As mentioned before, it is the strength of the beam that determines the axial loads in the columns, and the overturning moment developed in the frame, especially Frame A'. Had the beams been assigned a negative moment strength corresponding to a slab width of 120 inches, tension would have been produced in the exterior columns of Frame A' and Frame B. Since it was the columns that were loaded in tension (due to the earthquake loading alone) that yielded first, it is clear that using a beam with a larger negative moment strength could drastically alter the response.

6.2.2.5 The Takeda Model

Another source of error in the analysis deals with the way the degrading stiffness characteristics of the model were defined. In Fig. 5.3, the bi-linear Takeda model which was used in the analysis of the prototype, is shown. Although this model

certainly represents an improvement over no degrading stiffness, it still leaves much to be desired. The main problem with the model is that it poorly represents the behavior of a T-beam as responding to cyclic load reversals. Compare, for example, the response of a typical beam element from the Miyagi-Oki analysis, to the force deformation relationship obtained from the testing of a 1/2-scale beam-column subassembly in which the weak (controlling) element is the beam. These curves are shown in Figs 6.6 and 6.7 respectively. There is essentially no similarity. The response from the sub-assembly tests displays a pronounced pinching on the hysteresis loop and there is even distinct pinching in the first cycles of loading, as is typical of T-beam sections, since the large cracks which open up during application of loads producing tension in the bottom of the section do not close up immediately under the reversal of load. What this means in terms of the analytical response presented in the previous chapters, is that the energy dissipative properties of the beam elements have been over-estimated.

Another source of pinching in the hysteresis loop of Fig.6.7 is cyclic bond deterioration in the principal beam reinforcement embedded in the joint. This fixed end rotation of the beam elements is a low energy dissipating system, and is very difficult to model directly. Some researchers have attempted to derive degrading stiffness beam elements that include the effect of fixed end rotations, but it will be awhile before this can be reliably incorporated into our model.[23,24]

6.2.3 Shearwall Elements

Since the shearwall dominates the response of the entire structure to lateral loading, it is essential that the wall be modeled as accurately as possible. Assuming that the shearwall yields in a flexural mode, the response of the prototype as described in Chapters 3,4,and 5 is probably representative of the way the actual structure would behave, at least on a global basis. On the other hand, if the shearwall were to yield in a shear mode, or in a combination flexural-shear mode, the discussion presented in the last few chapters is only academic.

There are two indications of the likely behavior of the shearwall with regards to flexural or shear yielding. First, if the nominal shear stresses in the wall exceed about $7\sqrt{f'_c}$, or 434 psi, and the wall has undergone several cycles of inelastic deformation, there is a possibility that a shear failure, accompanied by large shear

deformations in the first story of the shearwall will ensue.[9] This sort of failure (see Fig.2.18) is usually triggered by the crushing of the diagonal compression strut which is contained within the panel of the wall. For the Miyagi-Oki response, the maximum base shear in the wall is 547 kips, which results in a shear stress in the base of the wall of 401 psi, or $6.47\sqrt{f'_c}$. (the shear stress is based on an effective area in shear of the wall equal to 0.8 times the gross area of the panel, or 1363 in².) Note however, that this occurred during the first cycle of flexural inelastic behavior, so it may or may not be an indication of impending shear failure. For the second pulse, however, the maximum shear was 500 kips, resulting in a shear stress of 376 psi or $5.9\sqrt{f'_c}$. This was preceded by several cycles of flexural inelastic behavior, so the indication is that a shear sliding failure, associated with large shear deformations in the lower portion of the wall may be possible, although the nominal shear stress is somewhat less than $7\sqrt{f'_c}$.

For the DPD response, the maximum base shear developed was 648 kips, resulting in a stress of 475 psi, which is $7.66\sqrt{f'_c}$. Here again, however, this occurred during the first pulse, so the possibility of large shear deformations is not clearly established.

The second indication of the possibility of shear yielding comes from the results of the Japanese pseudo-dynamic tests. In the first of these tests, the uncracked structure was loaded with an upper triangular distribution as shown in Fig.6.8a. The behavior of the wall in this case was reported to be mostly flexural. In later tests, the (already damaged) structure was loaded with a uniform lateral load, and the failure was in shear at the base of the wall. This is shown in Fig.6.8b.

Since there is a possibility of a shear-hinging mechanism occurring during the response, especially during a Miyagi-Oki type earthquake, it is essential that a model be developed that takes into account this mode of behavior. For future analysis, it would be possible to include a shear hinging mechanism in the model, where the wall would hinge in a shear mode only after a certain force was developed (this might also be tied in with previous flexural hinging). There are several ways of incorporating this mechanism into the DRAIN model, one of which is to use the beam-column model of DRAIN, together with truss bars which would work as lateral springs. In this model, shown in Fig. 6.9, the base of the wall would

develop increasing shear and moment until one of the two components yield. The shear-yielding would be produced by the yielding of the lateral springs, since the lower portion of the beam has no shear stiffness. The relative stiffnesses of the flexural and shear springs could be adjusted to provide any sequence of yielding. Typically, the wall would first yield in flexure, and then, after several cycles of inelastic deformation, shear yielding would occur. This indicates the necessity for some type of degrading stiffness mechanism in the shear springs.

6.2.4 Conclusions on Local Modeling

In the previous discussion, it has been shown that the modeling procedures used to determine the dynamic response of the prototype to earthquake induced loading were predicated upon a host of assumptions, and that a change in some of these assumptions could drastically alter the computed response. In future analysis, careful attention should be paid to the following items;

- 1) Better representation of the initial stiffness of the different elements.
- 2) Modelling of the base of the shearwall to include the possibility of large inelastic shear deformations.
- 3) Obtaining a more realistic value for the negative moment strength of the beam elements of Frames A' and B.
- 4) Deciding upon an appropriate value for strain hardening stiffness, especially for the negative moment regions of the beams.

6.3 Structural Loads, Mass, and Damping

6.3.1 Loads

For the analysis reported in Chapters 3,4,and 5, it was assumed that the prototype was loaded with its own self-weight, and superimposed dead and live load. For the gravity loading, a tributary area analysis was used in lieu of a more accurate method. See section 2.4 for a review of these more accurate methods. The errors resulting from using the tributary areas should be negligible for the response presented in Chapter 5. For future work, however, a more accurate method should be used to determine the gravity load distribution, particullary in the 1/5-scale model, because several tons of lead ballast will be used to adjust the

gravity load stresses, and to supply the proper mass for the scaling. Of special concern is the proper determination of the moment along the lengths of the beams to assure that there is no possibility of plastic hinges forming near midspan of the primary girders. If this type of hinge is possible, appropriate modifications can be made to the analytical model.

6.3.2 Mass

The masses were lumped at the lateral degrees of freedom for the analysis reported in Chapter 5, and this is probably a good approximation. Recall that no rotary mass was included for the wall. In the future, some parametric studies should be carried out in order to determine the type and magnitude of errors caused by leaving out the rotary mass. These errors would likely be of two types: first, the elastic response will be effected by changes in the period of vibration, and second, the inelastic response may be effected by equilibrium error correction procedures in DRAIN, or by numerical errors occurring during the solution of the incremental equilibrium equations.

6.3.3 Damping

It is difficult to accurately assign a damping to reinforced concrete structures since the value depends on the state of cracking in the structure at the onset of ground shaking. The average first three period damping ratios used in the analysis was about 6 percent is probably good if the assumption that the structure was well cracked prior the occurrence of the major earthquake is taken into consideration. From results obtained from the Japanese on the results of their pseudo-dynamic tests, the damping ratio increased from 2 percent critical for the uncracked specimen, to 3.1 percent after minor excitation, to 5.3 percent after moderate excitation, to 8.3% after major excitation.[2]

Recall that the damping used in this analysis is Rayleigh proportional damping, and is taken as proportional to the diagonal mass matrix, and the tangential stiffness matrix. From this point of view, the damping will decrease as the structure goes through the cycles of inelastic behavior, because the degrading stiffness model will reduce the stiffness of the elements each time the element yields. This is inconsistent with observed behavior since, in general, the damping will increase

(most likely due to displacement dependent Coulomb friction forces) as damage progresses. For this reason, in future work, the damping should be made proportional to initial stiffness, and not tangential stiffness.

6.4 Numerical Errors

Although the effects of numerical errors on the computed response of reinforced concrete structures are beyond the scope of this report, it is necessary to briefly mention the most important source of error, that is the manner in which the DRAIN program "corrects" equilibrium at the end of the time step.

Recall from Chapter 5 that whenever an element yields, the program "corrects" the equilibrium at the end of the time step by applying an impulsive load to the load vector for the subsequent time step. In general, the smaller the time-step, the smaller the equilibrium error corrective forces, and the more accurate the response. For the prototype, however, it is possible for large equilibrium errors to be introduced once the shearwall hinges. Subsequent to the yielding, an impulsive moment and shear is added to the first story of the shearwall. Although difficult to verify, it is felt that in some instances, this corrective force may momentarily overwhelm the response. Two illustrations are given. In Fig. 6.10(a) the inertial force profiles just before and after the wall hinges are shown. Note that before the hinge, all of the forces near the base of the structure are in the same direction, but that after the hinge, a rather large reverse force shows up at level one. This force can be followed up the structure as sort of a traveling wave for the next few time steps as shown in Fig. 6.10(b). Clearly, this corrective force is having a large influence on the subsequent response.

The best way to avoid these types of errors is to reduce the time step until such large equilibrium corrections are avoided. Another method, that may or may not work depending on the displacement increment, is to subdivide the base of the shearwall into several parallel elements, as shown in Fig. 6.11. As can be seen, it is possible that for a given displacement increment, Δ_y , the correction for a single element is much larger than that for the multi-component model. Note that if Δ_y is slightly larger though, the errors for the multi-component model might be slightly larger than for the single element. However, it seems that the multi-component

model would produce better results for a set of somewhat random displacement increments.

Finally, it should be noted that there is a new version of DRAIN, still in the developmental stages, that does not use the equilibrium correction procedure just described.[24] Instead, the program works on an event to event basis, much like the nonlinear static program ULARC. Here, if an event occurs during a time step, the program backs up a step, determines the time step that will just produce yielding, and goes on as before, but with equilibrium being satisfied exactly at the end of each timestep. Clearly, this is superior to the force modification procedure being used by the current version of the program.

CHAPTER 7

CONCLUSIONS AND RESEARCH NEEDS

7.0 Introductory Remarks

In the previous five chapters the design and the behavior of an analytical model of the reinforced concrete Test Building for the USA-Japan cooperative research program was discussed. First, the structure was reviewed to determine if it is a satisfactory design according to the 1979 version of the Uniform Building Code. Next, the inelastic analytical response of the structure to monotonically increasing lateral loads was presented, followed by a detailed description of the inelastic analytical response to two different earthquake ground motions. Finally, a discussion of errors that may have been introduced into the analytical response due to modelling procedures was given, and suggestions were made that might lead to a more accurate response in future analytical work.

In many cases, it is not possible to draw specific conclusions from the analysis carried out, since more computation needs to be done in order to quantify certain aspects of the response. This is particularly true for the procedures used to model the elements in the dynamic analysis, since there was simply not enough data accumulated to form a trend or pattern that leads to the source of specific errors in the response. These trends can only be traced via a systematic variation of the individual parameters that may affect the response. In other instances, however, it is possible to reach specific conclusions since the variables that govern these aspects of the analysis are well established. For example, it is easy to determine if the tie details in the critical regions of the beams are satisfactory according to UBC. In the following section, a list of the most basic general conclusions that can be reached is presented. Finally, some suggestions are given for future research needs, most having to do with methods for obtaining more realistic analytical responses to reinforced concrete structures subjected to earthquake induced loading.

7.1 Conclusions

The following are the main conclusions that can be drawn from the UBC analysis and from the analytical response of the Prototype to earthquake induced loading.

1) The design of the Prototype satisfies all of the requirements of the 1979 Uniform Building Code for structures classified as dual bracing systems ($k=0.8$) except as follows. First, the ties in the critical regions of the beams, columns, and in the edge members of the shearwall do not provide the required confinement. Second, the flexural strength of the shearwall is not adequate if the wall has to carry the entire factored overturning moment on its own.

2) The designed structure is a good example of the strong column-weak beam seismic design philosophy. This is so mainly because all of the inelastic behavior should occur in the ductile beams, or in the base of a relatively ductile shearwall, and the columns will not yield until the very end of the yield excursion. Also, the elements have been designed and detailed in such a way that relatively low shear stress can be developed and thus the danger of brittle shear failures is avoided. Higher energy dissipation capacity could be attained if the 1979 UBC requirements for ties in critical regions had been satisfied.

3) The analytical response of the Prototype to static and dynamic loadings is completely controlled by the centrally located shearwall. This wall, which is 1000 times stiffer, and 70 times stronger than any of the other elements, dominates the elastic response due to its stiffness, and the inelastic response due to its rigid body deformation mode after flexural yielding at its base.

4) After the shearwall hinges at its base, the frames are capable of resisting increased lateral loads, since the wall and the beams have been supplied with sufficient energy dissipation to allow the complete mechanism to form.

5) Although the shearwall was assumed to yield in a flexural mode, it may be possible for significant inelastic shear deformations to occur. This is particularly true for a Miyagi-Oki type ground motion, since large shear forces are preceded by several cycles of inelastic flexural deformation, including reversals.

6) In terms of selecting a ground motion to use in the shaking table tests of the 1/5-scale model, the Miyagi-Oki motion seems acceptable. Initial tests should be run with a maximum ground acceleration of about 0.15 g, followed by a motion with a peak acceleration of about 0.4 g. The first of these two motions should cause significant cracking without yielding the steel, and the second should produce significant inelastic response. If a serious failure (physical collapse) is not attained with the 0.4 g earthquake, a third run should be conducted under the MO earthquake normalized to a higher peak acceleration.

7) The global modeling of the structure using DRAIN does not allow an accurate and efficient modeling of frame to frame flexural-torsional coupling via the transverse slab-beam system. An approximate technique which uses a fictitious coupling beam has been described that will approximate this effect. However, in order to determine the true nature of this interaction between frames, a full three-dimensional analysis should be performed.

8) The methods available for the local modeling of the beams need improvement since the response of the structure is very sensitive to the behavior of these elements. In particular, the use of a bi-linear force deformation relationship is completely inadequate, since the parameters that are used to define the bi-linear model are difficult to establish. For example, only the initial and strain hardening stiffness, and the positive and negative moment "yield" strengths, are specified. In order to accurately model the strain hardening stiffness, some accuracy must be sacrificed in the specification of the yield moment. For T-beams, in which the positive or negative moment initial and strain hardening stiffnesses differ, an average must be used, and this averaging process may lead to errors in establishing the ductility demands.

9) For the columns, local modeling errors occur due to the difficulty in establishing the flexural and axial stiffness. The elements are assigned a yield surface, but this yield surface does not consider the effect of axial load on the flexural stiffness of the columns.

10) As mentioned earlier, there is a possibility of large inelastic shear deformations occurring at the base of the shearwall. This action may dominate if large shear forces occur after the wall has undergone several cycles of reverse

inelastic flexural deformation. It is necessary, therefore, to develop a procedure for the analytical modeling of shear yielding. A simplified approach has been recommended, but better models need to be created.

7.2 Future Analytical Research Needs

The vast majority of future research which needs to be performed has to do with the analytical techniques used to predict the response of reinforced concrete structures to earthquake ground motions. These needs go beyond what is required in academic research since designers need to be able to evaluate the capacity of their structures to resist major ground motions through the dissipation of energy, but without collapse. Although DRAIN allows a somewhat qualitative analysis of the response of a certain class of structures, it cannot be expected to accurately predict the response of all structures. The further removed a structure is from what may be modeled by DRAIN, the less accurate the analytical response. The Prototype structure is a good example of a structure that cannot be analyzed with precision using DRAIN (for a reasonable cost) since it is very difficult to include all of the important aspects of the design of the structure in the analytical model.

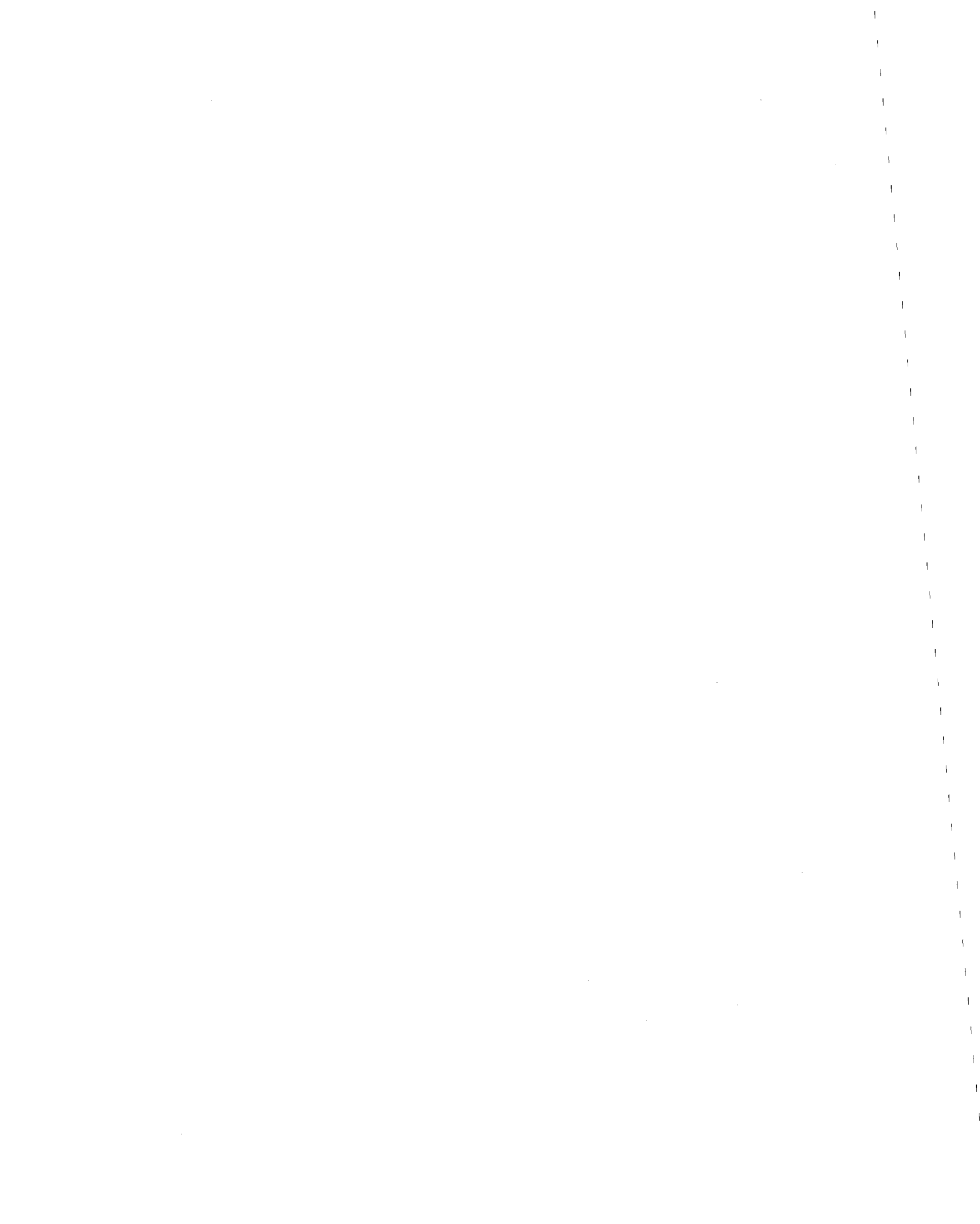
With minor modifications, however, it should be possible to obtain an accurate estimate of the important response parameters of reinforced concrete structures using DRAIN, or a similar program. What is needed is information on the way certain aspects of the local or global modeling affect the response of a structure. For example, in the analysis of the Prototype, decisions needed to be made with regard to assigning a value of strain hardening stiffness to the beam elements. Since only one stiffness could be assigned, which is independent of the direction of loading, an average positive-negative moment stiffness was used. What was the overall effect of this assumption on the response of the structure? This is impossible to answer since this was only one assumption of many that were simultaneously included in the modeling of the structure and, therefore, in the subsequent analytical response.

What is required then, is an analytical research program, in which a systematic series of analyses is carried out on a structure. In this analysis, certain parameters, such as initial stiffness, strain hardening stiffness, yield strength,

interaction of axial load and flexural stiffness for columns and walls, gravity loading, and shear-axial-flexure interaction should be varied one by one, until some sort of trend is established. This should be repeated for several types of structures, since the same parameters may affect different structures in different ways. Once this research is complete, guidelines may be established for accurate modeling of reinforced concrete structures.

7.3 Future Experimental Research Needs

Finally, as an experimental model the reinforced concrete test structure is adequate in most respects, except that it may not be representative of some frame-wall structures, especially those which may be required to develop considerably higher shear and bond stresses than will be the observed in the present model. Therefore, in terms of future experimental research needs, a similar series of tests should be carried out on another model, similar to the prototype, but designed to develop higher shear and bond forces.



REFERENCES

- [1] Penzien, J., "Recommendations for a U.S.-Japan Cooperative Research Program Utilizing Large Scale Testing Facilities", Report No. UCB/EERC-79/26, Earthquake Engineering Research Center, University of California, Berkeley, 1979.
- [2] Okamoto, S. et al, "A Progress Report on the Full Scale Seismic Experiment of a Seven Story Reinforced Concrete Building -- Part of the US Japan Cooperative Program", January, 1982.
- [3] Progress Report on Prototype Component Tests, by Japanese Participants, Japan-USA Project, Spring, 1981.
- [4] ACI Committee 318, "Building Code Requirements for Reinforced Concrete (ACI 318-77)" American Concrete Institute, Detroit, Michigan, 1979.
- [5] Uniform Building Code, 1979 Edition, International Conference of Building Officials, Whittier, California.
- [6] Park, R., and Paulay, T., Reinforced Concrete Structures, John Wiley and Sons, Inc., 1975.
- [7] Mahin, S.A., "RCCOLA A Computer Program For Reinforced Concrete Column Analysis", Department of Civil Engineering, University of California, Berkeley, 1977.
- [8] Ma, S., Popov, E.P., and Bertero, V.V., "Experimental and Analytical Studies on the Hysteretic Behavior of Reinforced Concrete and Rectangular T-Beams.", Report No. UCB/EERC-76/2, Earthquake Engineering Research Center, University of California, Berkeley, 1976.
- [9] Paulay, T., "Earthquake Resistant Structural Walls", Proceedings of a Workshop on Reinforced Concrete Building Construction (ERCBC), (V.V. Bertero, Organizer), Vol. III, pp 1339-1365, 1977.
- [10] Bertero, V.V., "Seismic Behavior of Reinforced Concrete Wall Structural Systems", paper presented at VIth World Conference on Earthquake Engineering, Istanbul, Turkey, 1980.
- [11] Jirsa, J.O., (Chairman), "Recommendations for Design of Beam Column Joints in Monolithic Reinforced Concrete Structures", Journal of the American Concrete Institute, July, 1976.
- [12] Wang, T.Y., Popov, E.P., and Bertero, V.V., "Hysteretic Behavior of Reinforced Concrete Framed Walls", Report No. UCB/EERC-75/23, University of California, Berkeley, 1975.
- [13] Vallenias, J.M., Popov, E.P., and Bertero, V.V., "Hysteretic Behavior of Reinforced Concrete Structural Walls", Report NO. UCB/EERC-79-20, University of California, Berkeley, 1979.

- [14] Fintel, Mark (Chairman), "Response of Buildings to Lateral Forces", Journal of the American Concrete Institute, February, 1971.
- [15] Zagajeski, S., and Bertero, V.V., "Optimum Design of Seismic Resistant Reinforced Concrete Frame Structures", Report No. UCB/EERC/80-03, Earthquake Engineering Research Center, University of California, Berkeley, 1980.
- [16] Charney, F.A., "ULARC3 - Users Manual", University of California at Berkeley, 1981.
- [17] Kaanan, A.E., and Powell, G.H., "DRAIN-2D, A General Purpose Computer Program for Dynamic Analysis of Planar Structures", Report No. UCB/EERC/73-6, Earthquake Engineering Research Center, University of California, Berkeley, 1973.
- [18] Adeli, H., Gere, J., and Weaver, W., "Algorithms for Nonlinear Structural Dynamics", Journal of the Structural Division, ACSE, February, 1978.
- [19] Higginbotham, M., "Computational Procedures for Nonlinear Structural Dynamics", Structural Engineering and Structural Mechanics Division Graduate Student Report #510, University of California, Berkeley, 1971.
- [20] Takeda, T., and Sozen, M., "Reinforced Concrete Response to Simulated Earthquakes", Journal of the Structural Division, ASCE, December, 1970.
- [21] Charney, F.A., "Supplimental Plots and Tables for the Report titled An Investigation to the Analytical Response of a Seven Story Reinforced Concrete Frame-Wall Structure to Static and Dynamic Loads", University of California at Berkeley, 1982.
- [22] Filippou, Philip, Modeling Techniques for Beam Critical Regions Under Deformation Reversals, CE299 Report, University of California, Berkeley.
- [23] Soleimani, D., "Reinforced Concrete Ductile Frames under Earthquake Loadings With Stiffness Degradation, Ph.D. Dissertation, Department of Civil Engineering, University of California, 1978.
- [24] Golafshani, A., "DRAIN-2D2, A Program For Inelastic Seismic Response of Structures", Ph.D Dissertation, Department of Civil Engineering, University of California, Berkeley, 1982.

* * * T A B L E S * * *

TABLE 2.1

(From Table 23-I of UBC)

**HORIZONTAL FORCE FACTOR K FOR BUILDINGS
AND OTHER STRUCTURES**

For buildings with a dual bracing system consisting of a ductile moment resisting space frame and a shear wall using the following criteria K shall be taken as 0.80.

- a. The frames and shear walls shall resist the total lateral forces in accordance with their relative rigidities considering the interaction of shearwalls and frames.
- b. The shear walls acting independently of the ductile moment resisting space frame shall resist the total required lateral forces.
- c. The ductile moment resisting space frame shall have the capacity to resist not less than 25 percent of the required lateral forces.

TABLE 2.2

AMERICAN and JAPANESE REINFORCEMENT PROPERTIES

METRIC BAR SIZE	DIAMETER (inches)	AREA (in ² in)	CLOSEST U.S. BAR	AREA (in ² in)	U.S. AREA/ METRIC AREA
D10	0.394	0.122	#3	0.110	0.90
D13	0.512	0.206	#4	0.196	0.95
D16	0.630	0.312	#5	0.307	0.98
D19	0.748	0.439	#6	0.442	1.01
D22	0.886	0.589	#7	0.601	1.02
D25	0.984	0.760	#8	0.785	1.03

TABLE 2.3
SUMMARY OF BEAM STRENGTHS

LOCATION	FLEXURAL STRENGTH (ACI)	FLEXURAL STRENGTH (RCCOLA)
+ Moment at Midspan	1561 in-k	1900 in-k
+ Moment at Support	1151 in-k	1420 in-k
- Moment at Support	2124 in-k	2137 in-k

[SHEAR STRENGTH = 70.7 kips]

TABLE 3.1
ELASTIC STIFFNESS OF FRAME ELEMENTS

ITEM	E (ksi)	A (in ²)	I (in ⁴)
Typical Column of Frame A'	3537	620	6848
Typical Beam of Frame A'	3537	*	5422
Typical Column of Frame B	3537	310	3424
Typical Beam of Frame B	3537	*	2711
Shearwall			
Level 0-1	3537	2270	2,940,000
Level 1-2	3537	2270	2,800,000
Level 2-3	3537	2270	2,650,000
Level 3-4	3537	2270	2,490,000
Level 4-5	3537	2270	2,320,000
Level 5-6	3537	2270	2,150,000
Level 6-7	3537	2270	1,970,000

* Beam Area not used with rigid diaphragm assumption

TABLE 3.2

JAPAN-USA FLEXIBILITY MATRICES
DISPLACEMENTS PER 1000 KIP FORCE AT EACH STORY

FRAME A'							
7	6	5	4	3	2	1	
29.05	25.49	21.25	16.89	12.53	8.19	3.92	7
25.49	24.39	21.03	16.84	12.51	8.18	3.92	6
21.25	21.03	19.98	16.65	12.47	8.17	3.92	5
16.89	16.84	16.65	15.60	12.28	8.13	3.91	4
12.53	12.51	12.47	12.28	11.25	7.96	3.88	3
8.19	8.18	8.17	8.13	7.96	6.95	3.73	2
3.92	3.92	3.92	3.91	3.88	3.73	2.80	1
FRAME B (Includes Wall)							
7	6	5	4	3	2	1	
13.36	10.43	7.80	5.38	3.29	1.63	0.50	7
10.43	8.50	6.50	4.57	2.84	1.42	0.44	6
7.80	6.60	5.15	3.72	2.36	1.21	0.38	5
5.38	4.57	3.72	2.81	1.86	0.97	0.31	4
3.29	2.84	2.36	1.86	1.30	0.72	0.24	3
1.63	1.42	1.21	0.97	0.72	0.44	0.16	2
0.50	0.44	0.38	0.31	0.24	0.16	0.07	1
WALL ONLY							
7	6	5	4	3	2	1	
20.70	16.24	12.00	8.17	4.92	2.39	0.72	7
16.24	12.98	9.76	6.75	4.12	2.02	0.61	6
12.00	9.76	7.52	5.32	3.31	1.65	0.51	5
8.17	6.75	5.32	3.89	2.50	1.28	0.40	4
4.92	4.12	3.31	2.50	1.70	0.91	0.30	3
2.39	2.02	1.65	1.28	0.91	0.53	0.19	2
0.72	0.61	0.51	0.40	0.30	0.19	0.08	1
TOTAL STRUCTURE = FRAME A'+B							
7	6	5	4	3	2	1	
8.531	6.841	5.183	3.632	2.259	1.140	0.357	7
6.841	5.686	4.439	3.180	2.012	1.029	0.326	6
5.183	4.439	3.612	2.680	1.739	0.906	0.291	5
3.632	3.180	2.680	2.094	1.419	0.763	0.251	4
2.259	2.012	1.739	1.419	1.034	0.590	0.202	3
1.140	1.029	0.906	0.763	0.590	0.377	0.142	2
0.357	0.326	0.291	0.251	0.202	0.142	0.068	1

TABLE 3.3

COMPARISON OF EXPERIMENTAL AND ANALYTICAL FLEXIBILITY

ANALYTICAL FLEXIBILITY MATRIX OF TOTAL STRUCTURE

7	6	5	4	3	2	1	
8.531	6.841	5.183	3.362	2.259	1.140	0.357	7
6.841	5.586	4.439	3.180	2.012	1.029	0.326	6
5.183	4.439	3.612	2.680	1.739	0.906	0.291	5
3.362	3.180	2.680	2.094	1.419	0.763	0.251	4
2.259	2.012	1.739	1.419	1.034	0.590	0.202	3
1.140	1.029	0.906	0.763	0.590	0.377	0.142	2
0.357	0.326	0.291	0.251	0.202	0.142	0.068	1

EXPERIMENTAL FLEXIBILITY OF TOTAL STRUCTURE

7	6	5	4	3	2	1	
2.34	1.78	1.35	0.98	0.64	0.39	0.19	7
1.78	1.46	1.19	0.86	0.60	0.33	0.15	6
1.35	1.19	1.04	0.76	0.55	0.30	0.14	5
0.98	0.86	0.76	0.64	0.48	0.26	0.12	4
0.64	0.60	0.55	0.48	0.41	0.22	0.11	3
0.39	0.33	0.30	0.26	0.22	0.15	0.08	2
0.19	0.15	0.14	0.12	0.11	0.08	0.08	1

TABLE 4.1

THE EFFECTS OF INTRODUCING A HINGE INTO THE BASE
OF THE WALL

FLEXIBILITY OF STRUCTURE BEFORE INTRODUCTION OF HINGE

7	6	5	4	3	2	1	
8.531	6.841	5.183	3.362	2.259	1.140	0.357	7
6.841	5.586	4.439	3.180	2.012	1.029	0.326	6
5.183	4.439	3.612	2.680	1.739	0.906	0.291	5
3.362	3.180	2.680	2.094	1.419	0.763	0.251	4
2.259	2.012	1.739	1.419	1.034	0.590	0.202	3
1.140	1.029	0.906	0.763	0.590	0.377	0.142	2
0.357	0.326	0.291	0.251	0.202	0.142	0.068	1

FLEXIBILITY OF STRUCTURE AFTER INTRODUCTION OF HINGE

7	6	5	4	3	2	1	
17.84	15.42	12.95	10.45	7.93	5.41	2.90	7
15.42	13.59	11.59	9.46	7.24	4.97	2.67	6
12.95	11.59	10.09	8.36	6.47	4.47	2.41	5
10.45	9.46	8.36	7.09	5.57	3.89	2.11	4
7.93	7.24	6.47	5.57	4.49	3.20	1.75	3
5.41	4.97	4.47	3.89	3.20	2.34	1.31	2
2.90	2.67	2.41	2.11	1.75	1.31	0.76	1

TABLE 5.1

Miyagi-Oki Pulse Analysis
T=2.40 to 3.60 Seconds

ITEM	UNITS	Positive		Negative	
		Quantity	@Time=	Quantity	@Time=
<hr/>					
1 Max. Ground Acc.	%g	20.9	2.54	25.1	2.92
2 Incremental Velocity	in/sec	19.9	2.17/2.68	30.6	2.69/3.28
3 Max. Roof Disp.	in	2.65	2.68	5.68	3.24
4 Max. Drift [1]	%	0.39	2.68	0.74	3.24
5 Max. Base Shear	kips	473.0	2.52	767.0	3.12
6 Max. Base Shear A'	kips	31.0	2.68	194.0	3.16
7 Max. Base Shear B	kips	454.0	2.52	587.0	3.12
8 Max. Base Shear Wall	kips	450.0	2.52	547.0	3.12
9 Max. O.T.M.[2]	in-kips	274000	2.68	370000	3.16
10 Max. O.T.M. A'	in-kips	76100	2.68	149000	3.20
11 Max. O.T.M. B	in-kips	198000	2.68	223500	3.16
12 Max. O.T.M. Wall	in-kips	150400	2.68	156500	3.16

Notes)

[1] Drift is inter-story drift.

[2] O.T.M. means overturning moment

TABLE 5.2

Miyagi-Oki Pulse Analysis
T=7.00 to 8.20 Seconds

ITEM	UNITS	Positive		Negative	
		Quantity	@Time=	Quantity	@Time=
1 Max. Ground Acc.	%g	24.0	7.18	36.0	7.56
2 Incremental Veloc.	in/sec	34.8	6.88/7.38	25.9	7.39/7.69
3 Max. Roof Disp.	in	6.35	7.44	5.01	7.92
4 Max. Drift [1]	%	0.83	7.44	0.67	7.92
5 Max. Base Shear	kips	641.0	7.28	510.0	7.80
6 Max. Base Shear A'	kips	203.0	7.44	147.0	7.96
7 Max. Base Shear B	kips	528.0	7.28	392.0	7.80
8 Max. Base Shear Wall	kips	500.0	7.28	366.0	7.80
9 Max. O.T.M. [2]	in-kips	378250	7.44	329600	7.92
10 Max. O.T.M. A'	in-kips	153710	7.44	133400	7.92
11 Max. O.T.M. B	in-kips	224500	7.44	196200	7.92
12 Max. O.T.M. Wall	in-kips	157100	7.44	136700	7.96

Notes)

[1] Drift is inter-story drift.

[2] O.T.M. means overturning moment

TABLE 5.3

Miyagi-Oki Pulse Analysis
T=10.40 to 11.60 Seconds

ITEM	UNITS	Positive		Negative	
		Quantity	@Time=	Quantity	@Time=
1 Max. Ground Acc.	%g	28.5	10.98	33.4	10.58
2 Incremental Velocity	in/sec	25.4	10.81/11.20	35.4	10.24/10.8
3 Max. Roof Disp.	in	4.94	11.36	7.03	10.88
4 Max. Drift [1]	%	0.66	11.36	0.91	10.88
5 Max. Base Shear	kips	445.0	11.20	644.0	10.88
6 Max. Base Shear A'	kips	153.0	11.44	223.0	10.88
7 Max. Base Shear B	kips	377.0	11.20	492.0	10.64
8 Max. Base Shear Wall	kips	361.0	11.20	471.0	10.64
9 Max. O.T.M.[2]	in-kips	314700	11.36	382200	10.88
10 Max. O.T.M. A'	in-kips	126400	11.36	156400	10.88
11 Max. O.T.M. B	in-kips	190100	11.40	225800	10.88
12 Max. O.T.M. Wall	in-kips	136700	11.40	157900	10.88

Notes)

[1] Drift is inter-story drift.

[2] O.T.M. means overturning moment

TABLE 5.4

Derived Pacoima Dam Pulse Analysis
T=2.60 to 4.00 Seconds

ITEM	UNITS	Positive		Negative	
		Quantity	@Time=	Quantity	@Time=
1 Max. Ground Acc.	%g	-40.0	3.28	+34.0	2.75
2 Incremental Velocity	in/sec	51.5	3.04/3.70	54.2	2.37/3.04
3 Max. Roof Disp.	in	11.10	3.68	8.03	3.04
4 Max. Drift [1]	%	1.39	3.68	1.02	3.04
5 Max. Base Shear	kips	749.0	3.44	868.0	2.84
6 Max. Base Shear A'	kips	277.0	3.68	241.0	3.04
7 Max. Base Shear B	kips	657.0	3.36	669.0	2.84
8 Max. Base Shear Wall	kips	648.0	3.36	614.0	2.84
9 Max. O.T.M.[2]	in-kips	395000	3.68	384000	3.04
10 Max. O.T.M. A'	in-kips	163000	3.68	159000	3.04
11 Max. O.T.M. B	in-kips	233000	3.68	225000	3.04
12 Max. O.T.M. Wall	in-kips	165000	3.68	159000	3.04

Notes)

[1] Drift is inter-story drift.

[2] O.T.M. means overturning moment

TABLE 5.5
COMPARISON OF MD and DPD RESPONSE

ITEM	MD		DPD	
	Quantity	@Time=	Quantity	@Time=
Duration(sec)	12	-	4	-
Max Acceleration (%g)	36	7.56	40	3.28
Max Inc. Velocity (in/sec)	35.4	10.24/10.80	54.2	2.37/3.04
Max Roof Displacement (in)	7.03	10.88	11.1	3.68
Max Drift (%)	0.91	10.88	1.39	3.68
Maximum Base Shear (Kips)	767	3.12	868	2.84
Max Base Shear Frame A'	223	10.88	277	3.68
Max Base Shear Frame B	587	3.12	669	2.84
Max Base Wall Shear	547	3.12	648	3.36
Maximum OTM [1] (in-k)	382200	10.88	395000	3.68
Maximum OTM Frame A'	156400	10.88	163000	3.68
Maximum OTM Frame B	225800	10.88	223000	3.68
Maximum OTM Wall	157900	10.88	165000	3.68
No. of Yield Reversals	2+	-	1	-
Max Beam +PHR [2] (rad)	.0053	10.88	.0124	3.70
Max Beam -PHR	.0087	10.88	.0163	3.70
Max Wall PHR	.0056	10.88	.0100	3.70

[1] OTM means Overturning Moment

[2] PHR means Plastic Hinge Rotation

TABLE 5.6
AVAILABLE SECTION CURVATURE DUCTILITY

ITEM	CURVATURE DUCTILITY
Beam Negative Moment	8.4
Beam Positive Moment	35.0
Column at N=130 kips	4.9
Column at N=195 kips	3.8
Column at N=260 kips	3.0
Column at N=325 kips	2.4
Shearwall at N=700 kips	18.9

TABLE 5.7
DUCTILITY DEMANDS FOR THE DPD ANALYSIS

ITEM	M (in-kips)	ϕ_y (rad/inch)	θ (rad)	L (inches)	μ_{ed}	μ_s	$V_{max}/V_{F_c}^1$
Center Bay of Frame A'							
+ Moment	1004.0	0.000134	0.0108	10.63	8.60	35.0	2.17
- Moment	2049.0	0.000179	0.00739	10.12	5.60	8.40	
Ext. Bay of Frame B							
+ Moment	1004.0	0.000134	0.0124	21.13	6.38	35.0	2.09
- Moment	2049.0	0.000179	0.0163	10.31	9.81	8.40	
Shear Wall							
	150000	0.000013	0.0101	147.80	6.26	18.9	7.65

Note:

μ_{ed} =ductility demand

μ_s =ductility supplied



*** FIGURES ***

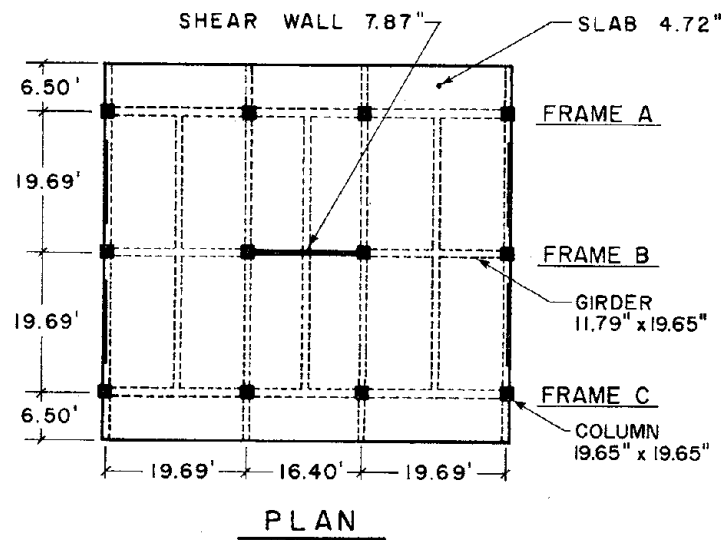


Fig. 1.1 Plan of Prototype Structure

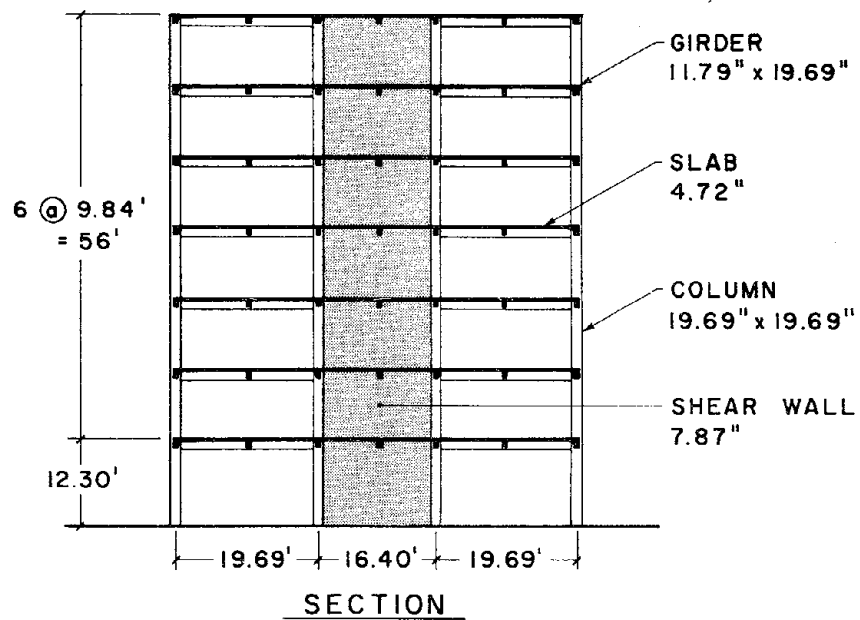


Fig. 1.2 Section of Prototype Structure

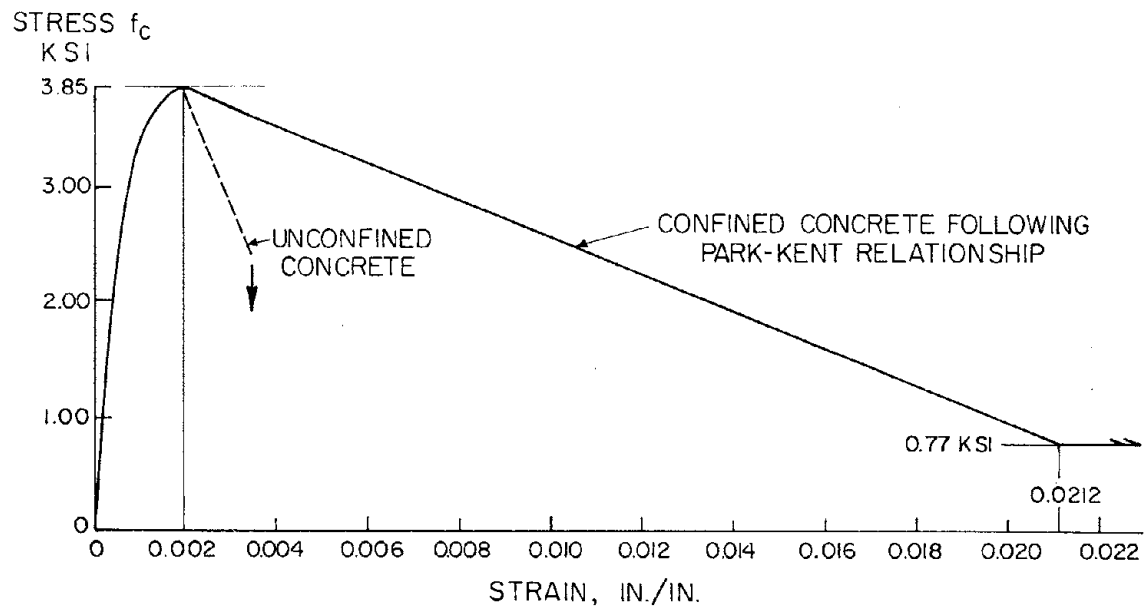


Fig. 2.1 Concrete Stress-Strain Curve

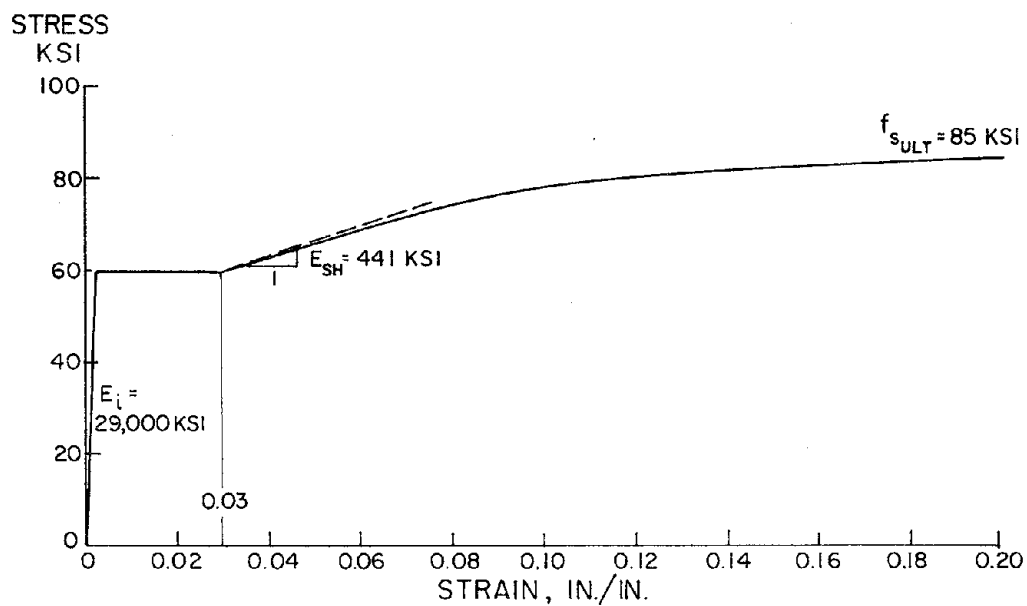


Fig. 2.2 Reinforcement Stress-Strain Curve

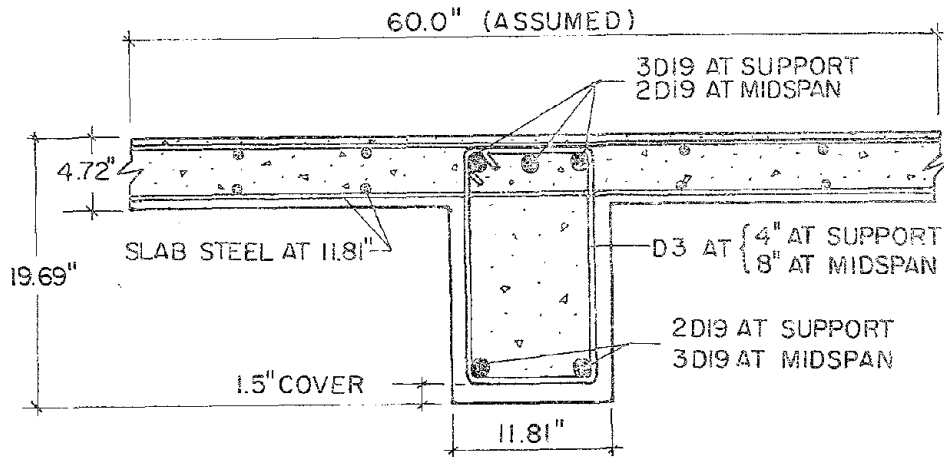


Fig. 2.3 Typical Beam Cross Section

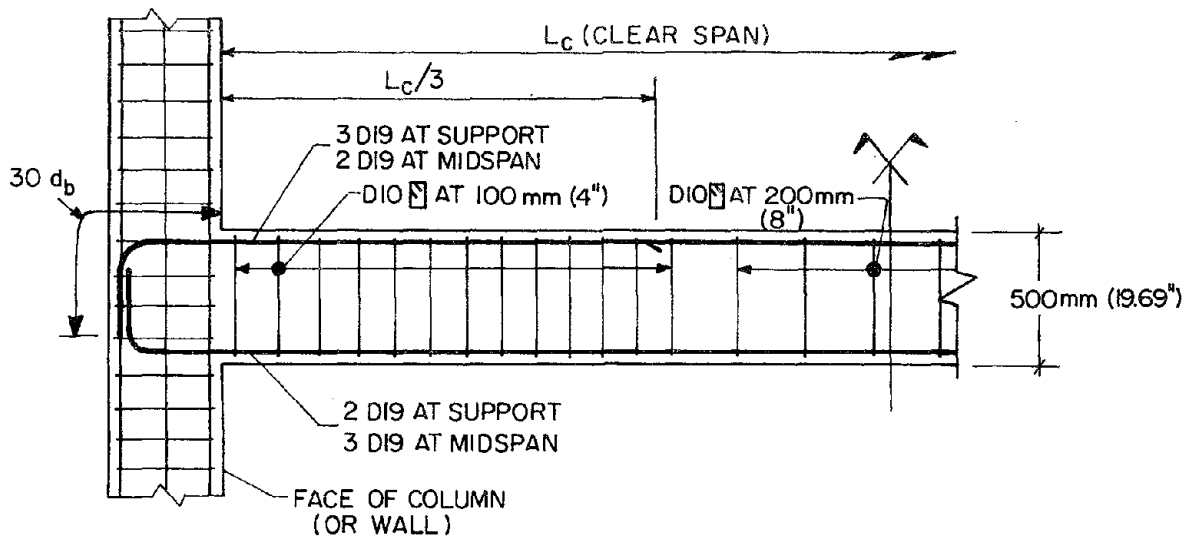


Fig. 2.4 Typical Beam Elevation

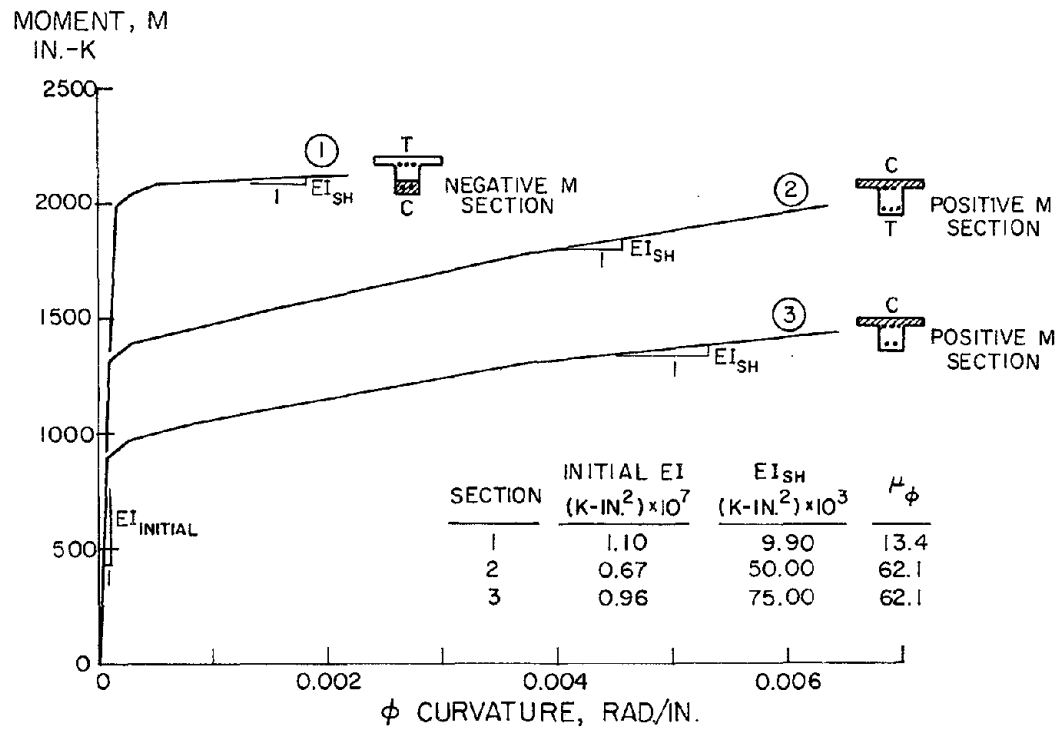


Fig. 2.5 Moment-Curvature Relationships for Typical Beam

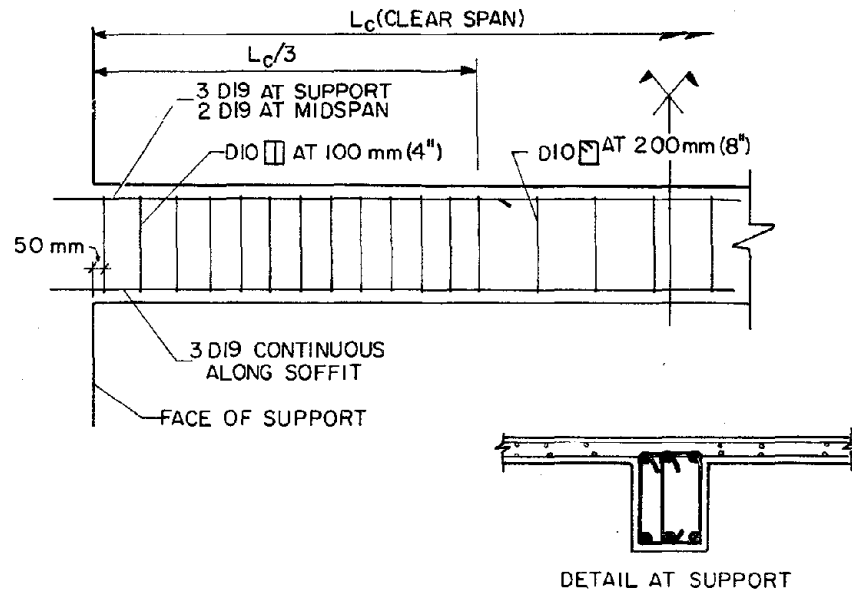


Fig. 2.6 Improved Detail for Typical Beam

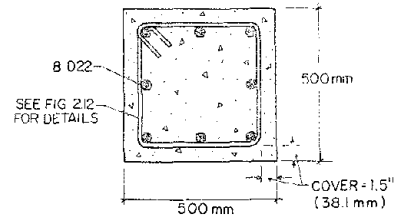


Fig. 2.7 Typical Column Cross Section

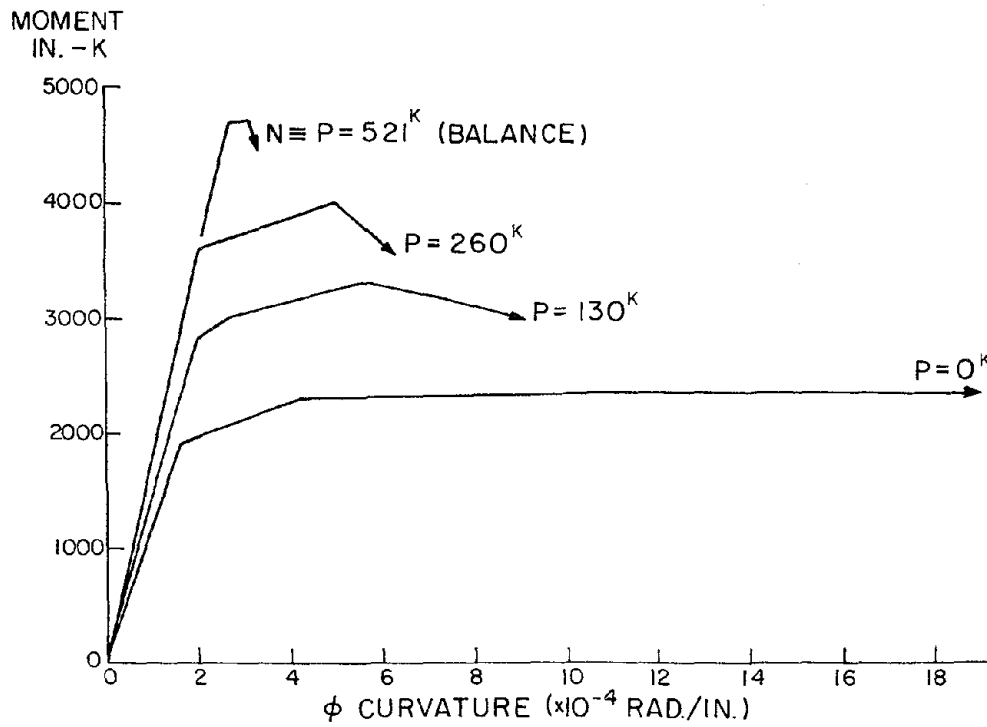


Fig. 2.8 Moment-Curvature Relationships for Typical Column

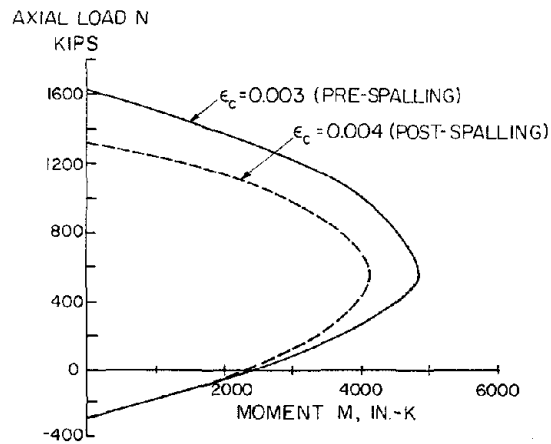


Fig. 2.9 Axial Load-Moment Interaction Diagram for Typical Column

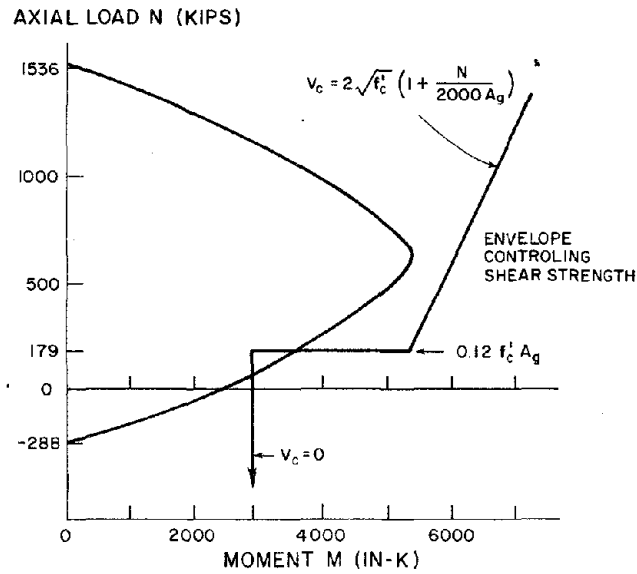


Fig. 2.10 Axial Load-Moment Controlled by Shear Strength Envelope for Typical Column

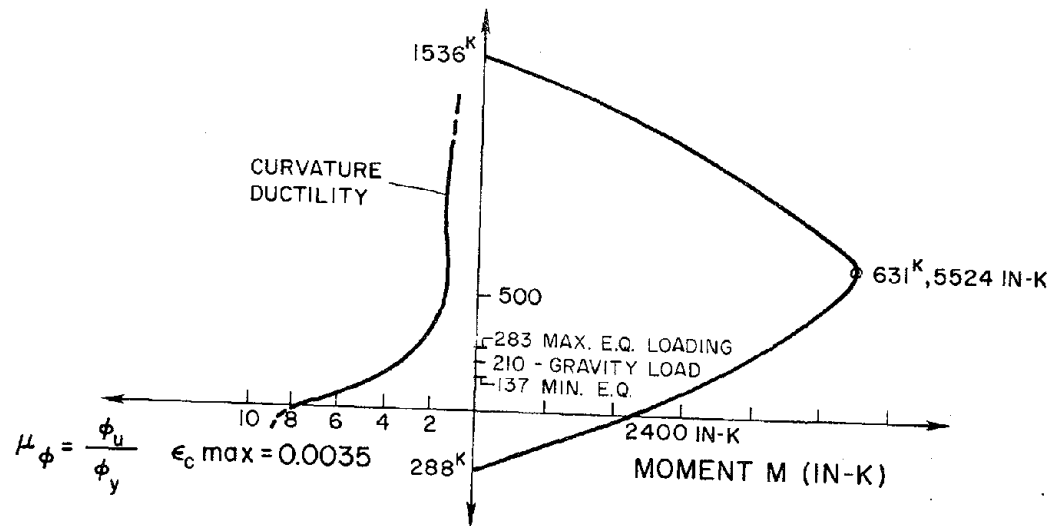


Fig. 2.11 Ductility Diagram for Typical Column

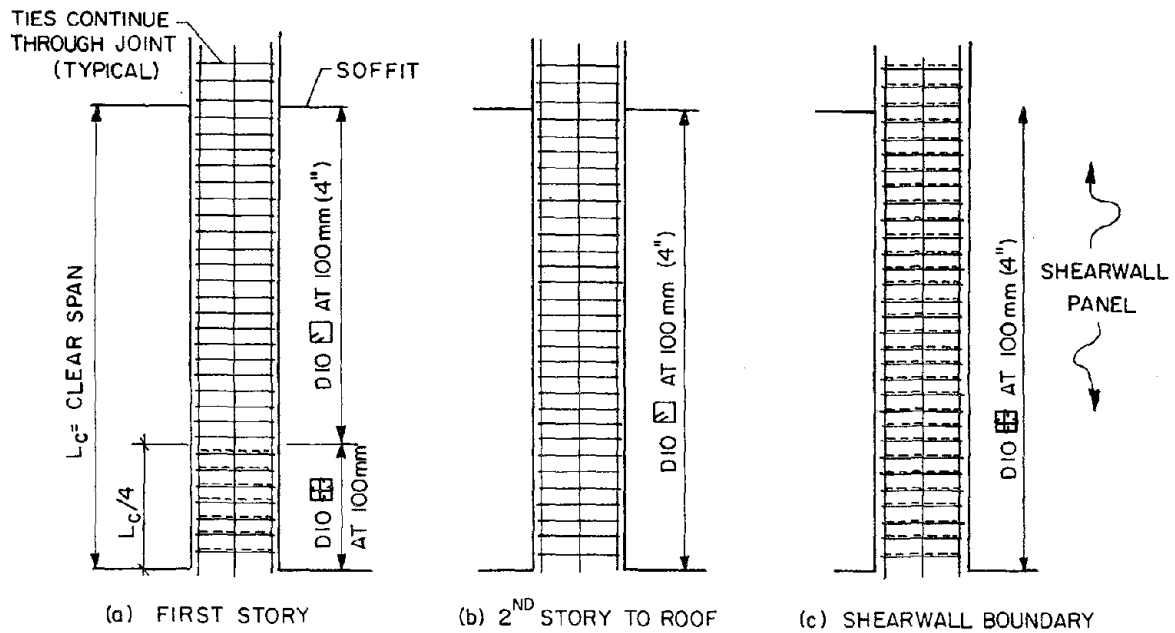


Fig. 2.12 Typical Column Tie Details

FROM THE UNIFORM BUILDING CODE:

$$S = \frac{A_{sh} f_{yh}}{0.3 f'_c h_c} \left(\frac{1}{(A_g / A_c) - 1} \right)$$

or

$$S = \frac{A_{sh} f_{yh}}{0.12 f'_c h_c}$$

Whichever is less, where

S is the required hoop spacing.

A_{sh} is the total area of hoop steel crossing a section with core dimension h_c

A_g is gross concrete area

A_c is core area

f_{yh} is yield strength of hoop steel (60 ksi)

f'_c is the 28 day concrete strength (3850 psi)

RESULTS


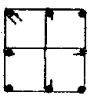

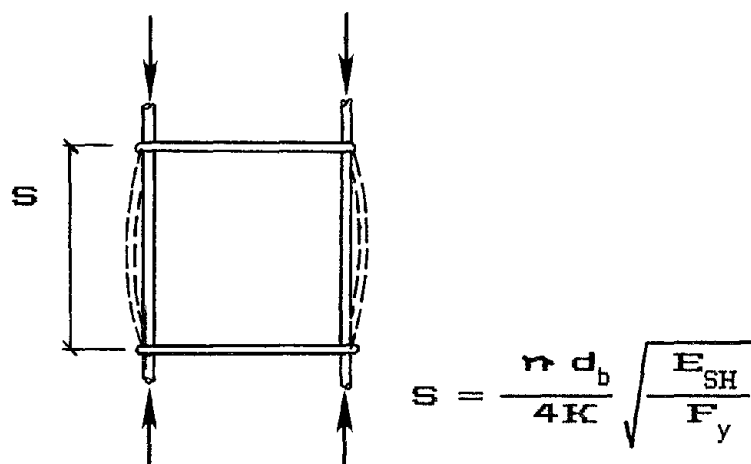
DETAIL	BAR SIZE	REQUIRED SPACING	
		inches	mm
	#3 (D10)	1.54	39
	#4 (D13)	2.80	71
	#3 (D10)	2.31	59
	#4 (D13)	4.20	107
	#3 (D10)	2.63	67
	#4 (D13)	4.87	121

Fig. 2.13 Tie Requirements According to UBC



where:

d_b = diameter of main bar (D22)

K = effective length factor (varies)

E_{SH} = strain hardening modulus for steel (500,000 psi)

F_y = steel yield strength

for $K =$	Spacing to prevent buckling =
0.5	3.96 inches
1.0	1.98 inches
2.0	1.00 inches

Fig. 2.14 Spacing of Ties to Prevent Buckling of Column Bars

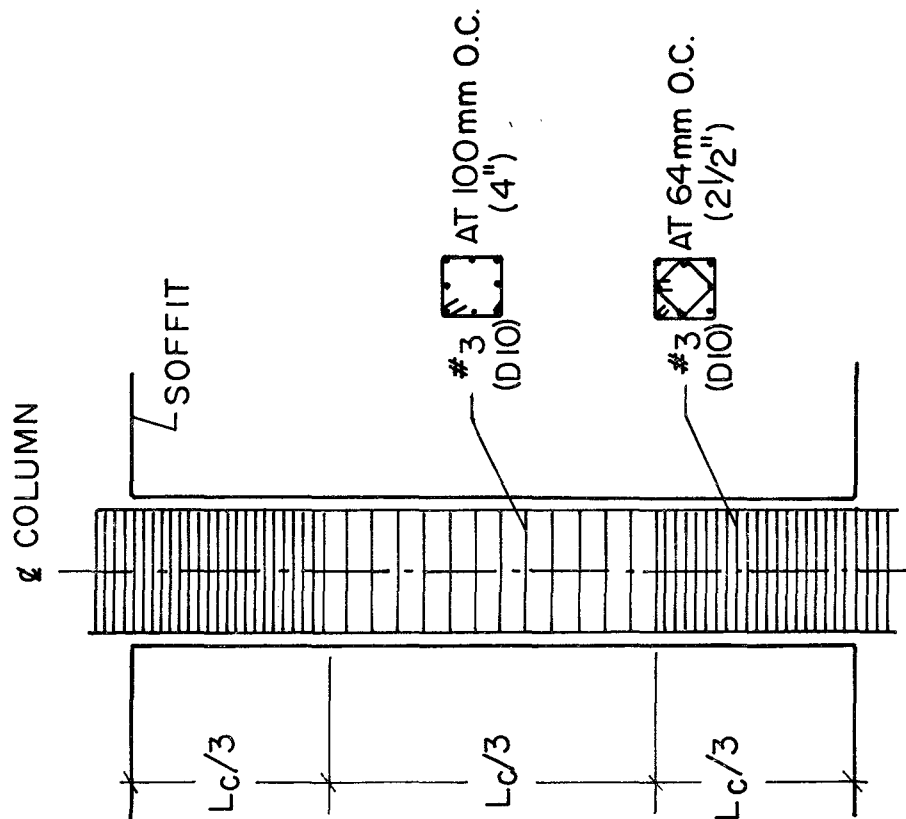


Fig. 2.15 Improved Detail for Typical Column

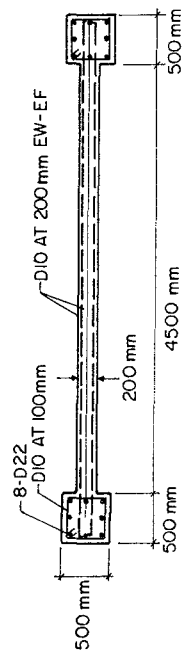


Fig. 2.16 Typical Cross-Section of Shearwall

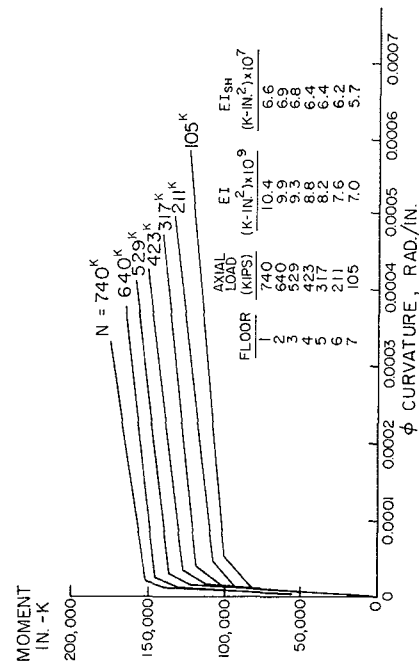


Fig. 2.17 Shearwall Moment-Curvature Diagram

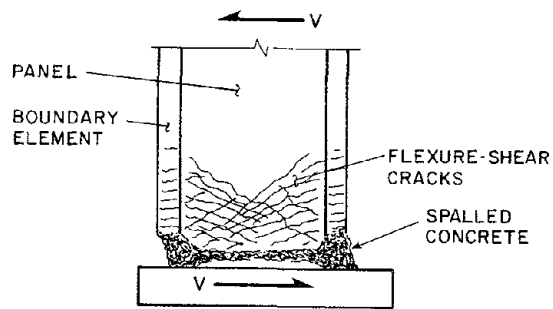


Fig. 2.18 The Mechanism of Sliding Shear Failure

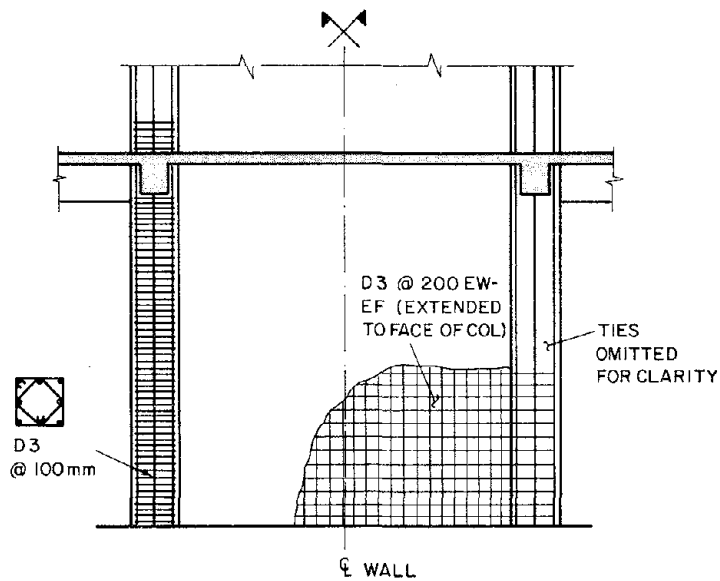


Fig. 2.19 Improved Shearwall Detail

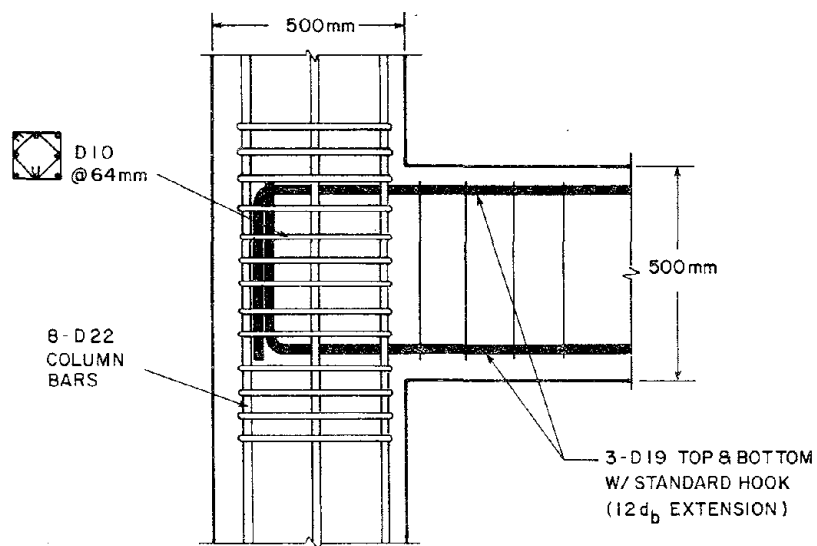
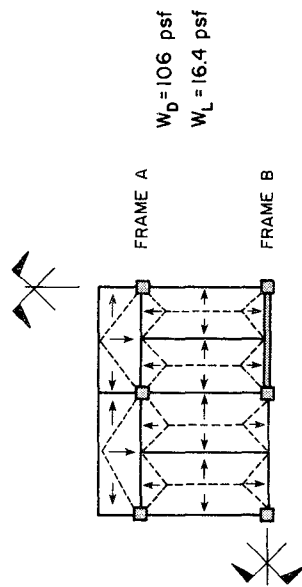
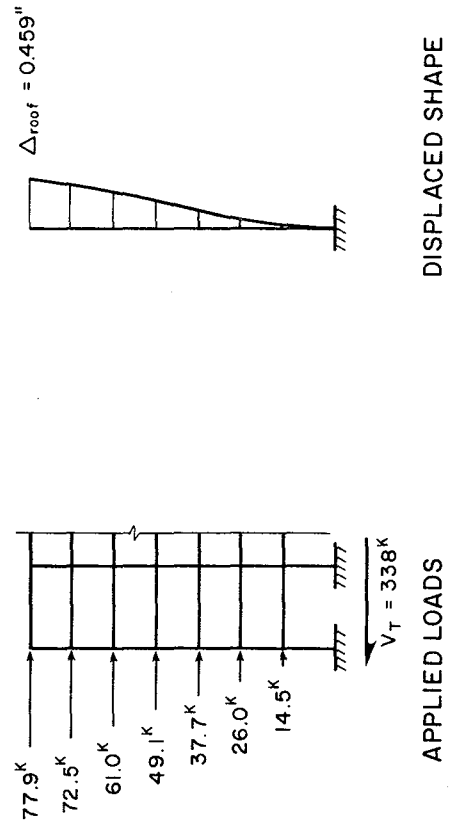
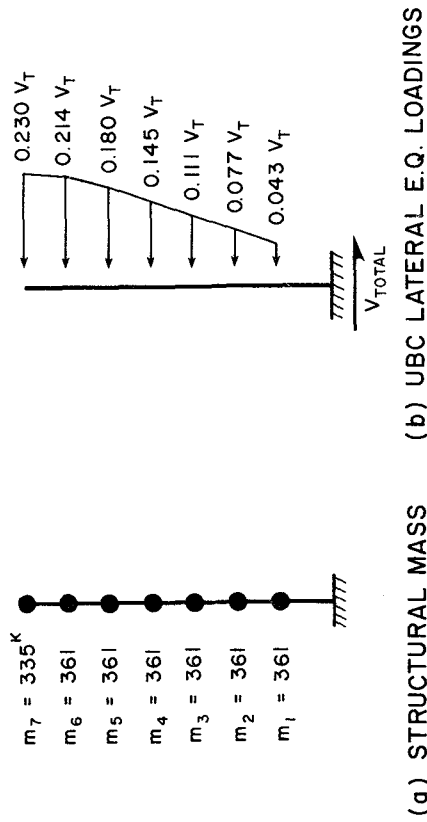


Fig. 2.20 Improved Joint Detail



TRIBUTARY AREAS FOR GRAVITY LOADING

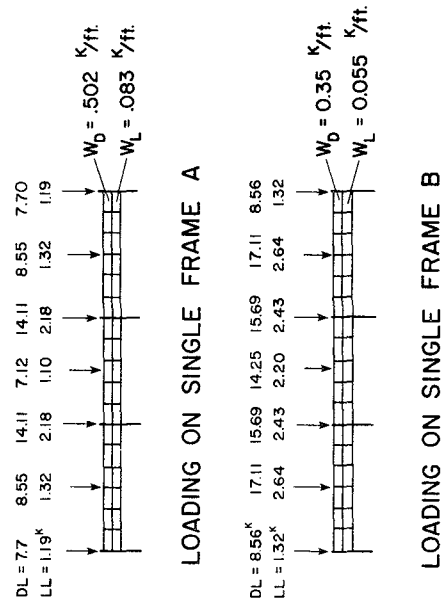
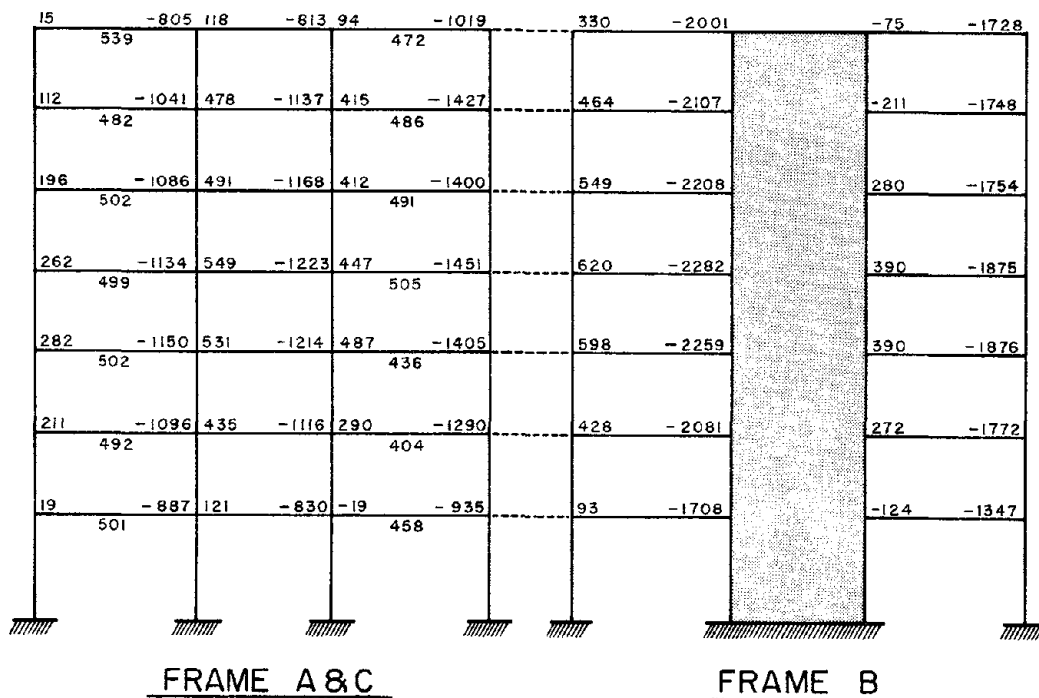
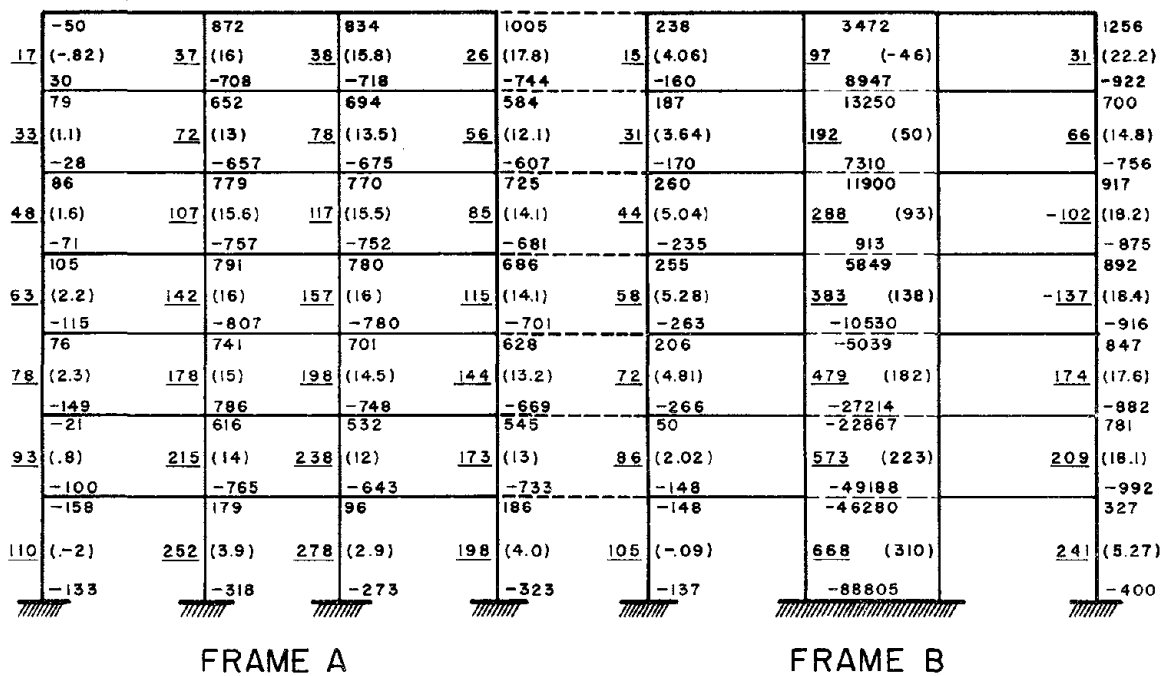


Fig. 2.21 Prototype Gravity Loading



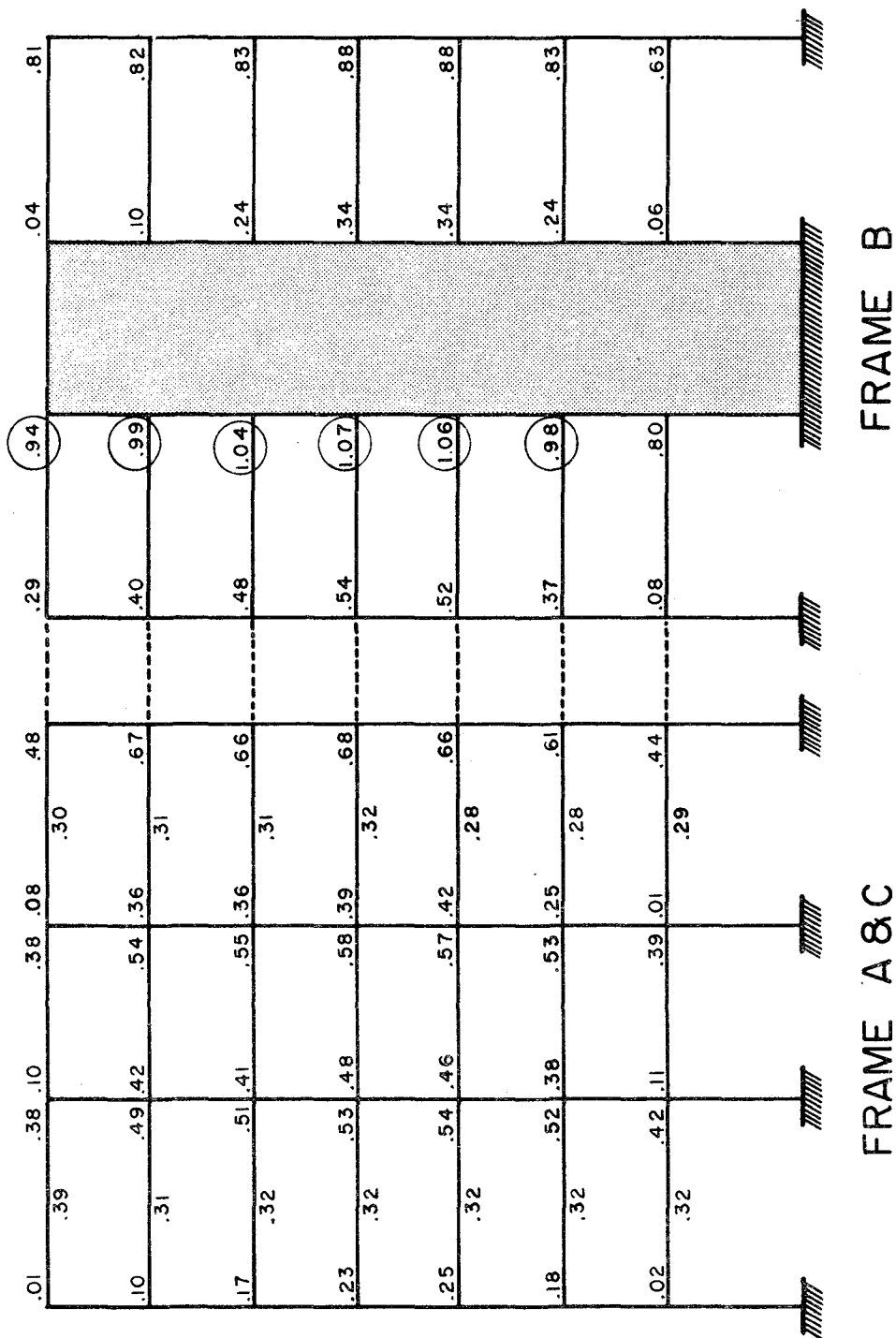
NOTE: ALL MOMENTS (IN-KIPS) ARE AT FACE OF SUPPORT EXCEPT THOSE WRITTEN BELOW BEAM WHICH ARE AT MIDSPAN, NEGATIVE MOMENTS ARE TENSION AT TOP

Fig. 2.24 Beam Moments from UBC Analysis



NOTE: UNITS ARE INCHES AND KIPS, UNDERLINED VALUES ARE AXIAL FORCES, VALUES IN PARENTHESIS ARE SHEARS, AND ALL OTHER VALUES ARE MOMENTS AT FACE OF SUPPORT

Fig. 2.25 Column Forces from UBC Analysis



NOTE: VALUES WHICH EXCEED 0.9 UBC REQUIREMENTS

Fig. 2.26 Beam Moments vs Beam Strengths from UBC Analysis

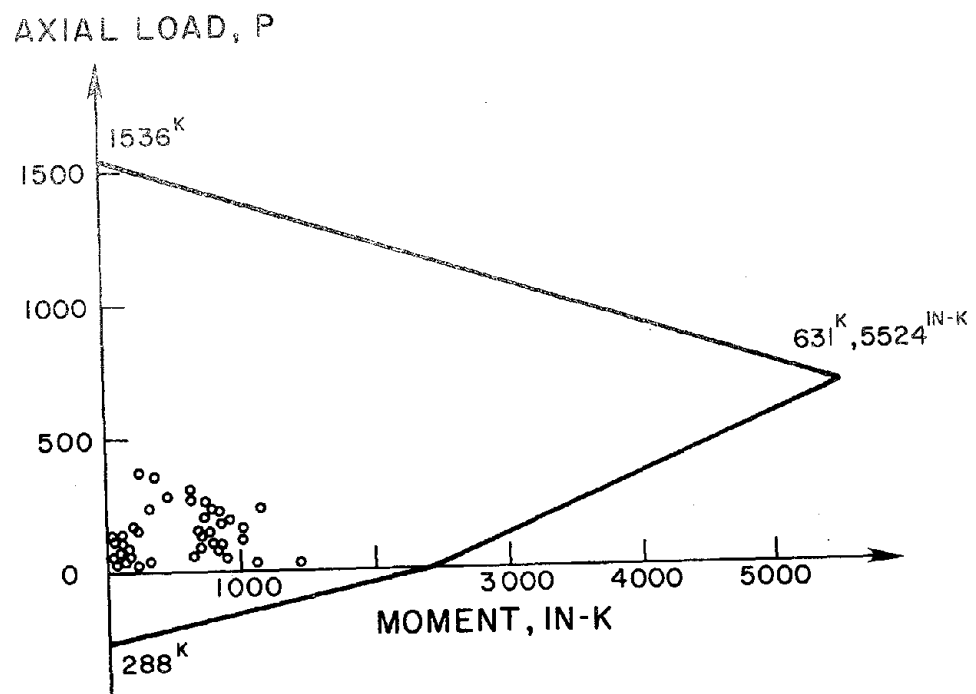


Fig. 2.27 Column Moments vs Column Strengths from UBC Analysis

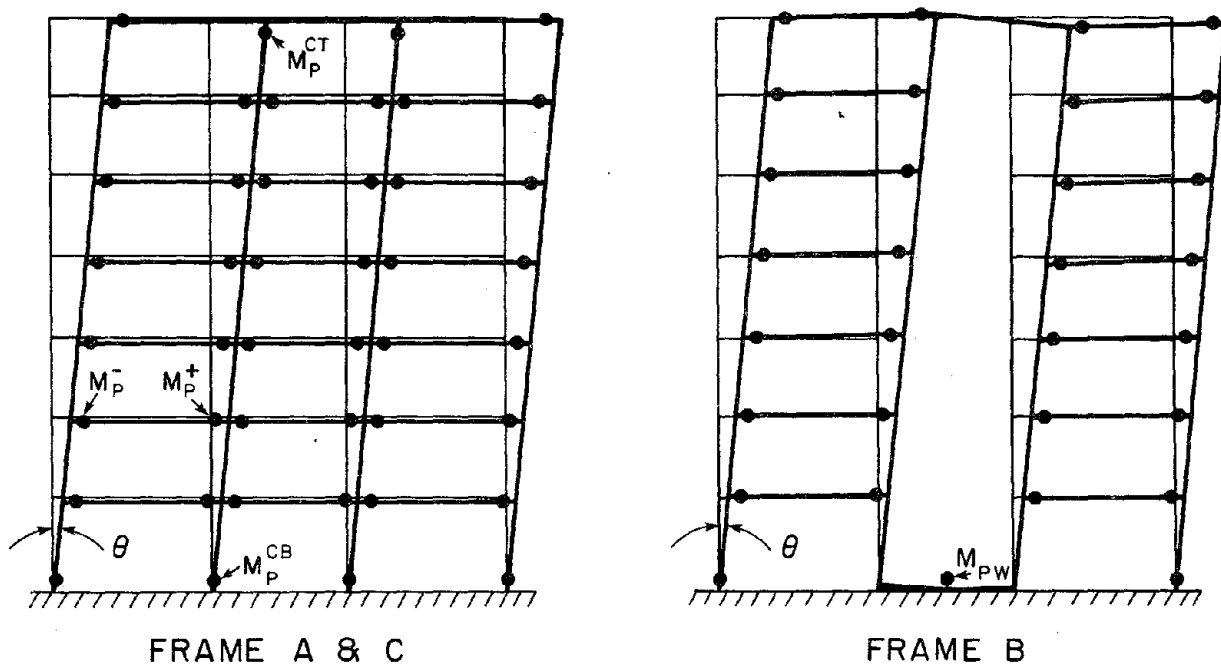


Fig. 2.28 Assumed Plastic Hinge Pattern for Strength Analysis

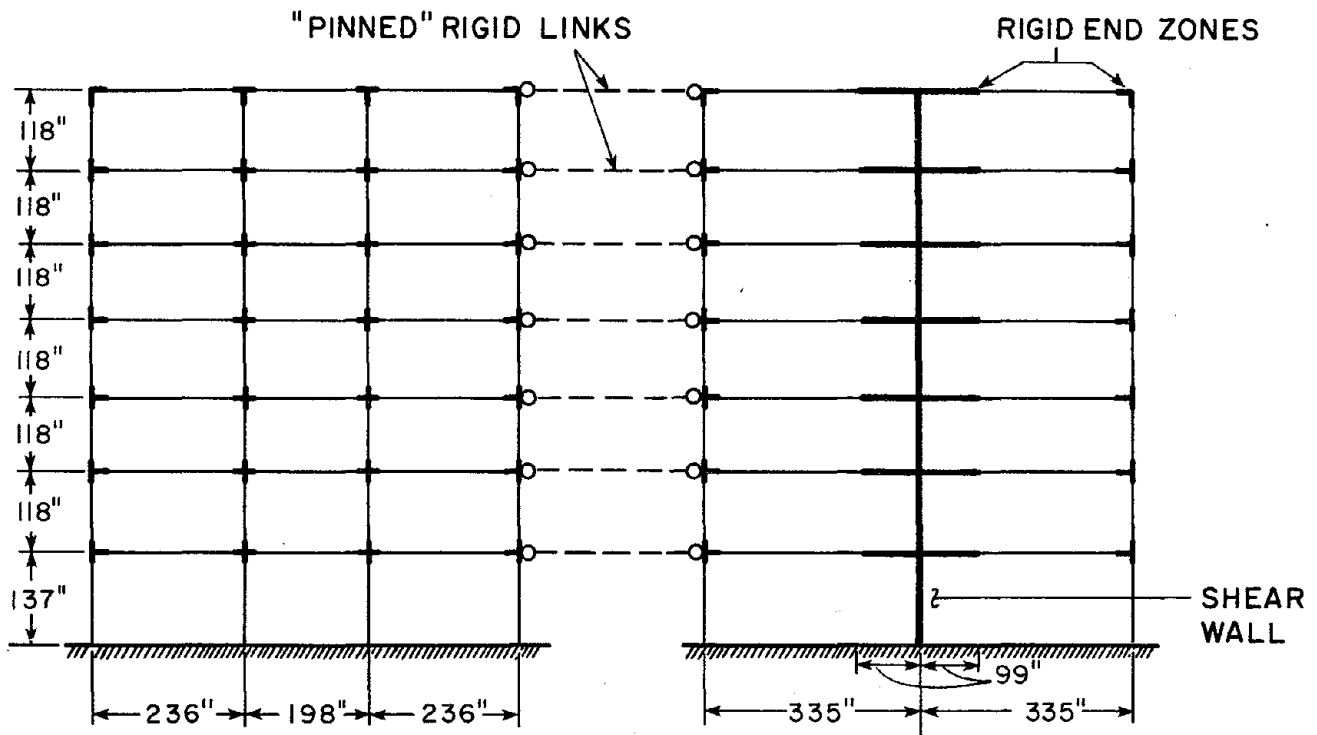


Fig. 3.1 Model of Prototype used for Linear and Nonlinear Analysis

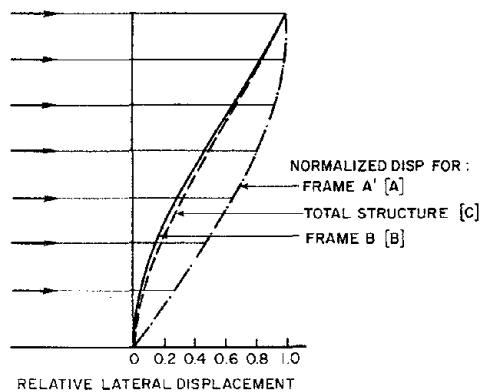


Fig. 3.2 Elastic Displacement Profiles for Component Frames

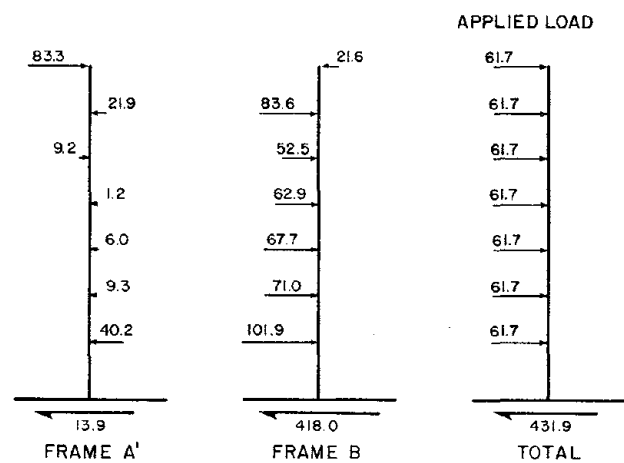


Fig. 3.3 Elastic Frame Interactive Forces

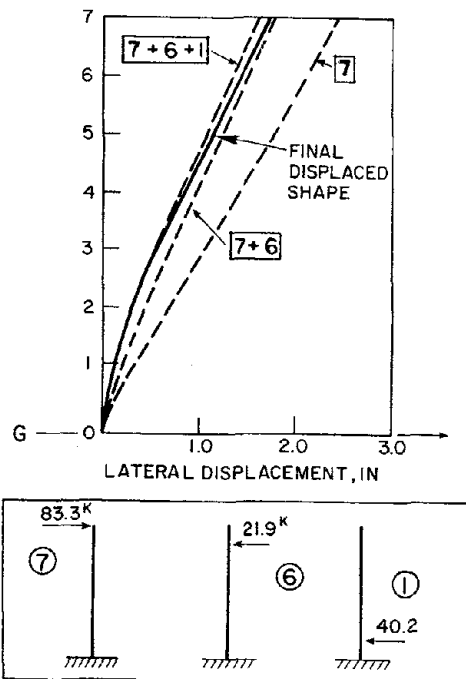


Fig. 3.4 Displacement Superposition for Interaction

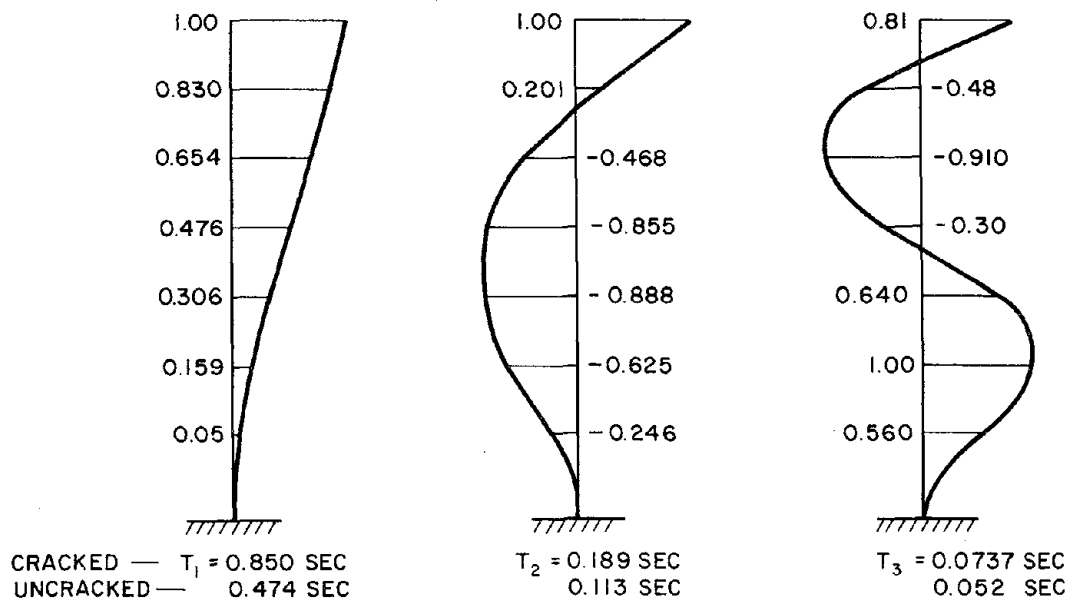


Fig. 3.5 Mode Shapes and Periods of Vibration

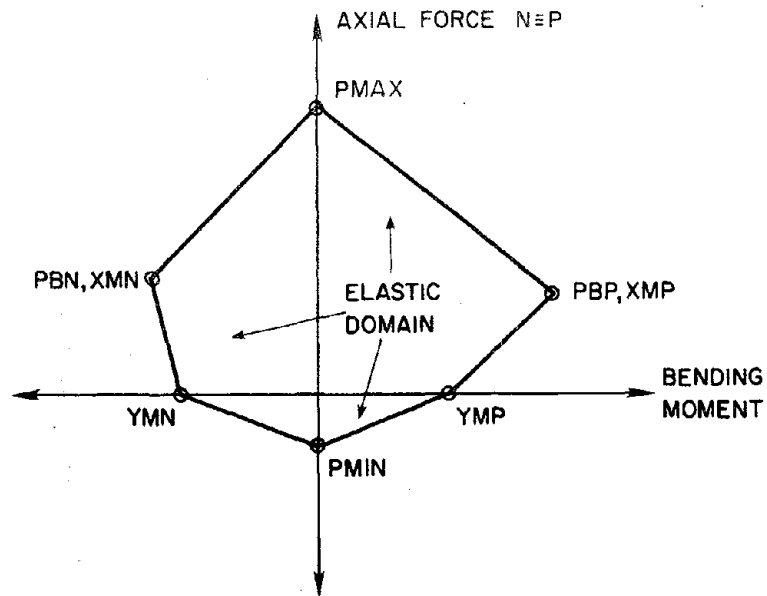


Fig. 4.1 ULARC3 Yield Surface for Beam-Columns

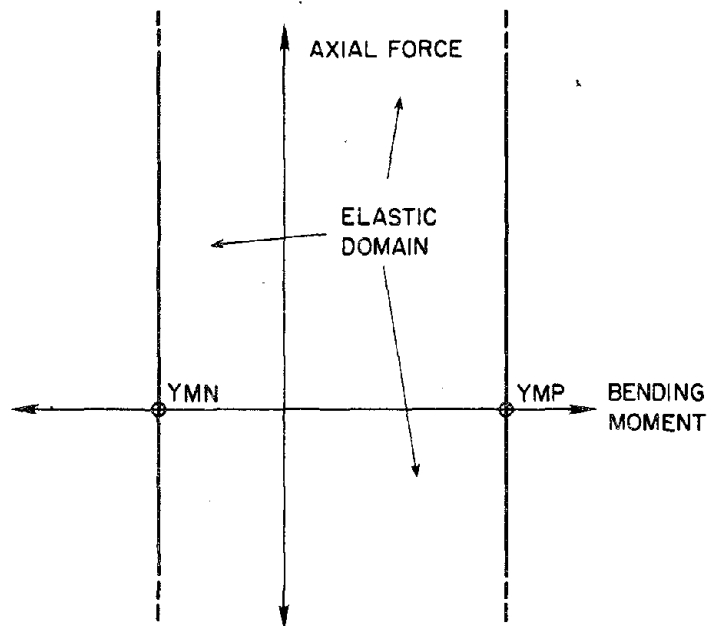


Fig. 4.2 ULARC3 Yield Surface for Beams

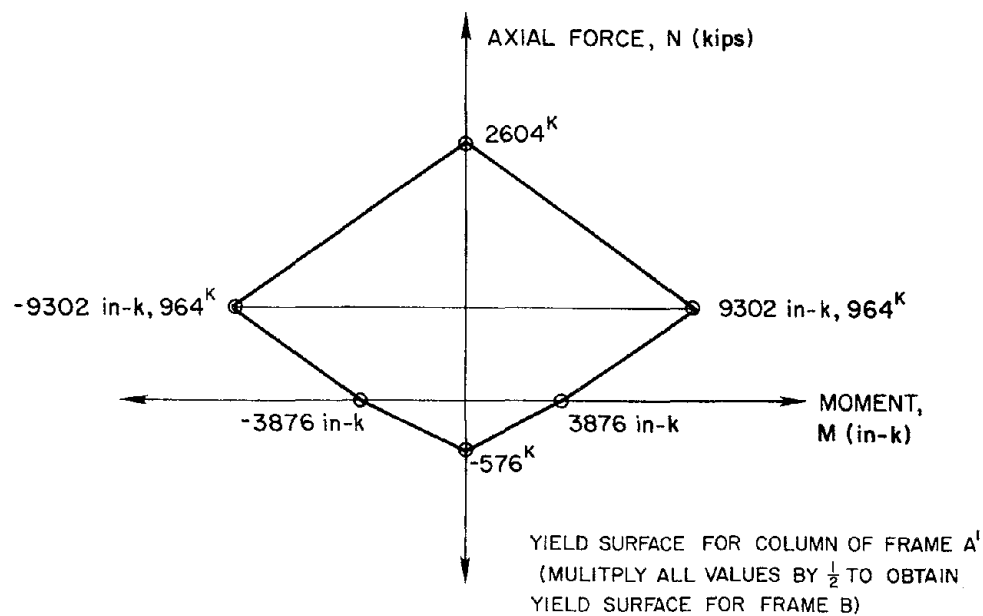


Fig. 4.3 Actual Yield Surface Used for Beam-Columns

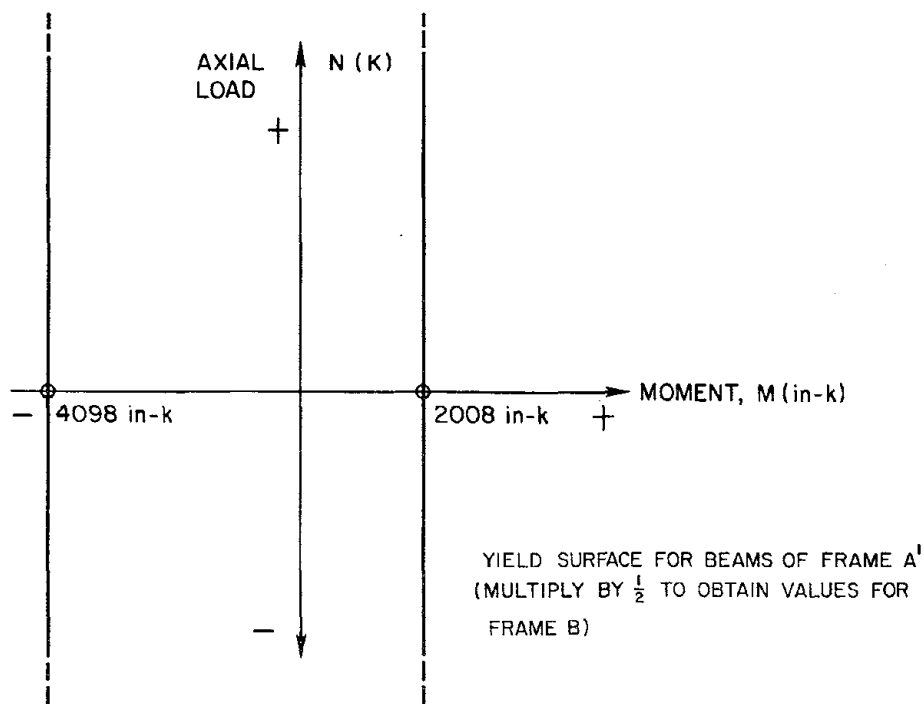


Fig. 4.4 Actual Yield Surface Used for Beams

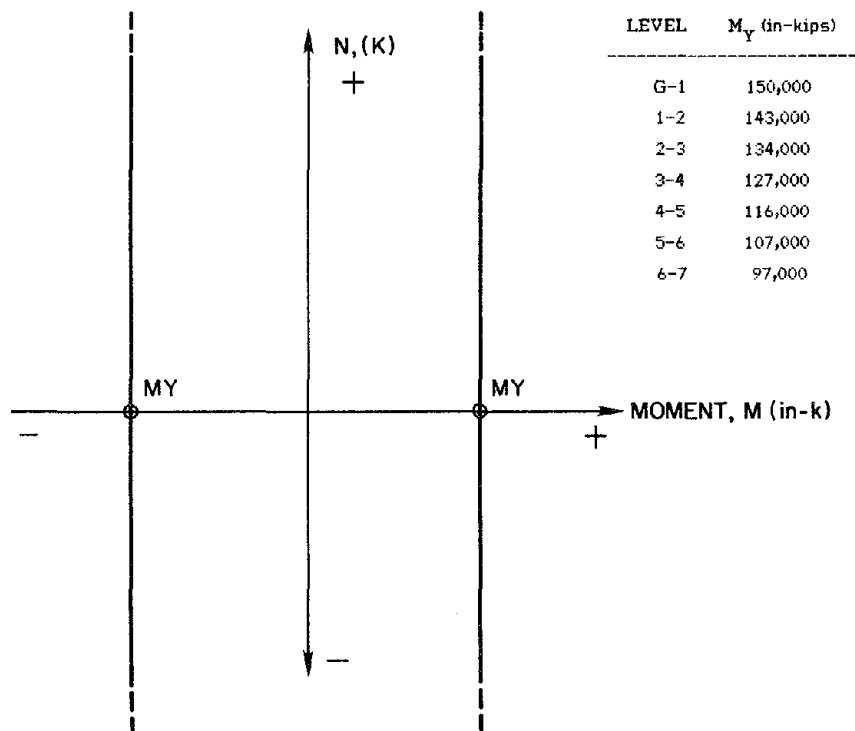


Fig. 4.5 Actual Yield Surface Used for Shearwall

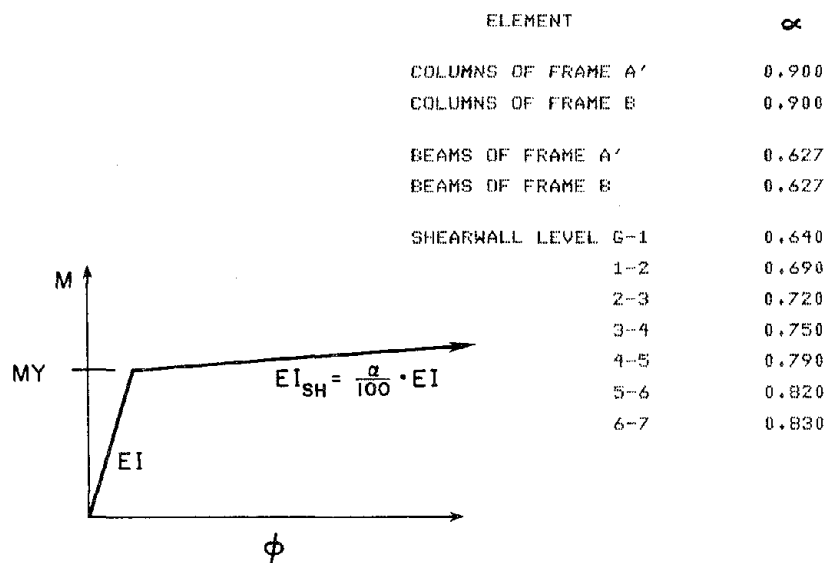


Fig. 4.6 Element Strain Hardening Parameters

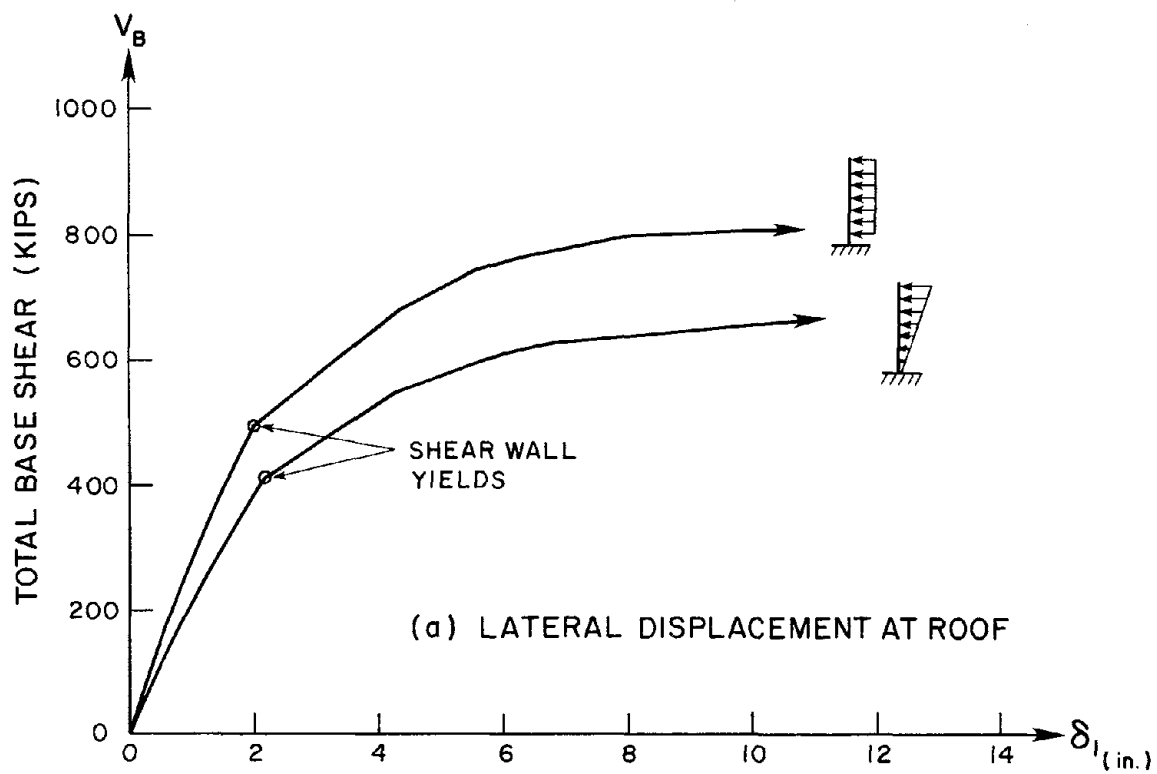


Fig. 4.7a Force vs Displacement at Roof from ULARC3 Analysis

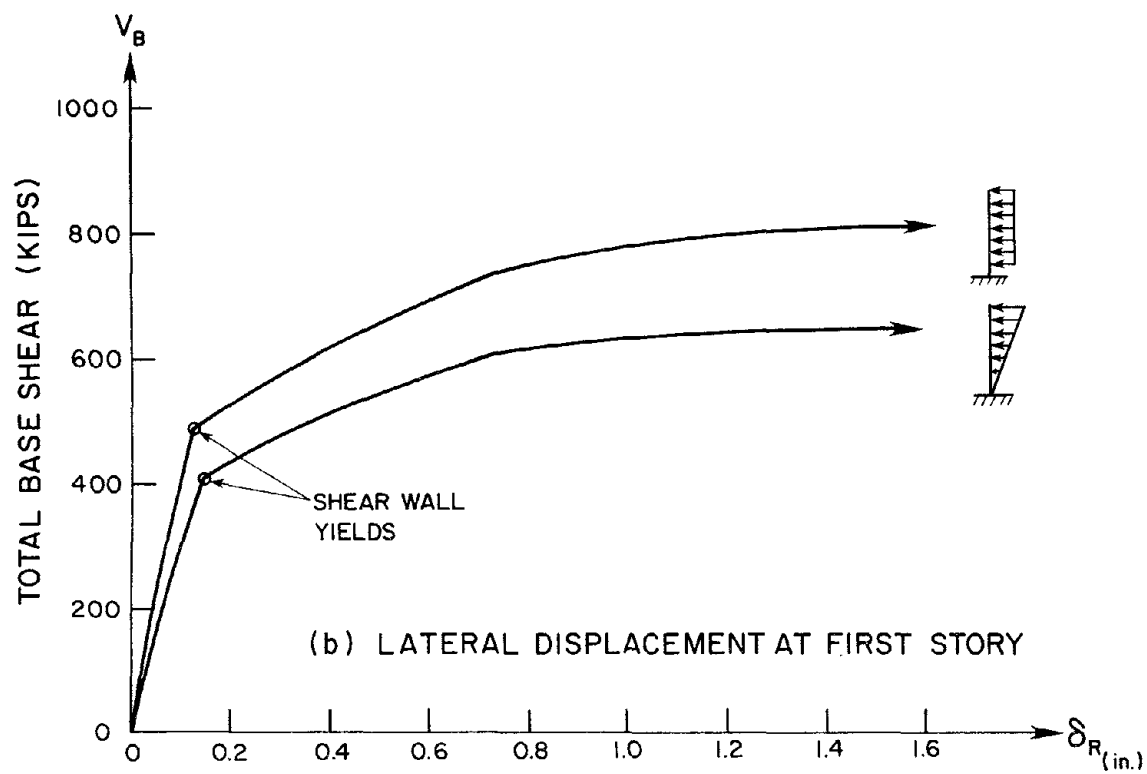


Fig. 4.7b Force vs Displacement at Level One from ULARC3 Analysis

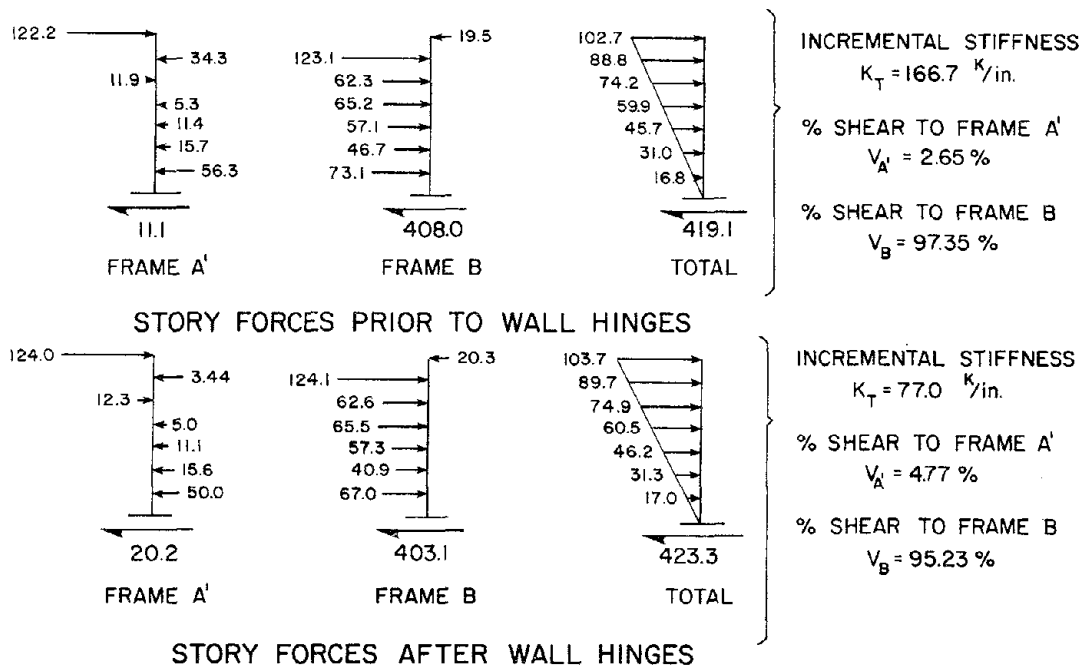


Fig. 4.8 Interactive Forces for Triangular Lateral Load from ULARC3 Analysis

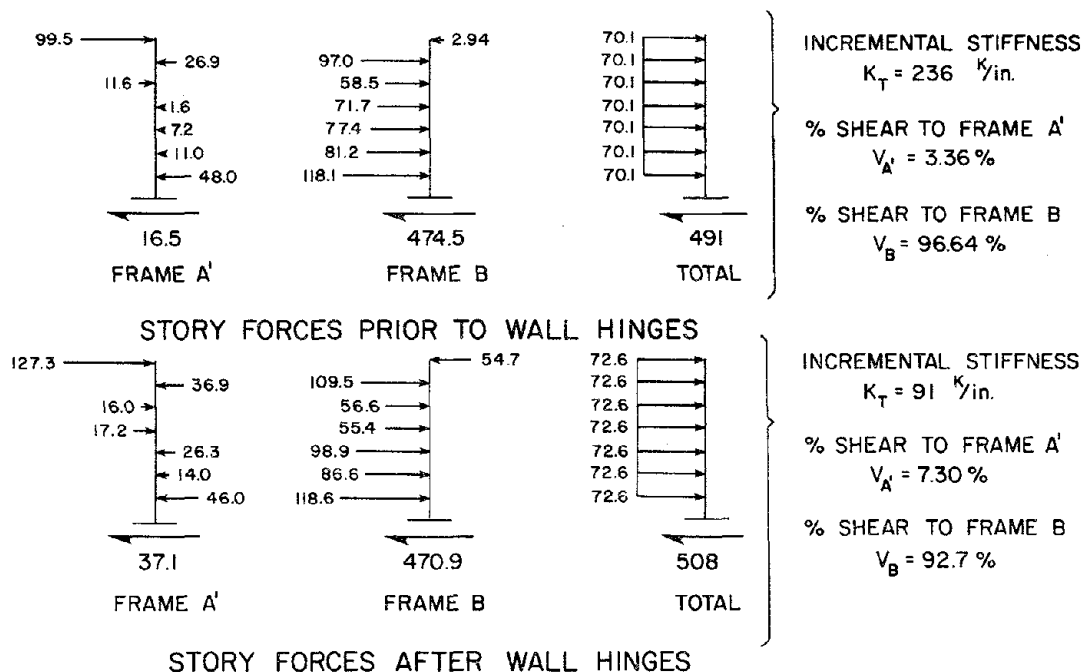


Fig. 4.9 Interactive Forces for Uniform Lateral Load from ULARC3 Analysis

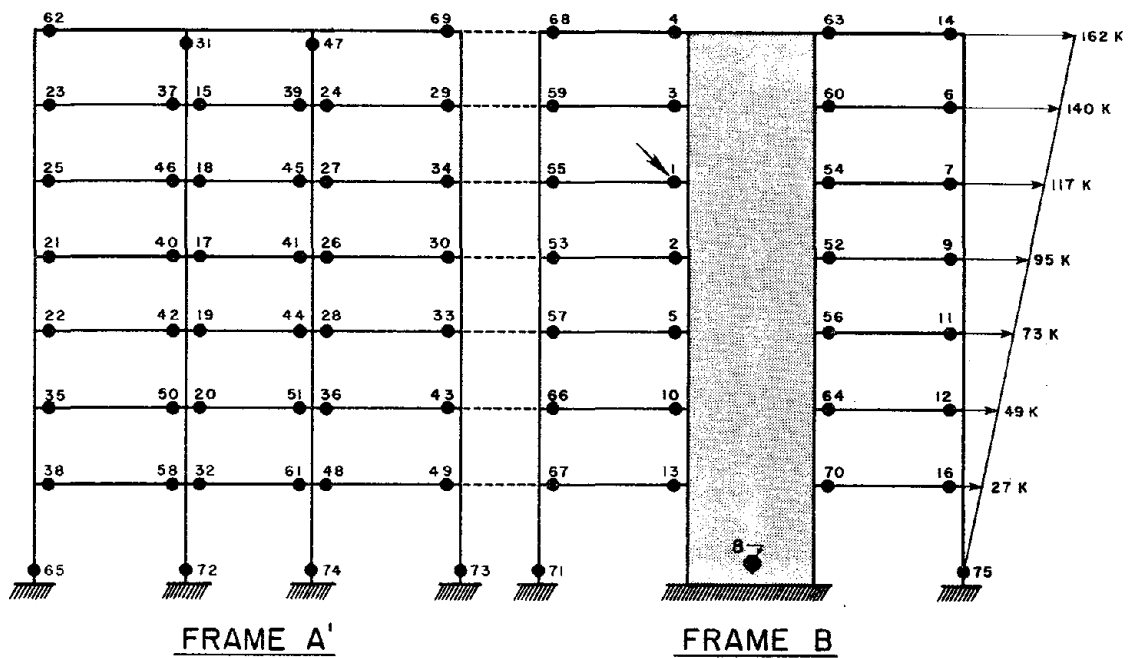


Fig. 4.10 Plastic Hinge Pattern for Triangular Lateral Loading

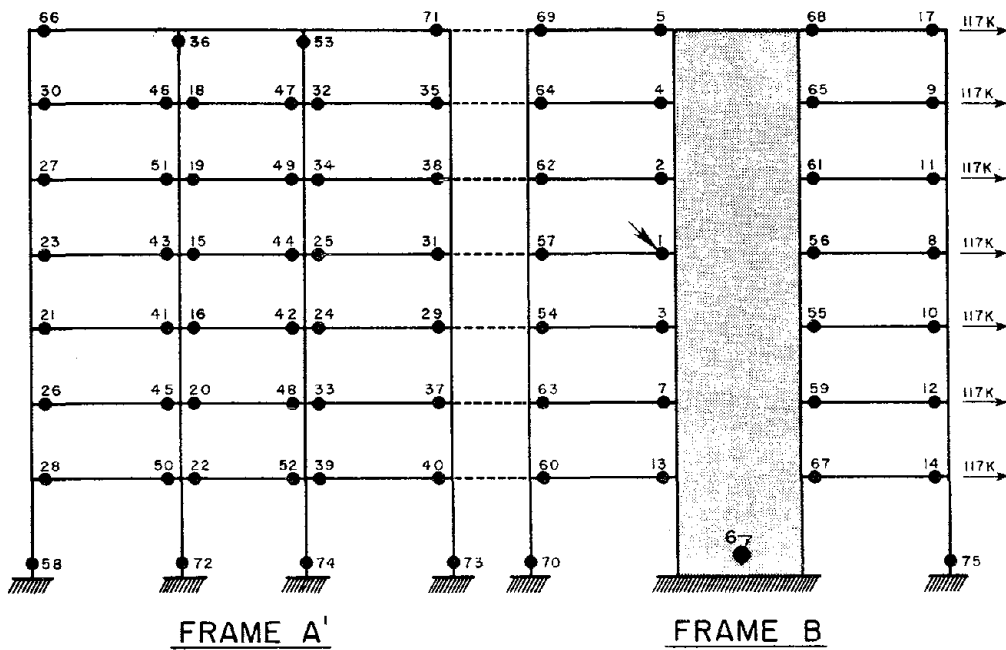
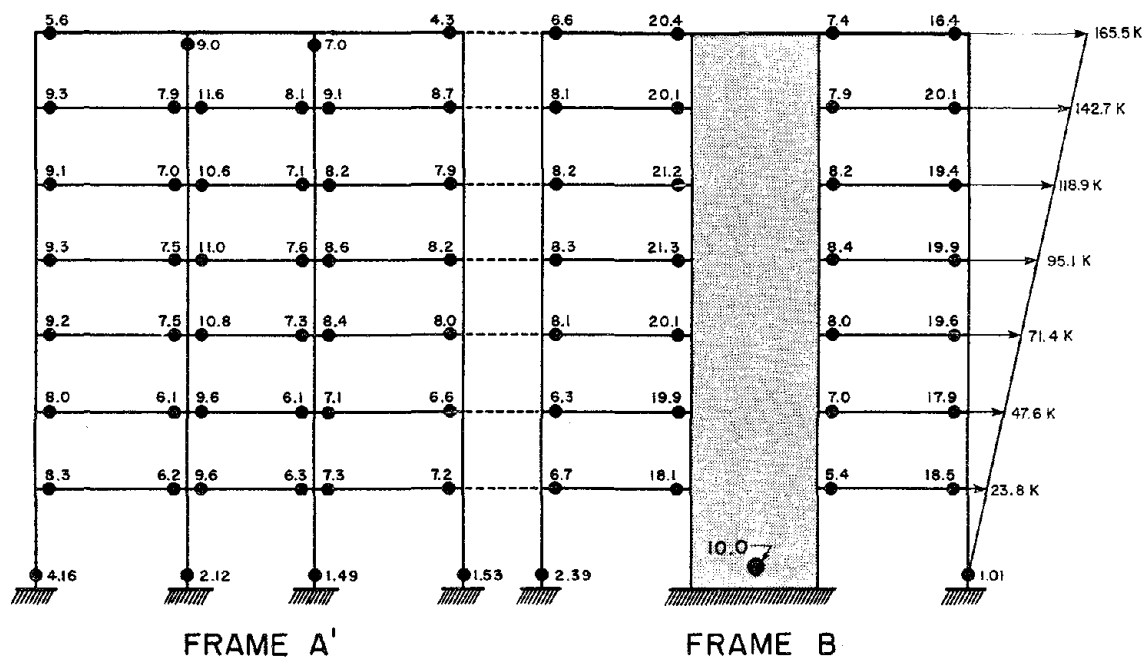


Fig. 4.11 Plastic Hinge Patterns for Uniform Lateral Loading



NOTE: DIVIDE INDICATED VALUE BY 1000 TO GET ROTATION IN RADIANS

Fig. 4.12 Maximum Plastic Hinge Rotations as a Result of Triangular Lateral Loading

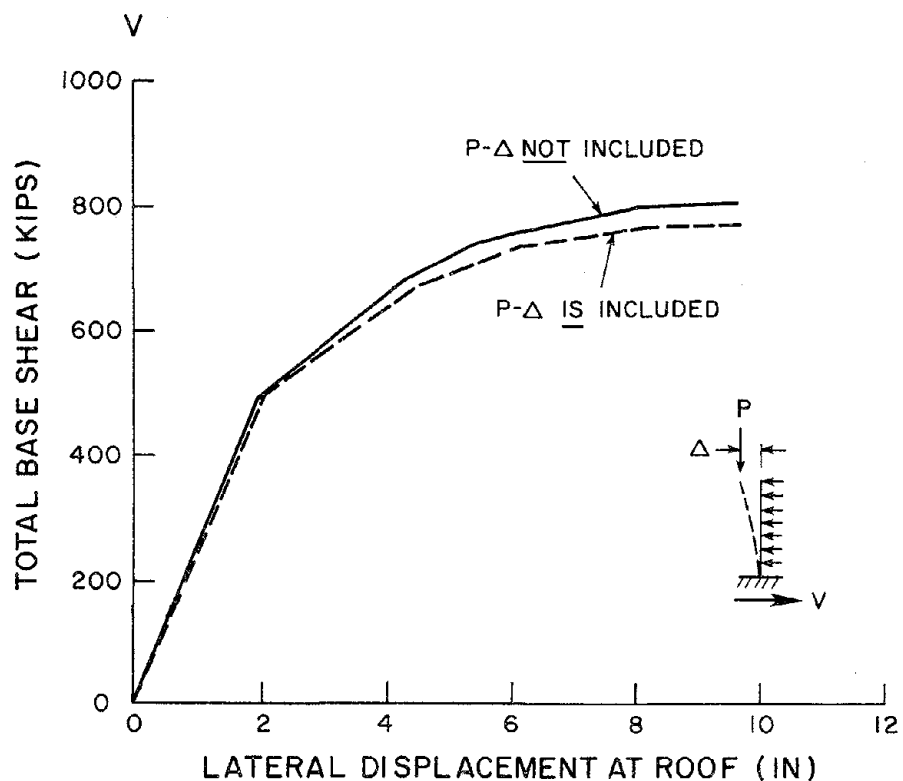
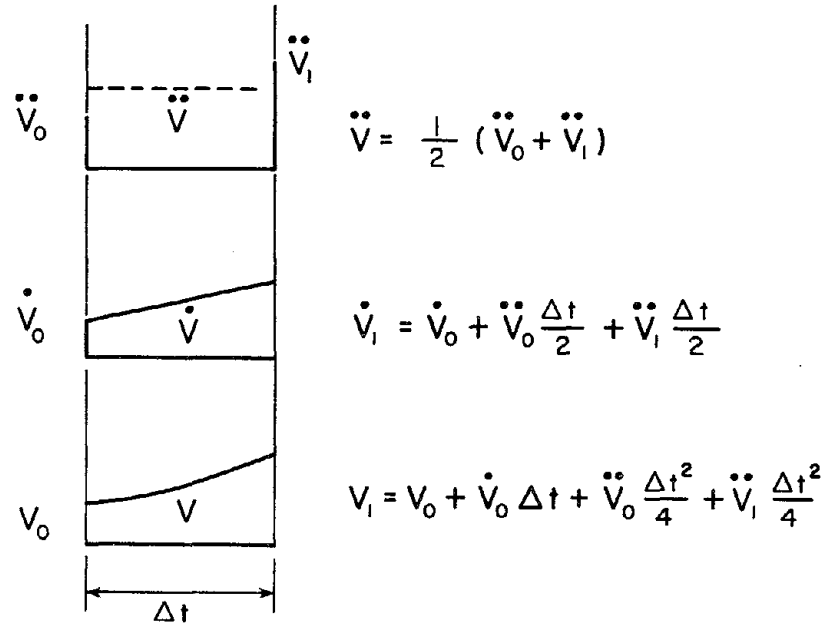


Fig. 4.13 Force vs Displacement Including P-Delta

[CONSTANT AVERAGE ACCELERATION]



$$\therefore \Delta \dot{V} = -2 \dot{V}_0 + \Delta V \frac{2}{\Delta t}$$

$$\Delta \ddot{V} = -2 \ddot{V}_0 - \dot{V}_0 \frac{4}{\Delta t} + \Delta V \frac{4}{\Delta t^2}$$

$$\text{and } K^* \Delta V = \Delta P + M \left[2 \ddot{V}_0 + \dot{V}_0 \frac{4}{\Delta t} + C 2 \dot{V}_0 \right]$$

$$\text{where } K^* = K + \frac{2}{\Delta t} C + \frac{4}{\Delta t^2} M$$

Fig. 5.1 Incremental Equations of Motion

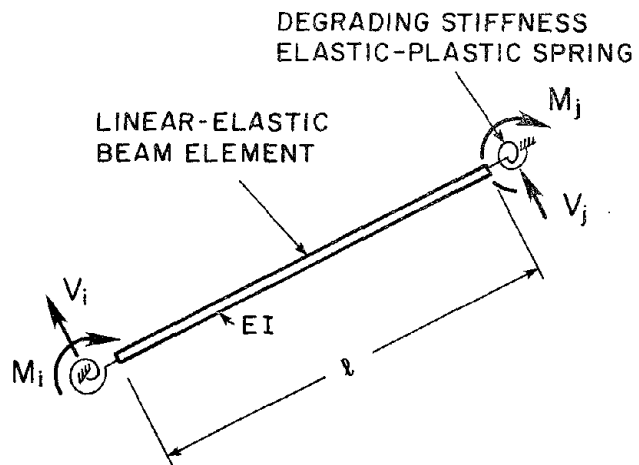


Fig. 5.2 Single Component Beam Model with Degrading Stiffness

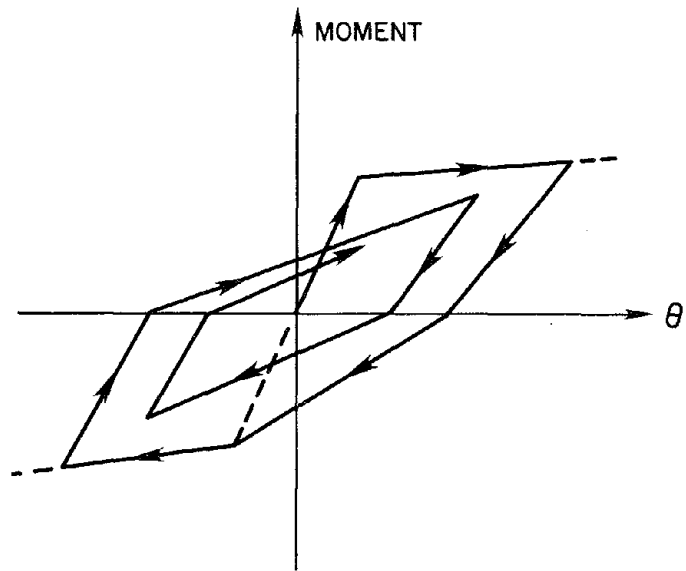


Fig. 5.3 Modified Takeda Bi-Linear Moment-Rotation Diagram

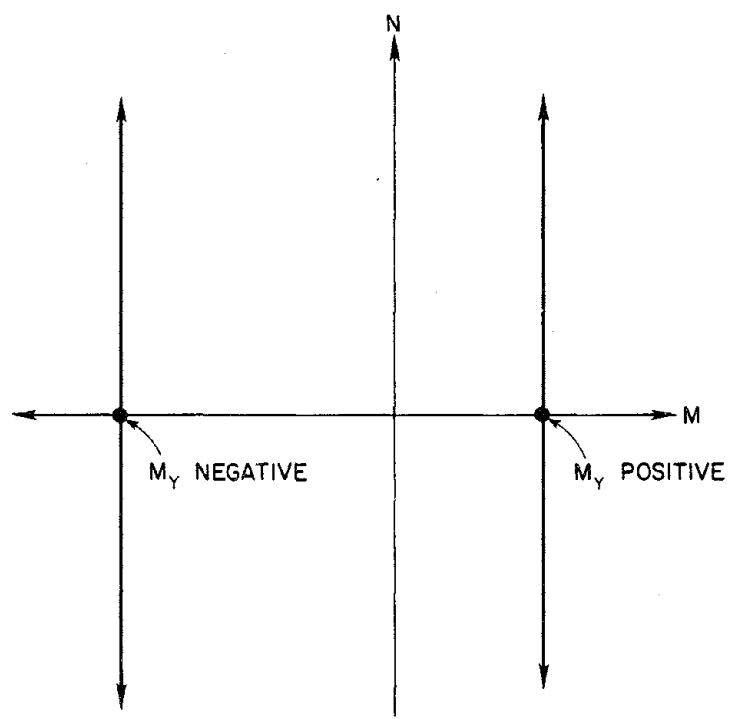


Fig. 5.4 Yield Surface for Single Component Model

ACCELERATION (PERCENT G)

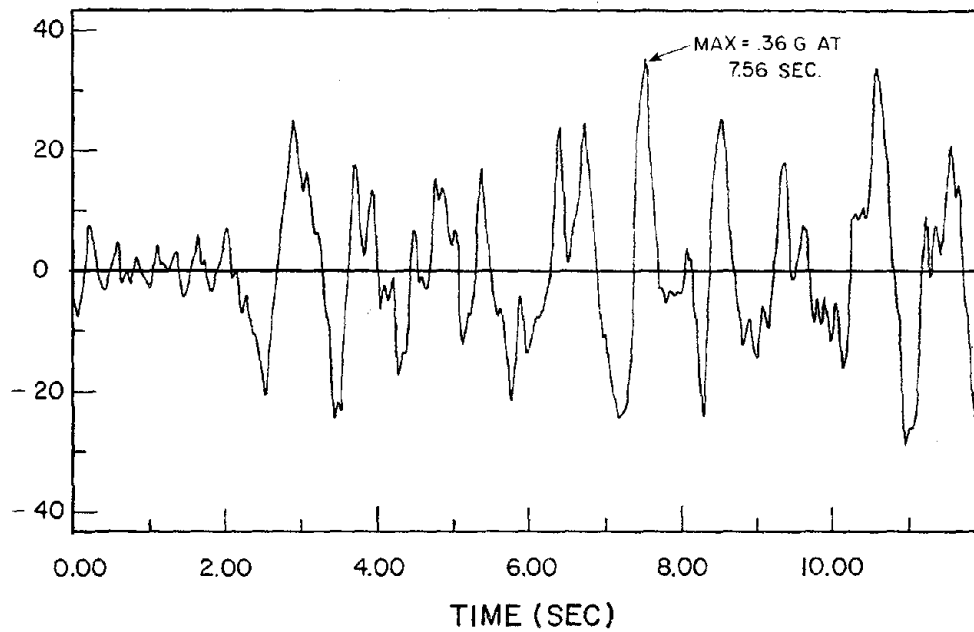


Fig. 5.5 Ground Acceleration Record for Miyagi-Oki Analysis

ACCELERATION (PERCENT G)

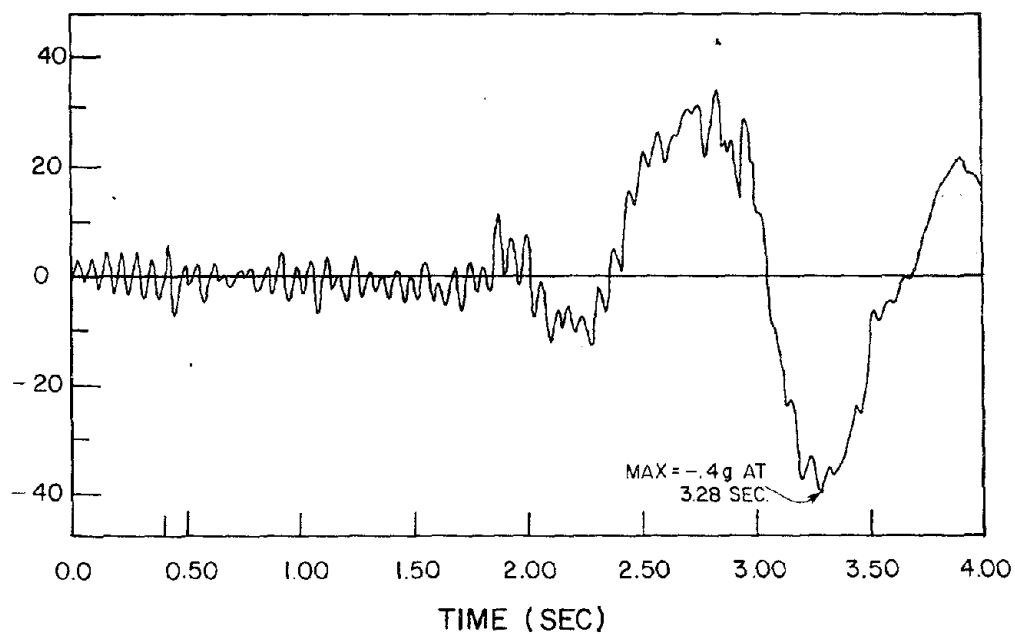


Fig. 5.6 Ground Acceleration Record for Derived Pacoima Dam Analysis

DISPLACEMENT (IN)

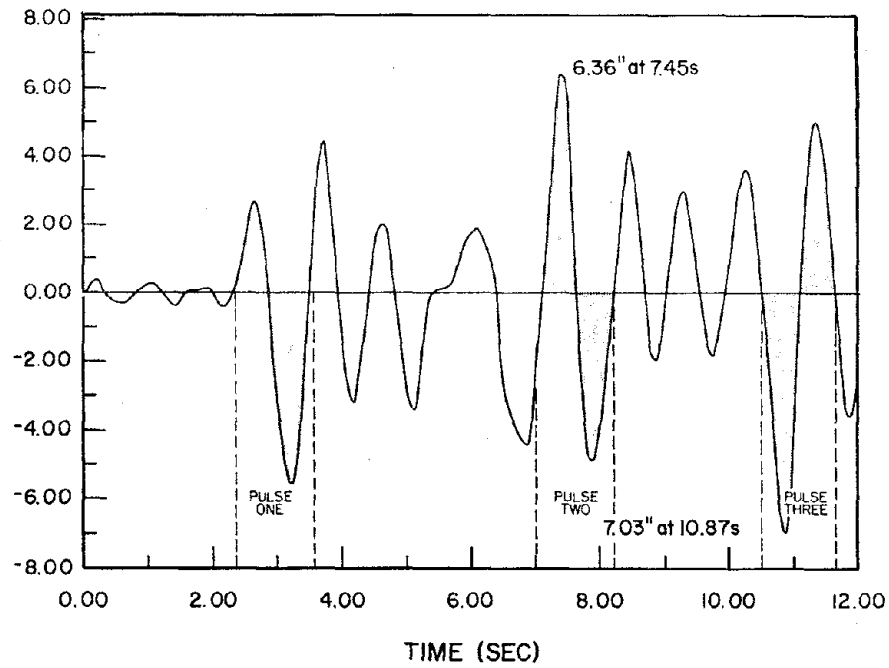


Fig. 5.7 Time-History of Top Story Displacement
Resulting from Miyagi-Oki Ground Motion

DISPLACEMENT (IN)

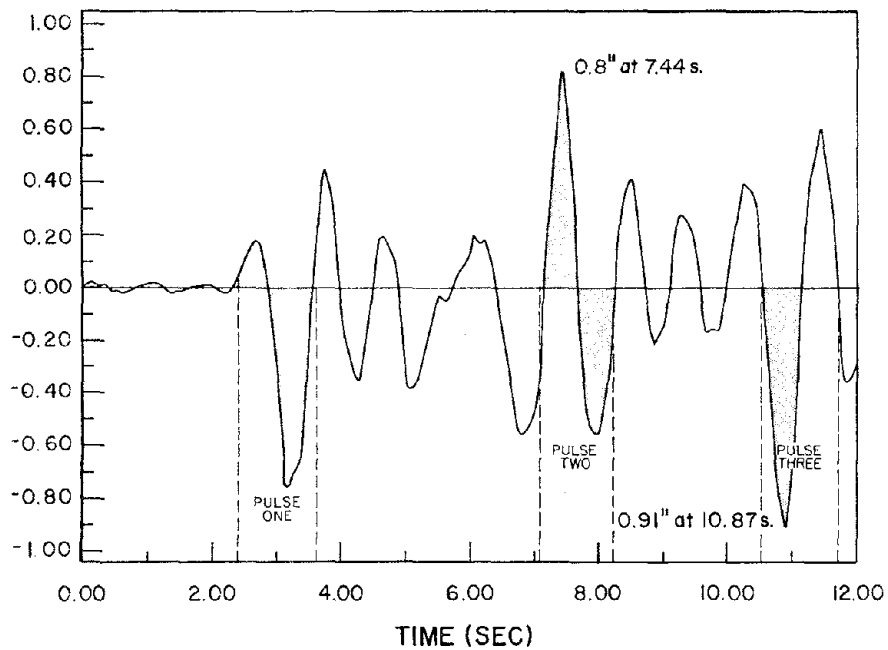


Fig. 5.8 Time-History of First Story Displacement
Resulting from Miyagi-Oki Ground Motion

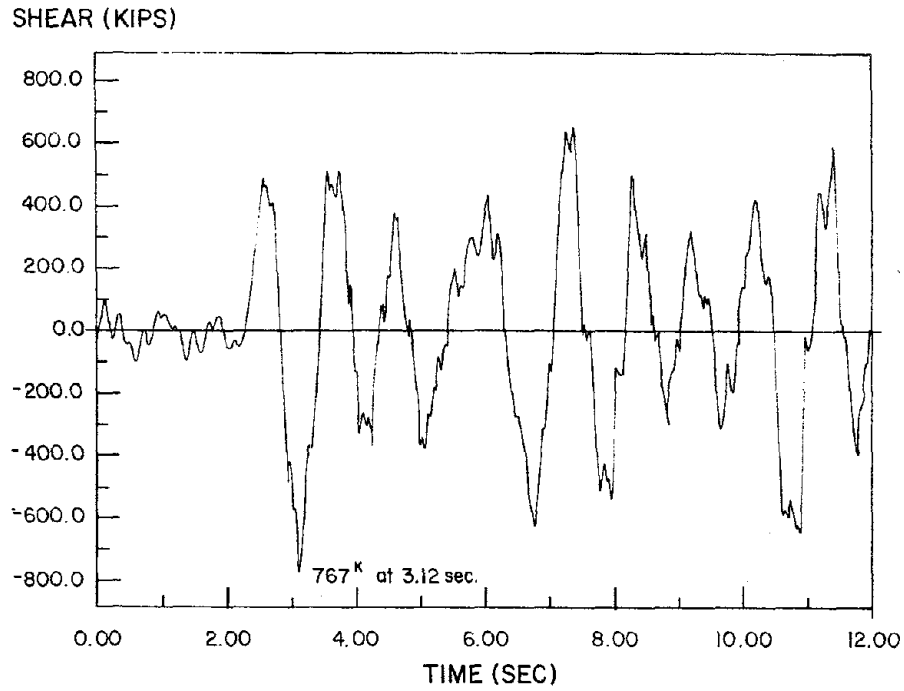


Fig. 5.9 Time-History of Structure Base Shear
Resulting from Miyagi-Oki Ground Motion

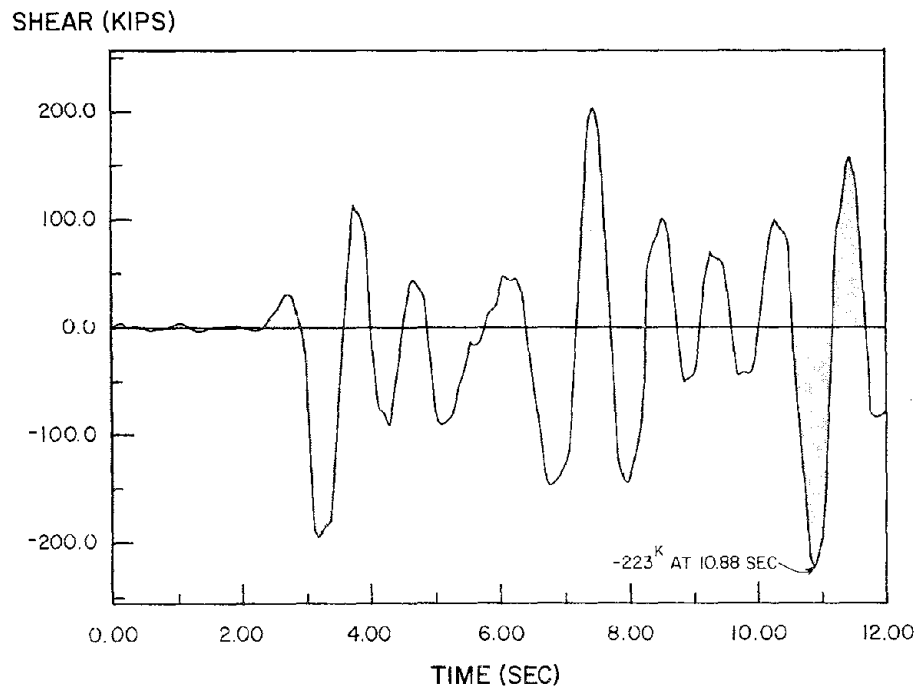


Fig. 5.10 Time-History of Frame A' Base Shear
Resulting from Miyagi-Oki Ground Motion

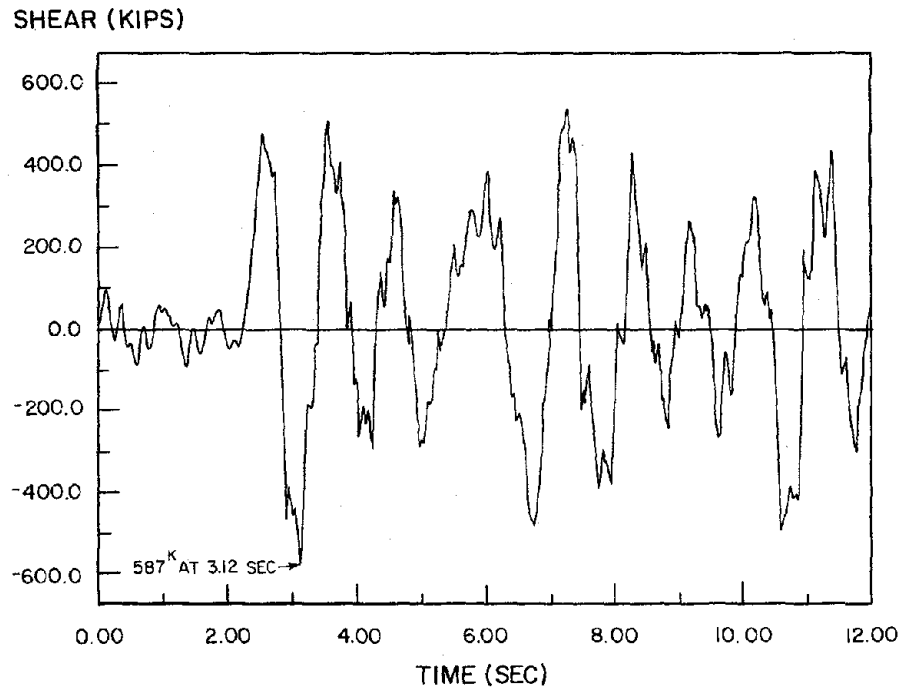


Fig. 5.11 Time-History of Frame B Base Shear
Resulting from Miyagi-Oki Ground Motion

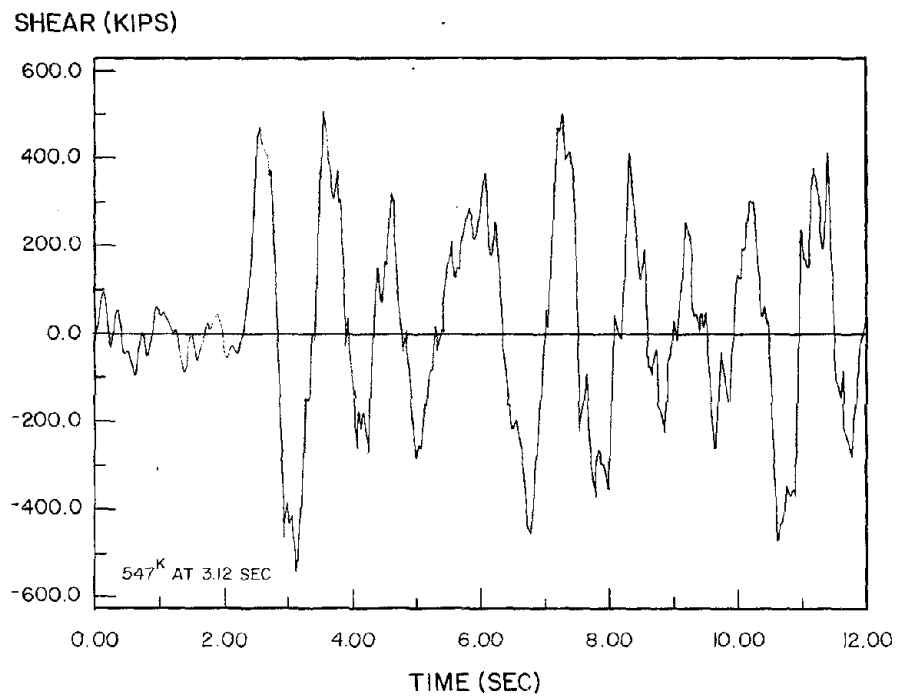


Fig. 5.12 Time-History of Shearwall Base Shear
Resulting from Miyagi-Oki Ground Motion

MOMENT (IN-K/1000)

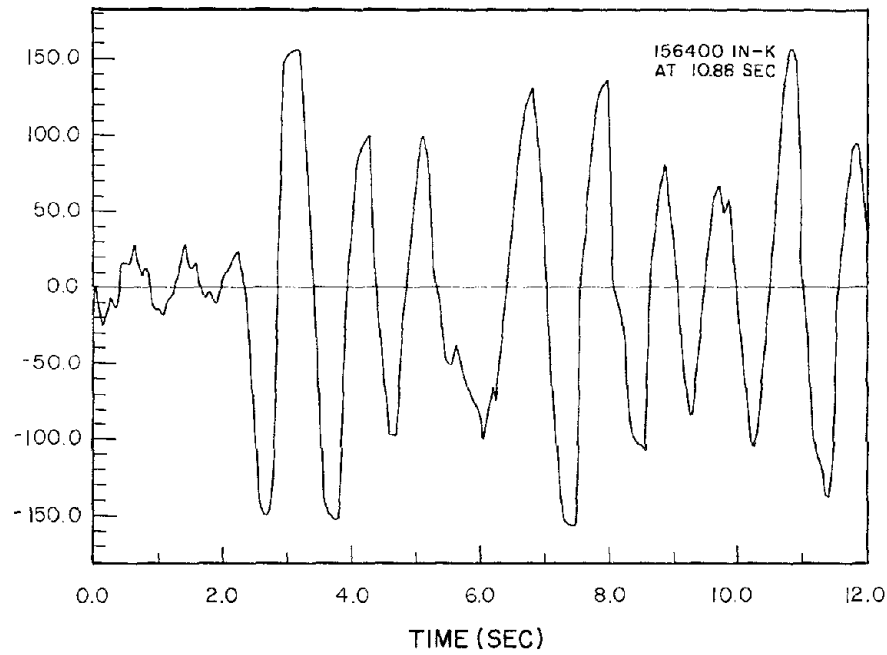


Fig. 5.13 Time-History of Shearwall Base Moment
Resulting from Miyagi-Oki Ground Motion

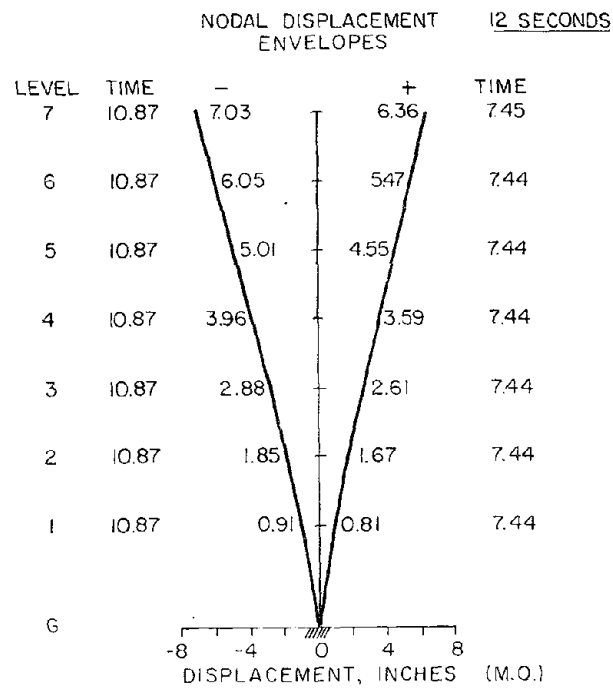
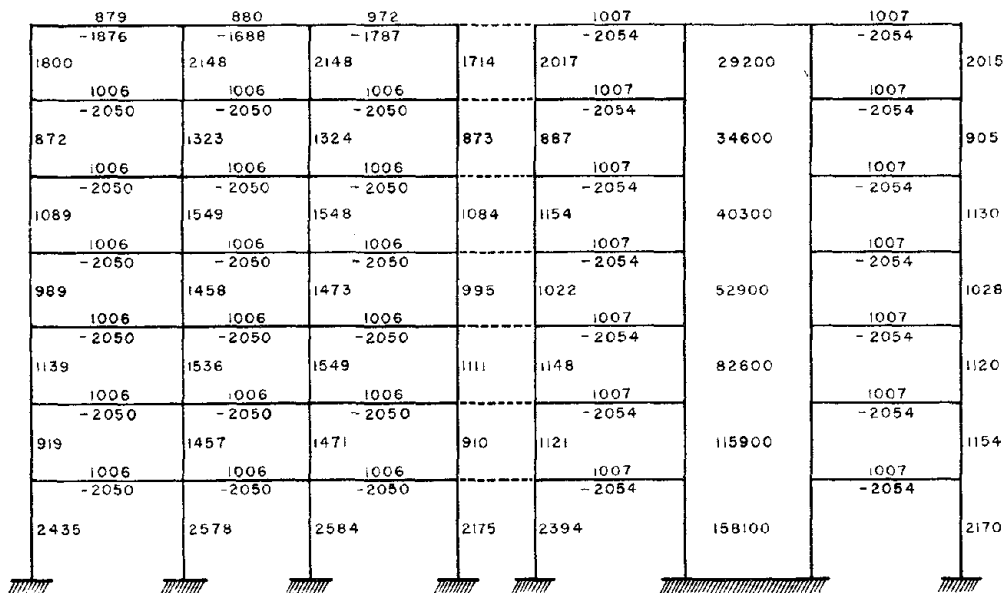


Fig. 5.14 Envelope of Maximum Lateral Displacements
Resulting from Miyagi-Oki Ground Motion

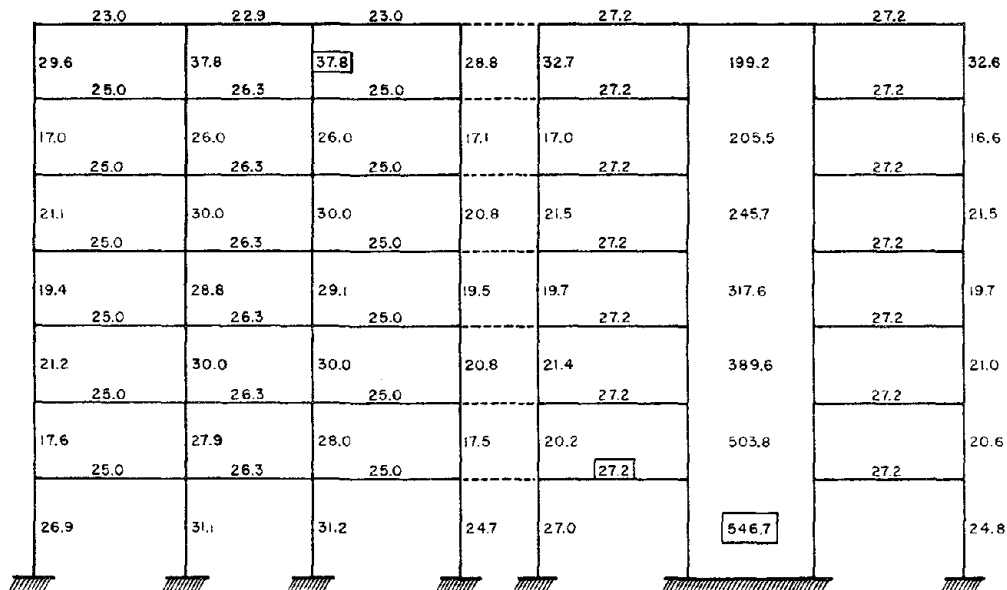


FRAME A'

FRAME B

NOTE: ALL MOMENTS, IN INCH-KIPS, ARE AT FACE OF SUPPORT. THE LARGEST ABSOLUTE VALUE OF ELEMENT MOMENT IS GIVEN FOR COLUMN AND WALL ELEMENTS. MAXIMUM POSITIVE AND NEGATIVE MOMENTS ARE GIVEN FOR BEAMS

Fig. 5.15 Envelope of Maximum Element Moments Resulting from Miyagi-Oki Ground Motion

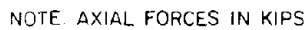


FRAME A'

FRAME B

NOTE: SHEAR FORCES IN KIPS

Fig 5.16 Envelope of Maximum Element Shears Resulting from Miyagi-Oki Ground Motion



FRAME A'						FRAME B			
2528	3017	4463	5344	2152	3433	1775	4057	2975	2851
2621	903	1874	986	1761	1726	4140	6077	7759	5064
2539	2527	3919	2824	1643	3411	3511	4572	3411	4634
2115	404	1380	472	1289	1242	7680	7058	8189	6557
2871	3026	4449	5355	2143	3757	3540	5068	3852	4740
2605	946	1901	944	1827	1720	7180	7484	8700	5960
2942	2840	4319	5175	2006	3783	3934	5366	4166	5126
2465	857	1727	871	1692	1624	7821	7768	8968	6628
2058	2121	3702	4479	1361	2797	3920	5197	4071	5052
1607	217	1023	244	1033	869	7645	7654	8780	6503
2093	1578	2801	3915	678	3221	2802	4429	3345	2328
1463		476		571	501	6645	6887	7971	6620
						2552	3021	1949	3789
						6131	5476	6548	4894

-127-

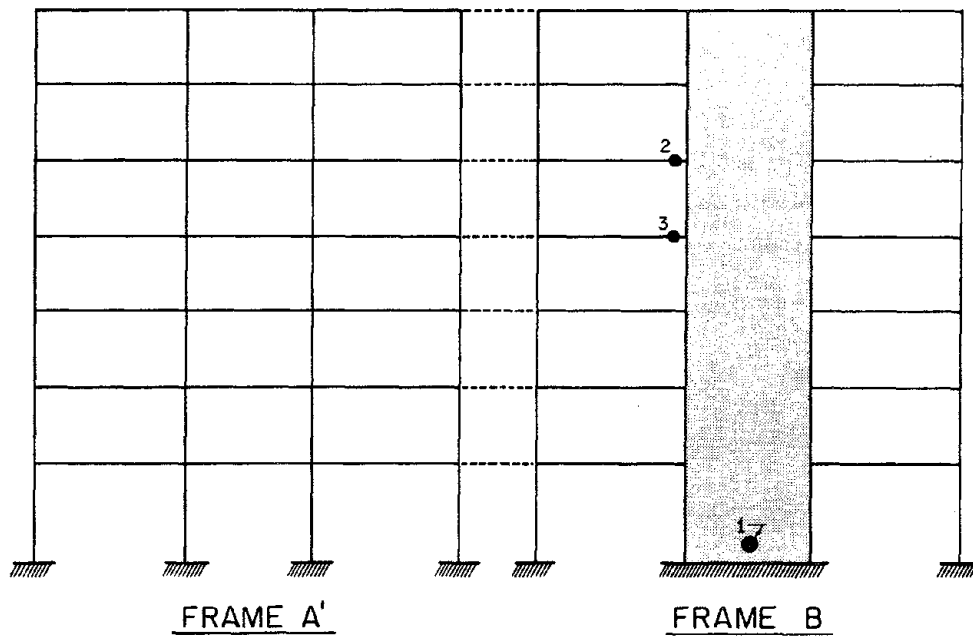


Fig. 5.19 Plastic Hinges Resulting from first part of Pulse One of Miyagi-Oki Ground Motion

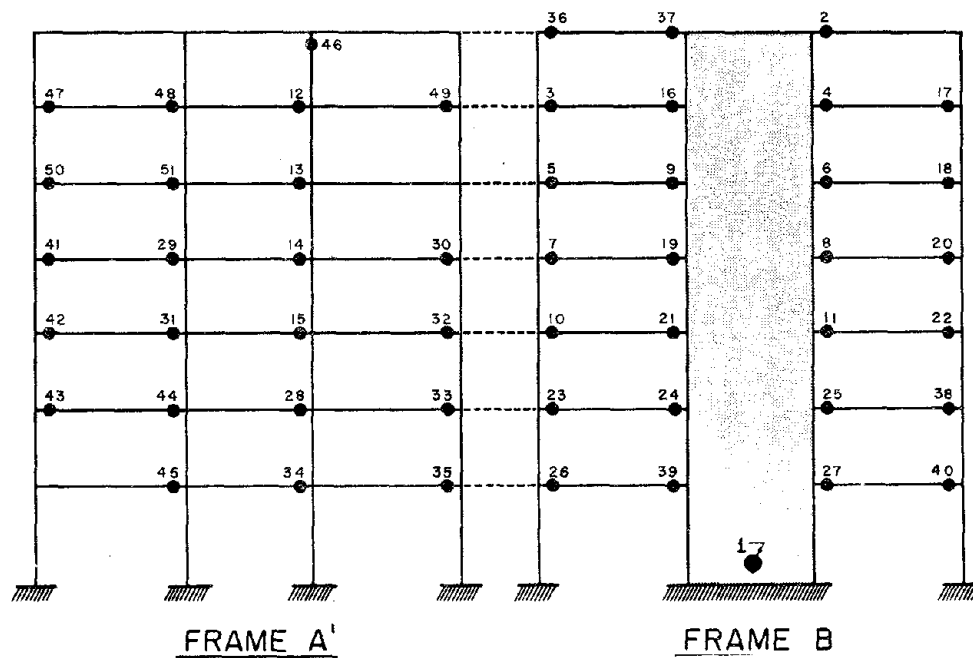


Fig. 5.20 Plastic Hinges Resulting from Second Part of Pulse One of Miyagi-Oki Ground Motion

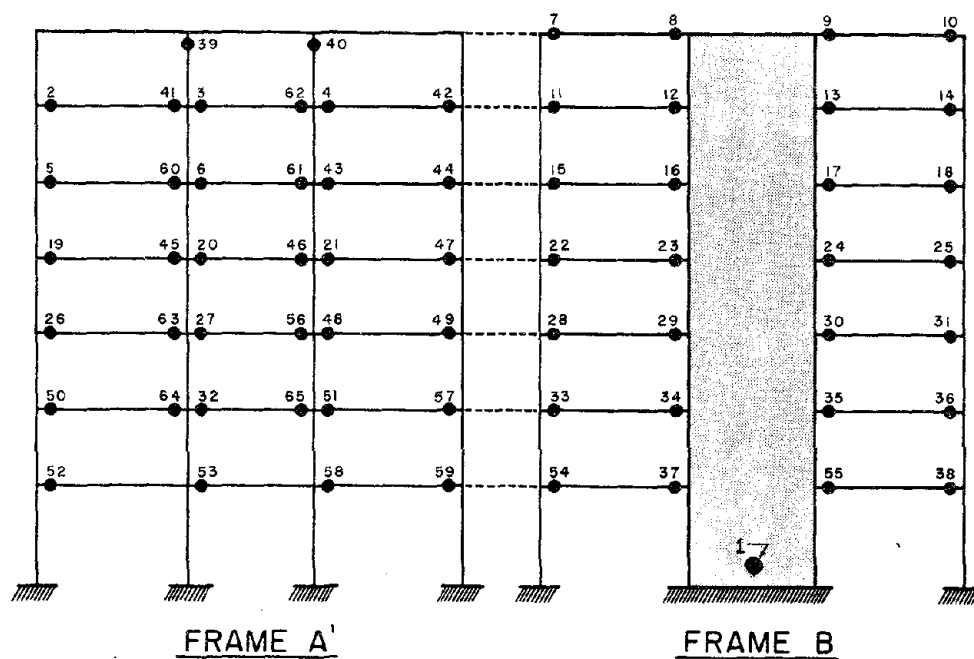


Fig. 5.21 Plastic Hinges Resulting from Pulse Two of Miyagi-Oki Ground Motion

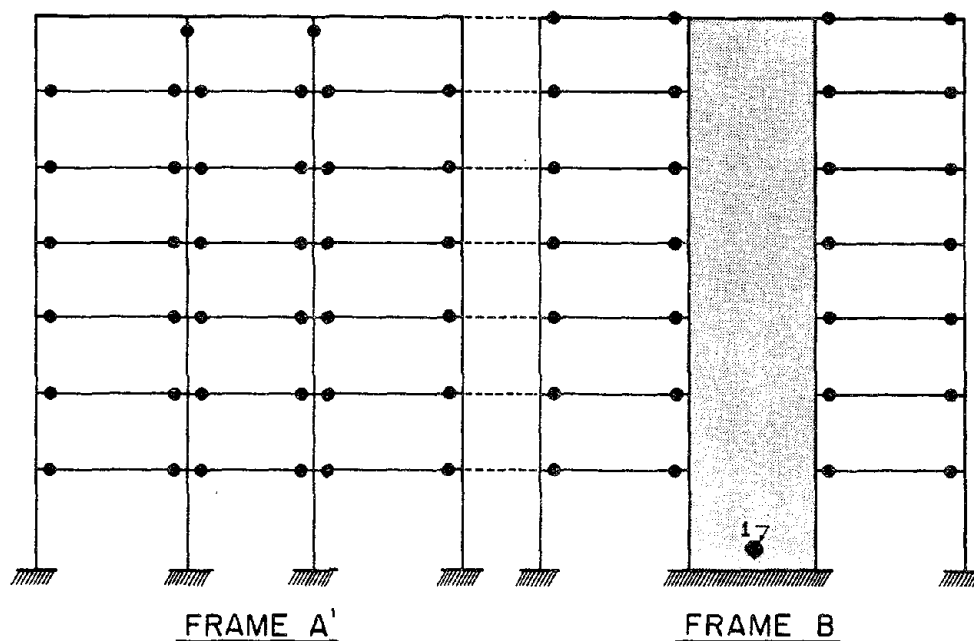


Fig. 5.22 Plastic Hinges Resulting from Pulse Three of Miyagi-Oki Ground Motion

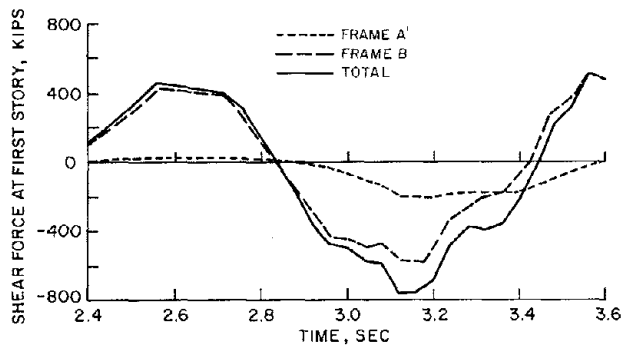


Fig. 5.23 Distribution of Base Shears Resulting from Pulse One of Miyagi-Oki Ground Motion

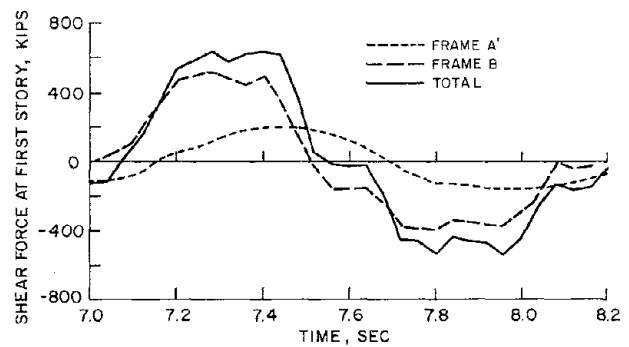


Fig. 5.24 Distribution of Base Shears Resulting from Pulse Two of Miyagi-Oki Ground Motion

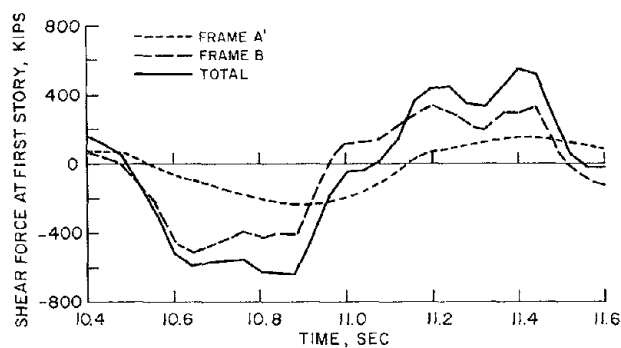
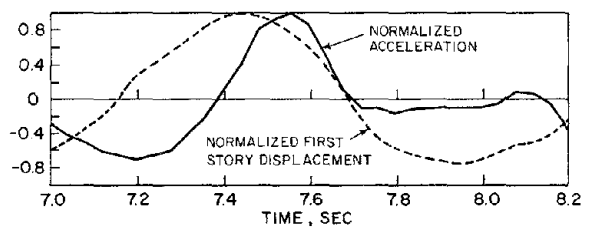
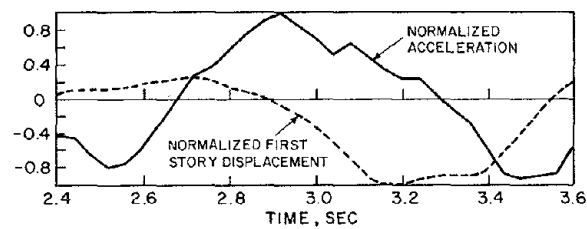
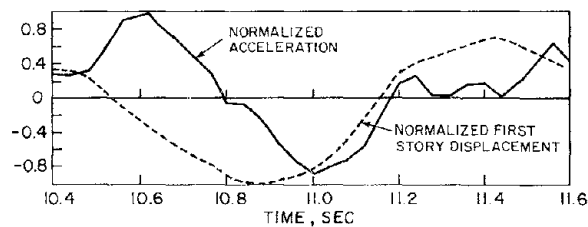


Fig. 5.25 Distribution of Base Shears Resulting from Pulse Three of Miyagi-Oki Ground Motion



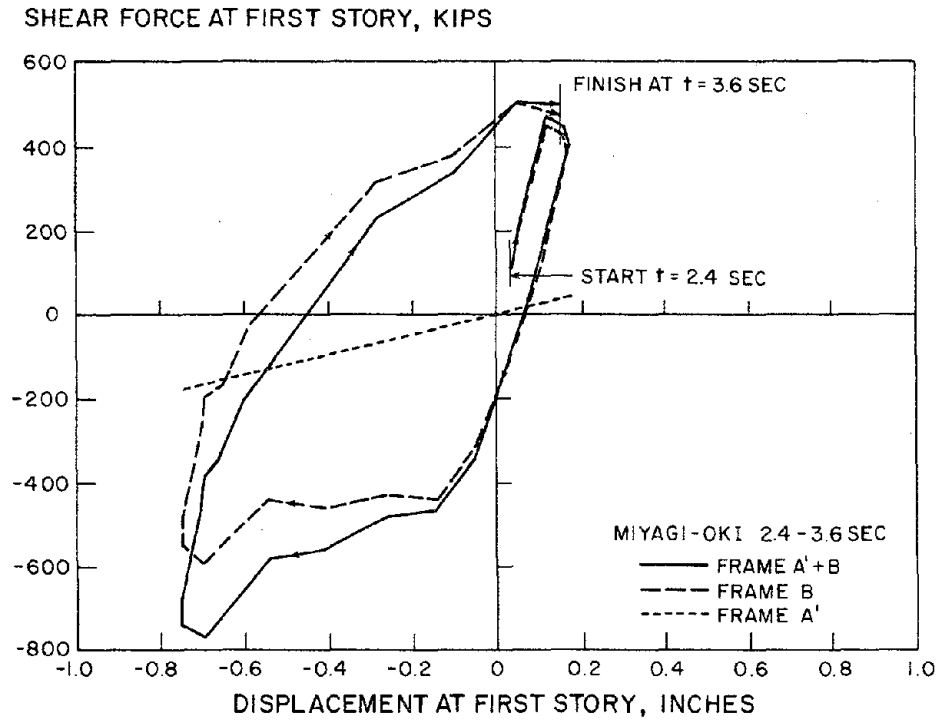


Fig. 5.26 Base Shear vs First Story Displacement Resulting from Pulse One of Miyagi-Oki Ground Motion

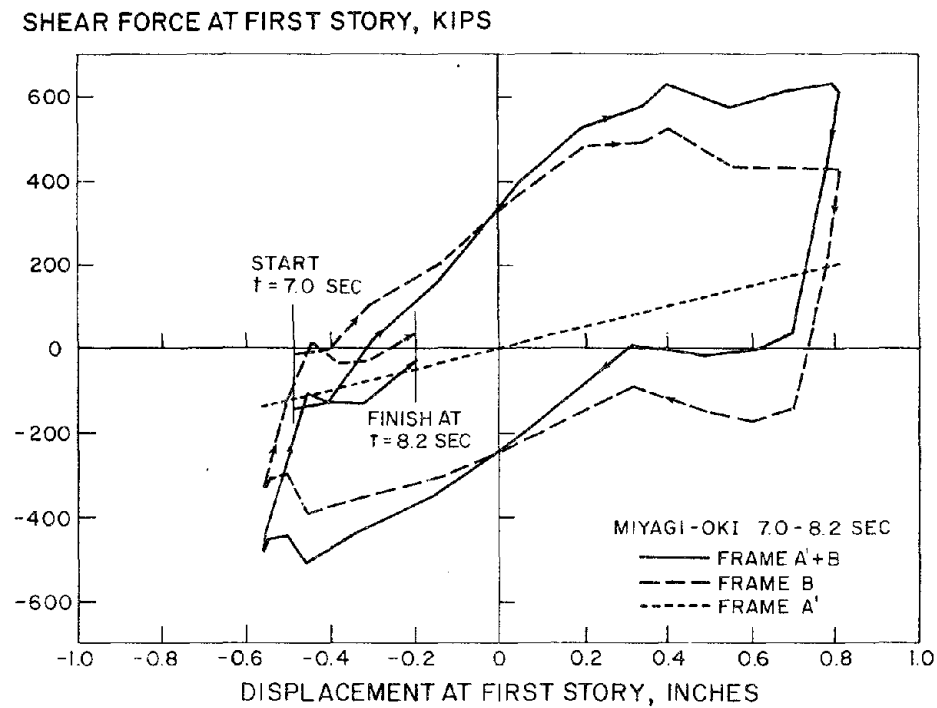


Fig. 5.27 Base Shear vs First Story Displacement Resulting from Pulse Two of Miyagi-Oki Ground Motion

SHEAR FORCE AT FIRST STORY, KIPS

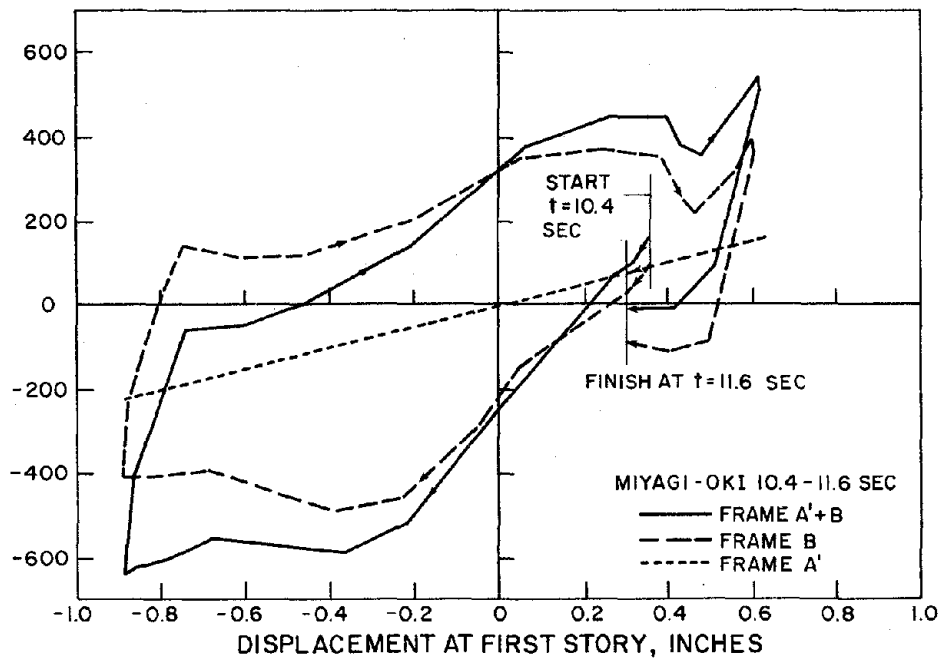


Fig. 5.28 Base Shear vs First Story Displacement Resulting from Pulse Three of Miyagi-Oki Ground Motion

SHEAR FORCE AT FIRST STORY, KIPS

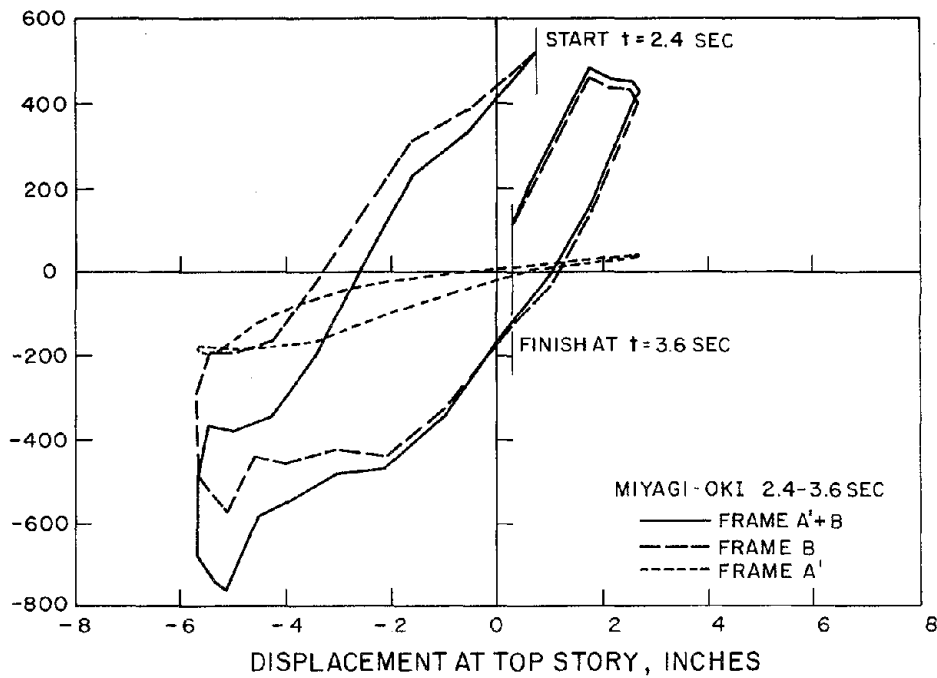


Fig. 5.29 Base Shear vs Roof Displacement Resulting from Pulse One of Miyagi-Oki Ground Motion

BASE SHEAR FORCE, KIPS

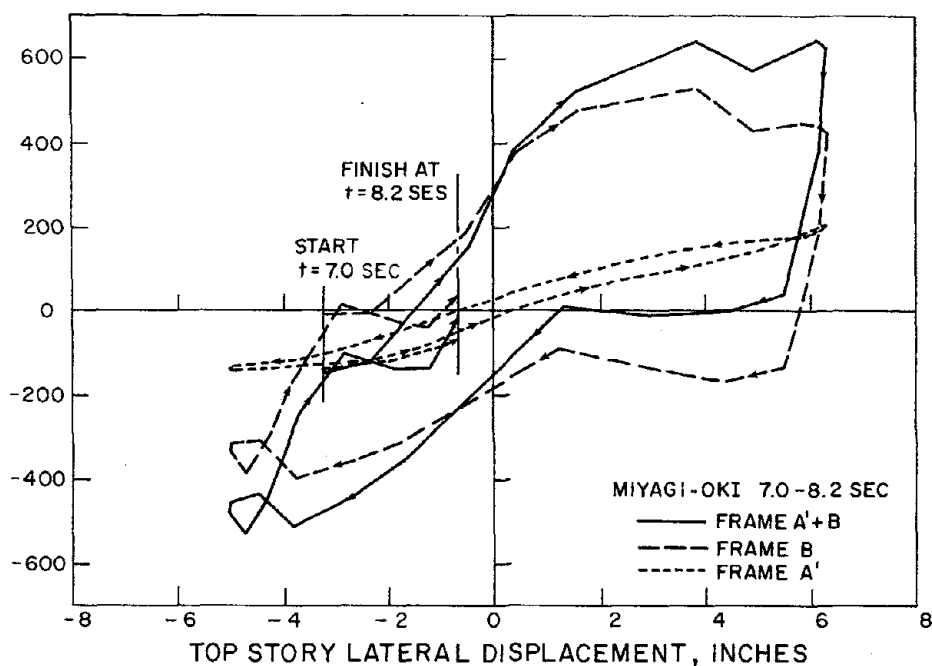


Fig. 5.30 Base Shear vs Roof Displacement Resulting from Pulse Two of Miyagi-Oki Ground Motion

BASE SHEAR FORCE, KIPS

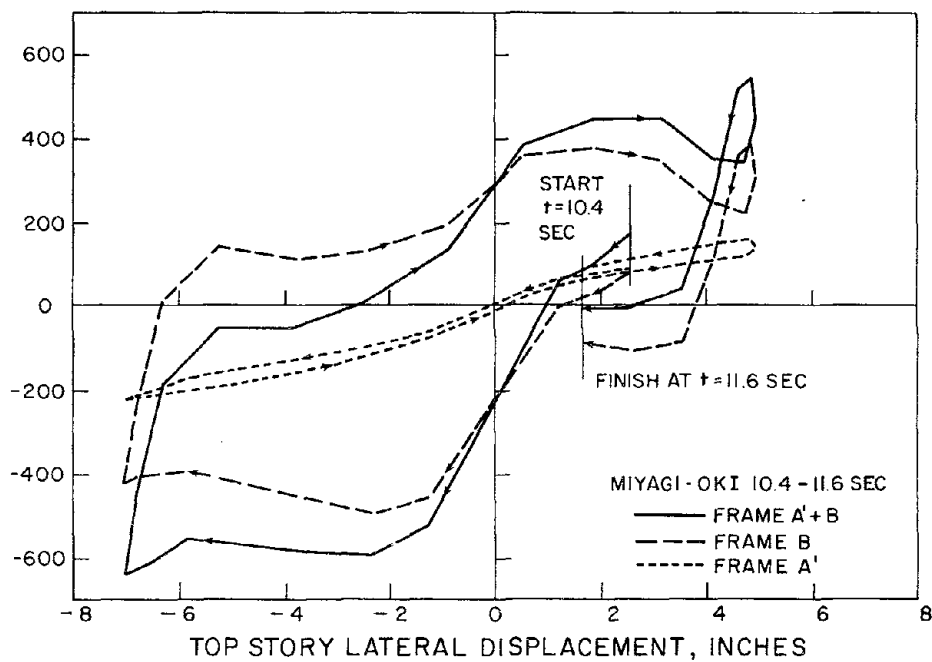
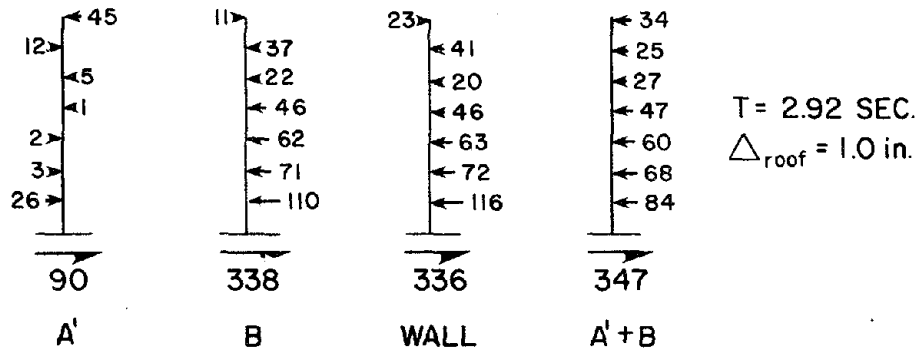
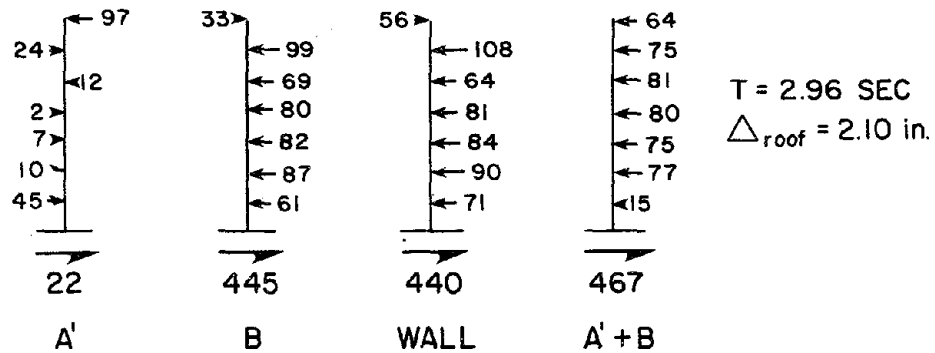


Fig. 5.31 Base Shear vs Roof Displacement Resulting from Pulse Three of Miyagi-Oki Ground Motion

PRIOR TO WALL HINGE FORMATION



AFTER WALL HINGE FORMATION



AT MAXIMUM LATERAL DISPLACEMENT

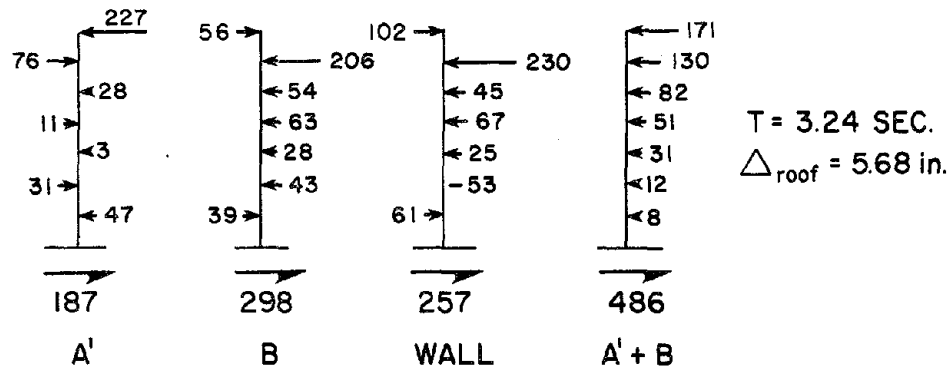
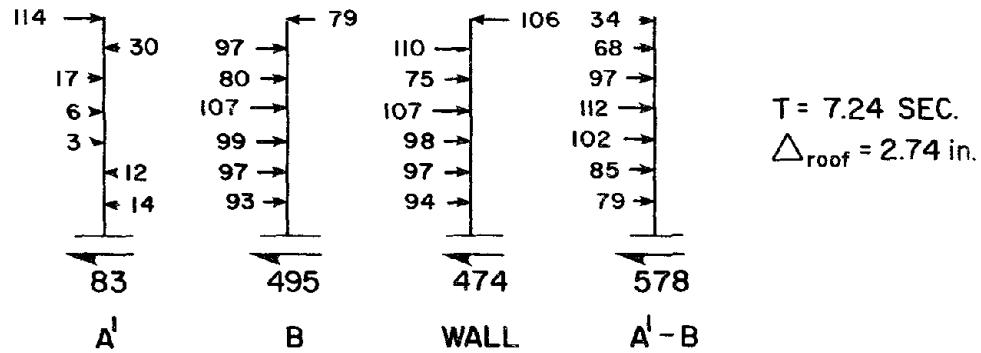
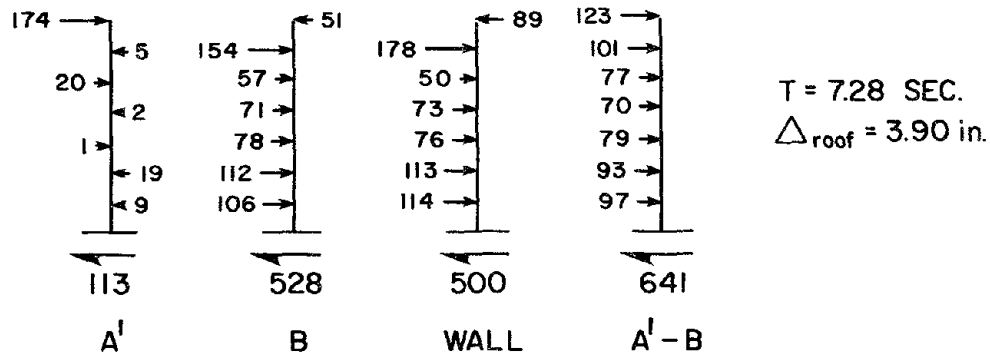


Fig. 5.32 Frame Interaction Forces Resulting from Pulse One of Miyagi-Oki Ground Motion

PRIOR TO WALL HINGE FORMATION



AFTER WALL HINGE FORMATION



AT MAXIMUM LATERAL DISPLACEMENT

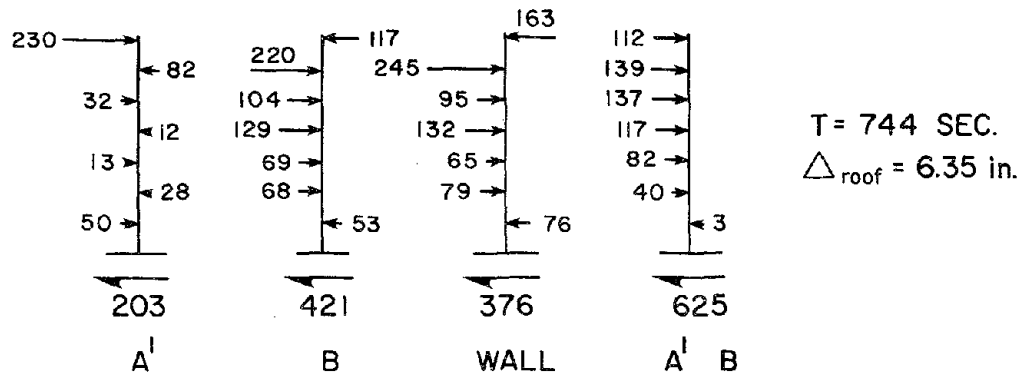
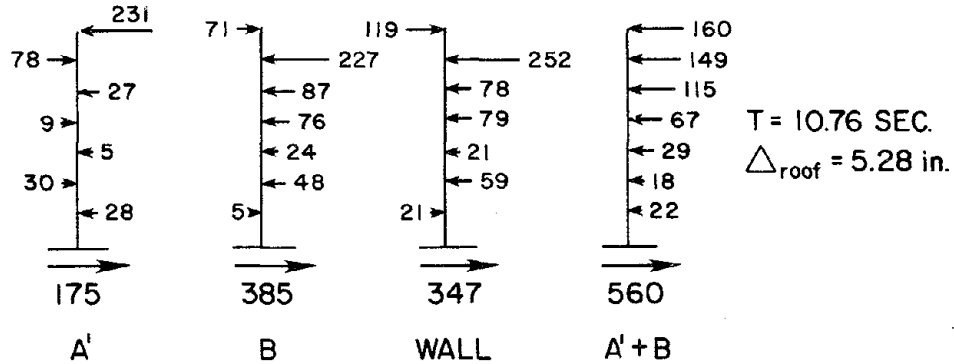
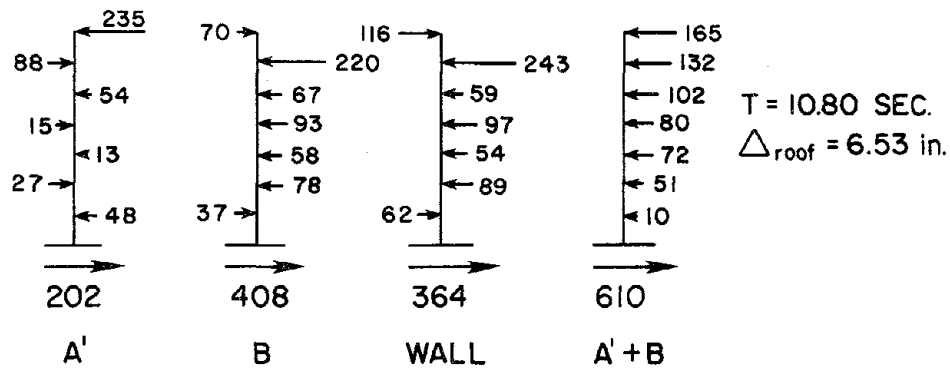


Fig. 5.33 Frame Interaction Forces Resulting from Pulse Two of Miyagi-Oki Ground Motion

PRIOR TO WALL HINGE FORMATION



AFTER WALL HINGE FORMATION



AT MAXIMUM LATERAL DISPLACEMENT

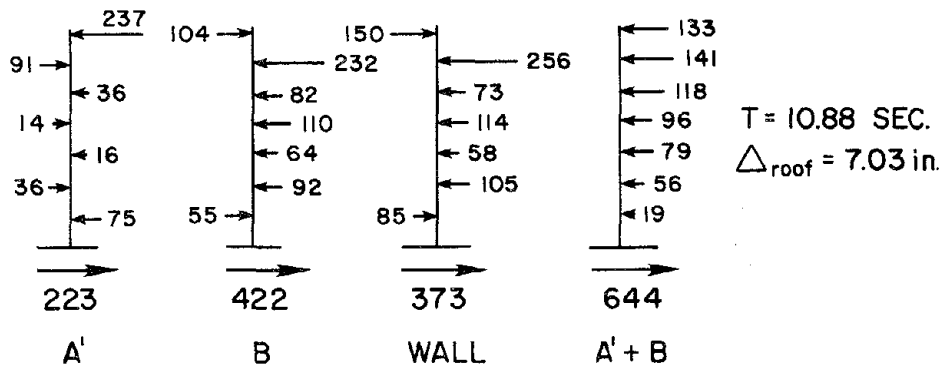


Fig. 5.34 Frame Interaction Forces Resulting from Pulse Three of Miyagi-Oki Ground Motion

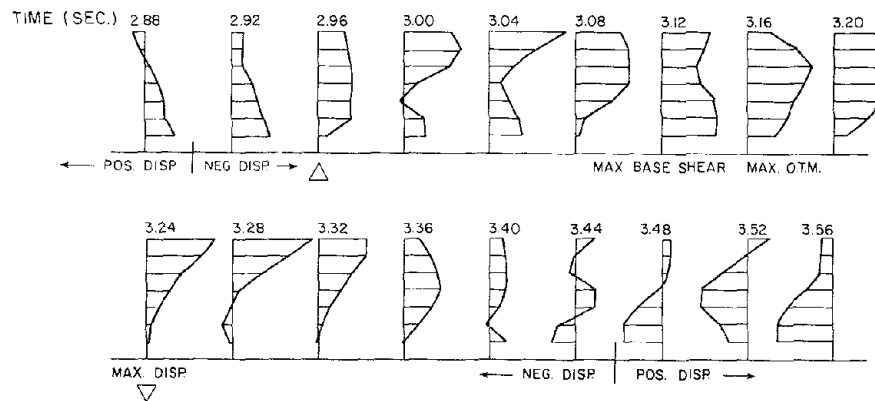


Fig. 5.35 Lateral Force Profile Time-History Resulting from Pulse One of Miyagi-Oki Ground Motion

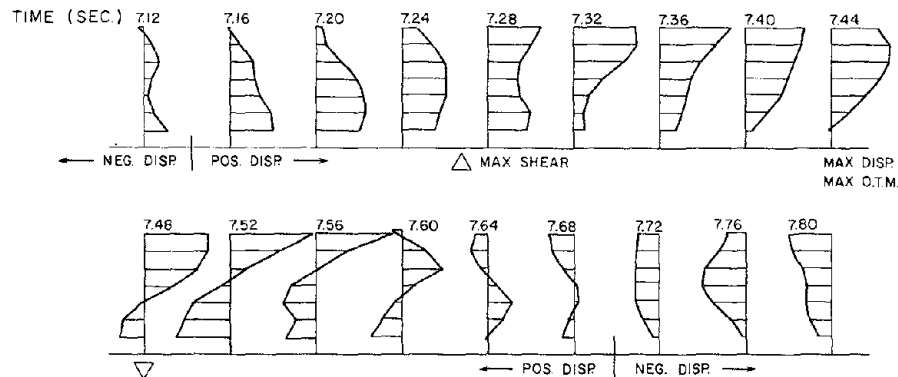


Fig. 5.36 Lateral Force Profile Time-History Resulting from Pulse Two of Miyagi-Oki Ground Motion

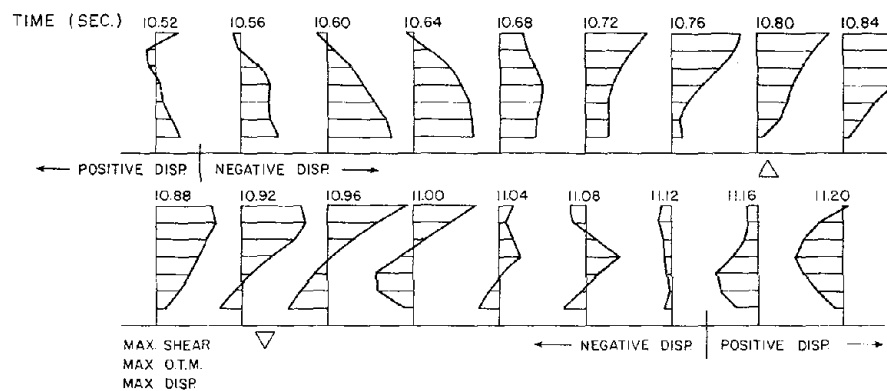


Fig 5.37 Lateral Force Profile Time-History Resulting From Pulse Three of Miyagi-Oki Ground Motion

DISPLACEMENT (IN)

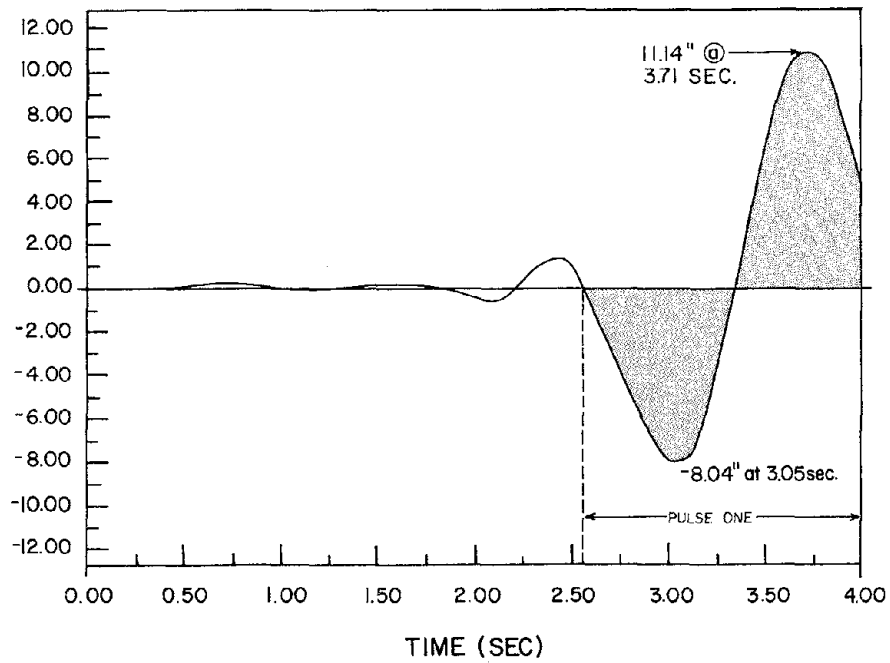


Fig. 5.38 Time-History of Roof Displacement Resulting from Derived Pacoima Dam Ground Motion

DISPLACEMENT (IN)

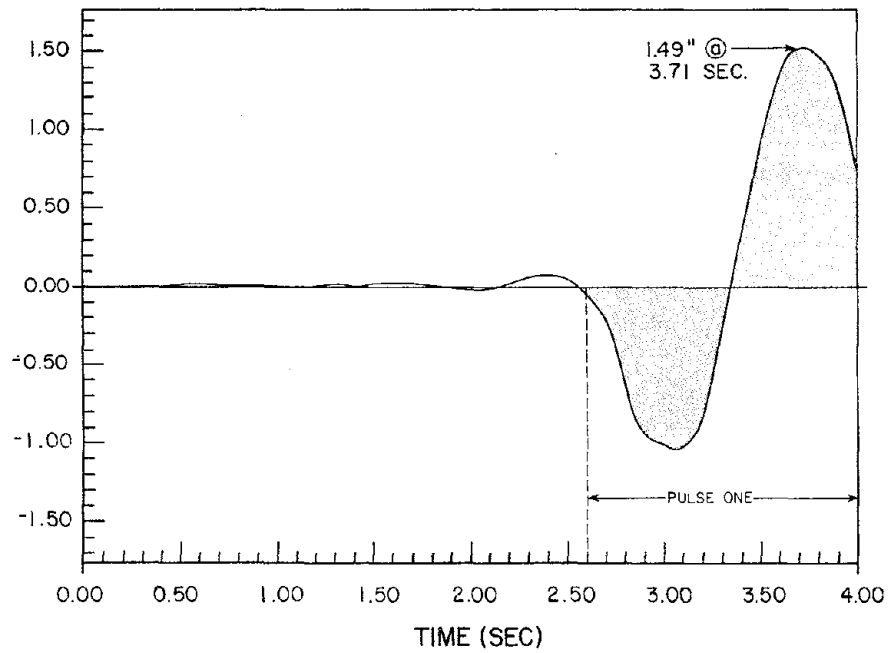


Fig. 5.39 Time History of First Story Displacement Resulting from Derived Pacoima Dam Ground Motion

SHEAR (KIPS)

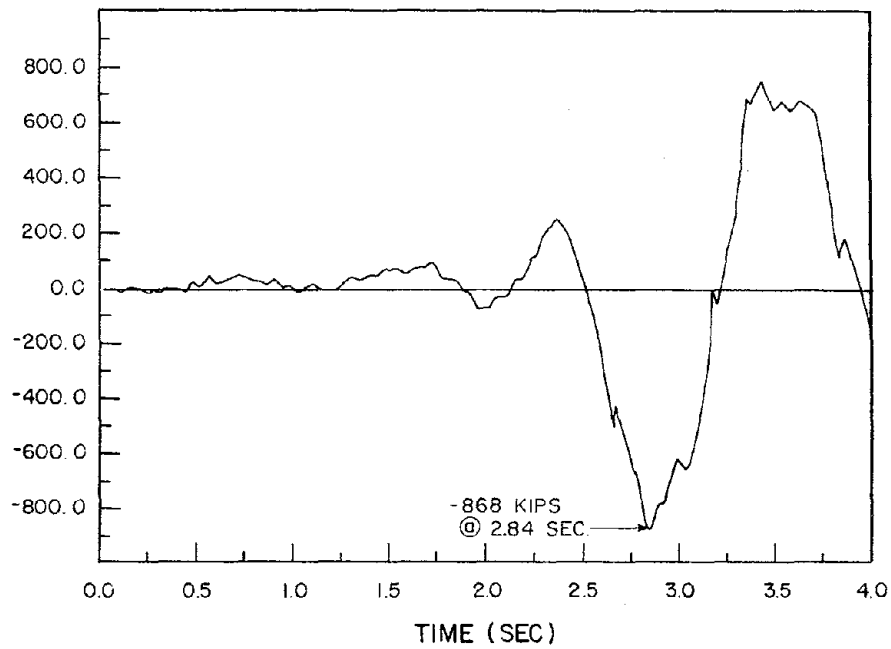


Fig. 5.40 Time-History of Structure Base Shear Resulting from Derived Pacoima Dam Ground Motion

SHEAR (KIPS)

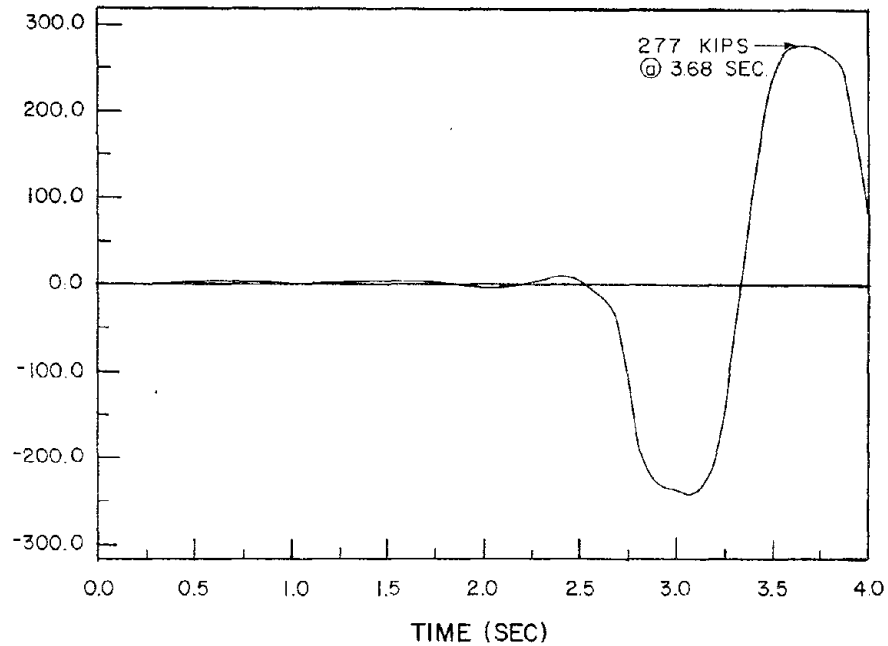


Fig. 5.41 Time-History of Frame A' Base Shear Resulting from Derived Pacoima Dam Ground Motion

SHEAR (KIPS)

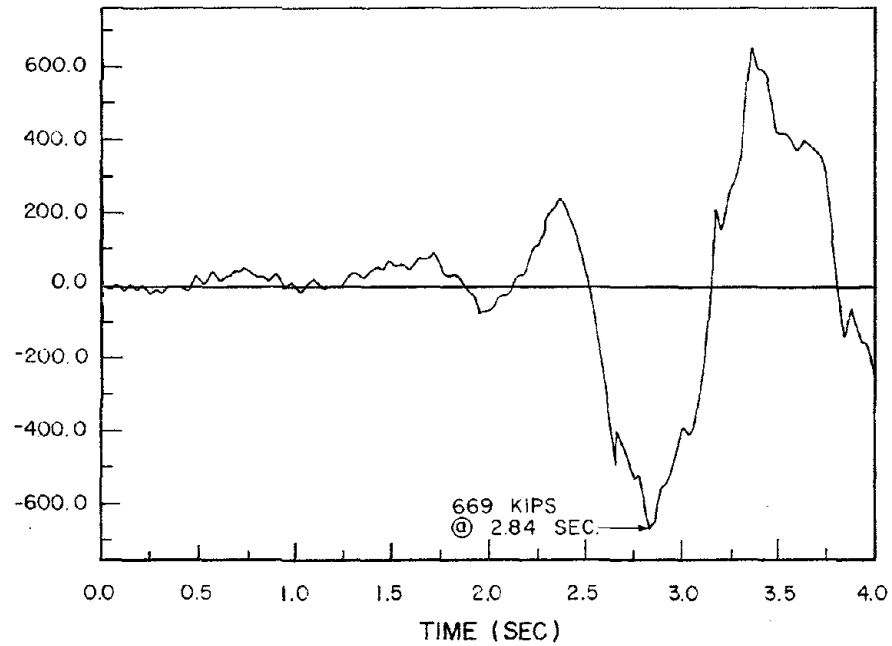


Fig. 5.42 Time-History of Frame B Base Shear Resulting from Derived Pacoima Dam Ground Motion

SHEAR (KIPS)

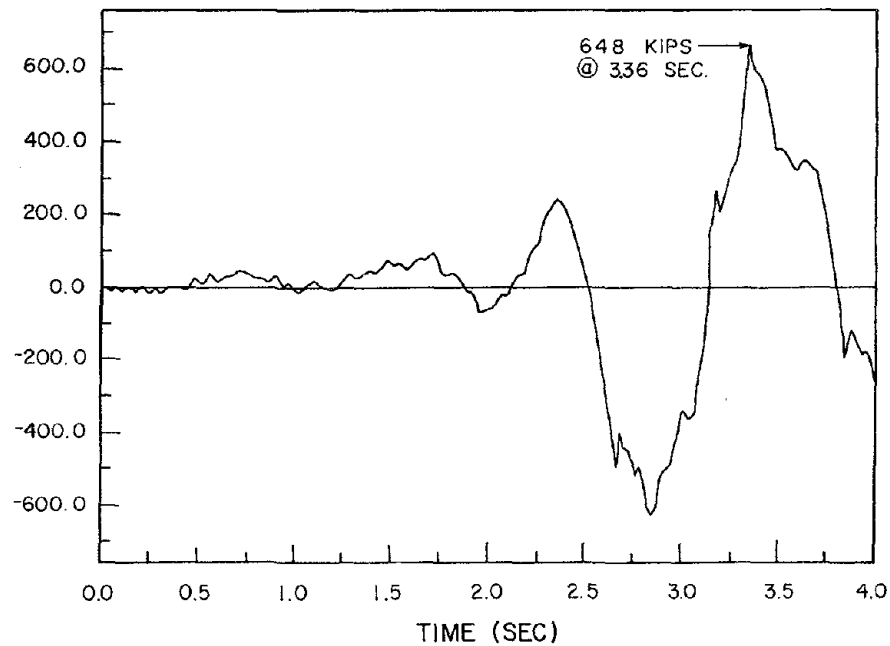


Fig. 5.43 Time-History of Shearwall Base Shear Resulting from Derived Pacoima Dam Ground Motion

MOMENT (IN-K/1000)

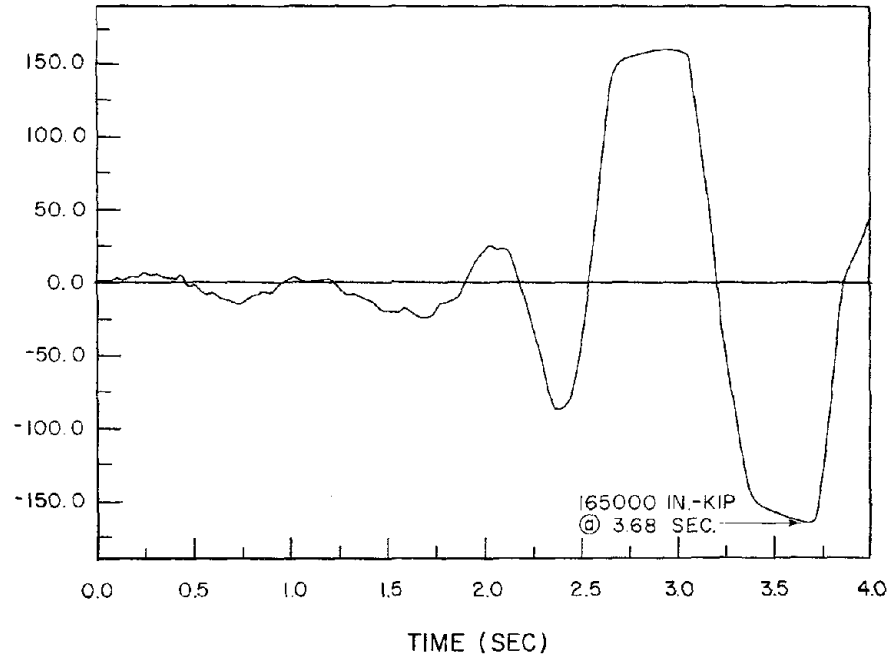


Fig. 5.44 Time-History of Shearwall Base Moment Resulting from Derived Pacoima Dam Ground Motion

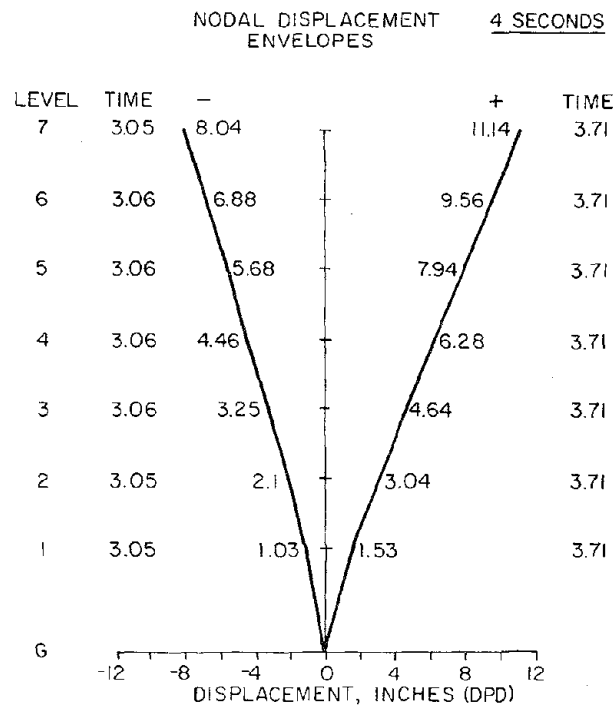
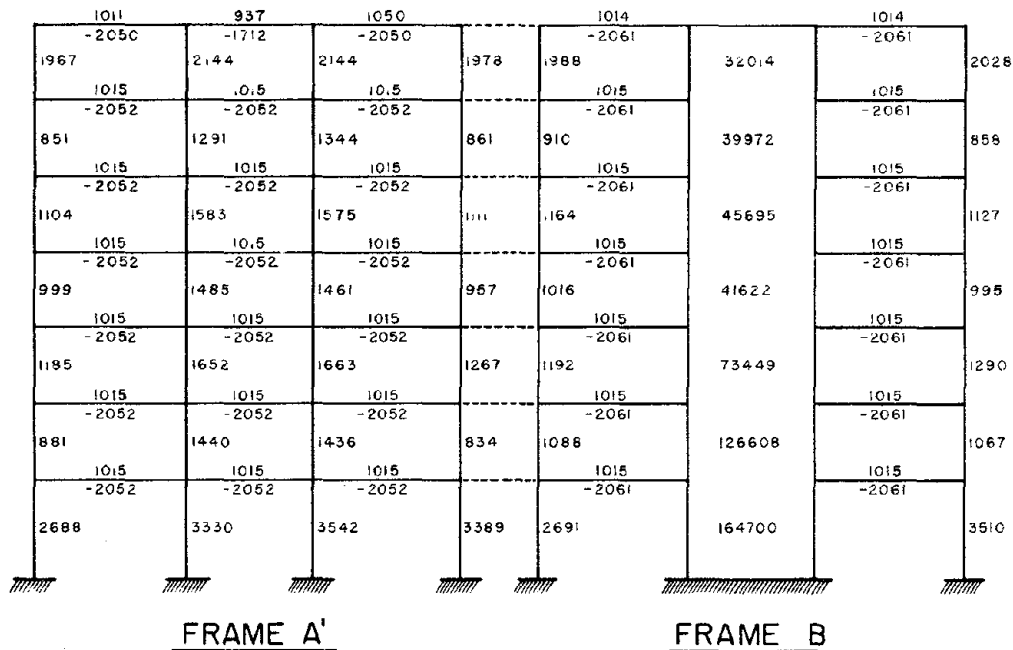
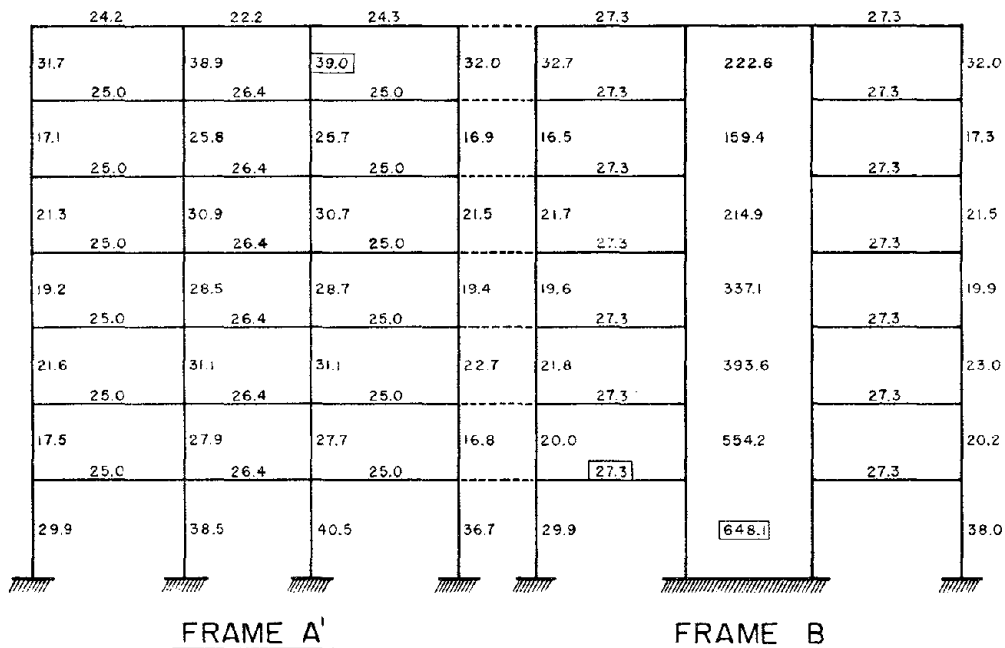


Fig. 5.45 Envelope of Maximum Lateral Displacements Resulting from Derived Pacoima Dam Ground Motion



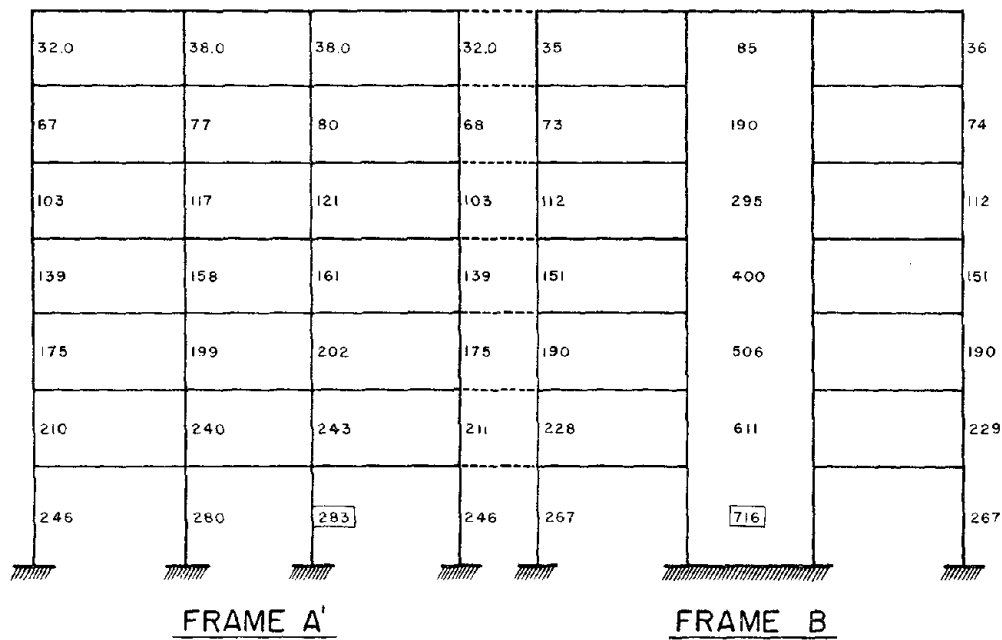
NOTE: ALL MOMENTS, IN INCH-KIPS, ARE AT FACE OF SUPPORT. THE LARGEST ABSOLUTE VALUE OF ELEMENT MOMENT IS GIVEN FOR COLUMN AND WALL ELEMENTS. MAXIMUM POSITIVE AND NEGATIVE MOMENTS ARE GIVEN FOR BEAMS

Fig. 5.46 Envelope of Maximum Element Moments Resulting from Derived Pacoima Dam Ground Motion



NOTE: SHEAR FORCES IN KIPS

Fig. 5.47 Envelope of Maximum Element Shears Resulting from Derived Pacoima Dam Ground Motion



NOTE: AXIAL FORCES IN KIPS

Fig. 5.48 Envelope of Maximum Element Axial Forces Resulting from Derived Pacoima Dam Ground Motion

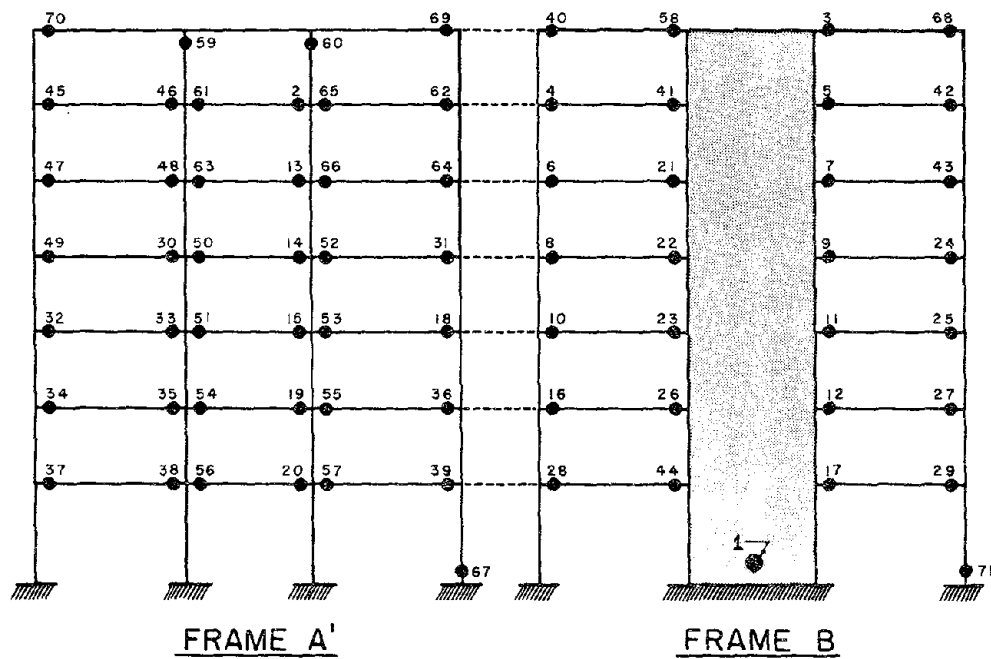


Fig. 5.49 Plastic Hinge Patterns Resulting from First Part of Pulse One of Derived Pacoima Dam Ground Motion

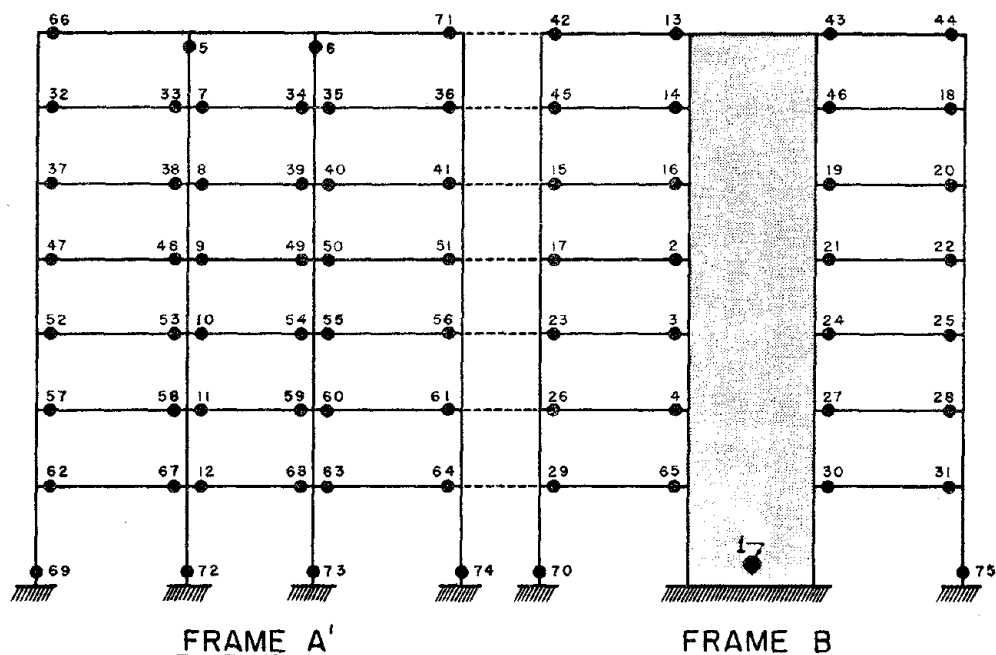
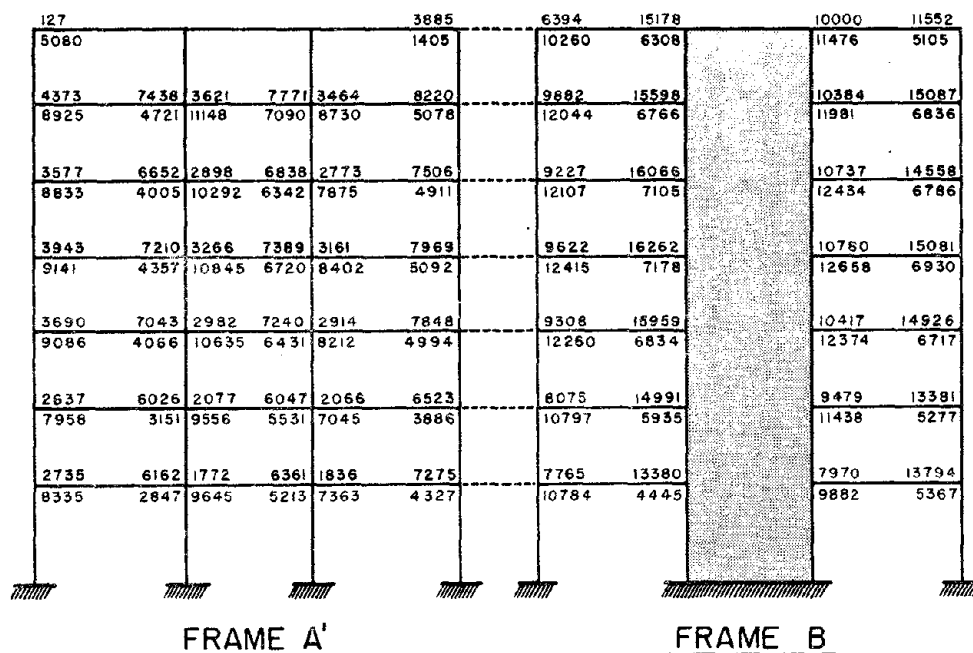


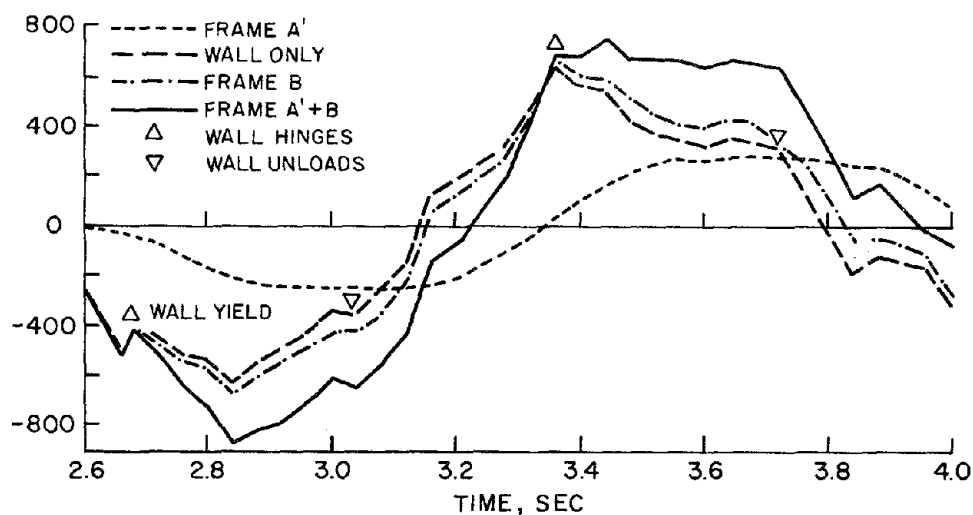
Fig. 5.50 Plastic Hinge Patterns Resulting from Second Part of Pulse One of Derived Pacoima Dam Ground Motion



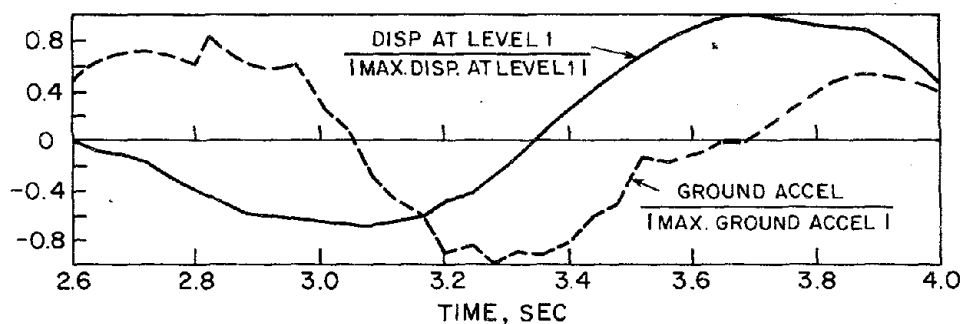
NOTE: MULTIPLY VALUES BY 10^6 TO OBTAIN ROTATIONS IN RADIANS.

Fig. 5.51 Maximum Plastic Hinge Rotations Resulting From Derived Pacoima Dam Ground Motion

SHEAR FORCE AT FIRST STORY, KIPS



(a) TIME-HISTORY OF STRUCTURE BASE SHEAR FORCES



(b) TIME-HISTORY DISPLACEMENTS AND GROUND ACCELERATION

Fig. 5.52 Distribution of Base Shears Resulting from
Pulse One of Derived Pacima Dam Ground Motion

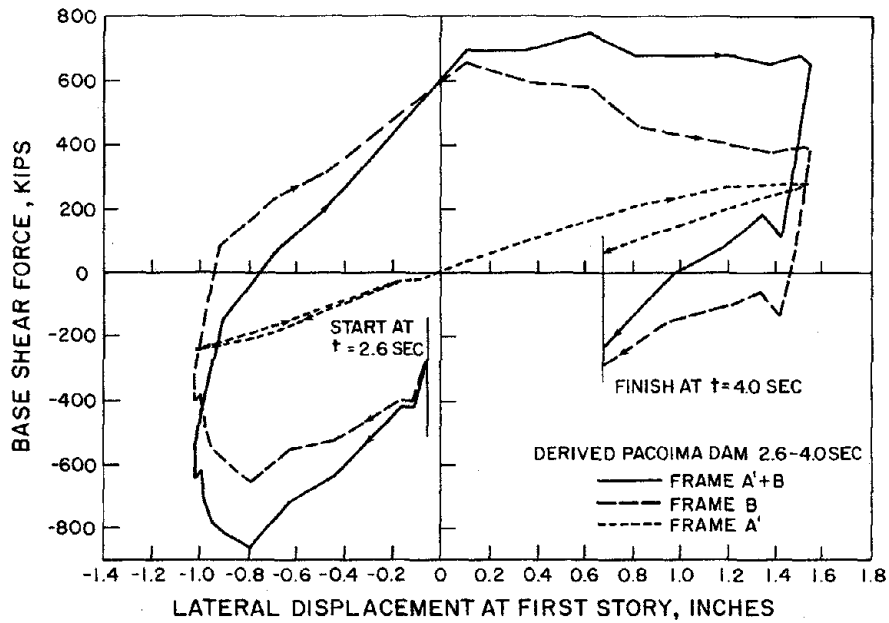


Fig. 5.53 Base Shear vs First Story Displacement Resulting from Pulse One of Derived Pacoima Dam Ground Motion

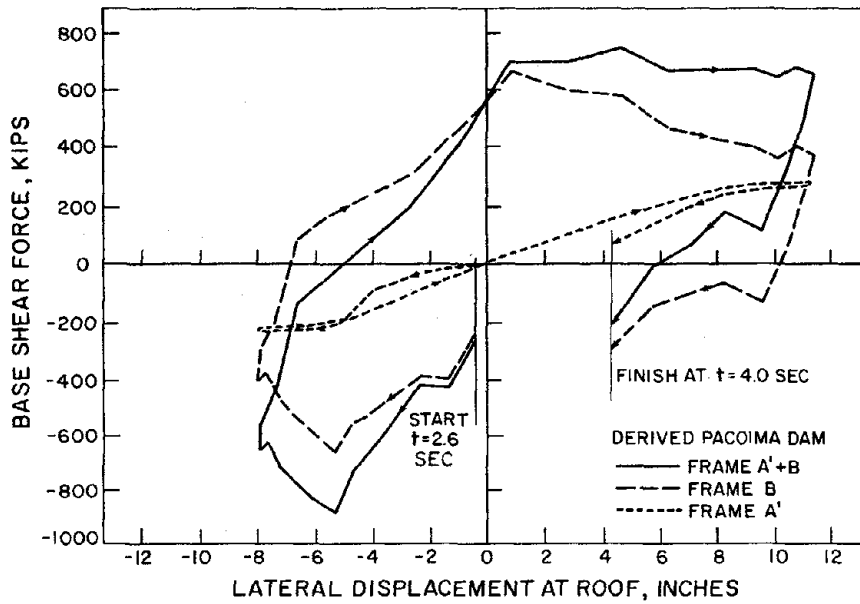
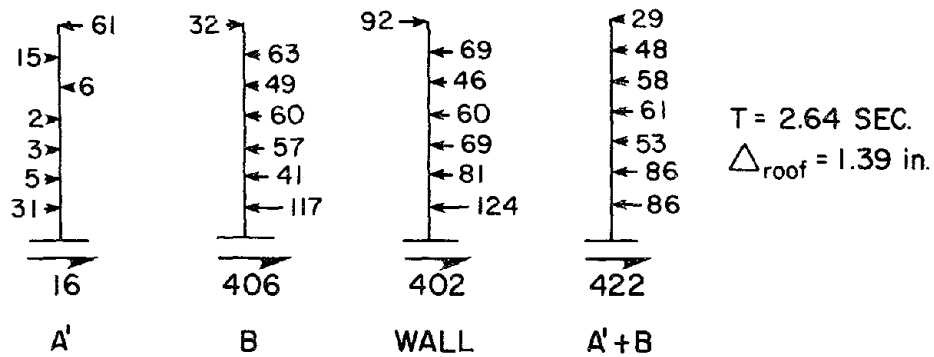
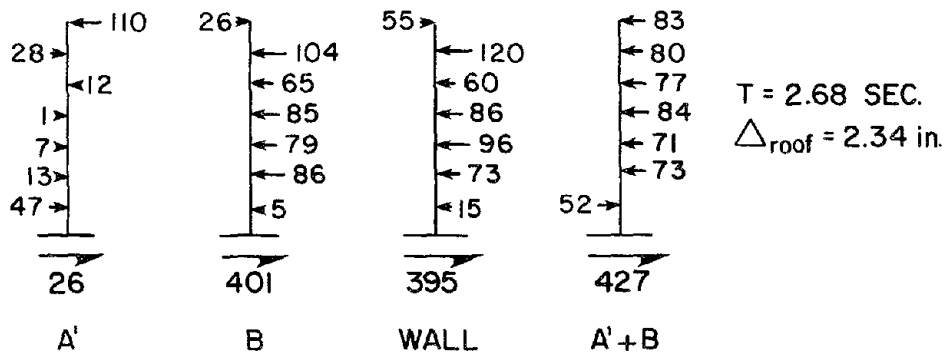


Fig. 5.54 Base Shear vs Roof Displacement Resulting from Pulse One of Derived Pacoima Dam Ground Motion

PRIOR TO WALL HINGE FORMATION



AFTER WALL HINGE FORMATION



AT MAXIMUM LATERAL DISPLACEMENT

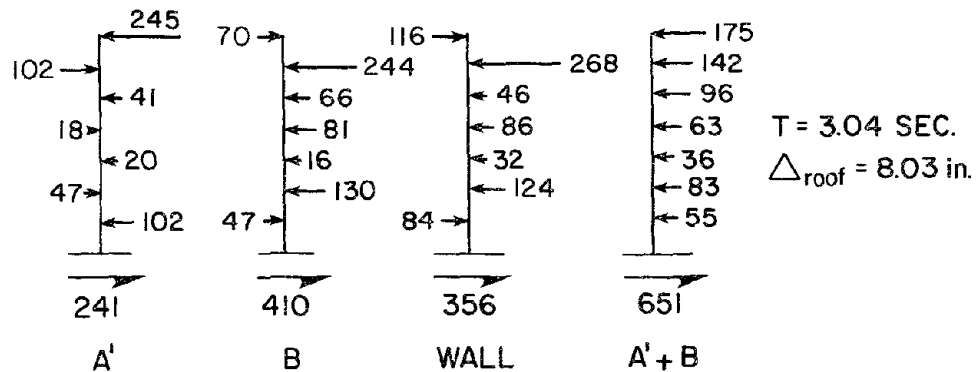
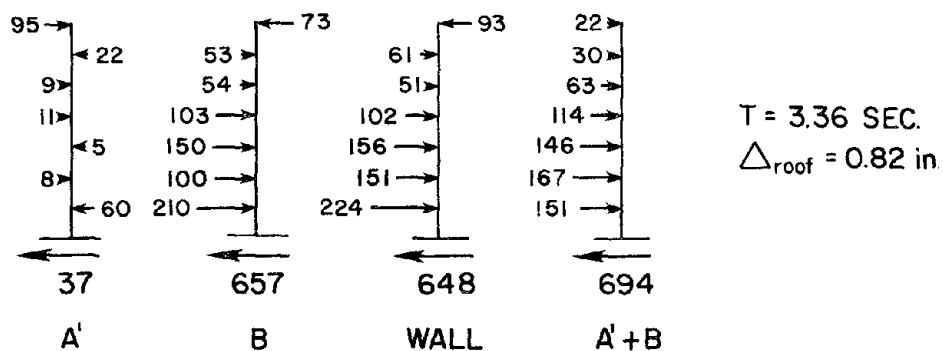
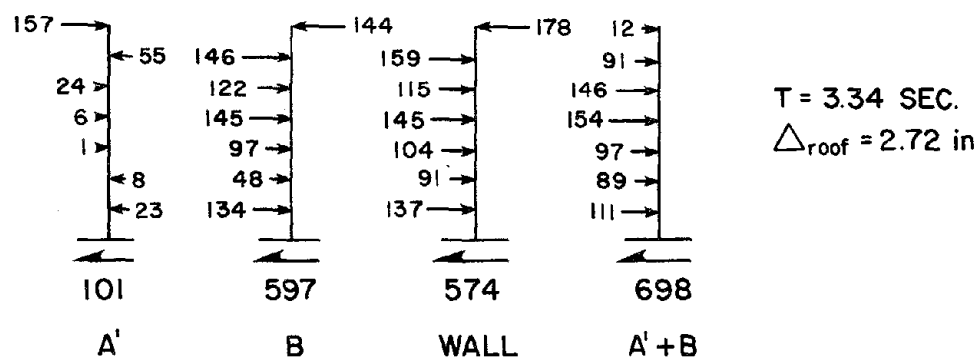


Fig. 5.55 Frame Interactive Forces Resulting from First Part of Pulse One of Derived Pacoima Dam Ground Motion

PRIOR TO WALL HINGE FORMATION



AFTER WALL HINGE FORMATION



AT MAXIMUM LATERAL DISPLACEMENT

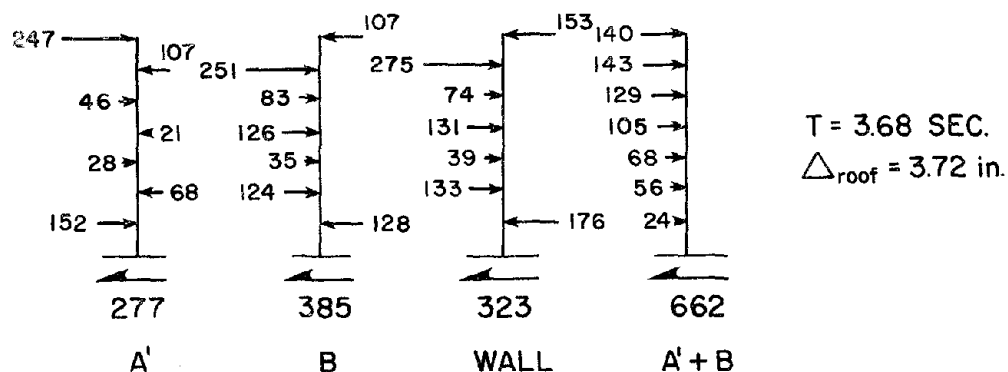


Fig. 5.56 Frame Interactive Forces Resulting from Second Part of Pulse One of Derived Pacoima Dam Ground Motion

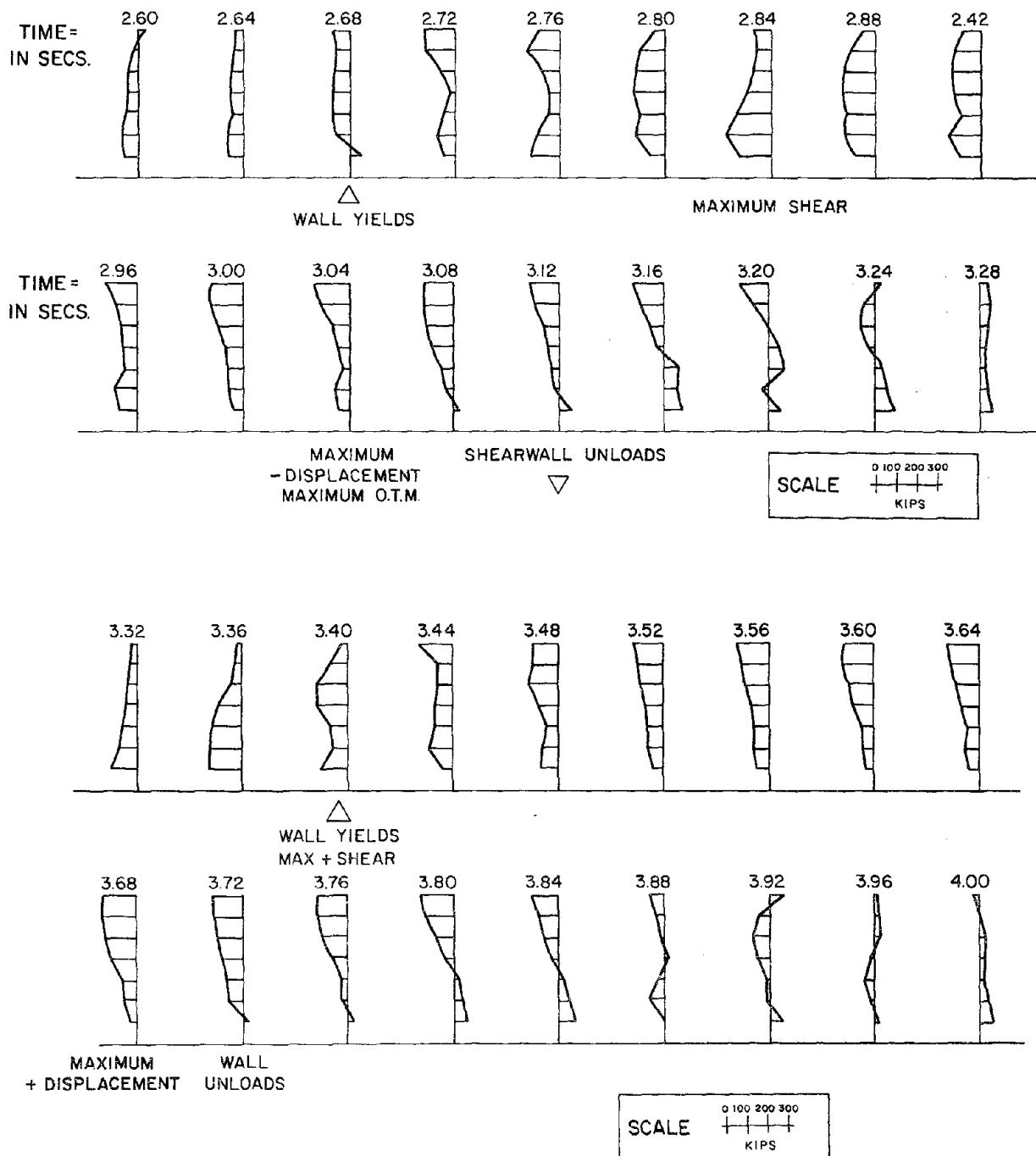


Fig. 5.57 Lateral Force Profile Time History Resulting from
Pulse One of Derived Pacoima Dam Ground Motion

Let ϕ_u = SECTION CURVATURE at maximum concrete strain
 ϕ_y = SECTION CURVATURE at steel yield
 L_p = equivalent PLASTIC HINGE LENGTH

Assume PLASTIC HINGE ROTATION Θ_u can be defined as follows:

$$\Theta_u = (\phi_u - \phi_y) / L_p$$

thus $\phi_u = (\Theta_u / L_p) + \phi_y$

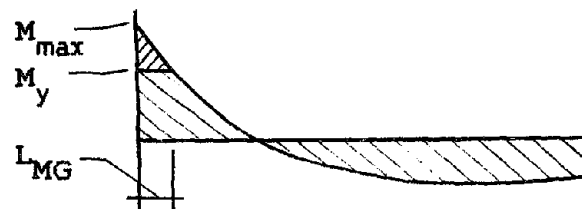
Define CURVATURE DUCTILITY μ_{cd} as:

$$\mu_{cd} = \phi_u / \phi_y$$

then $\mu_{cd} = [\Theta_u / (L_p * \phi_y)] + 1.0$

Define $L_p = d/2 + L_{MG}$

where "d" is section depth and L_{MG} is the distance between M_{max} and M_y for the critical region:



MOMENT DIAGRAM

Fig. 5.58 Relationship Between Plastic Hinge Rotation and Curvature Ductility

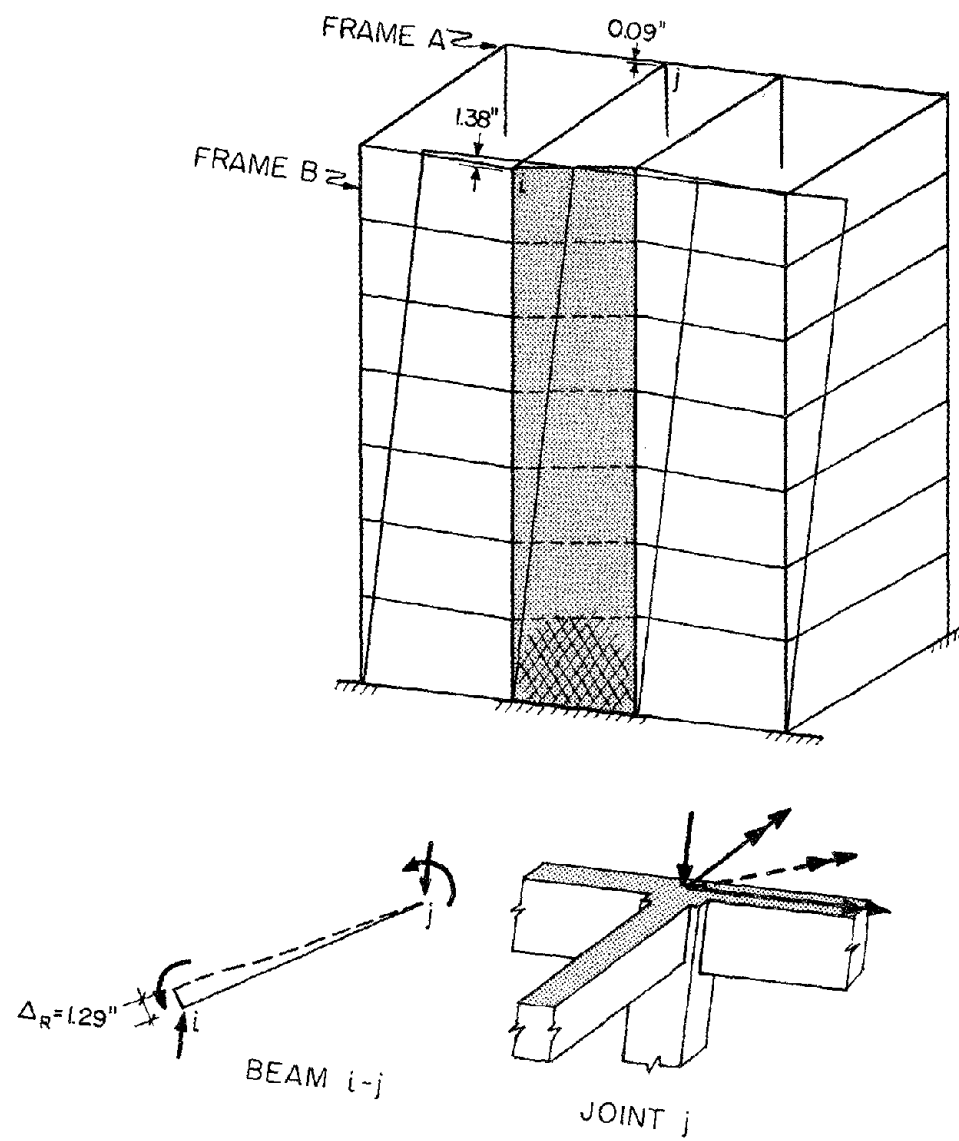


Fig. 6.1 Frame to Frame Flexural Coupling

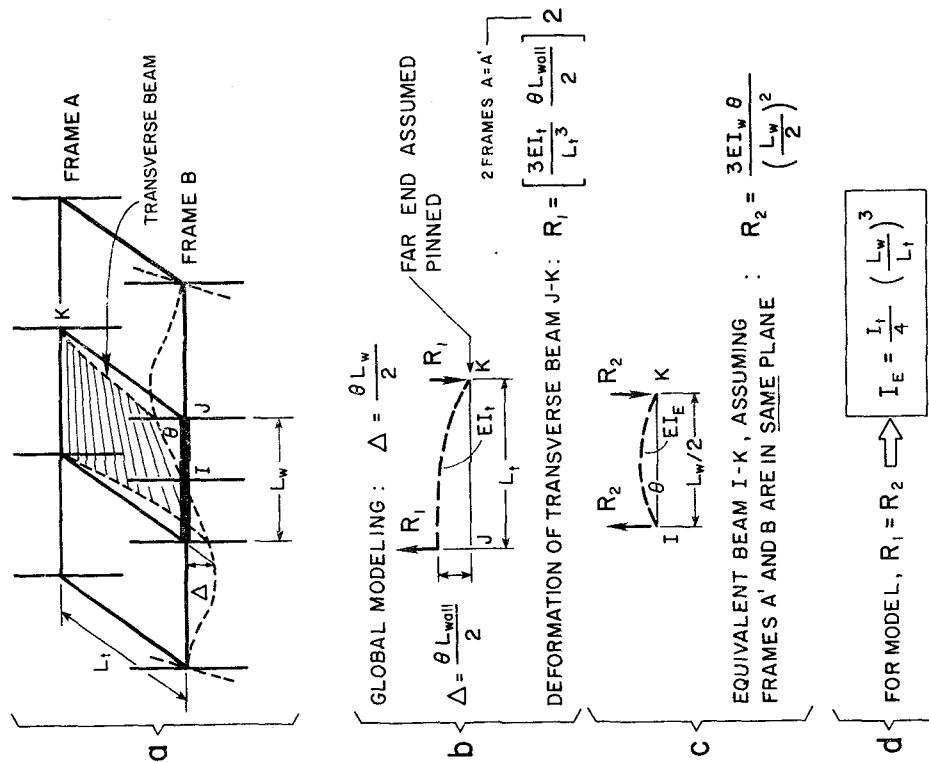


Fig. 6.2 Model Including Coupling

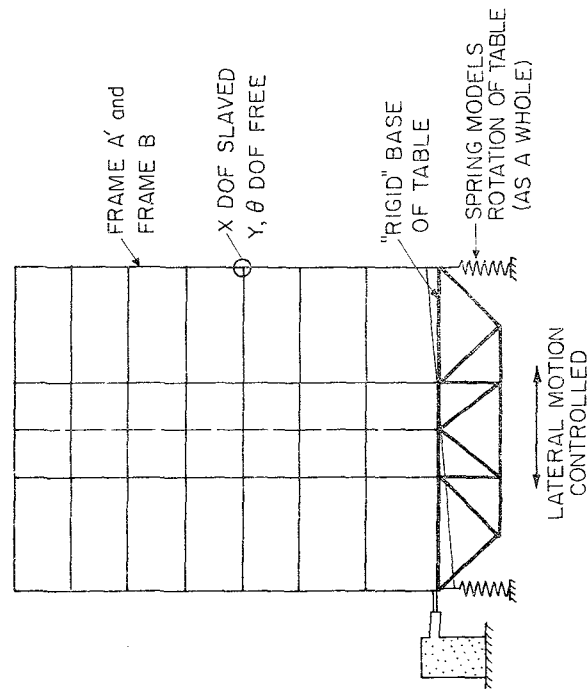
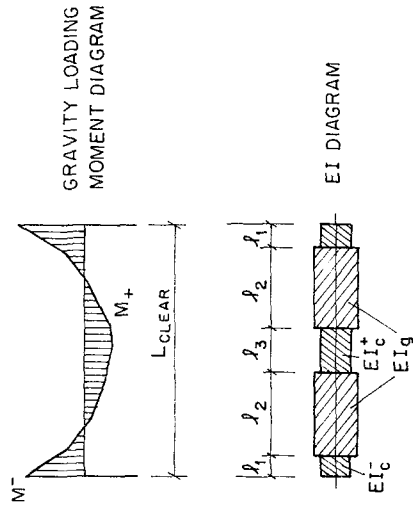
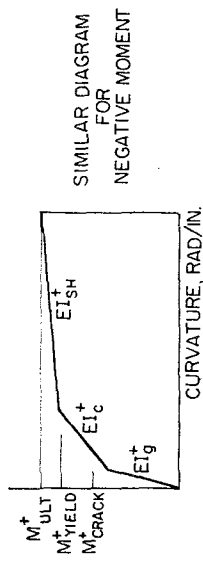
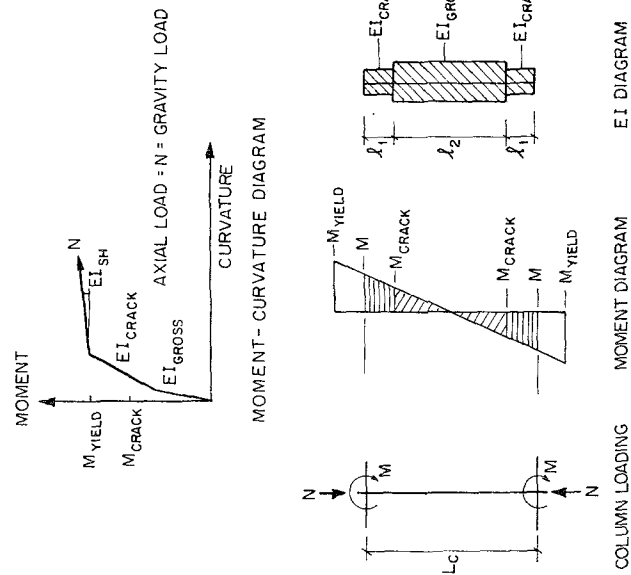


Fig. 6.3 Model of Base of Table



$$K_{BEAM} = \frac{EI_{GROSS}}{L_c} \begin{bmatrix} \alpha & \beta \\ \beta & \gamma \end{bmatrix} \quad \alpha, \beta, \gamma \text{ TO BE DETERMINED}$$

Fig. 6.5 Method for Obtaining Improved Beam Stiffness



$$K_{COLUMN} = \frac{EI_{GROSS}}{L_c} \begin{bmatrix} \alpha & \beta \\ \beta & \gamma \end{bmatrix} \quad \alpha, \beta, \gamma \text{ TO BE DETERMINED}$$

Fig. 6.4 Method for Obtaining Improved Column Stiffness

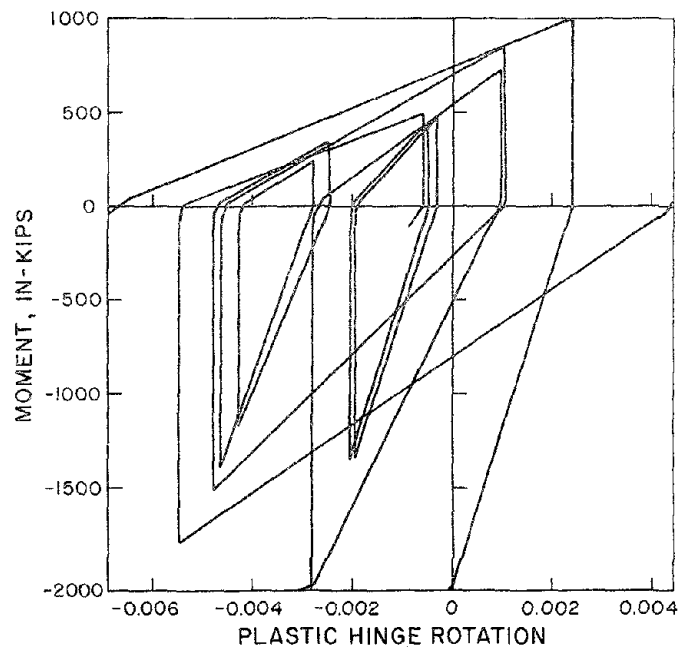


Fig. 6.6 Hysteresis for Typical Beam as Computed

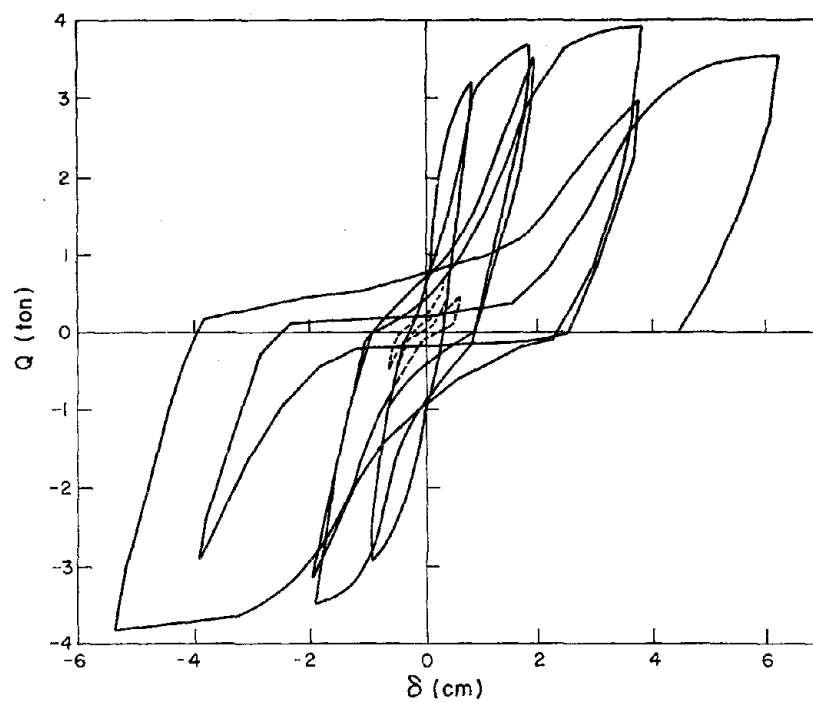


Fig. 6.7 Hysteresis for Japanese 1/2 Scale Model

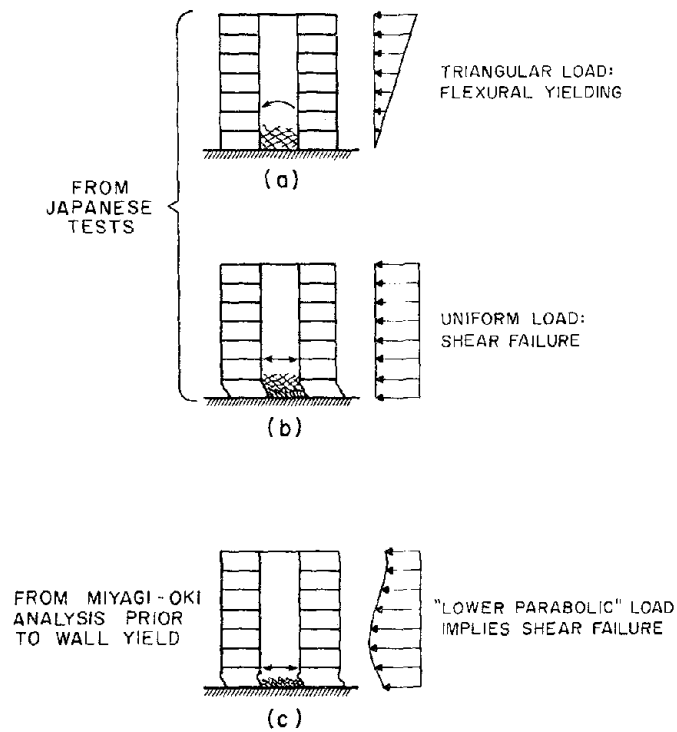


Fig. 6.8 Lateral Load Distributions Affecting Wall Hinging

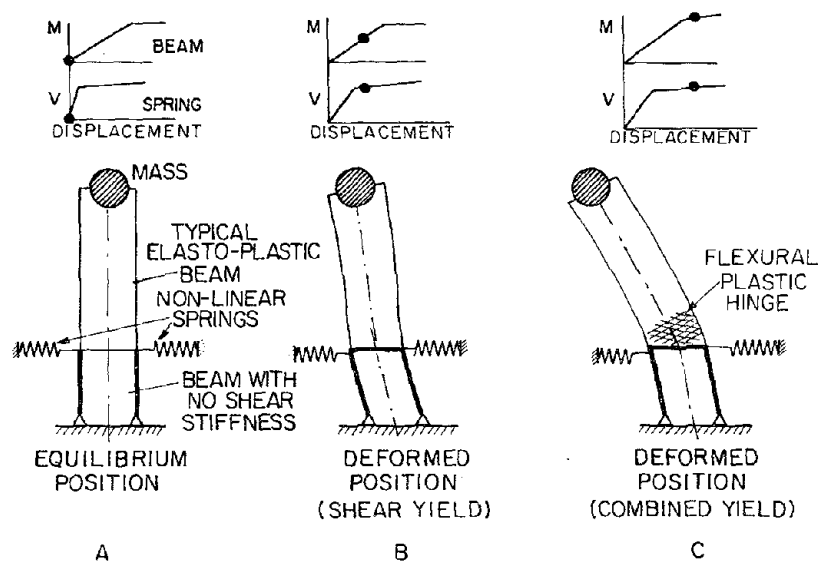
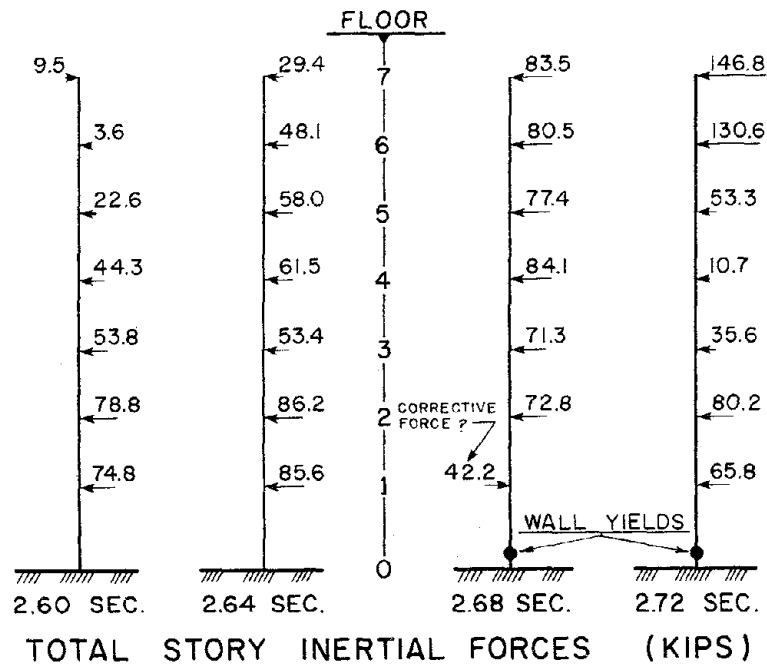
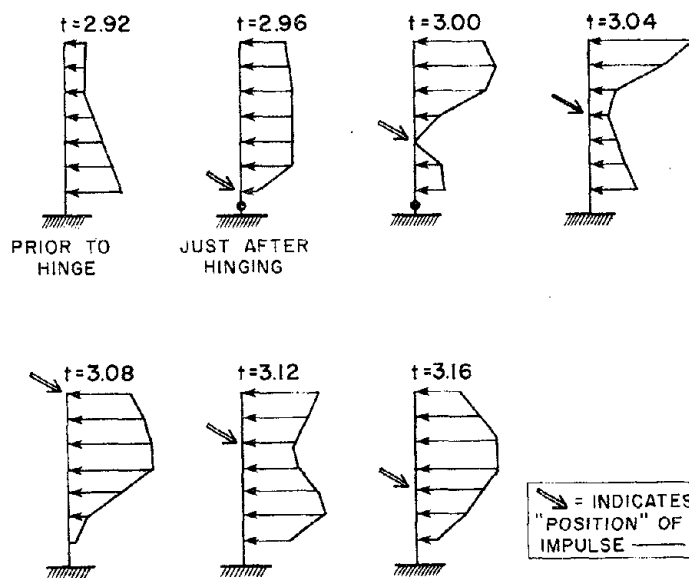


Fig. 6.9 Simple Shear Yielding Model



(A)



(B)

Fig. 6.10 Effect of Equilibrium Corrections on Response

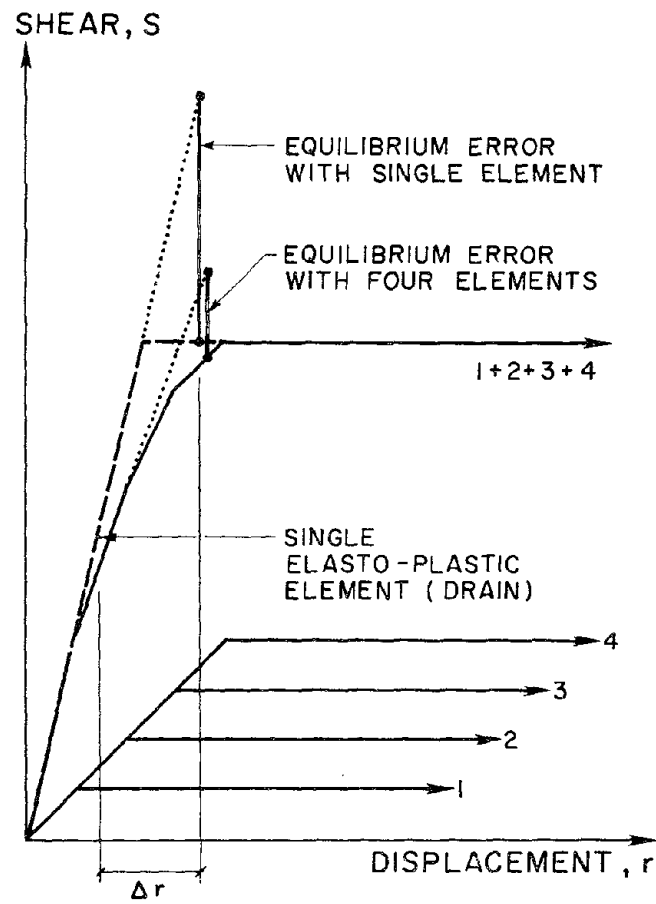


Fig. 6.11 Multi-Component Model to Reduce Equilibrium Errors

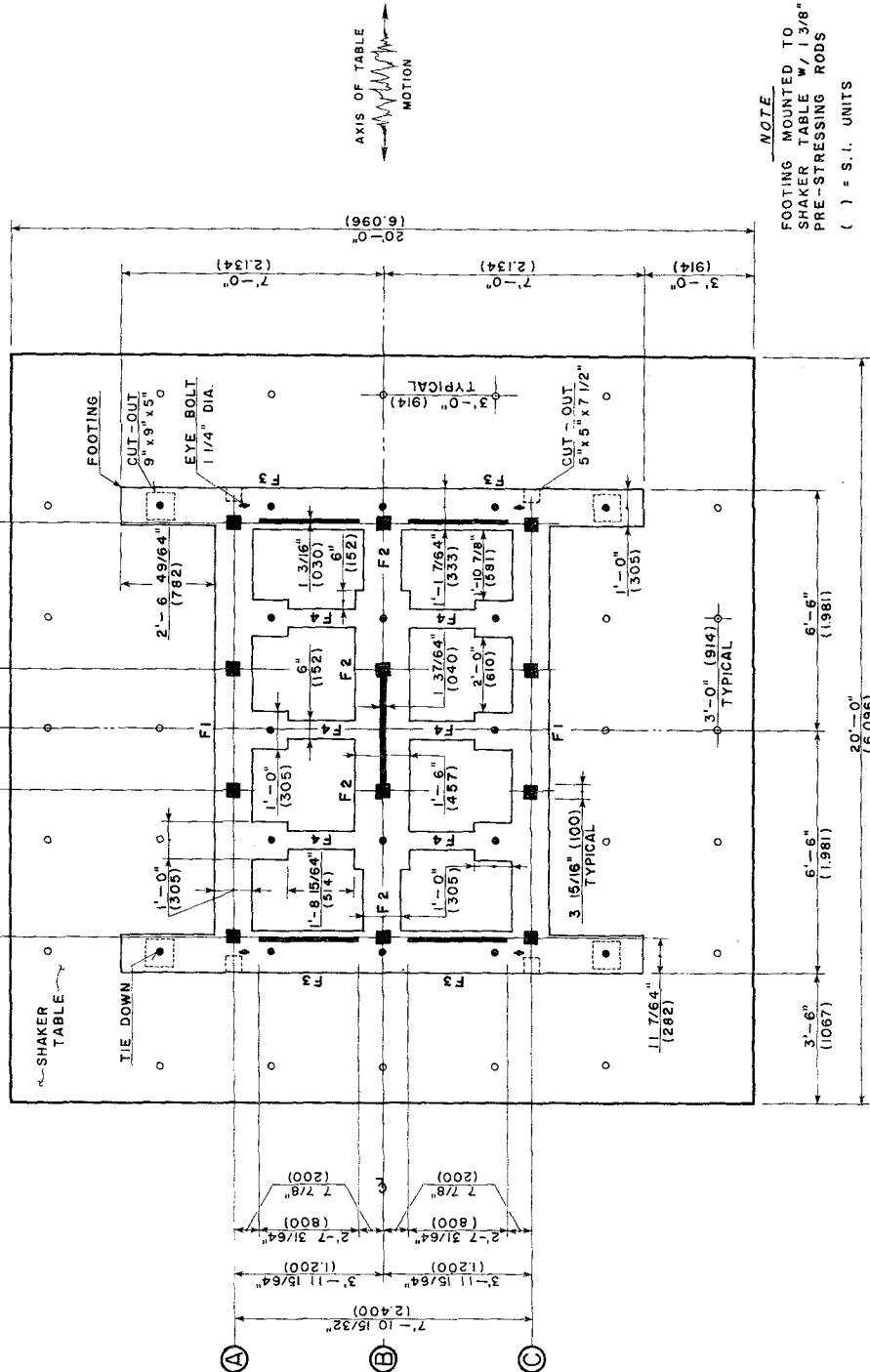
Appendix A

Plans for 1/5 Scale Model of Prototype

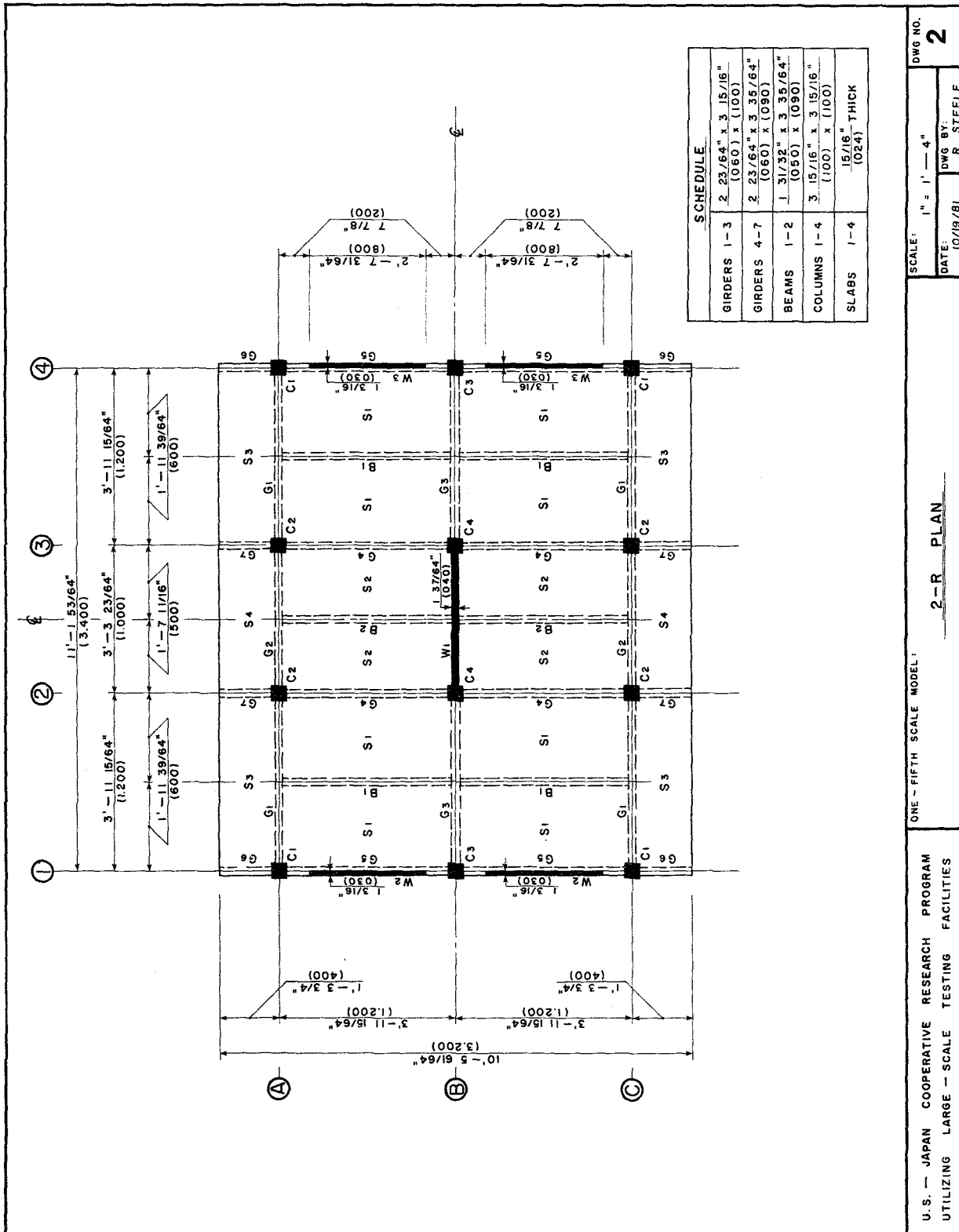
NOTE

THIS SET SUPERSEDES ALL
PREVIOUS SETS. REFER TO
CURRENT ADDENDA FOR
ADDITIONAL INFORMATION.

MINIMUM COVER	
MEMBERS	COVER
COLUMNS, BEAMS, BEARING WALLS	5/64" (006)
SLABS	5/32" (004)
WALLS except for BEARING WALLS	5/32" (004)
FOOTING	3/8" (010)

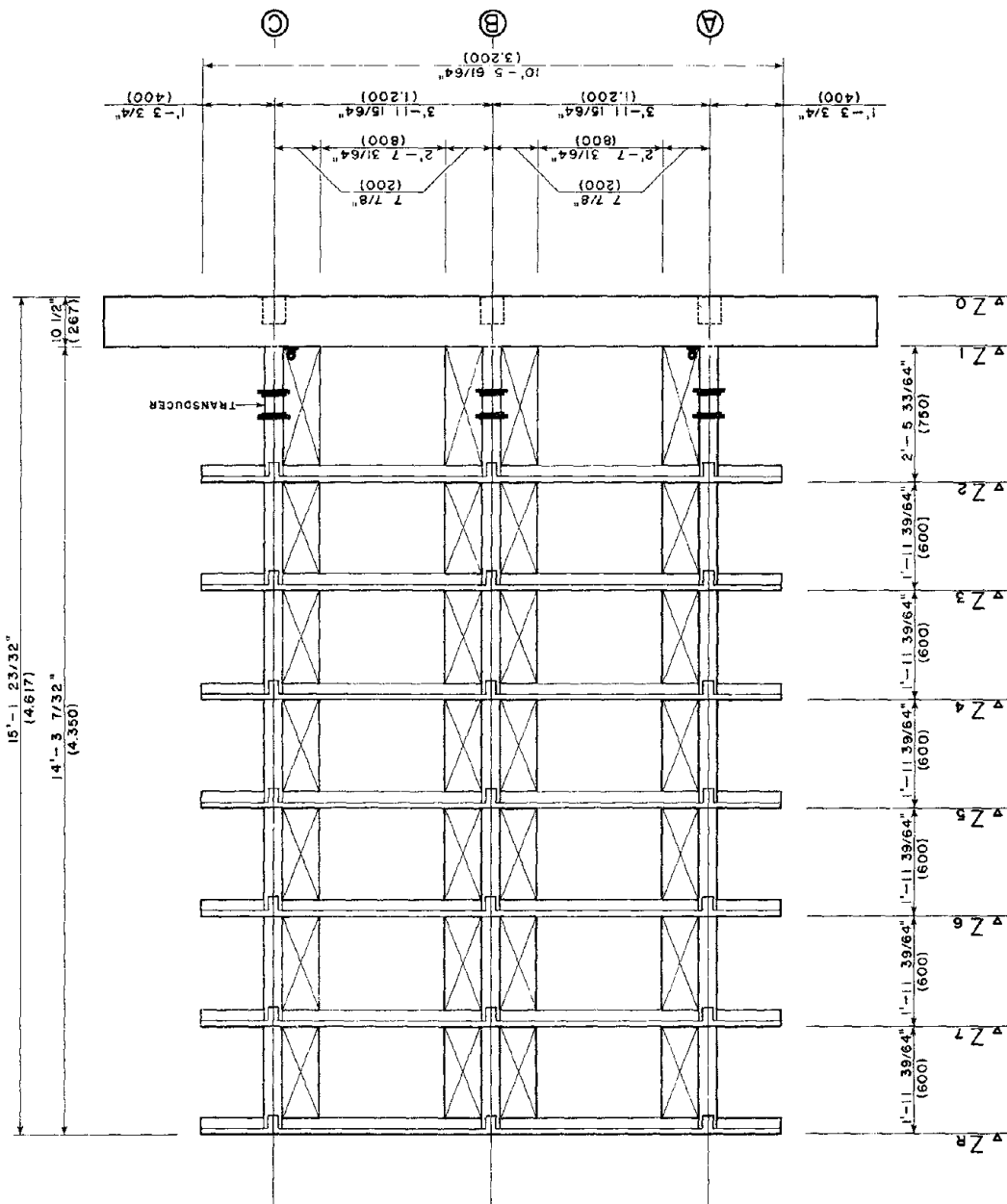


U.S. — JAPAN COOPERATIVE RESEARCH PROGRAM UTILIZING LARGE — SCALE TESTING FACILITIES		ONE — FIFTH SCALE MODEL		FOOTING PLAN		SCALE: 1" = 2' — 0"		DWG NO.
						DATE: 10/19/81		1
						DWG BY: R. STEELE		
								</



U.S. — JAPAN COOPERATIVE RESEARCH PROGRAM UTILIZING LARGE — SCALE TESTING FACILITIES	ONE — FIFTH SCALE MODEL		SCALE: 1" = 1' — 4"	DWG NO. 2
	2-R PLAN		DWG BY: R. STEELE	
			DATE: 10/19/81	





U.S. — JAPAN COOPERATIVE RESEARCH PROGRAM
UTILIZING LARGE — SCALE TESTING FACILITIES

ONE-FIFTH SCALE MODEL

④ FRAME SECTION

SCALE: 1" = 1'-4"

DWG NO. 4

DWG BY: R. STEELE

DATE: 10/19/81

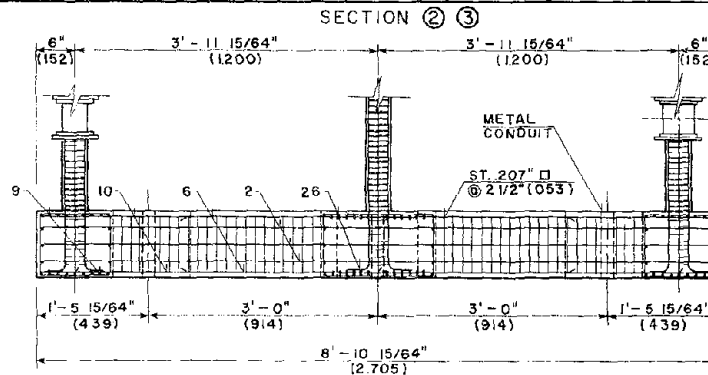
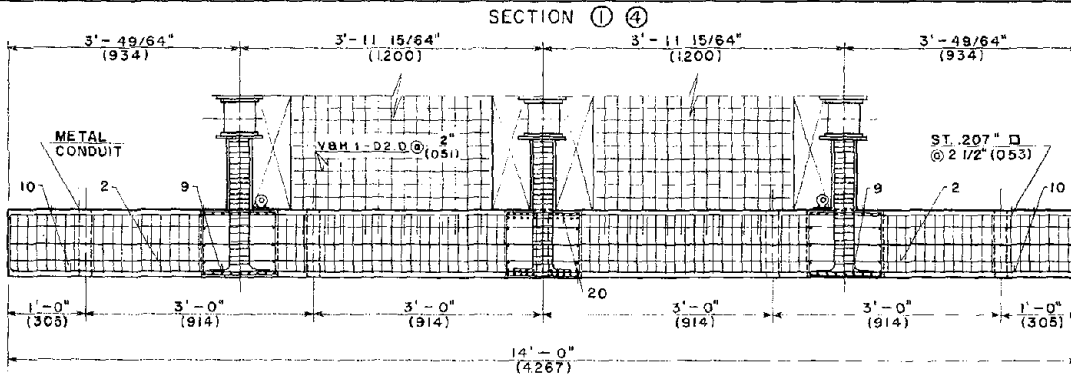
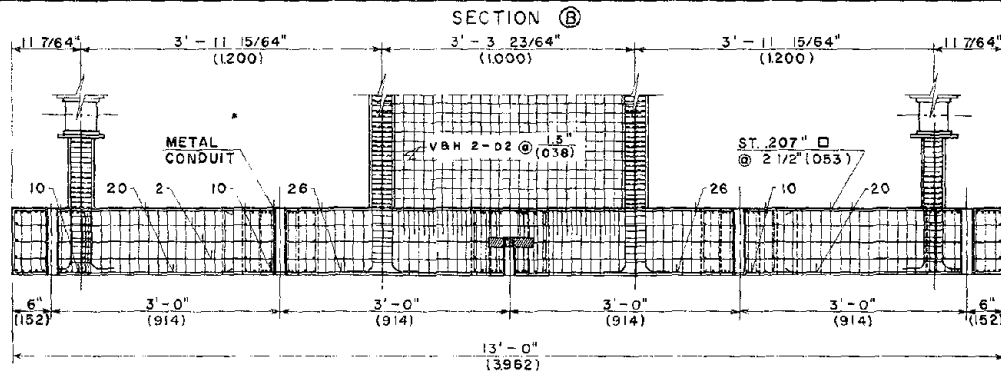
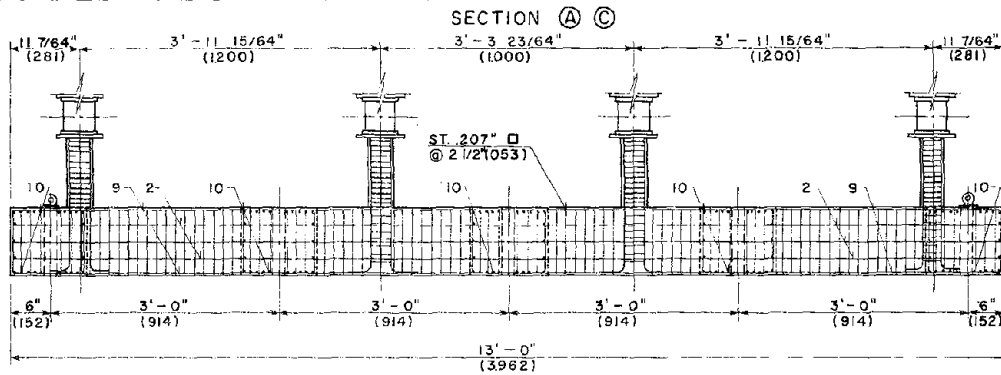
U.S. - JAPAN COOPERATIVE RESEARCH PROGRAM
UTILIZING LARGE - SCALE TESTING FACILITIES

ONE-FIFTH SCALE MODEL.

DETAIL OF FOOTING
REINFORCING - ELEVATION

SCALE: 1" = 1'-0"
DATE: 10/19/81
DWG NO: R. STEELE

DWG NO. 5



NOTES

HORIZONTAL FOOTING
STEEL #3 BAR -
TYPICAL

STIRRUPS 207" WIRE
@ 2 1/2" (053) O.C.

COVER 5/32" (004)

METAL CONDUIT
I.D. 2 1/16"
O.D. 2 3/16"

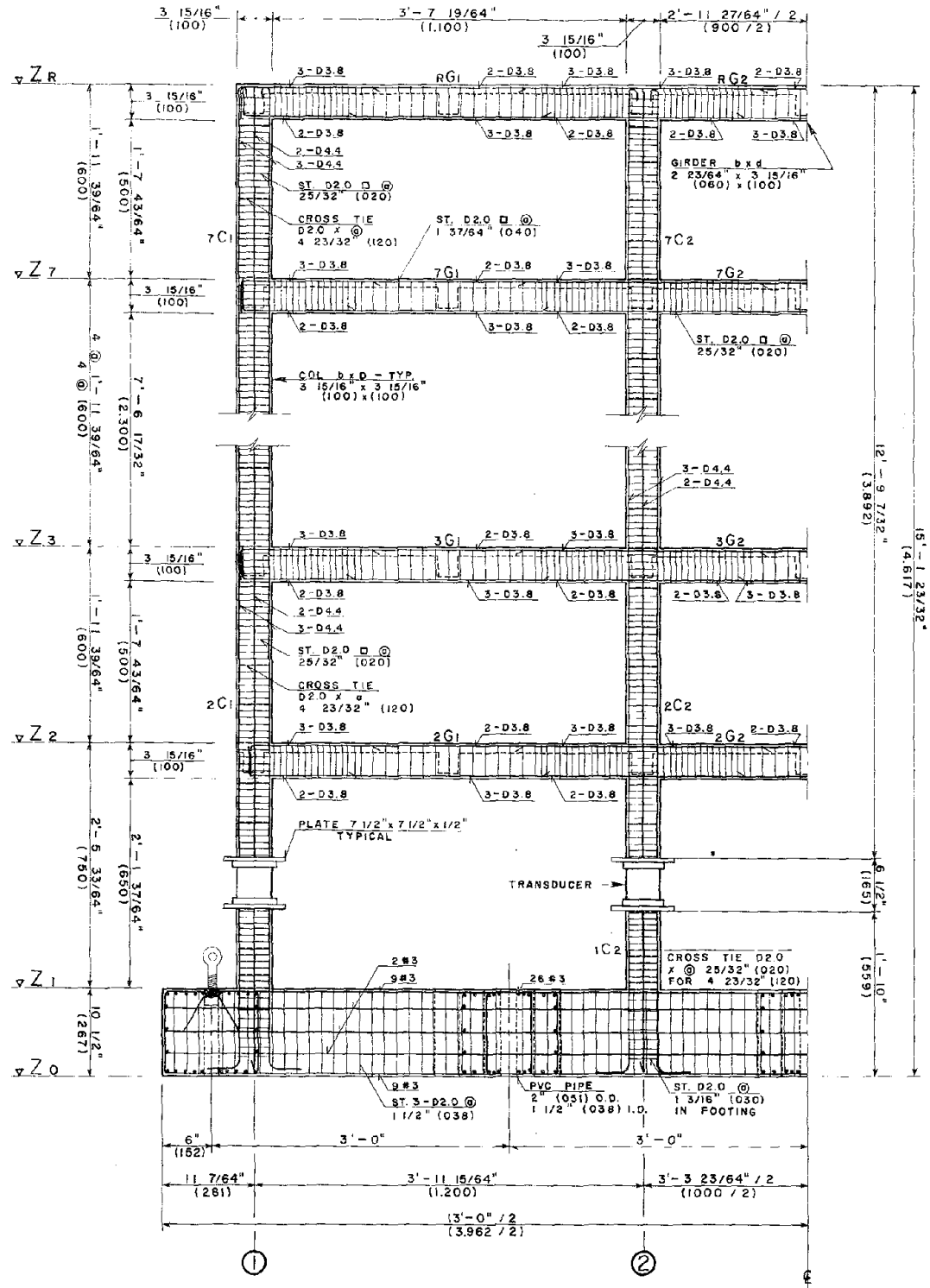
CUT-OUTS NOT
SHOWN THIS SHEET -
SEE DWG. NO. 6

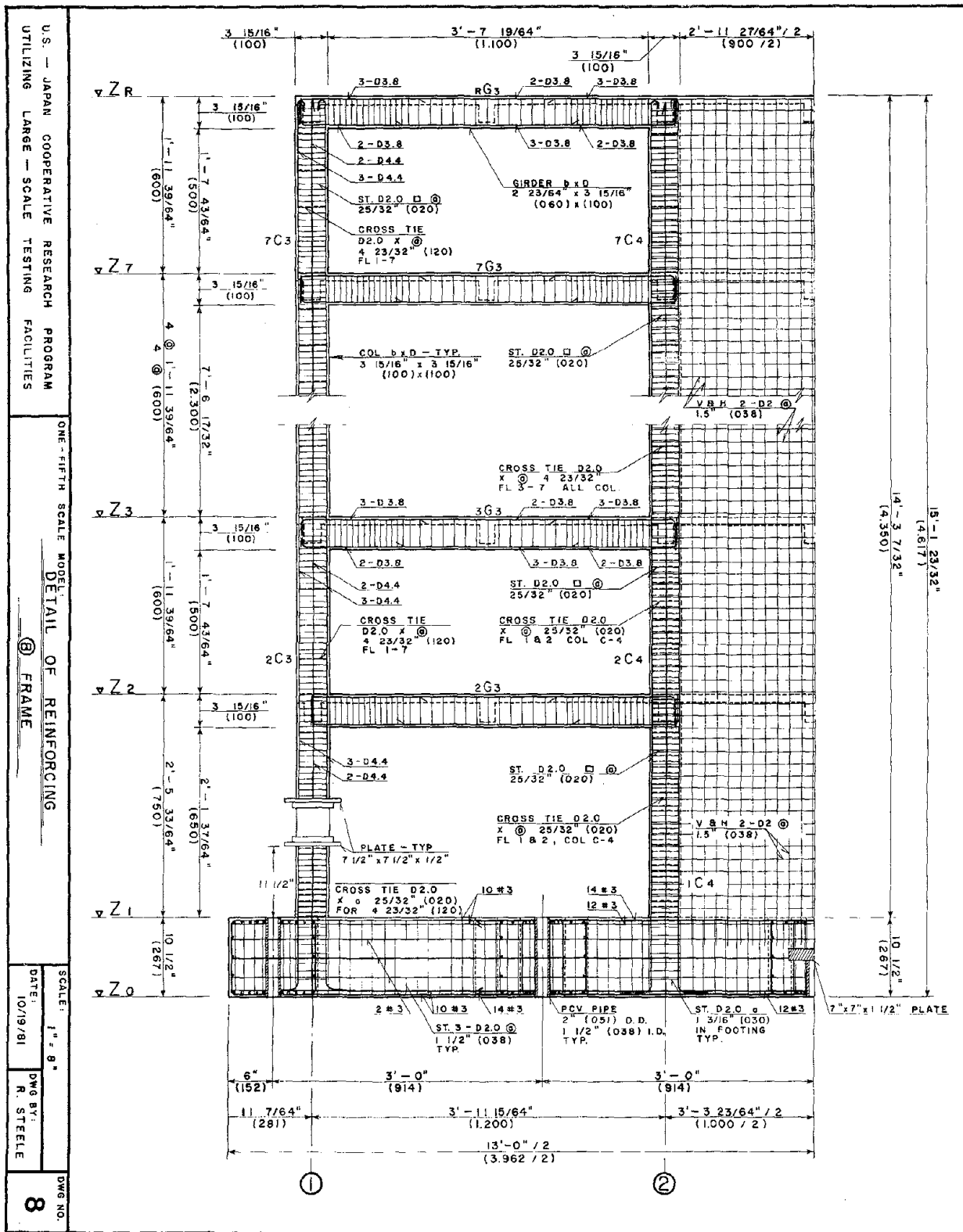
U.S. - JAPAN COOPERATIVE RESEARCH PROGRAM
UTILIZING LARGE-SCALE TESTING FACILITIES

ONE-FIFTH SCALE MODEL
DETAIL OF REINFORCING

SCALE: 1" = 8"
DATE: 10/19/81
DWG BY: R. STEELE

7





ONE-FIFTH SCALE MODEL:

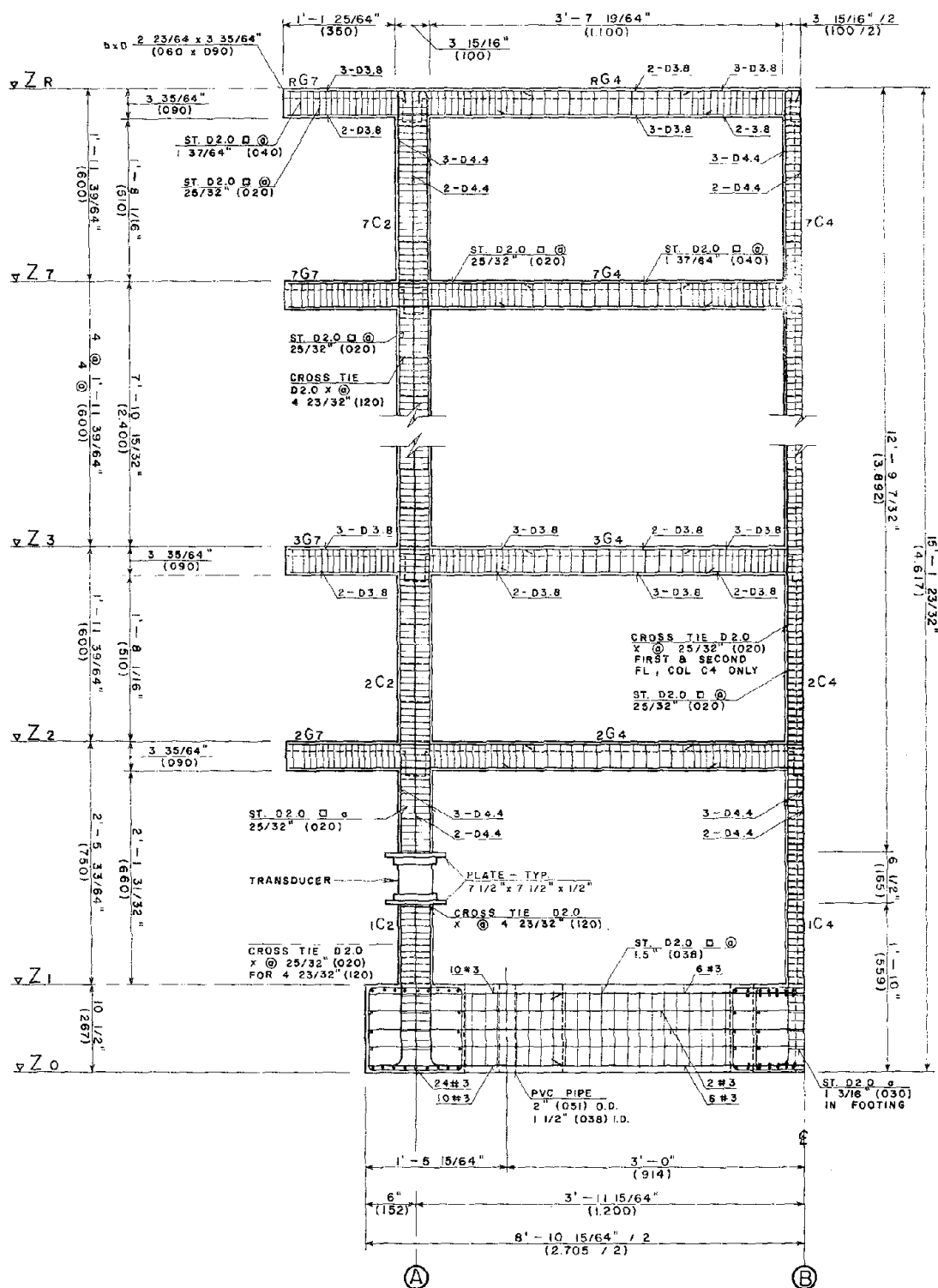
DETAIL OF REINFORCING

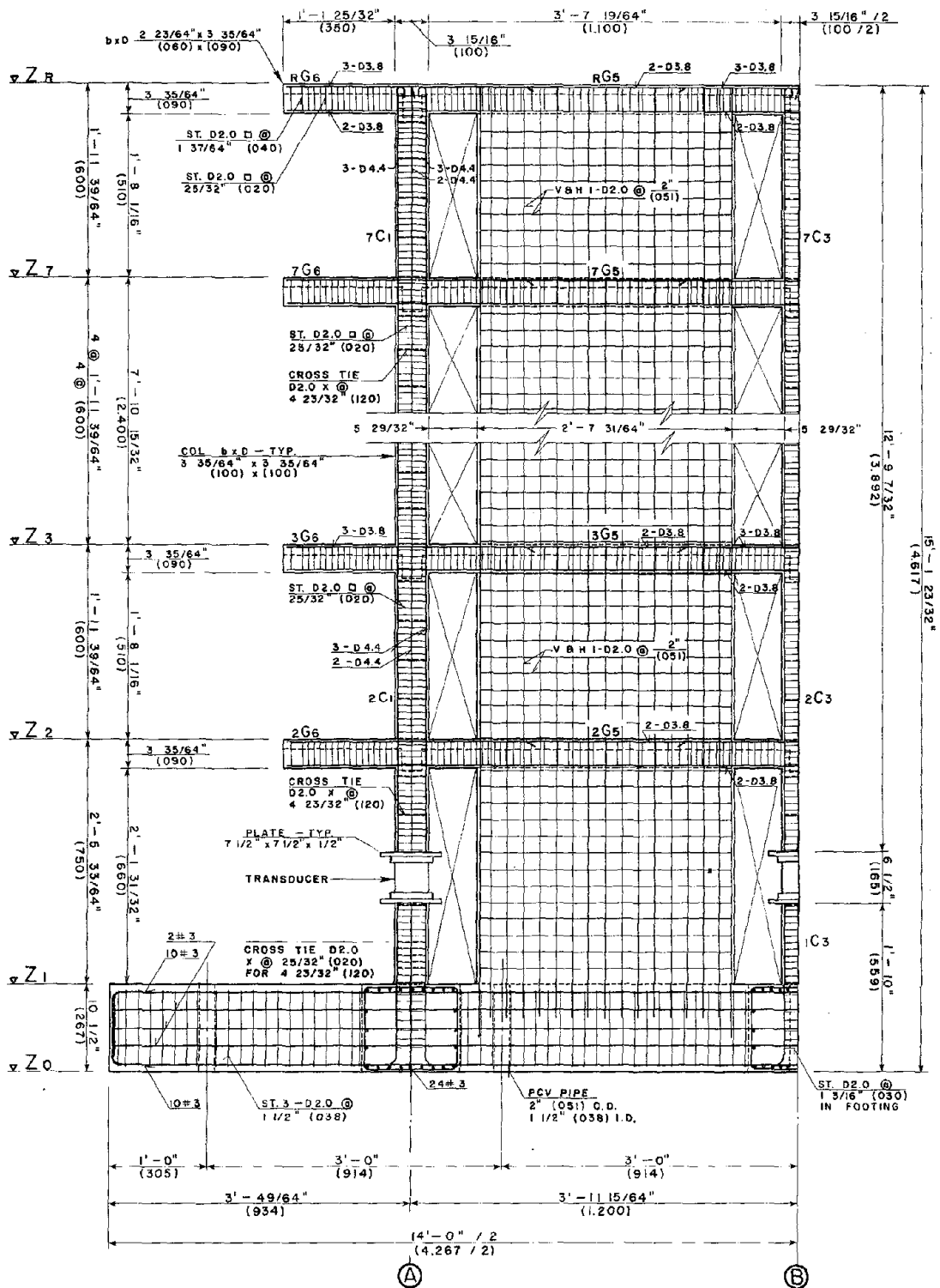
②, ③ FRAME

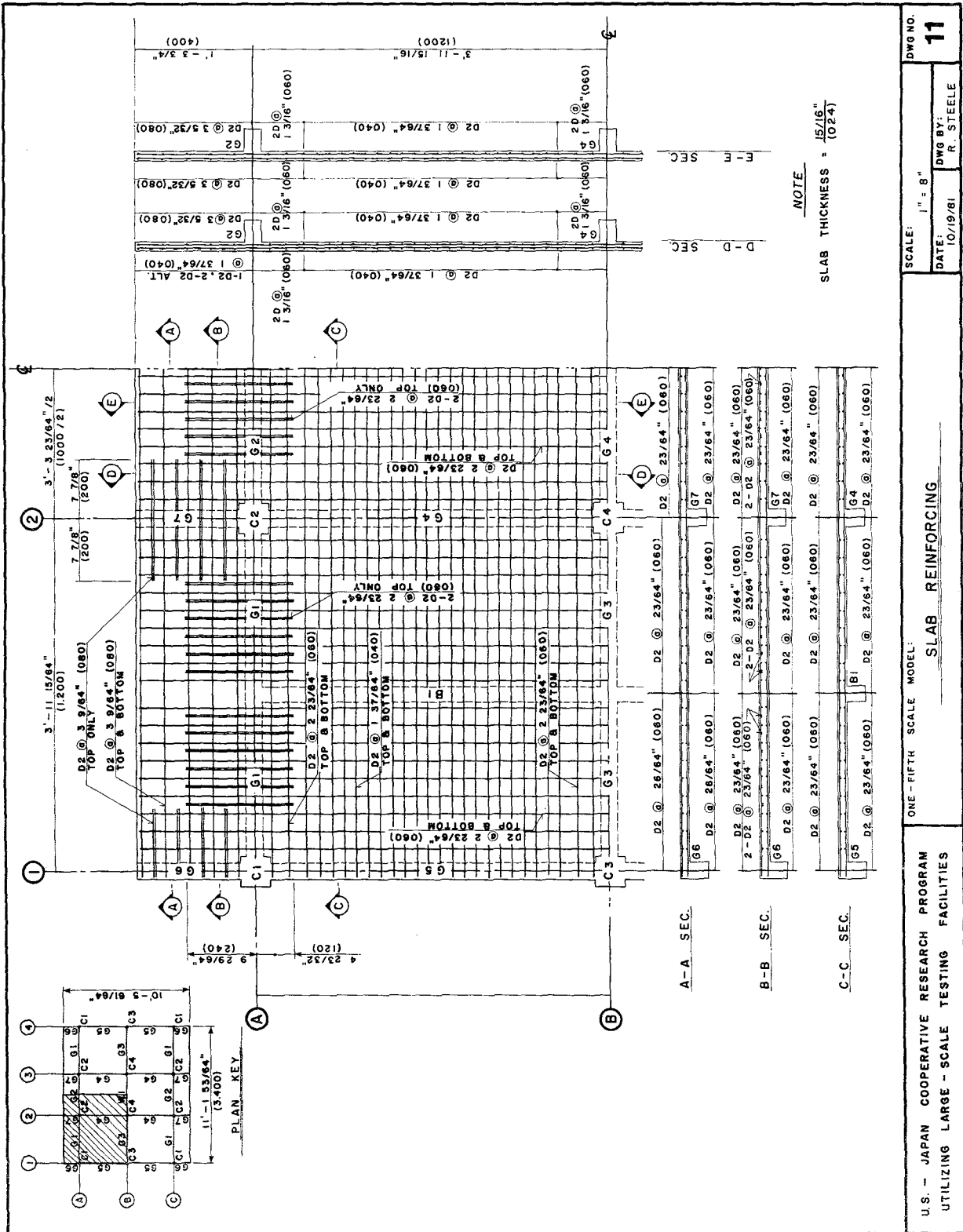
1" = 8"

DATE: 10/19/81	DWG BY: R. STEELE
-------------------	----------------------

60

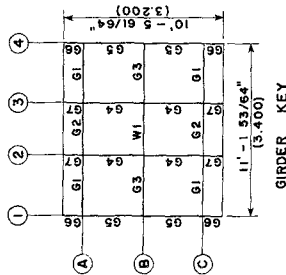






GIRDERS

MARK	POSITION	G1,3	G2	G4	G5	G6,7
		O.E. I.E. CENTER	END CENTER	O.E. I.E. CENTER	O.E. I.E. CENTER	ALL SECTION
ZR Z2						
b x D		2 23/64" x 3 15/16" (060 x 100)	2 23/64" x 3 15/16" (060 x 100)	2 23/64" x 3 35/64" (060 x 090)	2 23/64" x 3 35/64" (060 x 090)	2 23/64" x 3 35/64" (060 x 090)
TOP		3-D3.8	3-D3.8	3-D3.8	3-D3.8	3-D3.8
BOTTOM		2-D3.8	2-D3.8	2-D3.8	2-D3.8	2-D3.8
STIRRUP D-2		25/32" 1 37/64" (020)	25/32" 1 32/64" (020)	25/32" 1 37/64" (020)	25/32" 1 37/64" (020)	25/32" 1 37/64" (020)
SPACING O.C.						

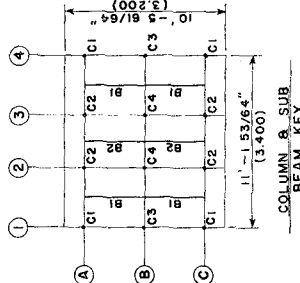


SUB BEAMS

MARK	POSITION	B1	B2
		O.E. CENTER I.E.	O.E. CENTER I.E.
b x D		1 31/32" x 3 35/64" (050 x 090)	1 31/32" x 3 35/64" (050 x 090)
TOP		2-D3.8	2-D3.8
BOTTOM		2-D3.8	2-D3.8
STIRRUP D-2		25/32" 1 37/64" (020)	25/32" 1 37/64" (020)
SPACING O.C.			

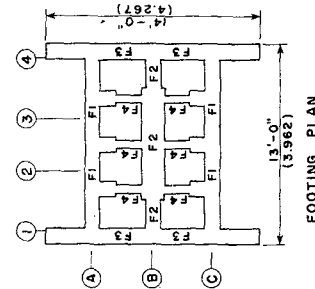
COLUMNS

MARK	POSITION	C1,2,3,4
		O.E. I.E. CENTER
Z7 Z1		
b x D		3 15/16" (100 x 100)
PRINCIPAL REIN		8-D4.4
HOOP D-2		25/32"
SPACING O.C.		(020)
CROSS REIN D-2		VARIES
SPACING O.C.		



FOOTING

MARK	POSITION	F1	F2	F3	F4
		ALL SECTION	END CENTER	ALL SECTION	O.E. I.E. CENTER
b x D		12" x 10 1/2" (305 x 267)	18" x 10 1/2" (457 x 267)	12" x 10 1/2" (305 x 267)	12" x 10 1/2" (305 x 267)
TOP		9-D3	20-D3	10-D3	10-D3
BOTTOM		9-D3	20-D3	10-D3	10-D3
WEB REIN		6-D3	6-D3	6-D3	6-D3
STIRRUP-20"		2 1/2"	2 1/2"	2 1/2"	2 1/2"
SPACING O.C.		(053)	(053)	(053)	(053)



U.S. — JAPAN COOPERATIVE RESEARCH PROGRAM
UTILIZING LARGE — SCALE TESTING FACILITIES

ONE-FIFTH SCALE MODEL: MEMBER SCHEDULE

SCALE: 1" = 10"

DATE: 10/19/81

DWG NO. 12

DWG BY: R. STEELE

1. HOOKS OF RE - BAR

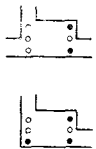
The end of deformed bars shall be hooked in the following cases:

- (1) Corner of column
- (2) Corner of beam
- (3) Hooks, stirrups and ties

COLUMN



BEAM



2. BENDING OF RE - BAR

BENDING ANGLE	TYPES	LOCATION
180°	D MIN 4 d I MIN 12 d	ENDS
135°	D MIN 4 d I MIN 12 d	
90°	D MIN 4 d I MIN 12 d	
135° 90°	D MIN 4 d I MIN 8 d I MIN 10 d	
NO MORE THAN 90°	D MIN 4 d D MIN 5 d D MIN 6 d	CENTERS

3. ANCHOR LENGTH & LAP LENGTH OF RE - BAR

RE-BAR	CONCRETE STRENGTH	S1	S2	BEAMS	SLABS
		50d	40d	25d	NO
					LESS THEN 1 3/16" (030)

- S1: For joints and anchor length except for the following cases.
S2: Anchor length of deformed bar without lap.
S3: Anchor length of bottom bar of sub-beam and slabs.

4. MINIMUM COVERING THICKNESS TO RE - BAR

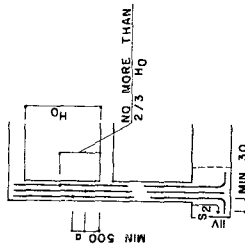
MEMBERS	COVERING THICKNESS
COLUMNS, BEAMS BEARING WALLS	15/64" (006)
SLABS, WALLS except for BEARING WALLS	5/32" (004)

The concrete covering covering for any reinforcement shall be not less than the minimum specified in the preceding table.

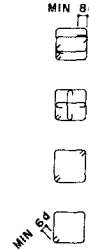
5. CLEARANCE BETWEEN MAIN RE - BAR

Clearance between main reinforcement bars shall not be less than 1 1/2 times the diameter of the bar.

6. JOINT AND ANCHORAGE (COLUMNS)



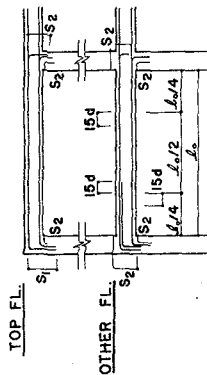
7. HOOPS



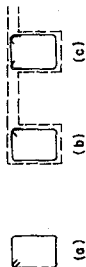
Hoops shall be placed alternately.

8. JOINT AND ANCHORAGE (GIRDERS)

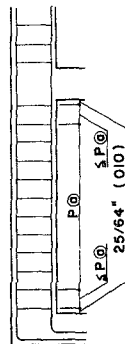
- (1) Joints shall be placed within the following limits.
Top bars - within $1/2$ of the center.
Bottom bars - within $1/4$ of the end.
- (2) Reinforcing bars shall be anchored across the center of the column when the bar is anchored in the column.



9. STIRRUPS



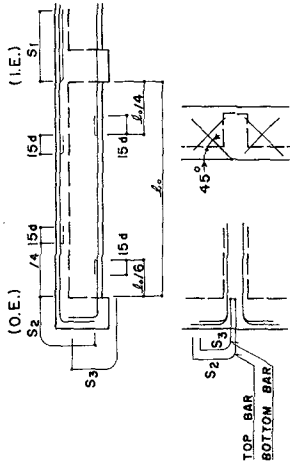
- (1) Stirrups shall be made as shown in the following figure.
- (2) Hooks shall be placed alternately in case of (a).



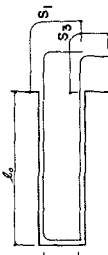
10. FOUNDATION



11. SUB BEAMS



12. CANTILEVER BEAMS



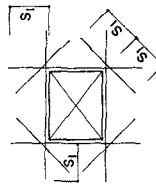
More than ten top bars shall be anchored in the column.

13. WALLS

- (1) Reinforcement of openings.

WALL	REINFORCEMENT BAR	VERTICAL	HORIZONTAL	DIAGONAL
t = 13/16"	2-D2	2-D2	2-D2	2-D2

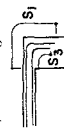
- (2) Length of lap joints and anchorage shall be S_1 .
- (3) Length of lap joint shall be S_1 and anchor length shall be S_2 in case of bearing walls.
- (4) Tie bars shall be spaced at $7/8$ (200) intervals.



- (5) Anchor length of reinforcement of openings.

14. SLABS

- (1) Anchor length shall be the following figure.



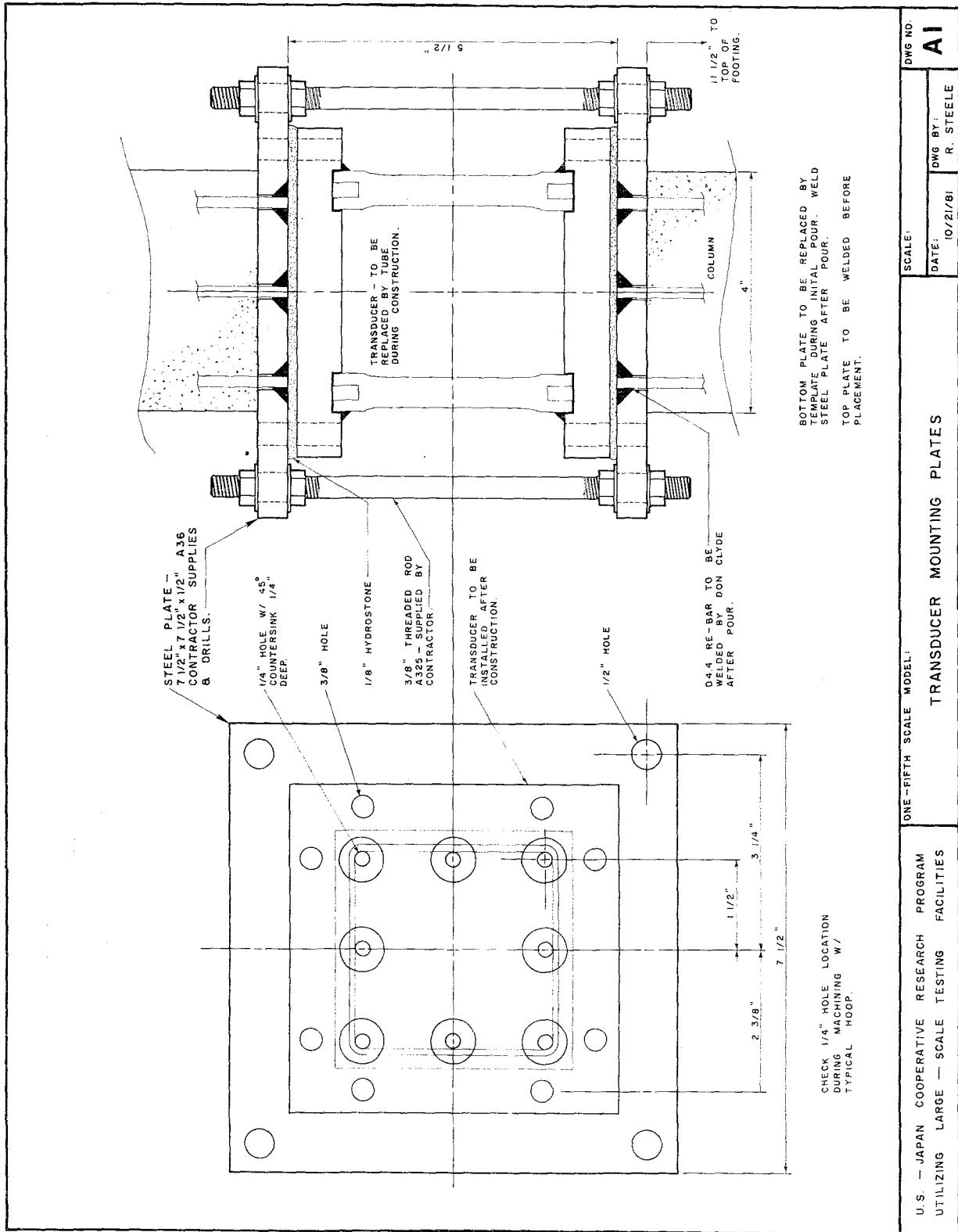
NOTE

THIS SET SUPERSEDES ALL PREVIOUS SETS. PLEASE REFER TO CURRENT ADDENDA FOR ADDITIONAL INFORMATION.

15. WEIGHT

Weight of typical floor = 2.8 kips
Weight of footing = 20 kips
Total weight = 30 kips

U.S. - JAPAN COOPERATIVE RESEARCH PROGRAM UTILIZING LARGE - SCALE TESTING FACILITIES		ONE - FIFTH SCALE MODEL		SPECIFICATIONS		SCALE: NONE	DWG NO. 14
				DATE: 10/19/81	DWG BY: R. STEELE		



DIMENSIONS OF LEAD PIGS

Detailed description of the technical drawing:

- Main Plan View:** A large rectangle divided into a grid of smaller rectangles. Each small rectangle contains a number (0, 1, 2, or 3). The grid is bounded by dimensions: 10'-5 61/64" / 2 (total width), 3'-11 15/64" (width of one section), 5'-6 29/64" (width of another section), 3'-11 15/64" (width of another section), and 1'-7 11/16" (width of another section). Vertical dimensions on the left include 6", 1'-5 5/8", 1'-3 5/8", 4", 4", 11 11/16", and 4".
- Callouts from Main Plan:**
 - "SHADED PIGS ABOVE TYPE 0 - TYPICAL"
 - "1' - 6\"
 - "2' - 6\"
 - "2' - 6\" ANGLE - TYPICAL"
- Elevation Details:**
 - Type 0:** PLAN: 24 1/2" (622); ELEVATION: 19" (483). Dimensions: 1 1/8" (029), 2 3/4" (070), 4 1/2" (114), 3" (076).
 - Type 1:** ELEVATION: 19" (483). Dimensions: 1 1/8" (029), 22 1/2" (572), 3" (076), 4 1/2" (114), 2 7/8" (073).
 - Type 2:** ELEVATION: 19" (483). Dimension: 3" (076).
 - Type 3:** ELEVATION: 17" (432). Dimension: 3" (076).
- Detail Views:**
 - Top Right Detail:** Shows a cross-section of a pig resting on a slab. Components include "1/4\"
 - Bottom Right Detail:** Shows a cross-section of a pig resting on a column. Components include "ANGLE 2 1/2\" x 1 1/2\" x 1/4\"", "1/4\" THREADED ROD A325 8\" LONG", "WASHER", "RUBBER STRIP 1\" x 1/4\"", "RUBBER STRIP 1\" x 1/4\"", "3/8\" I.D. PIPE OR TUBING", and "1/4\" PLATE".

TYPICAL LEAD MOUNTING DETAILS

ONE - FIFTH SCALE MODEL:	U.S. — JAPAN COOPERATIVE PROGRAM UTILIZING LARGE — SCALE TESTING FACILITIES	LEAD BALLAST DETAILS	SCALE: NOT TO SCALE	DWG. NO. A2
			DATE: 10/19/81	DWG. BY: R. STEELE

EARTHQUAKE ENGINEERING RESEARCH CENTER REPORTS

NOTE: Numbers in parentheses are Accession Numbers assigned by the National Technical Information Service; these are followed by a price code. Copies of the reports may be ordered from the National Technical Information Service, 5285 Port Royal Road, Springfield, Virginia, 22161. Accession Numbers should be quoted on orders for reports (PB --- ---) and remittance must accompany each order. Reports without this information were not available at time of printing. The complete list of EERC reports (from EERC 67-1) is available upon request from the Earthquake Engineering Research Center, University of California, Berkeley, 47th Street and Hoffman Boulevard, Richmond, California 94804.

- UCB/EERC-77/01 "PLUSH - A Computer Program for Probabilistic Finite Element Analysis of Seismic Soil-Structure Interaction," by M.P. Romo Organista, J. Lysmer and H.B. Seed - 1977 (PB81 177 651)A05
- UCB/EERC-77/02 "Soil-Structure Interaction Effects at the Humboldt Bay Power Plant in the Ferndale Earthquake of June 7, 1975," by J.E. Valera, H.B. Seed, C.F. Tsai and J. Lysmer - 1977 (PB 265 795)A04
- UCB/EERC-77/03 "Influence of Sample Disturbance on Sand Response to Cyclic Loading," by K. Mori, H.B. Seed and C.K. Chan - 1977 (PB 267 352)A04
- UCB/EERC-77/04 "Seismological Studies of Strong Motion Records," by J. Shoja-Taheri - 1977 (PB 269 655)A10
- UCB/EERC-77/05 Unassigned
- UCB/EERC-77/06 "Developing Methodologies for Evaluating the Earthquake Safety of Existing Buildings," by No. 1 - B. Bresler; No. 2 - B. Bresler, T. Okada and D. Zisling; No. 3 - T. Okada and B. Bresler; No. 4 - V.V. Bertero and B. Bresler - 1977 (PB 267 354)A08
- UCB/EERC-77/07 "A Literature Survey - Transverse Strength of Masonry Walls," by Y. Omote, R.L. Mayes, S.W. Chen and R.W. Clough - 1977 (PB 277 933)A07
- UCB/EERC-77/08 "DRAIN-TABS: A Computer Program for Inelastic Earthquake Response of Three Dimensional Buildings," by R. Guendelman-Israel and G.H. Powell - 1977 (PB 270 693)A07
- UCB/EERC-77/09 "SUBWALL: A Special Purpose Finite Element Computer Program for Practical Elastic Analysis and Design of Structural Walls with Substructure Option," by D.Q. Le, H. Peterson and E.P. Popov - 1977 (PB 270 567)A05
- UCB/EERC-77/10 "Experimental Evaluation of Seismic Design Methods for Broad Cylindrical Tanks," by D.P. Clough (PB 272 280)A13
- UCB/EERC-77/11 "Earthquake Engineering Research at Berkeley - 1976," - 1977 (PB 273 507)A09
- UCB/EERC-77/12 "Automated Design of Earthquake Resistant Multistory Steel Building Frames," by N.D. Walker, Jr. - 1977 (PB 276 526)A09
- UCB/EERC-77/13 "Concrete Confined by Rectangular Hoops Subjected to Axial Loads," by J. Vallenias, V.V. Bertero and E.P. Popov - 1977 (PB 275 165)A06
- UCB/EERC-77/14 "Seismic Strain Induced in the Ground During Earthquakes," by Y. Sugimura - 1977 (PB 284 201)A04
- UCB/EERC-77/15 Unassigned
- UCB/EERC-77/16 "Computer Aided Optimum Design of Ductile Reinforced Concrete Moment Resisting Frames," by S.W. Zagajski and V.V. Bertero - 1977 (PB 280 137)A07
- UCB/EERC-77/17 "Earthquake Simulation Testing of a Stepping Frame with Energy-Absorbing Devices," by J.M. Kelly and D.F. Tsztoo - 1977 (PB 273 506)A04
- UCB/EERC-77/18 "Inelastic Behavior of Eccentrically Braced Steel Frames under Cyclic Loadings," by C.W. Roeder and E.P. Popov - 1977 (PB 275 526)A15
- UCB/EERC-77/19 "A Simplified Procedure for Estimating Earthquake-Induced Deformations in Dams and Embankments," by F.I. Makdisi and H.B. Seed - 1977 (PB 276 820)A04
- UCB/EERC-77/20 "The Performance of Earth Dams during Earthquakes," by H.B. Seed, F.I. Makdisi and P. de Alba - 1977 (PB 276 821)A04
- UCB/EERC-77/21 "Dynamic Plastic Analysis Using Stress Resultant Finite Element Formulation," by P. Lukkunapvasit and J.M. Kelly - 1977 (PB 275 453)A04
- UCB/EERC-77/22 "Preliminary Experimental Study of Seismic Uplift of a Steel Frame," by R.W. Clough and A.A. Huckelbridge 1977 (PB 278 769)A08
- UCB/EERC-77/23 "Earthquake Simulator Tests of a Nine-Story Steel Frame with Columns Allowed to Uplift," by A.A. Huckelbridge - 1977 (PB 277 944)A09
- UCB/EERC-77/24 "Nonlinear Soil-Structure Interaction of Skew Highway Bridges," by M.-C. Chen and J. Penzien - 1977 (PB 276 176)A07
- UCB/EERC-77/25 "Seismic Analysis of an Offshore Structure Supported on Pile Foundations," by D.D.-N. Liou and J. Penzien 1977 (PB 283 180)A06
- UCB/EERC-77/26 "Dynamic Stiffness Matrices for Homogeneous Viscoelastic Half-Planes," by G. Dasgupta and A.K. Chopra - 1977 (PB 279 654)A06

UCB/EERC-77/27 "A Practical Soft Story Earthquake Isolation System," by J.M. Kelly, J.M. Eidinger and C.J. Derham - 1977 (PB 276 814)A07

UCB/EERC-77/28 "Seismic Safety of Existing Buildings and Incentives for Hazard Mitigation in San Francisco: An Exploratory Study," by A.J. Meltsner - 1977 (PB 281 970)A05

UCB/EERC-77/29 "Dynamic Analysis of Electrohydraulic Shaking Tables," by D. Rea, S. Abedi-Hayati and Y. Takahashi - 1977 (PB 282 569)A04

UCB/EERC-77/30 "An Approach for Improving Seismic - Resistant Behavior of Reinforced Concrete Interior Joints," by B. Galunic, V.V. Bertero and E.P. Popov - 1977 (PB 290 870)A06

ICB/EERC-78/01 "The Development of Energy-Absorbing Devices for Aseismic Base Isolation Systems," by J.M. Kelly and D.F. Tsztoo - 1978 (PB 284 978)A04

ICB/EERC-78/02 "Effect of Tensile Prestrain on the Cyclic Response of Structural Steel Connections," by J.G. Bouwkamp and A. Mukhopadhyay - 1978

ICB/EERC-78/03 "Experimental Results of an Earthquake Isolation System using Natural Rubber Bearings," by J.M. Eidinger and J.M. Kelly - 1978 (PB 281 686)A04

ICB/EERC-78/04 "Seismic Behavior of Tall Liquid Storage Tanks," by A. Niwa - 1978 (PB 284 017)A14

ICB/EERC-78/05 "Hysteretic Behavior of Reinforced Concrete Columns Subjected to High Axial and Cyclic Shear Forces," by S.W. Zagajski, V.V. Bertero and J.G. Bouwkamp - 1978 (PB 283 858)A13

ICB/EERC-78/06 "Three Dimensional Inelastic Frame Elements for the ANSR-I Program," by A. Riahi, D.G. Row and G.H. Powell - 1978 (PB 295 755)A04

ICB/EERC-78/07 "Studies of Structural Response to Earthquake Ground Motion," by O.A. Lopez and A.K. Chopra - 1978 (PB 282 790)A05

ICB/EERC-78/08 "A Laboratory Study of the Fluid-Structure Interaction of Submerged Tanks and Caissons in Earthquakes," by R.C. Byrd - 1978 (PB 284 957)A08

ICB/EERC-78/09 Unassigned

ICB/EERC-78/10 "Seismic Performance of Nonstructural and Secondary Structural Elements," by I. Sakamoto - 1978 (PB 281 154 593)A05

ICB/EERC-78/11 "Mathematical Modelling of Hysteresis Loops for Reinforced Concrete Columns," by S. Nakata, T. Sproul and J. Penzien - 1978 (PB 298 274)A05

ICB/EERC-78/12 "Damageability in Existing Buildings," by T. Blejwas and B. Bresler - 1978 (PB 30 166 978)A05

ICB/EERC-78/13 "Dynamic Behavior of a Pedestal Base Multistory Building," by R.M. Stephen, E.L. Wilson, J.G. Bouwkamp and M. Button - 1978 (PB 286 650)A08

ICB/EERC-78/14 "Seismic Response of Bridges - Case Studies," by R.A. Imbsen, V. Nutt and J. Penzien - 1978 (PB 286 503)A10

ICB/EERC-78/15 "A Substructure Technique for Nonlinear Static and Dynamic Analysis," by D.G. Row and G.H. Powell - 1978 (PB 288 077)A10

ICB/EERC-78/16 "Seismic Risk Studies for San Francisco and for the Greater San Francisco Bay Area," by C.S. Oliveira - 1978 (PB 81 120 115)A07

ICB/EERC-78/17 "Strength of Timber Roof Connections Subjected to Cyclic Loads," by P. Güllkan, R.L. Mayes and R.W. Clough - 1978 (HUD-000 1491)A07

UCB/EERC-78/18 "Response of K-Braced Steel Frame Models to Lateral Loads," by J.G. Bouwkamp, R.M. Stephen and E.P. Popov - 1978

UCB/EERC-78/19 "Rational Design Methods for Light Equipment in Structures Subjected to Ground Motion," by J.L. Sackman and J.M. Kelly - 1978 (PB 292 357)A04

UCB/EERC-78/20 "Testing of a Wind Restraint for Aseismic Base Isolation," by J.M. Kelly and D.E. Chitty - 1978 (PB 292 833)A03

UCB/EERC-78/21 "APOLLO - A Computer Program for the Analysis of Pore Pressure Generation and Dissipation in Horizontal Sand Layers During Cyclic or Earthquake Loading," by P.P. Martin and H.B. Seed - 1978 (PB 292 935)A04

UCB/EERC-78/22 "Optimal Design of an Earthquake Isolation System," by M.A. Bhatti, K.S. Pister and E. Polak - 1978 (PB 294 735)A06

UCB/EERC-78/23 "MASH - A Computer Program for the Non-Linear Analysis of Vertically Propagating Shear Waves in Horizontally Layered Deposits," by P.P. Martin and H.B. Seed - 1978 (PB 293 101)A05

UCB/EERC-78/24 "Investigation of the Elastic Characteristics of a Three Story Steel Frame Using System Identification," by I. Kaya and H.D. McNiven - 1978 (PB 296 225)A06

UCB/EERC-78/25 "Investigation of the Nonlinear Characteristics of a Three-Story Steel Frame Using System Identification," by I. Kaya and H.D. McNiven - 1978 (PB 301 363)A05

- JCB/EERC-78/26 "Studies of Strong Ground Motion in Taiwan," by Y.M. Hsiung, B.A. Bolt and J. Penzien - 1978 (PB 298 436)A06
- JCB/EERC-78/27 "Cyclic Loading Tests of Masonry Single Piers: Volume 1 - Height to Width Ratio of 2," by P.A. Hidalgo, R.L. Mayes, H.D. McNiven and R.W. Clough - 1978 (PB 296 211)A07
- JCB/EERC-78/28 "Cyclic Loading Tests of Masonry Single Piers: Volume 2 - Height to Width Ratio of 1," by S.-W.J. Chen, P.A. Hidalgo, R.L. Mayes, R.W. Clough and H.D. McNiven - 1978 (PB 296 212)A09
- JCB/EERC-78/29 "Analytical Procedures in Soil Dynamics," by J. Lysmer - 1978 (PB 298 445)A06
- JCB/EERC-79/01 "Hysteretic Behavior of Lightweight Reinforced Concrete Beam-Column Subassemblages," by B. Forzani, E.P. Popov and V.V. Bertero - April 1979(PB 298 267)A06
- JCB/EERC-79/02 "The Development of a Mathematical Model to Predict the Flexural Response of Reinforced Concrete Beams to Cyclic Loads, Using System Identification," by J. Stanton & H. McNiven - Jan. 1979(PB 295 875)A10
- JCB/EERC-79/03 "Linear and Nonlinear Earthquake Response of Simple Torsionally Coupled Systems," by C.L. Kan and A.K. Chopra - Feb. 1979(PB 298 262)A06
- JCB/EERC-79/04 "A Mathematical Model of Masonry for Predicting its Linear Seismic Response Characteristics," by Y. Mengi and H.D. McNiven - Feb. 1979(PB 298 266)A06
- JCB/EERC-79/05 "Mechanical Behavior of Lightweight Concrete Confined by Different Types of Lateral Reinforcement," by M.A. Manrique, V.V. Bertero and E.P. Popov - May 1979(PB 301 114)A06
- JCB/EERC-79/06 "Static Tilt Tests of a Tall Cylindrical Liquid Storage Tank," by R.W. Clough and A. Niwa - Feb. 1979 (PB 301 167)A06
- JCB/EERC-79/07 "The Design of Steel Energy Absorbing Restrainers and Their Incorporation into Nuclear Power Plants for Enhanced Safety: Volume 1 - Summary Report," by F.N. Spencer, V.F. Zackay, and E.R. Parker - Feb. 1979(UCB/EERC-79/07)A09
- JCB/EERC-79/08 "The Design of Steel Energy Absorbing Restrainers and Their Incorporation into Nuclear Power Plants for Enhanced Safety: Volume 2 - The Development of Analyses for Reactor System Piping," "Simple Systems" by M.C. Lee, J. Penzien, A.K. Chopra and K. Suzuki "Complex Systems" by G.H. Powell, E.L. Wilson, R.W. Clough and D.G. Row - Feb. 1979(UCB/EERC-79/08)A10
- JCB/EERC-79/09 "The Design of Steel Energy Absorbing Restrainers and Their Incorporation into Nuclear Power Plants for Enhanced Safety: Volume 3 - Evaluation of Commercial Steels," by W.S. Owen, R.M.N. Pelloux, R.O. Ritchie, M. Faral, T. Ohhashi, J. Toplosky, S.J. Hartman, V.F. Zackay and E.R. Parker - Feb. 1979(UCB/EERC-79/09)A04
- JCB/EERC-79/10 "The Design of Steel Energy Absorbing Restrainers and Their Incorporation into Nuclear Power Plants for Enhanced Safety: Volume 4 - A Review of Energy-Absorbing Devices," by J.M. Kelly and M.S. Skinner - Feb. 1979(UCB/EERC-79/10)A04
- JCB/EERC-79/11 "Conservatism in Summation Rules for Closely Spaced Modes," by J.M. Kelly and J.L. Sackman - May 1979(PB 301 328)A03
- JCB/EERC-79/12 "Cyclic Loading Tests of Masonry Single Piers: Volume 3 - Height to Width Ratio of 0.5," by P.A. Hidalgo, R.L. Mayes, H.D. McNiven and R.W. Clough - May 1979(PB 301 321)A08
- JCB/EERC-79/13 "Cyclic Behavior of Dense Course-Grained Materials in Relation to the Seismic Stability of Dams," by N.G. Banerjee, H.B. Seed and C.K. Chan - June 1979(PB 301 373)A13
- JCB/EERC-79/14 "Seismic Behavior of Reinforced Concrete Interior Beam-Column Subassemblages," by S. Viathanatepa, E.P. Popov and V.V. Bertero - June 1979(PB 301 326)A10
- JCB/EERC-79/15 "Optimal Design of Localized Nonlinear Systems with Dual Performance Criteria Under Earthquake Excitations," by M.A. Bhatti - July 1979(PB 80 167 109)A06
- JCB/EERC-79/16 "OPTDYN - A General Purpose Optimization Program for Problems with or without Dynamic Constraints," by M.A. Bhatti, E. Polak and K.S. Pister - July 1979(PB 80 167 091)A05
- JCB/EERC-79/17 "ANSR-II, Analysis of Nonlinear Structural Response, Users Manual," by D.P. Mondkar and G.H. Powell - July 1979(PB 80 113 301)A05
- JCB/EERC-79/18 "Soil Structure Interaction in Different Seismic Environments," A. Gomez-Masso, J. Lysmer, J.-C. Chen and H.B. Seed - August 1979(PB 80 101 520)A04
- JCB/EERC-79/19 "ARMA Models for Earthquake Ground Motions," by M.K. Chang, J.W. Kwiakowski, R.F. Nau, R.M. Oliver and K.S. Pister - July 1979(PB 301 166)A05
- JCB/EERC-79/20 "Hysteretic Behavior of Reinforced Concrete Structural Walls," by J.M. Valienas, V.V. Bertero and E.P. Popov - August 1979(PB 80 165 905)A12
- JCB/EERC-79/21 "Studies on High-Frequency Vibrations of Buildings - 1: The Column Effect," by J. Lubliner - August 1979 (PB 80 158 553)A03
- JCB/EERC-79/22 "Effects of Generalized Loadings on Bond Reinforcing Bars Embedded in Confined Concrete Blocks," by S. Viathanatepa, E.P. Popov and V.V. Bertero - August 1979(PB 81 124 018)A14
- JCB/EERC-79/23 "Shaking Table Study of Single-Story Masonry Houses, Volume 1: Test Structures 1 and 2," by P. Gülkan, R.L. Mayes and R.W. Clough - Sept. 1979 (HUD-000 1763)A12
- JCB/EERC-79/24 "Shaking Table Study of Single-Story Masonry Houses, Volume 2: Test Structures 3 and 4," by P. Gülkan, R.L. Mayes and R.W. Clough - Sept. 1979 (HUD-000 1836)A12
- JCB/EERC-79/25 "Shaking Table Study of Single-Story Masonry Houses, Volume 3: Summary, Conclusions and Recommendations," by R.W. Clough, R.L. Mayes and P. Gülkan - Sept. 1979 (HUD-000 1837)A06

UCB/EERC-79/26 "Recommendations for a U.S.-Japan Cooperative Research Program Utilizing Large-Scale Testing Facilities," by U.S.-Japan Planning Group - Sept. 1979(PB 301 407)A06

UCB/EERC-79/27 "Earthquake-Induced Liquefaction Near Lake Amatitlan, Guatemala," by H.B. Seed, I. Arango, C.K. Chan, A. Gomez-Masso and R. Grant de Ascoli - Sept. 1979(NUREG-CR1341)A03

UCB/EERC-79/28 "Infill Panels: Their Influence on Seismic Response of Buildings," by J.W. Axley and V.V. Bertero Sept. 1979(PB 80 163 371)A10

UCB/EERC-79/29 "3D Truss Bar Element (Type 1) for the ANSR-II Program," by D.P. Mondkar and G.H. Powell - Nov. 1979 (PB 80 169 709)A02

UCB/EERC-79/30 "2D Beam-Column Element (Type 5 - Parallel Element Theory) for the ANSR-II Program," by D.G. Row, G.H. Powell and D.P. Mondkar - Dec. 1979(PB 80 167 224)A03

UCB/EERC-79/31 "3D Beam-Column Element (Type 2 - Parallel Element Theory) for the ANSR-II Program," by A. Riahi, G.H. Powell and D.P. Mondkar - Dec. 1979(PB 80 167 216)A03

UCB/EERC-79/32 "On Response of Structures to Stationary Excitation," by A. Der Kiureghian - Dec. 1979(PB 80166 929)A03

UCB/EERC-79/33 "Undisturbed Sampling and Cyclic Load Testing of Sands," by S. Singh, H.B. Seed and C.K. Chan Dec. 1979(ADA 087 298)A07

UCB/EERC-79/34 "Interaction Effects of Simultaneous Torsional and Compressional Cyclic Loading of Sand," by P.M. Griffin and W.N. Houston - Dec. 1979(ADA 092 352)A15

UCB/EERC-80/01 "Earthquake Response of Concrete Gravity Dams Including Hydrodynamic and Foundation Interaction Effects," by A.K. Chopra, P. Chakrabarti and S. Gupta - Jan. 1980(AD-A087297)A10

UCB/EERC-80/02 "Rocking Response of Rigid Blocks to Earthquakes," by C.S. Yim, A.K. Chopra and J. Penzien - Jan. 1980 (PB80 166 002)A04

UCB/EERC-80/03 "Optimum Inelastic Design of Seismic-Resistant Reinforced Concrete Frame Structures," by S.W. Zagajeski and V.V. Bertero - Jan. 1980(PB80 164 635)A06

UCB/EERC-80/04 "Effects of Amount and Arrangement of Wall-Panel Reinforcement on Hysteretic Behavior of Reinforced Concrete Walls," by R. Iliya and V.V. Bertero - Feb. 1980(PB81 122 525)A09

UCB/EERC-80/05 "Shaking Table Research on Concrete Dam Models," by A. Niwa and R.W. Clough - Sept. 1980(PB81 122 368)A06

UCB/EERC-80/06 "The Design of Steel Energy-Absorbing Restrainers and their Incorporation into Nuclear Power Plants for Enhanced Safety (Vol 1A): Piping with Energy Absorbing Restrainers: Parameter Study on Small Systems," by G.H. Powell, C. Oughourlian and J. Simons - June 1980

UCB/EERC-80/07 "Inelastic Torsional Response of Structures Subjected to Earthquake Ground Motions," by Y. Yamazaki April 1980(PB81 122 327)A08

UCB/EERC-80/08 "Study of X-Braced Steel Frame Structures Under Earthquake Simulation," by Y. Ghanaat - April 1980 (PB81 122 335)A11

UCB/EERC-80/09 "Hybrid Modelling of Soil-Structure Interaction," by S. Gupta, T.W. Lin, J. Penzien and C.S. Yeh May 1980(PB81 122 319)A07

UCB/EERC-80/10 "General Applicability of a Nonlinear Model of a One Story Steel Frame," by B.I. Sveinsson and H.D. McNiven - May 1980(PB81 124 377)A06

UCB/EERC-80/11 "A Green-Function Method for Wave Interaction with a Submerged Body," by W. Kioka - April 1980 (PB81 122 269)A07

UCB/EERC-80/12 "Hydrodynamic Pressure and Added Mass for Axisymmetric Bodies," by F. Nilrat - May 1980(PB81 122 343)A08

UCB/EERC-80/13 "Treatment of Non-Linear Drag Forces Acting on Offshore Platforms," by B.V. Dao and J. Penzien May 1980(PB81 153 413)A07

UCB/EERC-80/14 "2D Plane/Axisymmetric Solid Element (Type 3 - Elastic or Elastic-Perfectly Plastic) for the ANSR-II Program," by D.P. Mondkar and G.H. Powell - July 1980(PB81 122 350)A03

UCB/EERC-80/15 "A Response Spectrum Method for Random Vibrations," by A. Der Kiureghian - June 1980(PB81 122 301)A03

UCB/EERC-80/16 "Cyclic Inelastic Buckling of Tubular Steel Braces," by V.A. Zayas, E.P. Popov and S.A. Mahin June 1980(PB81 124 885)A10

UCB/EERC-80/17 "Dynamic Response of Simple Arch Dams Including Hydrodynamic Interaction," by C.S. Porter and A.K. Chopra - July 1980(PB81 124 000)A13

UCB/EERC-80/18 "Experimental Testing of a Friction Damped Aseismic Base Isolation System with Fail-Safe Characteristics," by J.M. Kelly, K.E. Beucke and M.S. Skinner - July 1980(PB81 148 595)A04

UCB/EERC-80/19 "The Design of Steel Energy-Absorbing Restrainers and their Incorporation into Nuclear Power Plants for Enhanced Safety (Vol 1B): Stochastic Seismic Analyses of Nuclear Power Plant Structures and Piping Systems Subjected to Multiple Support Excitations," by M.C. Lee and J. Penzien - June 1980

UCB/EERC-80/20 "The Design of Steel Energy-Absorbing Restrainers and their Incorporation into Nuclear Power Plants for Enhanced Safety (Vol 1C): Numerical Method for Dynamic Substructure Analysis," by J.M. Dickens and E.L. Wilson - June 1980

UCB/EERC-80/21 "The Design of Steel Energy-Absorbing Restrainers and their Incorporation into Nuclear Power Plants for Enhanced Safety (Vol 2): Development and Testing of Restraints for Nuclear Piping Systems," by J.M. Kelly and M.S. Skinner - June 1980

UCB/EERC-80/22 "3D Solid Element (Type 4-Elastic or Elastic-Perfectly-Plastic) for the ANSR-II Program," by D.P. Mondkar and G.H. Powell - July 1980(PB81 123 242)A03

UCB/EERC-80/23 "Gap-Friction Element (Type 5) for the ANSR-II Program," by D.P. Mondkar and G.H. Powell - July 1980 (PB81 122 285)A03

UCB/EERC-80/24 "U-Bar Restraint Element (Type 11) for the ANSR-II Program," by C. Oughourlian and G.H. Powell July 1980(PB81 122 293)A03

UCB/EERC-80/25 "Testing of a Natural Rubber Base Isolation System by an Explosively Simulated Earthquake," by J.M. Kelly - August 1980(PB81 201 360)A04

UCB/EERC-80/26 "Input Identification from Structural Vibrational Response," by Y. Hu - August 1980(PB81 152 308)A05

UCB/EERC-80/27 "Cyclic Inelastic Behavior of Steel Offshore Structures," by V.A. Zayas, S.A. Mahin and E.P. Popov August 1980(PB81 196 180)A15

UCB/EERC-80/28 "Shaking Table Testing of a Reinforced Concrete Frame with Biaxial Response," by M.G. Oliva October 1980(PB81 154 304)A10

UCB/EERC-80/29 "Dynamic Properties of a Twelve-Story Prefabricated Panel Building," by J.G. Bouwkamp, J.P. Kollegger and R.M. Stephen - October 1980(PB82 117 128)A06

UCB/EERC-80/30 "Dynamic Properties of an Eight-Story Prefabricated Panel Building," by J.G. Bouwkamp, J.P. Kollegger and R.M. Stephen - October 1980(PB81 200 313)A05

UCB/EERC-80/31 "Predictive Dynamic Response of Panel Type Structures Under Earthquakes," by J.P. Kollegger and J.G. Bouwkamp - October 1980(PB81 152 316)A04

UCB/EERC-80/32 "The Design of Steel Energy-Absorbing Restrainers and their Incorporation into Nuclear Power Plants for Enhanced Safety (Vol 3): Testing of Commercial Steels in Low-Cycle Torsional Fatigue," by P. Spencer, E.R. Parker, E. Jongewaard and M. Drory

UCB/EERC-80/33 "The Design of Steel Energy-Absorbing Restrainers and their Incorporation into Nuclear Power Plants for Enhanced Safety (Vol 4): Shaking Table Tests of Piping Systems with Energy-Absorbing Restrainers," by S.F. Stiemer and W.G. Godden - Sept. 1980

UCB/EERC-80/34 "The Design of Steel Energy-Absorbing Restrainers and their Incorporation into Nuclear Power Plants for Enhanced Safety (Vol 5): Summary Report," by P. Spencer

UCB/EERC-80/35 "Experimental Testing of an Energy-Absorbing Base Isolation System," by J.M. Kelly, M.S. Skinner and K.E. Beucke - October 1980(PB81 154 072)A04

UCB/EERC-80/36 "Simulating and Analyzing Artificial Non-Stationary Earthquake Ground Motions," by R.F. Nau, R.M. Oliver and K.S. Pister - October 1980(PB81 153 397)A04

UCB/EERC-80/37 "Earthquake Engineering at Berkeley - 1980," - Sept. 1980(PB81 205 974)A09

UCB/EERC-80/38 "Inelastic Seismic Analysis of Large Panel Buildings," by V. Schricker and G.H. Powell - Sept. 1980 (PB81 154 338)A13

UCB/EERC-80/39 "Dynamic Response of Embankment, Concrete-Gravity and Arch Dams Including Hydrodynamic Interaction," by J.F. Hall and A.K. Chopra - October 1980(PB81 152 324)A11

UCB/EERC-80/40 "Inelastic Buckling of Steel Struts Under Cyclic Load Reversal," by R.G. Black, W.A. Wenger and E.P. Popov - October 1980(PB81 154 312)A08

UCB/EERC-80/41 "Influence of Site Characteristics on Building Damage During the October 3, 1974 Lima Earthquake," by P. Repetto, I. Arango and H.B. Seed - Sept. 1980(PB81 161 739)A05

UCB/EERC-80/42 "Evaluation of a Shaking Table Test Program on Response Behavior of a Two Story Reinforced Concrete Frame," by J.M. Blondet, R.W. Clough and S.A. Mahin

UCB/EERC-80/43 "Modelling of Soil-Structure Interaction by Finite and Infinite Elements," by F. Medina - December 1980(PB81 229 270)A04

UCB/EERC-81/01 "Control of Seismic Response of Piping Systems and Other Structures by Base Isolation," edited by J.M. Kelly - January 1981 (PB81 200 735)A05

UCB/EERC-81/02 "OPTNSR - An Interactive Software System for Optimal Design of Statically and Dynamically Loaded Structures with Nonlinear Response," by M.A. Bhatti, V. Ciampi and K.S. Pister - January 1981 (PB81 213 851)A09

UCB/EERC-81/03 "Analysis of Local Variations in Free Field Seismic Ground Motions," by J.-C. Chen, J. Lysmer and H.B. Seed - January 1981 (AD-AC99508)A13

UCB/EERC-81/04 "Inelastic Structural Modeling of Braced Offshore Platforms for Seismic Loading," by V.A. Zayas, P.-S.B. Shing, S.A. Mahin and E.P. Popov - January 1981(PB82 138 777)A07

UCB/EERC-81/05 "Dynamic Response of Light Equipment in Structures," by A. Der Kiureghian, J.L. Sackman and B. Nour-Omid - April 1981 (PB81 218 497)A04

UCB/EERC-81/06 "Preliminary Experimental Investigation of a Broad Base Liquid Storage Tank," by J.G. Bouwkamp, J.P. Kollegger and R.M. Stephen - May 1981(PB82 140 385)A03

UCB/EERC-81/07 "The Seismic Resistant Design of Reinforced Concrete Coupled Structural Walls," by A.E. Aktan and V.V. Bertero - June 1981(PB82 113 358)A11

UCB/EERC-81/08 "The Undrained Shearing Resistance of Cohesive Soils at Large Deformations," by M.R. Pyles and H.B. Seed - August 1981

UCB/EERC-81/09 "Experimental Behavior of a Spatial Piping System with Steel Energy Absorbers Subjected to a Simulated Differential Seismic Input," by S.F. Stiemer, W.G. Godden and J.M. Kelly - July 1981

- UCB/EERC-81/10 "Evaluation of Seismic Design Provisions for Masonry in the United States," by B.I. Sveinsson, R.L. Mayes and H.D. McNiven - August 1981
- UCB/EERC-81/11 "Two-Dimensional Hybrid Modelling of Soil-Structure Interaction," by T.-J. Tzong, S. Gupta and J. Penzien - August 1981(PB82 142 118)A04
- UCB/EERC-81/12 "Studies on Effects of Infills in Seismic Resistant R/C Construction," by S. Brokken and V.V. Bertero - September 1981
- UCB/EERC-81/13 "Linear Models to Predict the Nonlinear Seismic Behavior of a One-Story Steel Frame," by H. Valdimarsson, A.H. Shah and H.D. McNiven - September 1981(PB82 138 793)A07
- UCB/EERC-81/14 "TLUSH: A Computer Program for the Three-Dimensional Dynamic Analysis of Earth Dams," by T. Kagawa, L.H. Mejia, H.B. Seed and J. Lysmer - September 1981(PB82 139 940)A06
- UCB/EERC-81/15 "Three Dimensional Dynamic Response Analysis of Earth Dams," by L.H. Mejia and H.B. Seed - September 1981 (PB82 137 274)A12
- UCB/EERC-81/16 "Experimental Study of Lead and Elastomeric Dampers for Base Isolation Systems," by J.M. Kelly and S.B. Hodder - October 1981
- UCB/EERC-81/17 "The Influence of Base Isolation on the Seismic Response of Light Secondary Equipment," by J.M. Kelly - April 1981
- UCB/EERC-81/18 "Studies on Evaluation of Shaking Table Response Analysis Procedures," by J. Marcial Blondet - November 1981
- UCB/EERC-81/19 "DELIGHT.STRUCT: A Computer-Aided Design Environment for Structural Engineering," by R.J. Balling, K.S. Pister and E. Polak - December 1981
- UCB/EERC-81/20 "Optimal Design of Seismic-Resistant Planar Steel Frames," by R.J. Balling, V. Ciampi, K.S. Pister and E. Polak - December 1981
- UCB/EERC-82/01 "Dynamic Behavior of Ground for Seismic Analysis of Lifeline Systems," by T. Sato and A. Der Kiureghian - January 1982 (PB82 218 926) A05
- UCB/EERC-82/02 "Shaking Table Tests of a Tubular Steel Frame Model," by Y. Ghanaat and R. W. Clough - January 1982 (PB82 220 161) A07
- UCB/EERC-82/03 "Experimental Behavior of a Spatial Piping System with Shock Arrestors and Energy Absorbers under Seismic Excitation," by S. Schneider, H.-M. Lee and G. W. Godden - May 1982
- UCB/EERC-82/04 "New Approaches for the Dynamic Analysis of Large Structural Systems," by E. L. Wilson - June 1982
- UCB/EERC-82/05 "Model Study of Effects on the Vibration Properties of Steel Offshore Platforms," by F. Shahrivar and J. G. Bouwkamp - June 1982
- UCB/EERC-82/06 "States of the Art and Practice in the Optimum Seismic Design and Analytical Response Prediction of R/C Frame-Wall Structures," by A. E. Aktan and V. V. Bertero - July 1982.
- UCB/EERC-82/07 "Further Study of the Earthquake Response of a Broad Cylindrical Liquid-Storage Tank Model," by G. C. Manos and R. W. Clough - July 1982
- UCB/EERC-82/08 "An Evaluation of the Design and Analytical Seismic Response of a Seven Story Reinforced Concrete Frame - Wall Structure," by A. C. Finley and V. V. Bertero - July 1982